DEUTERIUM AND PHOSPHORUS-31 NUCLEAR MAGNETIC RESONANCE INVESTIGATIONS OF HUMAN PLASMA LOW- AND HIGH- DENSITY LIPOPROTEINS

by

David B. Fenske

B.Sc., Simon Fraser University, 1981

THESIS SUBMITTED IN PARTIAL FULFILLMENT OF

THE REQUIREMENTS FOR THE DEGREE OF

DOCTOR OF PHILOSOPHY

in the Department

of

Chemistry

SIMON FRASER UNIVERSITY

July 1988

APPROVAL

Name: David B. Fenske

Degree: Doctor of Philosophy

Title of thesis: DEUTERIUM AND PHOSPHORUS-31 NUCLEAR MAGNETIC RESONANCE INVESTIGATIONS OF HUMAN PLASMA LOW- AND HIGH- DENSITY LIPOPROTEINS

Examining Committee:

Chairman: Dr. E. J. Wells

Dr. R. J. Cushley
Senior Supervisor

Dr. I. D. Gay

Dr. W. R. Richards

Dr. G. Tibbits
Department of Kinesiology

Dr. P. R. Cullis
External Examiner
Department of Biochemistry
University of British Columbia

Date Approved: 8/4/88, 1988

PARTIAL COPYRIGHT LICENSE

I hereby grant to Simon Fraser University the right to lend my thesis, project or extended essay (the title of which is shown below) to users of the Simon Fraser University Library, and to make partial or single copies only for such users or in response to a request from the library of any other university, or other educational institution, on its own behalf or for one of its users. I further agree that permission for multiple copying of this work for scholarly purposes may be granted by me or the Dean of Graduate Studies. It is understood that copying or publication of this work for financial gain shall not be allowed without my written permission.

Title of Thesis/Project/Extended Essay

DEUTERIUM AND PHOSPHORUS-31 NUCLEAR MAGNETIC RESONANCE INVESTIGATIONS OF HUMAN PLASMA LOW- AND HIGH- DENSITY LIPOPROTEINS

Author:

(signature)

DAVID B. FENSKE

(name)

SEPT. 12, 1988

(date)

ABSTRACT

Interactions between the surface phospholipids and core lipids of reconstituted high density lipoprotein (rHDL) have been studied by ^2H NMR. Temperature-dependent ^2H NMR spectra of rHDLs containing either cholesteryl [18,18,18-$^2H_3$]oleate or tri-[16,16-$^2H_2$]oleoyl glycerol ([$^2H_6$]triolein) as the core lipids surrounded by either dipalmitoylphosphatidylcholine (DPPC) or egg PC were obtained to assess the effect of the monolayer on the core. To examine the effect of core on monolayer, rHDLs composed of [5,5-$^2H_2$]PC and either cholesteryl oleate or triolein were studied. The acyl chains of both the monolayer and core components showed increased order when in contact with neighboring lipids of higher order, demonstrating considerable interactions between the core and monolayer of HDL.

Lateral diffusion coefficients D of phospholipids in low density lipoprotein (LDL) and HDL_3, obtained from the viscosity-dependence of the ^{31}P NMR linewidths, were (1.4±0.5) x 10^{-9} cm^2/s and (2.3±0.8) x 10^{-8} cm^2/s at 25°C, respectively. The value for HDL_3 is close to that observed in HDL_2 and phospholipid bilayers, while that for LDL is an order of magnitude slower. At 45°C, the value for LDL increased to (1.1±0.3) x 10^{-8} cm^2/s, suggesting that the slow diffusion observed at 25°C may arise from interactions with the core cholesteryl esters.

The residual chemical shift anisotropy $\Delta\sigma$ of phospholipids in LDL at 25°C, obtained from the viscosity- and field- dependence of the ^{31}P NMR linewidths, was 49±1 and 50±4 ppm, respectively. These values are similar to those observed in phospholipid bilayers (≃45 ppm). In HDL_3 at 25°C, unusually high values of 136±11 and 156±30 ppm were obtained from the

viscosity- and field- dependence, respectively, suggesting significantly different motions and/or unique orientations of the headgroup.

The formation of soluble complexes of LDL with the glycosaminoglycans (GAGs) heparin and chondroitin sulfate (CS) was studied by ^{2}H and ^{31}P NMR and light scattering. Heparin was found to form multiple-LDL complexes only over a narrow range of heparin concentrations, while with CS the proportion of complexes was fewer, increasing continuously over the range of CS concentrations studied. The mean size of LDL-heparin complexes varied with protein concentration at heparin/LDL $\simeq$0.02. Analysis of ^{2}H NMR linewidths of $C^{2}H_{3}$ groups yielded correlation times of [^{2}H]GAG suggesting that both heparin and CS have similar motions when bound to LDL. LDL-heparin insoluble complexes were studied by ^{31}P NMR. Powder-type spectra were observed at temperatures <30°C, with $\Delta\sigma$ of the heparin complexes similar to pelleted LDL.

ACKNOWLEDGEMENTS

I am grateful to my supervisor, Dr. R. J. Cushley, for his guidance and support during the course of these investigations. I also wish to thank Dr. I. D. Gay and Dr. W. R. Richards for their efforts as members of my supervisory committee. In addition, Dr. Gay made available several of his computer programs, and his generosity is much appreciated. I also wish to thank Dr. Elliott Burnell (Department of Chemistry, University of British Columbia) for providing his computer program for simulating ^{31}P NMR lineshapes, and for assistance in making it run.

I am indebted to past and present members of the research group for their assistance and advice. Dr. S. R. Wassall, Dr. Y. I. Parmar, Dr. W. D. Treleaven, and Dr. J. L. Thewalt provided many helpful ideas and interesting discussions. Ravinder Chana and Dr. Y. I. Parmar provided assistance with electron microscopy, and deuterated lipids were synthesized by Ravinder Chana and Dr. H. Gorrissen.

Financial support from the Natural Sciences and Engineering Research Council of Canada and from Simon Fraser University is gratefully acknowledged.

Finally, I wish to thank my wife, Beth, for her support and patience during the course of these studies.

DEDICATION

To Beth, Jenny, and Michael

LIST OF ABBREVIATIONS

rHDL, reconstituted high density lipoprotein; HDL, high density lipoprotein; LDL, low density lipoprotein; VLDL, very low density lipoprotein; ^{2}H NMR, deuterium nuclear magnetic resonance; ^{31}P NMR, phosphorus-31 nuclear magnetic resonance; DSC, differential scanning calorimetry; QELS, quasi-elastic light scattering; [$^{2}H_{3}$]CO, cholesteryl [18,18,18-$^{2}H_{3}$]oleate; [$^{2}H_{2}$]PC, phosphatidylcholine synthesized from egg L-*a*-lysophosphatidylcholine and [5,5-$^{2}H_{2}$]palmitic acid; [$^{2}H_{31}$]PC, phosphatidylcholine synthesized from egg L-*a*-lysophosphatidylcholine and [$^{2}H_{31}$]palmitic acid; [$^{2}H_{6}$]TO, tri-[16,16-$^{2}H_{2}$]oleoyl glycerol; PC, phosphatidylcholine; egg PC, egg phosphatidylcholine; DPPC, dipalmitoylphosphatidylcholine; SPM, sphingomyelin; TO, triolein; CO, cholesteryl oleate; CE, cholesteryl ester; TG, triglyceride; apoHDL$_{3}$, apoproteins isolated from HDL$_{3}$; GAG, glycosaminoglycan; HEP, heparin; CS, chondroitin sulfate; C4S, chondroitin 4-sulfate; C6S, chondroitin 6-sulfate; PG, proteoglycan.

TABLE OF CONTENTS

LIST OF TABLES

LIST OF FIGURES

CHAPTER I

INTRODUCTION

The plasma lipoproteins are spherical macromolecular assemblies of specific apoproteins and lipid which transport hydrophobic lipids within the aqueous environment of the circulatory system. The lipids, whose origin may be dietary or endogenous, are delivered to cells for oxidative metabolism, triglyceride synthesis for storage, steroid hormone biosynthesis, and maintenance of cellular membrane integrity (Dolphin, 1985). This complex flow of lipids is regulated by the various apoproteins whose functions include activation of metabolic enzymes and membrane receptor binding (Dolphin, 1985).

Lipoprotein Structure

The plasma lipoproteins share a common structure, which is represented in Figure 1. The hydrophobic lipids (cholesteryl esters, triglycerides, and possibly some free cholesterol) are partitioned into the center or core of the particle, and are surrounded by an interfacial monolayer of phospholipids, free cholesterol, and protein. The phospholipids and cholesterol are oriented with their polar moieties (headgroups and hydroxyl groups, respectively) facing the aqueous environment and their hydrophobic portions in contact with the core lipid. The apoproteins form amphipathic helices which allow opposite sides of the helix to interact with the aqueous and lipid environments (Segrest *et al.*, 1974; Assman and Brewer, 1974).

Figure 1: Structural model of low density lipoprotein.

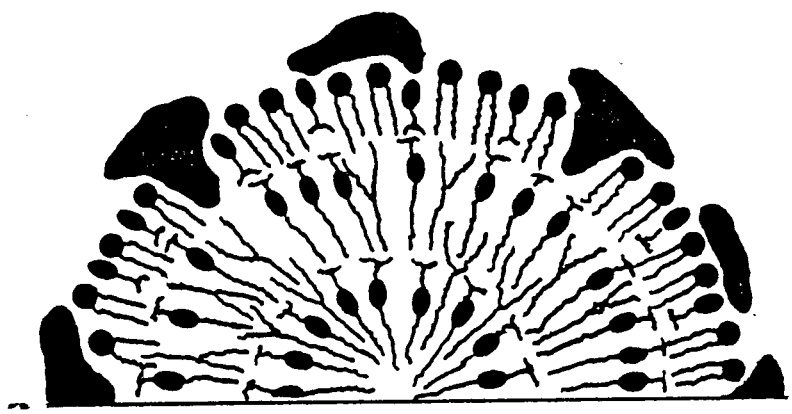

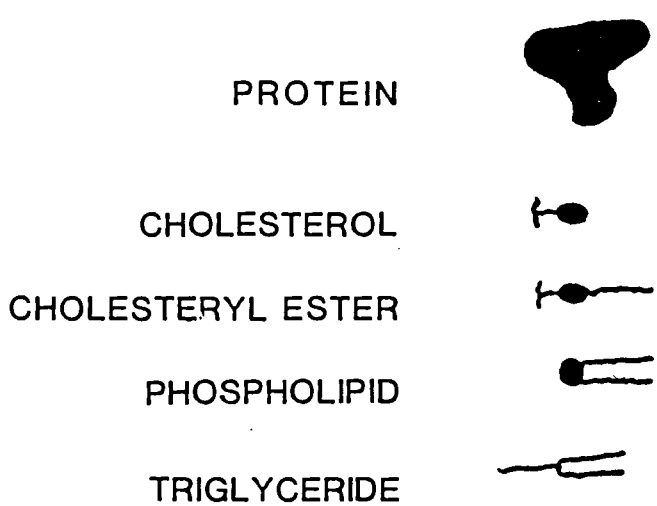

Lipoproteins are classified according to their bouyant densities and are commonly isolated by sequential ultracentrifugal flotation. The major groupings, followed by the density range in which they are isolated, are chylomicrons (CM, <0.94 g/mL), very low density lipoprotein (VLDL, <1.006 g/mL), low density lipoprotein (LDL, 1.019-1.063 g/mL), and high density lipoprotein (HDL_2, 1.063-1.125 g/mL; HDL_3, 1.125-1.21 g/mL). Their properties and composition are listed in Table I.

Table I: Composition (weight-%) of the human plasma lipoproteins.[a]

Component	CM	VLDL	LDL	HDL_2	HDL_3
Protein	2	8	21	46	61
Triglyceride	90	55	5	3	2
Cholesterol	1	7	9	4	2
Cholesteryl ester	3	12	42	19	14
Phospholipids	4	18	24	28	20
Diameter (nm)	≈300	55	22	11	8.8
MW x 10^6	10^3	5-27	2.5	0.22	0.16
Density (g/mL)	<0.95	<1.006	1.019-1.063	1.063-1.125	1.125-1.21

[a] Table adapted from Dolphin (1985) and Scanu (1979).

Physical Studies of Human Plasma Lipoproteins

Much information on lipoprotein structure has come from physical techniques such as NMR (Hamilton and Morrissett, 1986; Parmar *et al.*, 1983; 1985; Treleaven *et al.*, 1986), electron microscopy (Forte *et al.*, 1968), differential scanning calorimetry (Deckelbaum *et al.*, 1977), X-ray diffraction (Atkinson *et al.*, 1977; 1980; Laggner and Muller, 1978; Baumstark *et al.*, 1983), and neutron diffraction (Laggner *et al.*, 1981). In the following discussion, attention will first be focused on common structural elements of the plasma lipoproteins, followed by a more detailed discussion of the structure of LDL and HDL.

Phosphatidylcholine (PC) and sphingomyelin (SPM) are the major phospholipids in all classes of lipoproteins, the former being the most abundant (Scanu, 1973). X-ray diffraction studies have shown that all of the phospholipid head-groups are located with the apoproteins in an electron-dense region at the surface of the particle (Laggner and Muller, 1978; Baumstark *et al.*, 1983). The same result was obtained from neutron diffraction studies of LDL containing incorporated PC selectively deuterated in the head group (Laggner *et al.*, 1981). ^{31}P NMR studies utilizing paramagnetic shift reagents generally support this view. Hydrated transition metal ions caused quenching of all ^{31}P resonances in HDL and LDL (Henderson *et al.*, 1975), and Pr^{3+} was found to shift all of the ^{31}P resonances in LDL (Yeagle *et al.*, 1978), suggesting that all of the phosphate are located at the surface of the particle. However, Mn^{2+} in the presence of excess EDTA was found to selectively quench 50% and 80% of the ^{31}P intensity of LDL and HDL, respectively (Henderson *et al.*, 1975). This has been explained by postulating that the Mn-EDTA complex is too large to

access all the phosphates (Hamilton and Morrisset, 1986).

Several workers have attempted to use absolute intensity measurements to determine what percentage of the phospholipids contribute to the high-resolution ^{1}H and ^{31}P NMR spectra. This is done by comparing the ratio of lipoprotein to external reference compound obtained from NMR intensities with the same ratio determined from chemical analysis. Using ^{31}P NMR, it was determined that all of the HDL phospholipid was observable, while only $\simeq$80% of the LDL phospholipid was (Yeagle *et al.*, 1977; 1978). Trypsin-treatment of LDL resulted in close to 100% detection, suggesting that interactions with protein had immobilized $\simeq$20% of the phospholipid. Similarly, a ^{1}H NMR study of porcine lipoproteins found that all of the choline methyl protons of HDL phospholipids and $\simeq$70% of those of LDL are observed in the high-resolution spectrum (Finer *et al.*, 1975).

The majority of NMR investigations have utilized ^{13}C NMR to investigate the motional properties of lipids (Hamilton and Morrissett, 1986). This technique allows a wide range of lipid resonances to be studied, and has proved useful in demonstrating the anisotropic nature of the motions of the steroid ring of both cholesterol and cholesteryl esters (Hamilton and Morrissett, 1986). In particular, the temperature-dependence of the C-6 and C-3 resonances of LDL cholesteryl esters are found to be characteristic of a liquid to liquid crystalline phase transition, an observation corroborated by DSC and ^{1}H NMR (see below). Also, ^{13}C NMR studies suggest that at least 1/3 of the unesterified cholesterol pool of LDL is present in the core. Nevertheless, the amount of novel information provided by ^{13}C NMR is small; in general, the chemical shifts and T_1 values of most resonances are the same in lipoproteins and in simple model

systems. As well, the fatty acyl resonances of the different lipids are not resolved (Hamilton and Morrissett, 1986). What ^{13}C NMR does demonstrate clearly is that the lipid components of lipoproteins possess a great deal of motional freedom.

Structure of LDL

Human plasma LDL isolated in the density range 1.019-1.063 g/mL has a molecular weight range of 2 to 3.5 x 10^6 and a diameter of 20-25 nm (Goldstein and Brown, 1977). The composition of the particle is approximately 20% protein, 24% phospholipid, 42% cholesteryl ester, 9% free cholesterol, and 5% triglyceride (Dolphin, 1985). The cholesteryl ester fatty acid is predominantly linoleate (50%), followed by oleate (20%) and palmitate (15%) (Goldstein and Brown, 1977). The phospholipids are primarily PC (64%) and SPM (26%) (Scanu, 1973). Some glycosphingolipids are also present (Dawson *et al.*, 1976).

LDL undergoes a thermal transition between 20 and 40°C which corresponds to a smectic to disordered transition of the core cholesteryl esters (Deckelbaum *et al.*, 1977). Small-angle x-ray scattering studies suggest that the cholesteryl esters are radially packed in two concentric layers below the phase transition (Atkinson *et al.*, 1977, 1980). The radial electron density shows two maxima at approximately 3 and 6 nm, which originate from the steroid rings of the ester molecules. Above the phase transition, these maxima are gone, suggesting a more uniform distribution of esters within the core (Atkinson *et al.*, 1980). The enthalpy of the LDL transition was found by DSC to be less (per gram of cholesteryl ester) than that of either the isolated esters or of neat ester mixtures, and it was found that the esters in LDL could not be crystallized (Deckelbaum *et*

al., 1977). This was taken to suggest that the behaviour of esters in LDL is constrained relative to the free esters, a suggestion corroborated by ^{13}C NMR (Sears *et al.*, 1976). This could result from the spherical packing imposed by the particle and/or from interactions with the surface components (Deckelbaum *et al.*, 1977). The observed transition temperature of a single LDL sample varies with the triglyceride content of the core (Deckelbaum *et al.*, 1977). None of the surface components, when isolated from the particle, undergo phase transitions between 0 and 45°C (Deckelbaum *et al.*, 1977).

The dynamics of LDL cholesteryl esters have been studied by ^{13}C NMR (Hamilton *et al.*, 1979). The temperature-dependence of the ^{13}C NMR linewidths of the steroid ring carbons of the core esters were indicative of an order - disorder transition. Similar results were obtained from a ^{1}H NMR study of the temperature-dependence of the intensities of the acyl chain resonances (Kroon, 1981). More recently, cholesteryl oleate, selectively deuterated along the acyl chain, has been incorporated into LDL from microemulsion donor particles using plasma exchange proteins (Treleaven *et al.*, 1986). Temperature-dependent ^{2}H NMR spectra of the C-2' and C-5' deuterons of the acyl chain revealed the presence of two spectral components, corresponding to regions of high and low order in the core. At 25°C, values of the C-^{2}H order parameter S_{CD} were 0.20 and 0.12 for the C-2' and C-5' deuterons, respectively. Both domains were observed above the phase transition. ^{2}H spin-lattice relaxation time measurements were indicative of an increased rate of motion towards the free end of the chain.

The phospholipid monolayer has also been studied by ^2H NMR via incorporation of selectively deuterated palmitic acid (Treleaven, 1985). As in the core, two regions of different order were detected, with S_{CD} ≃0.31 and ≃0.05-0.07. This was taken to reflect a non-uniform distribution of phospholipid, cholesterol, and protein in the surface monolayer.

The microviscosities of the hydrophobic lipid regions of human serum lipoproteins have been determined from fluorescence polarization measurements using 1,6-diphenyl-1,3,5-hexatriene as the fluorescent probe (Jonas, 1977). LDL had the highest microviscosity at 25°C (6.1 P). Differences in the microviscosity of intact LDL compared with the isolated lipids suggested an immobilizing effect of the protein on lipid. Interestingly, no evidence of a phase transition was observed over the temperature range of 0-40°C, which raises questions about the location of the bulky reporting group and its perturbing effects.

LDL contains a single molecule of apo B-100, a monomeric protein 4536 amino acids in length with an apparent M_r ≃549,000, making it the largest polypeptide ever studied (Chen *et al.*, 1986; Patterson *et al.*, 1987; Li *et al.*, 1988). Another form of apo B, termed apo B-48, is found in chylomicrons and has a M_r ≃ 264,000. Both are products of a single gene (Li *et al.*, 1988). Apo B-100 is unique among the apoprotein family in possessing a high content of β-structure (Li *et al.*, 1988) and it does not transfer among lipoprotein particles (Kane, 1983). Elucidation of the stucture of apo B-100 was hampered for years by its low solubility in aqueous buffers and by its propensity to aggregate when delipidated (Sparks and Sparks, 1985). Its primary sequence, obtained from the sequencing of apo B-100 cDNA's (Chen *et al.*, 1986), has been found to contain two kinds

of internal repeats (Li *et al.*, 1988). The first corresponds to amphipathic α-helices, as in the other apoproteins, and the second to hydrophobic proline-rich domains. The latter are unique to apo B-100 and are thought to form β-turns and β-structure, which may penetrate deeper into LDL than the amphipathic helices. Evidence for this comes from an FT-IR study dealing with changes in secondary structure of apo B-100 upon Cu^{2+}-oxidation (Herzyk *et al.*, 1987). The α-helical, random coil, and β-turn structures were affected by oxidation and showed fast ^1H-^2H exchange, suggesting a location on or near the surface of LDL. In contrast, the β-structure was resistant to oxidation and exchange.

Structure of HDL

HDL are a heterogeneous class rich in phospholipid and free cholesterol. There are two major kinds known as HDL_2 and HDL_3, the former being larger with a higher cholesteryl ester content. The HDLs are small particles 8-11 nm in diameter with a composition that is high in protein (46-61%). The main proteins are apo A-I (60%) and apo A-II (30%), with the remainder consisting largely of apo C-III and apo E (Lusis, 1988). Neither HDL_2 nor HDL_3 exhibit any thermal phase transitions as does LDL, although the isolated esters show reversible transitions between 20 and 40°C (Tall *et al.*, 1977). This may indicate that the small number of esters in HDL are in a domain too small for cooperative changes to occur (Phillips, 1977). Tall (1980) has noted that HDL particles smaller than 14 nm will not have sufficient core volume to accomodate a single extended layer of cholesteryl esters, a prerequisite for cooperative interactions. This is exemplified by HDL_C, a large ($\simeq$18 nm) cholesterol-rich HDL containing apo A-I and apo E isolated from atherosclerotic swine, which exhibits a thermal

transition of its core esters over the range 25-45°C (Atkinson *et al.*, 1978). The core contains only a single layer of cholesteryl esters, whereas LDL has two (Atkinson *et al.*, 1977).

A great deal of discussion has centered on the nature of the interaction between the core and monolayer of HDL. Hamilton and Cordes (1978) and Shen *et al.* (1977), on the basis of ^{13}C NMR and size/composition correlations, respectively, concluded that the core components exist in a separate liquid phase in HDL, with a sharply defined boundary between the hydrophobic core and the amphipathic layer surrounding it. In contrast, interdigitation of core components with phospholipid acyl chains is a feature of several models of HDL structure, based on size and compositional data (Verdery and Nichols, 1975), differential scanning calorimetry (Tall *et al.*, 1977), and X-ray diffraction (Laggner and Muller, 1978; Baumstark *et al.*, 1983). Based on ^{2}H NMR studies of selectively deuterated cholesteryl palmitate in the core of reconstituted HDL, Parmar *et. al.* (1983) demonstrated that the ester adopts an extended conformation in the core. This would make penetration of esters into the monolayer likely. The order parameters of esters in the HDL core were significantly higher ($S_{CD} \simeq 0.35$ for deuterons C-2' to C-6') than in LDL (see above).

The acyl chain order in the HDL_3 monolayer ($S_{CD} \simeq 0.4$), determined from ^{2}H NMR studies of selectively deuterated palmitic acids, is approximately 1.5 - 2 times higher than in PC multilamellar dispersions (Parmar *et al.*, 1985), and is significantly higher than in VLDL (R.S. Chana, unpublished results) or LDL (Treleaven, 1985).

Lipoprotein Metabolism

The following discussion is a brief summary of the current knowledge on lipoprotein metabolism. For more details, the reader is referred to recent reviews by Brown and Goldstein (1986), Atkinson and Small (1986), Dolphin (1985), and Mahley and Innerarity (1983). An excellent discussion on the apoproteins and the apoprotein multigene family is given by Li *et al.* (1988); the genetic factors affecting blood lipoprotein expression are discussed by Lusis (1988).

The largest lipoprotein particles, the triglyceride-rich chylomicrons, with diameters ranging from 100 to 500 nm, are synthesized by the intestine in response to dietary fat. The particles contain apo B-48, which is synthesized only in the intestine, and apo A-I, A-II, and A-IV. Chylomicrons pass through the lymphatic system en route to the circulatory system. In plasma, apo C-I, C-II and E bind to the surface and the cholesterol content increases, with the loss of some phospholipid and apo A-IV, which then enters the HDL pool. The chylomicron is then modified by lipoprotein lipase, which is activated by apo C-II and results in hydrolysis of triglyerides and shrinkage of the core. The end products are core and surface remnants, of which the former are enriched in cholesterol and are rapidly removed by the B,E-receptor and chylomicron-receptor of the liver, and the latter enter the HDL pool.

VLDL are triglyceride-rich particles that are secreted by the liver, and contain apo B-100, apo C, and apo E. Once in the plasma, VLDL are subjected to triglyceride hydrolysis by lipoprotein lipase, producing a VLDL-remnant called intermediate density lipoprotein (IDL), which is

further metabolized to LDL. During the VLDL to LDL transformation, some phospholipids and the apo C's and E are lost to the HDL pool. LDL contains a single molecule of apo B-100 as its only protein, and a core that is predominantly cholesteryl ester. High levels of LDL have been linked with an increased risk of coronary heart disease (Goldstein and Brown, 1977). LDL is the major carrier of cholesterol to the peripheral tissues, and is involved in the regulation of cholesterol biosynthesis at these sites by the LDL pathway (Goldstein and Brown, 1977). Although cells outside the liver have the capacity to synthesize cholesterol *de novo*, they generally obtain it from LDL instead. The apo B-100 in LDL is recognized by the apo B,E-receptor, a glycoprotein of M_r ≃164,000 (Schneider *et al.*, 1982), which is located in clathrin-coated pits upon the cell membrane of many tissues. Binding of LDL to the LDL receptor results in internalization of the receptor-LDL complex by endocytosis. The resulting vesicles fuse with lysosomes, and both the protein and cholesteryl ester components of the LDL particle undergo hydrolytic degradation. The liberated unesterified cholesterol plays an important role in cell cholesterol regulation; it suppresses the synthesis of cholesterol and LDL receptors, resulting in a decrease of both *de novo* cholesterol synthesis and cholesterol uptake from LDL (Goldstein and Brown, 1977). The role of LDL in the pathogenesis of atherosclerosis will be further discussed in detail in a later section.

In contrast to LDL, high plasma concentrations of HDL have been inversely correlated with the risk of atherosclerosis (Miller and Miller, 1975). HDL are synthesized by both the liver and intestine in two forms: (i) discoidal HDLs of high cholesterol to phospholipid ratio, in which the lipid is arranged in a bilayer, with protein around the periphery of the discs, and (ii) small (≃8 nm) spherical HDL_3 particles which contain a

small core of cholesteryl ester and triglyceride (Atkinson and Small, 1986). The nascent discoidal HDL containing apo A-I are transformed into small HDL_3-like particles by the enzyme lecithin-cholesterol-acyltransferase (LCAT), which is activated by apo A-I and converts some of the phospholipid and free cholesterol to cholesteryl ester. The further transformations of the small HDL_3 provides the basis for the process of reverse cholesterol transport, by which cholesterol is transported, via HDL, from the peripheral tissues to the liver for excretion from the body (Dolphin, 1985; Atkinson and Small, 1986). The HDL_3 may fuse with the surface remnants of chylomicrons and VLDL to form phospholipid-rich HDL_{2a}. These particles can interact with cells and acquire free cholesterol, which is esterified by LCAT and stored in the core. As this process continues, the size of the core increases, resulting in the formation of the larger HDL_{2b}, which can then acquire apo E with displacement of apo A-I (Gordon *et al.*, 1983). The apo E containing particles are removed by the B,E-receptors or chylomicron receptors of the liver, completing the process. The hepatic apo A-I receptor may also contribute to cholesterol removal of apo A-I containing particles (Rifici and Eder, 1984). HDL cholesteryl esters may also be transfered to the other lipoproteins by the action of lipid transfer proteins present in the plasma (Zilversmit, 1984; Tall, 1986).

The Relationship between Lipoprotein-Glycosaminoglycan Interactions and Atherosclerosis

Atherosclerosis, an arterial disease characterized by lipid-containing lesions, is the chief cause of death in North America and Western Europe (Ross and Glomset, 1976). The atherosclerotic lesions (fatty streak,

fibrous plaque, and complicated lesion) are formed by three processes; smooth muscle cell proliferation, intra- and extracellular lipid deposition, and extracellular matrix component accumulation (collagen, elastic fibers, and proteoglycan (PG)) (Ross and Glomset, 1976). Most of the lipid present in these lesions (predominantly cholesteryl esters) is thought to originate from plasma LDL (Goldstein and Brown, 1977). Thus, understanding the pathogenesis of atherosclerosis requires elucidation of the factors which contribute to deposition of LDL in the arterial matrix. The primary route by which LDL is removed from the plasma by the smooth muscle cells of the inner arterial wall is the LDL-receptor pathway discussed above (Brown and Goldstein, 1986). Individuals with genetic disorders resulting in abnormal receptors or apolipoproteins (and thus abnormal LDL-receptor interactions) are predisposed toward accelerated atherosclerosis (Mahley and Innerarity, 1983). Also, in some human populations the mean levels of LDL in the plasma are too high for effective clearance to occur. In either of these cases, LDL is taken up by a phagocytic, receptor-independent process that results in cholesteryl ester accumulation within smooth muscle cells, eventually leading to the development of fatty streaks and fibrous plaques (Goldstein and Brown, 1977). While the exact mechanism of lipid deposition is not yet known, a great deal of work implicates the macromolecules of the extracellular matrix, especially the glycosaminoglycan (GAG) components of PGs, as instumental in this regard. The GAGs are long linear polysaccharide chains composed of repeating disaccharide units, many of which are linked to a central core protein to form a PG (Kennedy, 1979; Roden, 1980). Each disaccharide unit contains a hexosamine residue (either D-glucosamine or D-galactosamine), along with a uronic acid residue (either D-glucuronic

acid, L-iduronic acid, or both) (Roden, 1980). The seven GAGs are chondroitin 4-sulfate (C4S), chondroitin 6-sulfate (C6S), dermatan sulfate (DS), keratan sulfate (KS), heparin (HEP), heparan sulfate (HS), and hyaluronic acid (HA). Only the last is not sulfated. C4S and C6S contain D-glucuronic acid and N-acetyl-D-galactosamine, and are sulfated on the 4- and 6- positions of the latter residue, respectively. HEP is more complex in its structure, being composed of two repeating disaccharides (glucosamine and either L-iduronic acid (70-90%) or D-glucuronic acid (10-30%) which vary in their modifications. HEP has a high content of O-sulfate and N-sulfate groups, and a smaller percentage of N-acetyl groups. HEP is the most highly sulfated GAG, with the highest charge density (Iverius, 1972).

A possible role for the GAG components of PGs in the binding and sequestration of extracellular LDL was originally proposed on the basis of *in vitro* binding studies. LDL is known to form both soluble and insoluble complexes with GAGs and PGs *in vitro* (Bernfeld *et al.*, 1960; Srinivasan *et al.*, 1970; Iverius, 1972; Srinivasan *et al.*, 1975a; Pan *et al.*, 1978; Camejo *et al.*, 1980; Mourao *et al.*,, 1981; Bihari-Varga *et al.*, 1981; 1982; 1983; Camejo *et al.*, 1983; Mourao and Bracamonte, 1984; Yla-Herttuala *et al.*, 1986; Steele *et al.*, 1987; Kokkonen and Kovanen, 1987; Cardin *et al.*, 1986; 1987). If divalent cations are absent or present at low concentrations (2-3 m*M*), LDL and GAG form soluble complexes in which positively charged surface groups are proposed to interact with the negatively charged GAG sulfate and carboxyl groups (Iverius, 1972; Cardin *et al.*, 1987). In the presence of divalent metal ions such as Ca^{2+} at concentrations >5 m*M*, it has been proposed that an additional cross-linking occurs between the GAG and the negatively charged phosphate moiety of the

phospholipid headgroups of LDL, resulting in the formation of insoluble complexes (Srinivasan *et al.*, 1975a). However, recent studies suggest that the interaction of basic amino acid residues of LDL with acidic groups on HEP is the dominant interaction in insoluble complex formation as well (Cardin *et al.*, 1987). Such an interaction *in vivo* has been implicated in the deposition of LDL cholesterol in the arterial wall and in the pathogenesis of atherosclerosis. Evidence for this view has been provided by the isolation of LDL-GAG complexes (Srinivasan *et al.*, 1972; 1975b; 1979; 1980; Kuznetsov, 1982) and LDL-PG complexes (Srinivasan *et al.*, 1975b; Walton and Williamson, 1968) from atherosclerotic lesions, and of a PG with a high affinity for LDL from arterial tissues (Camejo *et al.*, 1980; 1983). As well, studies dealing with experimentally induced atherosclerosis in laboratory animals have correlated increases in arterial PG (Alavi and Moore, 1987) and changes in aortic GAG (Hoff and Wagner, 1986) with arterial injury and tissue LDL accumulation, respectively. Recent evidence also suggests that LDL-PG complex formation may lead to increased uptake of LDL by intimal macrophages during the early stages of atherosclerosis (Vijayagopal *et al.*, 1985; Yla-Herttuala *et al.*, 1986), a process which may be receptor-mediated (Vijayagopal *et al.*, 1988). In addition, it has been observed that insoluble complex formation leads to alterations in the structure of the LDL core such as to raise the transition temperature of the cholesteryl esters (Bihari-Varga *et al.*, 1981; 1982; 1983; Mateu *et al.*, 1984), a factor which may enhance deposition in the arterial matrix. Much work has been directed towards identifying the GAG moieties of PGs which are involved in the extracellular binding of LDL. Of all GAGs, CS, particularly the C6S isomer, seems to be most closely associated with changes in the arterial wall. C6S is increased

in GAGs isolated from fatty streaks relative to those isolated from uninvolved aortic intima (Dalferes *et al.*, 1971), and has been identified in LDL-GAG complexes isolated from human aortic fatty streaks and fibrous plaques (Srinivasan *et al.*, 1975b; Kuznetsov, 1982). In rabbits, a marked increase in both C6S and C4S is observed in PG isolated from areas of injured arterial wall covered by regenerated endothelium (Alavi and Moore, 1987). In hypercholesterolemic swine, an enrichment in CS at the expense of dermatan sulfate occurs in the early stages of atherosclerosis (Hoff and Wagner, 1986). Furthermore, C6S has been identified as the GAG moiety responsible for the lipoprotein-complexing capacity of a lipoprotein-complexing PG isolated from human aorta (Camejo *et al.*, 1983). HEP, which has the highest affinity for LDL (Iverius, 1972) is not usually present in the extracellular matrix, but is found in the form of a HEP-PG in mast cells within their cytoplasmic granules (Fransson, 1985). Recently, it has been demonstrated that LDL can bind to the negatively-charged HEP-PG of rat serosal mast cell granules (Kokkonen and Kovanen, 1987). Stimulation of mast cells, followed by release of their granules into the extracellular space, could result in the formation of LDL-HEP-PG complexes. HEP has been detected in LDL-GAG complexes isolated from human aortic fibrous plaques (Srinivasan *et al.*, 1975b; Kuznetsov, 1982). Thus, both CS and HEP may play a role in the sequestration of LDL within the extracellular space.

The physiological significance of soluble complexes in the plasma has not received as much attention as has the role of complexes in the arterial matrix. At concentrations much higher than those found physiologically, heparin has been found to reduce uptake of LDL by cultured fibroblasts (Goldstein *et al.*, 1976), and the uptake of LDL by aortic tissue *in vivo* can be inhibited by the presence of GAG (Sirtori *et al.*,

1976; Weber *et al.*, 1979). Also, GAGs have been found to act as effective anti-atherosclerotic agents (Caruzzo, 1974; Morrison, 1971; Radhakrishnamurthy *et al.*, 1978), presumably via saturation of LDL binding sites. CS is the predominant GAG found in human plasma, in which it exists in both low-charge and high-charge forms in non-covalent association with plasma proteins (Staprans and Felts, 1985). The presence of HEP has never been demonstrated. Nakashima *et. al.* (1975) have observed that the high-charge plasma GAGs can modify LDL conformation, an effect that can be prevented by the low-charge species. This has led to the suggestion that the rheological properties of lipoproteins may be maintained by interactions with plasma GAGs. These observations suggest the possibility of a role for soluble complex formation in the many factors which regulate the deposition of LDL cholesterol in the arterial wall.

Research Objectives

One of the objectives of the present research is to obtain a better understanding of the behaviour of the lipoprotein monolayer. The results from ^{2}H NMR (Treleaven *et al.*, 1986; Parmar *et al.*, 1985; R. S. Chana, unpublished results), ^{31}P NMR (Yeagle *et al.*, 1977; 1978), and fluorescence (Jonas, 1977) studies suggest that the properties of the lipid regions of VLDL, LDL, and HDL differ significantly. Also, it is known that proteins and phospholipid headgroups are both located at the particle surface, and that the protein probably adopts an amphipathic helical form, but it is unclear to what extent these two components interact. ^{31}P NMR suggests that protein-lipid interactions are operative in LDL only (Yeagle *et al.*, 1977; 1978), whereas fluorescence suggests that protein effects are present in

all the lipoproteins, particularly LDL and HDL. Two parameters of the monolayer phospholipids which may reveal important structural information are the lateral diffusion coefficients D and the residual chemical shift anisotropy $\Delta\sigma$ of the phosphate group. These have previously been determined using ^{31}P NMR for HDL_2 (Parmar, 1985). While the diffusion coefficient was similar to values observed in phospholipid bilayers, $\Delta\sigma$ was significantly larger ($\simeq$70 ppm). Hence, these values have been determined for LDL and HDL_3, in the hope that a comparison of these values with those determined for HDL_2 and VLDL (R. S. Chana, unpublished results) will provide information on the dynamics and orientational properties of lipoprotein phospholipids within the framework of compositional differences. ^{31}P NMR is ideally suited to this task, as the ^{31}P nucleus is a 100% abundant non-perturbing probe. As well, the presence of only two phospholipids in the lipoproteins makes spectral interpretation relatively easy.

Another aspect of lipoprotein structure which is still unclear is the extent of interaction between the monolayer and the core. This is a matter of some importance, especially in cholesteryl-ester rich lipoproteins, as it is conceivable that the composition of the core may affect the properties of the monolayer, which could affect the metabolism of the particle. In order to study this problem, we have chosen to examine reconstituted HDL (rHDL) using ^{2}H NMR. ^{2}H NMR is a powerful technique for studying molecular order and dynamic structure in membrane systems as it monitors a non-perturbing probe. Selective deuteration, combined with the low natural abundance of deuterium, make spectral assignments relatively unambiguous. The strong quadrupolar interaction allows dipolar interactions with neighboring nuclei to be ignored, with the result that linewidths and relaxation times are directly related to reorientations of the C-^{2}H bond.

The extent of averaging of the quadrupolar interaction provides information on the orientational order of anisotropic systems, information not easily obtained from ^{13}C NMR. The use of rHDL particles provides a means of placing deuterium probes at almost any position within the lipoprotein complex, thereby allowing selective information on lipid motions and organization to be monitored. rHDL particles are easily formed by sonication of isolated apo-HDL_3 in the presence of phospholipid and one or more of the core components (CE, TG). The apoprotein is isolated from HDL_3 by chloroform-methanol precipitation (Scanu *et al.*, 1969). The properties of rHDL are very similar to the native lipoproteins (Parmar *et al.*, 1983; Hirz and Scanu, 1970) and thus they are excellent models for the systematic study of lipoprotein structure. Furthermore, as HDLs are the smallest lipoproteins, the proportion of core components in contact with the monolayer is maximized, making it easier to detect any effects that the monolayer may impose on the core.

A second objective to this reseach is the study of LDL-GAG interactions. The observation that both soluble and insoluble complex formation may affect LDL stucture, especially the phase transition temperature of the core esters, suggests that core-monolayer interactions may have important physiological effects. Hence, NMR studies of LDL-GAG complexes were performed to characterize the complexes formed and to assess the prospects for further research in this area, specifically, the study of complex formation on LDL structure using ^{2}H NMR. With respect to the latter point, a technique was developed for the incorporation of phospholipids and cholesteryl esters into LDL from rHDL donor particles using plasma exchange proteins.

CHAPTER II

NMR THEORY

^{2}H NMR

The application of ^{2}H NMR to membranes is discussed by Seelig (1977), Smith *et al.* (1977), Stockton *et al.* (1976), and Davis (1983). The material in this chapter follows the approach of Seelig (1977), Smith *et al.* (1977), and Stockton *et al.* (1976).

The energy of a ^{2}H nucleus in a magnetic field H_o, applied in the z-direction, is the sum of the magnetic energy E_M and the quadrupolar energy E_Q. The magnetic (Zeeman) energy results from the interaction of the nuclear magnetic moment $\mu = g\mu_N m$ with the magnetic field H_o, and is given by

$$E_M = -g\mu_N H_o m \qquad (1)$$

where g is the nuclear g-factor, μ_N the nuclear magneton, and m the quantum number defining the 2I + 1 non-degenerate energy levels in the magnetic field. For ^{2}H, with spin I = 1, m = -1, 0, +1. Nuclei with spin $I \geq 1$ depart from spherical charge symmetry at the nucleus and thus may possess an electric quadrupole moment Q. The quadrupole moment may interact with the electric field gradient (EFG) at the site of the nucleus. The EFG is properly represented as a symmetric, traceless tensor with principal components V_{XX}, V_{YY}, and V_{ZZ}. For sp^3-hybridized carbons, the electric field is approximately axially symmetric, with the largest component V_{ZZ} = eq (where e is the charge on the electron and q is the second derivative of the electric potential at the nucleus) coincident with the C-^{2}H bond.

The departure of the C-^{2}H bond from axial symmetry is measured by an asymmetry parameter $\eta = (V_{XX} - V_{YY})/V_{ZZ}$, which varies between 0 and 1 (by definition, $V_{ZZ} \geq V_{XX} \geq V_{YY}$). The quadrupolar interaction ($\simeq$200 kHz) is dominated by the Zeeman interaction at high fields (38.8 MHz in the present study), allowing the former to be treated as a perturbation which shifts the Zeeman levels as shown in Figure 2. If we consider a homogeneously oriented sample, for example, a crystal in which all the C-^{2}H bonds (and therefore V_{ZZ}) are aligned parallel to H_o, then the energy levels are given by

$$E_M = -g\mu_N H_o m + [(e^2qQ)(3m^2 - 2)/4] \qquad (2)$$

The three energy levels for this orientation are

$$\begin{aligned} E_{+1} &= -g\mu_N H_o + (1/4)(e^2qQ) \\ E_o &= -(1/2)(e^2qQ) \\ E_{-1} &= g\mu_N H_o + (1/4)(e^2qQ) \end{aligned} \qquad (3)$$

The selection rule $\Delta m = \pm 1$ allows two transitions with corresponding transition energies

$$\begin{aligned} h\nu_+ &= E_{-1} - E_o = g\mu_N H_o + (3/4)(e^2qQ) \\ h\nu_- &= E_o - E_{+1} = g\mu_N H_o - (3/4)(e^2qQ) \end{aligned} \qquad (4)$$

giving rise to two resonances separated by the quadrupolar splitting $\Delta\nu_Q$

$$\Delta\nu_Q = \nu_+ - \nu_- = (3/2)(e^2qQ/h) \qquad (5)$$

where (e^2qQ/h) is the static quadrupolar coupling constant, which is $\simeq$170 kHz for sp^3-hybridized C-^{2}H bonds. Eq 5 represents the largest possible

Figure 2: The nuclear Zeeman energy levels of a quadrupolar nucleus (I = 1) for a zero (*left*) or finite (*right*) electric field gradient at the nucleus.

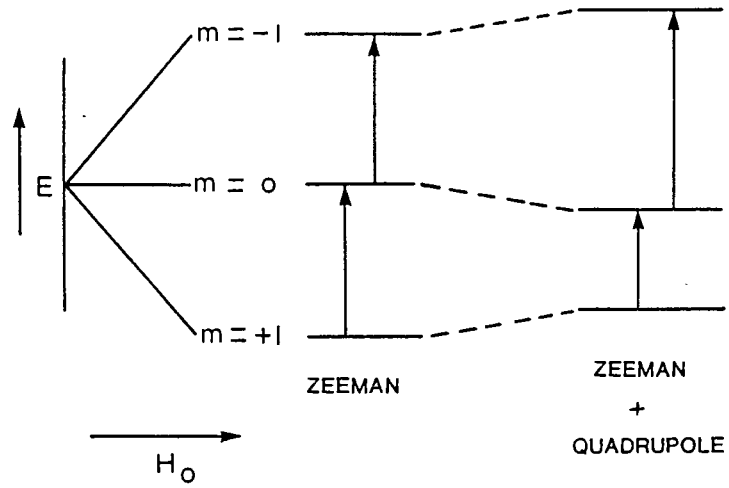

Figure 3: Rotation of a single crystal in a magnetic field, beginning from V_{ZZ} parallel to H_o. The Euler angles ϕ and θ define the relative orientation of the molecule-fixed principal axis coordinate system with the laboratory coordinate system (x, y, z; H_o parallel to z).

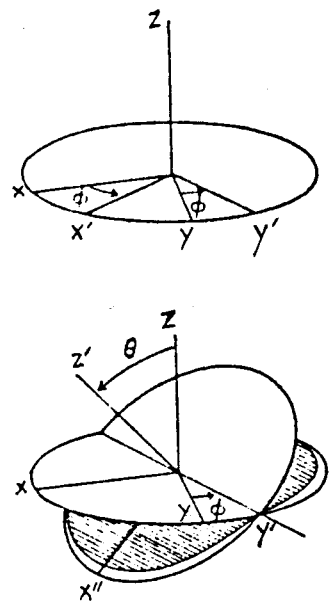

quadrupolar splitting, with V_{ZZ} parallel to the magnetic field. This will be reduced for any other orientation of the crystal in the magnetic field. Any arbitrary orientation can be achieved by two successive rotations, beginning from H_0 parallel to V_{ZZ}. The crystal is first rotated about the z-axis by an angle ϕ, followed by a rotation about the new y-axis by an angle θ as shown in Figure 3. The angular variation of the quadrupolar splitting is given by (Abragam, 1961a)

$$\Delta\nu_Q = (3/2)(e^2qQ/h)[((3\cos^2\theta - 1)/2) + (\eta\sin^2\theta\cos2\phi/2)] \quad (6)$$

For C-^{2}H bonds, $\eta = 0$ (Seelig, 1977), giving

$$\Delta\nu_Q = (3/2)(e^2qQ/h)[(3\cos^2\theta - 1)/2] \quad (7)$$

where θ is the angle between the C-^{2}H bond and H_0.

For the case of a polycrystalline powder sample, the EFG's will adopt a random distribution with respect to H_0. The probability distribution of the EFG's is given by $p(\theta) = (1/2)\sin\theta$ for the case of axial symmetry. The resulting spectrum will be a superposition of splittings for all θ, with intensities scaled by $p(\theta)$. Thus, the least intense resonances occur for $\theta = 0°$, and the most intense for $\theta = 90°$. A typical powder spectrum is shown in Figure 4. The quadrupolar splitting is defined as the separation of the two most intense peaks ($\theta = 90°$), and thus for a powder sample

$$\Delta\nu_Q(\text{powder}) = (3/4)(e^2qQ/h) = 126 \text{ kHz} \quad (8)$$

Thus far we have considered ^{2}H NMR in the absence of motion. In biological and model membranes, which are examples of lamellar liquid crystals, the constituent molecules are free to undergo rapid, anisotropic motions. These include rotation about the long molecular axis which results

Figure 4: A theoretical ^2H powder pattern.

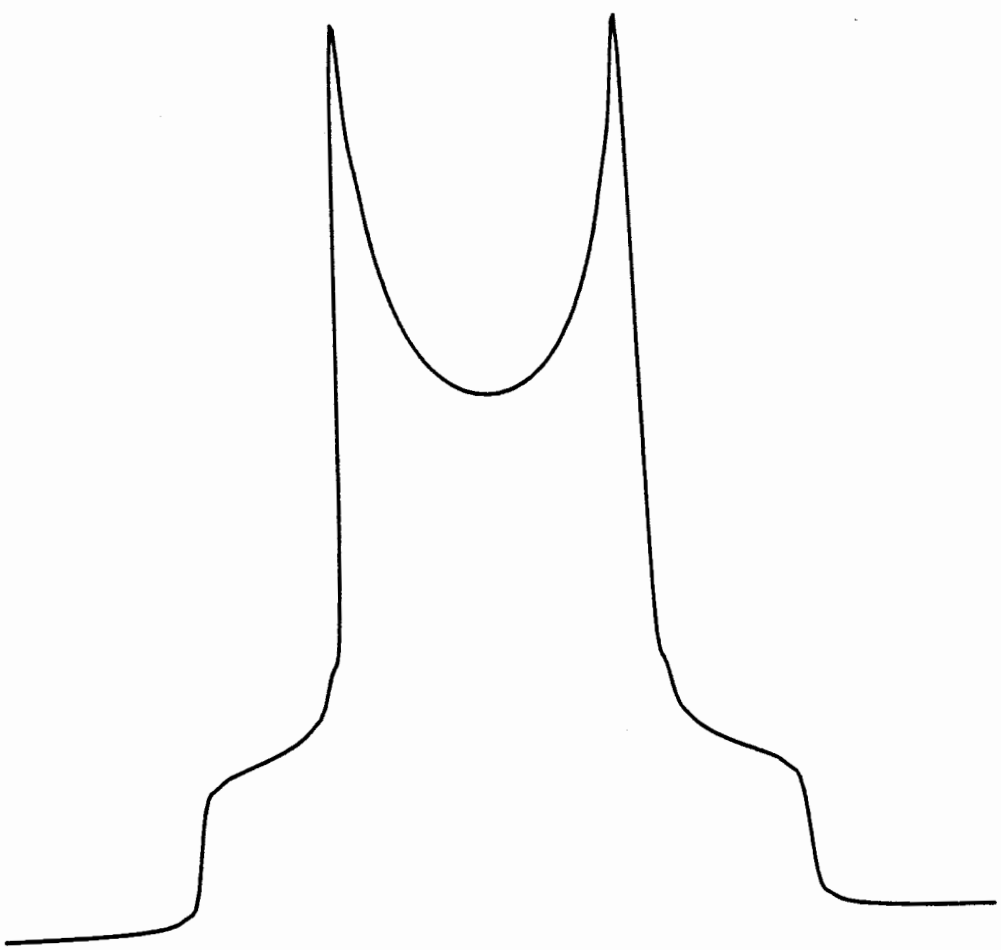

from the parallel packing of the phospholipid molecules, and restricted angular oscillations perpendicular to the long molecular axis. These motions occur about a director axis, z', which is the normal to the membrane surface. The effect of these anisotropic motions is to partially average the quadrupolar interaction, giving rise to a reduced quadrupolar splitting $\Delta\nu_r$. For the case of axial symmetry

$$\Delta\nu_Q = (3/4)(e^2qQ/h)S_{CD} \tag{9}$$

where the C-^{2}H bond order parameter S_{CD} is given by

$$S_{CD} = (1/2)(3\langle\cos^2\beta\rangle - 1) \tag{10}$$

where $\langle\cos^2\beta\rangle$ denotes the time average of the angular fluctuations of the C-^{2}H bond with respect to the director. The fast, anisotropic motions in bilayers are seen to reduce the static quadrupolar splitting by a factor S_{CD}. $|S_{CD}|$ varies between 0 and 1.

Model systems such as multilamellar dispersions are very large (diameter $\simeq$1000 nm) and tumble slowly on the ^{2}H NMR time scale; hence, the quadrupolar splitting is observed directly. By contrast, systems such as plasma lipoproteins and unilamellar vesicles are very small, with diameters ranging from 8 to 50 nm. The rapid isotropic tumbling experienced by these particles averages the quadrupolar interaction, giving rise to Lorentzian lineshapes with linewidths ranging from less than a hundred Hz to a few kilohertz. This reduction in $\Delta\nu_Q$ is most conveniently seen from consideration of the second moment M_2 of the powder pattern, which has the general form

$$M_2 = \int_{-\infty}^{\infty} \omega^2 f(\omega)d\omega \; / \; \int_{-\infty}^{\infty} f(\omega)d\omega \tag{11}$$

where $f(\omega)$ is the intensity of the powder pattern at frequency ω from the center of the Pake doublet. The linewidth at half height $\Delta\nu_{1/2}$ for the Lorentzian line is related to M_2 by (Abragam, 1961b)

$$\pi\Delta\nu_{1/2} = M_2\tau_e + C \tag{12}$$

where C is a constant containing contributions from τ_e-independent processes, such as magnetic field inhomogeneity and spin-lattice relaxation. The effective correlation time τ_e for isotropic motions is given by (Stockton *et al.*, 1976)

$$1/\tau_e = 1/\tau_t + 1/\tau_d \tag{13}$$

where τ_t is the correlation time for particle tumbling and τ_d is the correlation time for phospholipid lateral diffusion in the HDL monolayer. These are given by

$$\tau_t = 4\pi\eta R^3/3kT \tag{14}$$

$$\tau_d = R^2/6D \tag{15}$$

where η is the solvent viscosity, R is the particle radius, k is the Boltzmann constant, and D is the lateral diffusion coefficient for phospholipids in the HDL monolayer. M_2 is also related to the quadrupolar splitting $\Delta\nu_Q$ by (Davis, 1983)

$$M_2 = (4/5)\pi^2\Delta\nu_Q^2. \tag{16}$$

For C^2H_2 groups, the static quadrupolar splitting $\Delta\nu_Q$ in eq 16 is $\simeq$126 kHz (Burnett and Muller, 1971). Fast, anisotropic acyl chain reorientations reduce the second moment from its rigid lattice value to a residual second

moment M_{2_r}. Under the assumption that the rate of local molecular reorientations is much faster than the isotropic motions described by τ_e the linewidth may be expressed by

$$\pi\Delta\nu_{1/2} = M_{2_r}\tau_e + 1/T_1 \tag{17}$$

where $1/T_1$ is the spin-lattice relaxation rate. This equation assumes that the linewidth arises from only two types of motion, these being the isotropic motions giving rise to τ_e and the fast, local, anisotropic reorientations represented by T_1. Thus, the possibility that slow anisotropic motions are also present is not considered. Assuming that the molecular motions within the lipoprotein monolayer are axially symmetric about the normal to the particle surface, i.e., the radial direction (as found for phospholipids in unilamellar vesicles), we can write

$$M_{2_r} = (4/5)\pi^2\Delta\nu_r^2 \tag{18}$$

where $\Delta\nu_r$ is given by eq 9. Substitution of eq 9 and 18 into eq 17 yields (Stockton *et al.*, 1976)

$$\Delta\nu_{1/2} = (9\pi/20)(e^2qQ/h)^2S_{CD}^2\tau_e + (1/\pi T_1). \tag{19}$$

^{31}P NMR

Excellent reviews of the application of ^{31}P NMR to membranes are given by Seelig (1978), Cullis and De Kruijff (1979), and Griffin (1981).

^{31}P is a spin 1/2 nucleus with a relative sensitivity of 0.06 compared to ^{1}H (Buldt and Wohlgemuth, 1981). It is the only naturally occuring isotope of phosphorus, and is found in membranes only in the headgroup of

phospholipids and sphingolipids. ^{31}P is thus an ideal non-perturbing probe for studying the motion and average orientation of the phosphate group in membrane phospholipids.

The broad ^{31}P NMR spectra of membranes arise from ^{1}H-^{31}P dipolar interactions and from the chemical shift anisotropy (CSA) of the phosphorus nuclei (Seelig, 1978). The dipolar interactions can be removed by proton-decoupling. The CSA arises from the anisotropic shielding of the nucleus by the bonding electrons, and is the parameter which provides the most information on headgroup structure.

The chemical shift tensor of the phosphate group is not axially symmetric, but has three distinct principal components. The static chemical shielding tensor σ_p is given by

$$\sigma_p = \begin{bmatrix} \sigma_{11} & 0 & 0 \\ 0 & \sigma_{22} & 0 \\ 0 & 0 & \sigma_{33} \end{bmatrix} \qquad (20)$$

where the subscript p refers to the molecule-based principal coordinate system. Because phospholipid crystals large enough to examine by NMR have proven impossible to obtain, the principal components σ_{ii} are obtained from the spectra of phospholipid powders, where the phosphate group is completely immobilized. The ^{31}P NMR spectra of anhydrous DPPC is shown in Figure 5*a*. The discontinuities in the lineshape represent the principal components, which are σ_{11} = -98, σ_{22} = -34, and σ_{33} = 134 ppm. These values are reduced in the monohydrate, and remain unchanged with the addition of further water (Griffin, 1976).

Figure 5*a*: ^{1}H-decoupled ^{31}P NMR spectrum (121.5 MHz) of anhydrous DPPC acquired with Hahn echo (from Rance and Byrd (1983)).

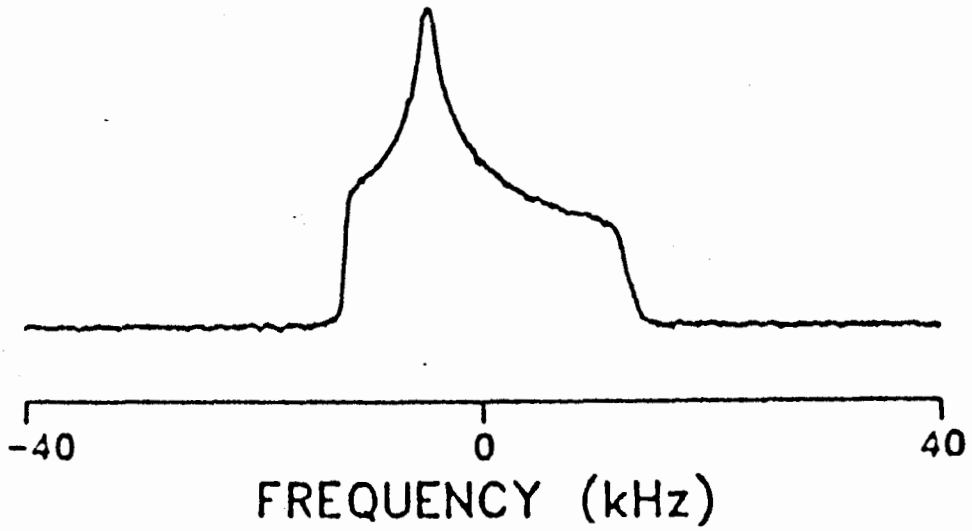

Figure 5*b*: Orientation of the ^{31}P chemical shift tensor (principle components σ_{ii} in the molecular frame of the phosphate segment. O3 and O4 are the non-esterified oxygens. O1 and O2 connect the phosphate group with the glycerol backbone and the headgroup, respectively. The orientation is based on a single crystal study of barium diethylphosphate (Herzfeld *et al.*, 1978). Figure from Buldt and Wohlgemuth (1981).

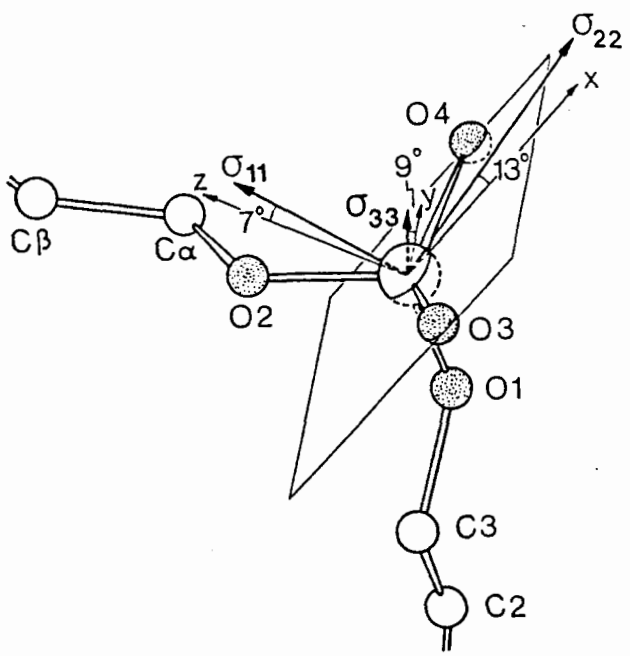

Unfortunately, the orientation of the shielding tensor on the phosphate group cannot be obtained from powder samples, but can only be obtained from single crystals. A single crystal of a suitable reference compound yields a spectrum which, when ^1H-decoupled, consists of a few sharp lines whose positions vary as the crystal is rotated in the magnetic field. A complete rotation pattern of a single crystal allows determination of the orientation of the principal axes and the magnitude of the principal components. Such studies have been performed on phosphoethanolamine (Kohler and Klein, 1976) and barium diethylphosphate (Herzfeld *et al.*, 1978), and have provided the basis for the interpretation of phospholipid spectra, as to date it has proven impossible to obtain sufficiently large crystals of any of the common phospholipids. The orientation of the chemical shift tensor of barium diethylphosphate is shown in Figure 5*b*. The values of the principal components of barium diethylphosphate (σ_{11} = -76, σ_{22} = -18, σ_{33} = 110 ppm) are very close to those obtained for phospholipid monohydrate powders (approximately σ_{11} = -80, σ_{22} = -20, σ_{33} = 110 ppm (Seelig, 1978)), and hence the tensor orientation has been assumed to be similar. This is probably valid as the shielding tensor of the phospholipid analogue 1-hexadecyl-2-deoxyglycerophosphoric acid has recently been determined (Hauser *et al.*, 1988), and its orientation differs only by 7-13° from that of barium diethylphosphate.

In membranes, the phospholipids undergo rapid rotation around the director axis (perpendicular to membrane surface), also referred to as the z axis. This averages the components of the shielding tensor in the plane of the membrane, giving rise to an effective tensor σ_{eff} which is axially symmetric about the director axis

$$\sigma_{eff} = \begin{bmatrix} \sigma_\perp & 0 & 0 \\ 0 & \sigma_\perp & 0 \\ 0 & 0 & \sigma_\parallel \end{bmatrix} \quad (21)$$

where $\sigma_{//}$ and $\sigma_\perp$ are the time-averaged components parallel and perpendicular, respectively, to the director axis. The residual chemical shift anisotropy $\Delta\sigma$ is defined as

$$\Delta\sigma = \sigma_{//} - \sigma_\perp \quad (22)$$

Planar oriented bilayers yield a single resonance whose position varies according to the angle δ between the applied magnetic field H_0 and the director axis. In such a system, $\sigma_{//}$ and $\sigma_\perp$, which represent the two extreme chemical shifts, are observed when $\delta = 0$ and 90°, respectively. For a randomly oriented membrane sample, a powder pattern is observed which is the superposition of spectra for all angles δ. A bilayer type powder pattern is shown in Figure 6. $\Delta\sigma$ is easily obtained from powder-type spectra; $\sigma_{//}$ corresponds to the chemical shift of the low-intensity shoulder, and $\sigma_\perp$ to that of the high-intensity shoulder (Seelig, 1978). For bilayers in the liquid crystalline state, $\Delta\sigma$ varies between 40-50 ppm (Seelig, 1978).

The quantitative relationship between the static components σ_{ii} and the time-averaged components $\sigma_{//}$ and $\sigma_\perp$ is given by (Mehring *et al.*, 1971; Seelig, 1978)

$$\sigma_{//} = \sigma_{11}\sin^2\theta\cos^2\phi + \sigma_{22}\sin^2\theta\sin^2\phi + \sigma_{33}\cos^2\theta \quad (23)$$

$$\sigma_\perp = (1/2)[(\sigma_{11} + \sigma_{22} + \sigma_{33}) - \sigma_{//}] \quad (24)$$

where ϕ and θ are the Euler angles relating the orientation of the rotation axis (director) with respect to the principal axis frame of the

Figure 6: Theoretical ^{31}P NMR lineshapes for lamellar phospholipids undergoing slow (a) and fast (b) isotropic motion. Spectrum (a) is an axially symmetric powder pattern which was simulated using $\Delta\sigma$ = 50 ppm and a correlation time τ for isotropic rotation of 0.01 s; 200 ppm is plotted. Spectrum (b), simulated using $\Delta\sigma$ = 50 ppm and τ = 1.57 x 10^{-6} s, is the theoretical spectrum for an LDL particle tumbling rapidly in solution.

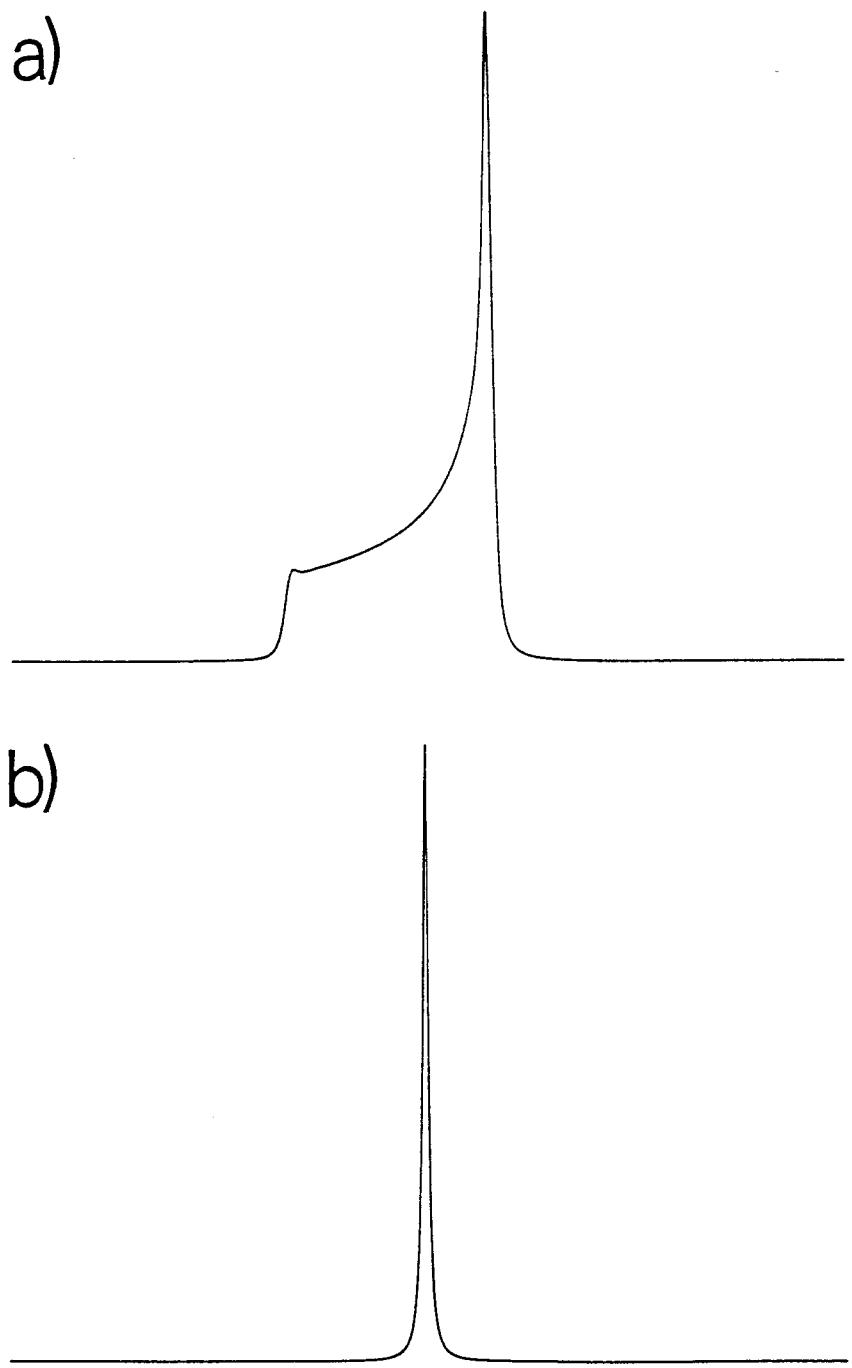

shielding tensor, as defined in Figure 2*b*. Substitution of eq 23 and 24 into eq 22, and introduction of the order parameters S_{ii} (representing the motion of the *i*th principal coordinate axis of the chemical shielding tensor about the director) leads to

$$\Delta\sigma = S_{11}(\sigma_{11} - \sigma_{22}) + S_{33}(\sigma_{33} - \sigma_{22}) \qquad (25)$$

where S_{11} is the order parameter of the axis connecting the esterified oxygens, and S_{33} that of the axis connecting the non-esterified oxygens. Only two order parameters are independent, the third is fixed by the relationship $\Sigma_i S_{ii} = 0$ (Seelig, 1978). The order parameters depend on both the orientation of the ^{31}P shielding tensor with respect to the rotation axis, and also on the extent of angular fluctuations about that axis (Seelig and Gally, 1976). Unfortunately, a measured $\Delta\sigma$ cannot be used to ascertain details of head-group motion, as two unknowns would need to be determined from a single measurement. In general, a head-group orientation and a model of motional averaging are assumed, and the calculated $\Delta\sigma$ is compared with experimental results. This approach, when combined with information from other sources (e.g., ^{2}H NMR), can provide detailed information on headgroup motions.

Some lipids such as phosphatidylethanolamine can form hexagonal mesophases in which the lipids are packed in elongated cylinders (Cullis and de Kruijjf, 1979). The rapid diffusion of phospholipids about the cylinder axis provides an additional mechanism of motional narrowing. For a random distribution of cylinders, a powder pattern is obtained, which, compared to a bilayer, is reduced by a factor of two and has the opposite sign (Cullis and de Kruijjf, 1979; Seelig, 1978). It should be noted that certain headgroup orientations in the lamellar phase are predicted to give

rise to hexagonal-like spectra (Thayer and Kohler, 1981), although this has not been observed experimentally.

In small unilamellar vesicles and serum lipoproteins, $\Delta\sigma$ cannot be observed directly. Rapid, isotropic tumbling of the lipoprotein particle averages the chemical shift anisotropy, with the result that a single Lorentzian line with linewidth $\Delta\nu_{1/2}$ as defined in eq 12 is observed for each species of phospholipid. For ^{31}P, the second moment is given by (McLaughlin *et al.*, 1975)

$$M_2 = (4/45)(2\pi\nu_0)^2\Delta\sigma^2 \qquad (26)$$

CHAPTER III

EXPERIMENTAL PROCEDURES

Materials.

[18,18,18-$^2H_3$]oleic acid and [5,5-$^2H_2$]palmitic acid were generous gifts from the late Dr. A.P. Tulloch, Plant Biochemistry Institute, National Research Council of Canada, Saskatoon, Saskatchewan. [$^2H_3$]CO, [$^2H_2$]PC and [$^2H_{31}$]PC, [$^2H_9$]DPPC, and [$^2H_6$]TO were generous gifts from Dr. W. D. Treleaven, R. Chana, Dr. R. J. Cushley, and Dr. H. Gorrissen, respectively, the latter presently at BASF AG, Abt. Kunststofflabor, D-6700, Ludwigshafen, F.R.G. DPPC, CO, TO, Heparin (Porcine Intestinal Mucosa, Grade 1, sodium salt), chondroitin sulfate Type A (C4S) (whale cartilage, sodium salt), chondroitin sulfate Type C (C6S) (shark cartilage, sodium salt), perdeuterated acetic anhydride ([$^2H_6$]acetic anhydride), and deuterium depleted water were purchased from Sigma Chemical Co. Cholesterol was obtained from Fisher Scientific Co., and was recrystallized three times from benzene.

Isolation of LDL and HDL_3

LDL was isolated from fresh (<3 days old) plasma by ultracentrifugal flotation in the density range 1.025-1.063 g/mL (Havel *et al.*, 1955). HDL_3 was isolated in the density range 1.125-1.21 g/mL. In general, several units of each lipoprotein were pooled and purified by reisolation in the same density range. The lipoproteins were stored at 4°C under N_2. The purity of the lipoproteins isolated in this manner has been demonstrated

previously by immunoelectrophoresis (Treleaven, 1985; Parmar, 1985). Sodium dodecyl sulfate gel electrophoresis of freshly isolated LDL reveals no degradation of the apo B-100.

Isolation of apoHDL$_3$

ApoHDL$_3$ was isolated using the technique of Scanu *et al.* (1969). Approximately 46 mLs of cold (-20°C) chloroform:methanol (2:1) was poured into a large test tube containing 0.5 mLs of HDL$_3$ at a protein concentration of ≃35 mg/mL (in ≃2 *M* KBr). The tubes were stored at -20°C for one hour, following which they were centrifuged on an IEC clinical centrifuge for 10-15 minutes. The solvent was removed, and the protein/KBr pellet was washed 4-5 times in cold diethyl ether, allowing the tubes to stand for 15-20 minutes each washing at -20°C. The ether was decanted, and the tubes were placed under high vacuum overnight. The protein content of the final product, determined by the method of Lowry *et al.* (1951), was ≃7 weight-%.

Preparation of rHDL

Reconstituted HDL particles were prepared by the established procedure of Hirz and Scanu (1970). For the [$^2H_3$]CO/DPPC(egg PC) and [$^2H_2$]PC/CO(TO) rHDLs, 18 mg of core component ([$^2H_3$]CO, CO, or TO) was co-dissolved in chloroform with 27 mg of egg PC, DPPC, or [$^2H_2$]PC. The chloroform was removed under a stream of N_2, and the lipids were placed under high vacuum overnight. A lipid-water emulsion was formed by mixing the lipids with approximately 6 mL of deuterium-depleted water at 50°C. ApoHDL$_3$/KBr (55 mg

protein) was added to the mixture as a solid and gently stirred until dissolved. When a homogeneous dispersion was obtained, the mixture was sonicated, under nitrogen, until translucent using a Heat Systems W-375 Sonicator operating at 35-40% output power. The sonication time varied from 6-30 minutes, using 1.5 minute pulses followed by 2 minute cooling periods. The temperature in the vessel was maintained at 48-52°C (near the isotropic melt of CO). The temperature was monitored by inserting a thermocouple directly into the sonication mixture. Titanium particles were removed by centrifugation on a clinical centrifuge followed by filtration (Gelman Acrodisc polysulfone filters; 0.2μm). The preparation of [$^2H_{31}$]PC/TO rHDL was identical except that the amount of starting materials was increased slightly (60 mg protein, 30 mg [$^2H_{31}$]PC, 20 mg TO).

[$^2H_6$]TO/DPPC(egg PC) rHDLs of mean diameter $\simeq$13 nm were prepared as described above except that the amount of starting material was reduced (25 mg protein, 12.3 mg DPPC or egg PC, 8.2 mg [$^2H_6$]TO), and the lipid-protein emulsions were sonicated for 4-6 minutes at 37°C on a Biosonics sonicator, using 2 minute pulses followed by 1 minute cooling periods. These particles were reduced in size to $\simeq$11 nm diameter by sonication for 10 minutes at 37-47°C ([$^2H_6$]TO/egg PC/apoHDL$_3$) or 46-50°C ([$^2H_6$]TO/DPPC/apoHDL$_3$) on a Heat Systems W-375 Sonicator operating at $\simeq$35% output power. One or two minute pulses were used, followed by two minute cooling periods.

rHDL was isolated in the density range 1.125-1.210 g mL^{-1}. Density adjustments were performed using solid KBr or a saturated KBr solution prepared in deuterium-depleted water. The samples were run as isolated, in $\simeq$2 *M* KBr. In order to determine the solvent viscosities, a solution of KBr (1.21 g/mL) was centrifuged under identical conditions as the rHDL samples,

and an aliquot equal in volume to the rHDL samples was removed. Solvent viscosities η as a function of temperature were determined over the temperature range 2-48°C using an Ostwald viscometer. Viscosity values below 0°C were obtained by extrapolation of a plot of log η vs. 1/T.

The preparation of the rHDLs used to incorporate DPPC and CO into LDL was the same as above except that the rHDL was isolated by centrifugation at density 1.063 g/mL. The material floating at the top of the tube was discarded, and the rHDL pellet was resuspended for use in the exchange experiments. The composition of each sonication mixture used in the 3 studies is given in Table II.

Gel Electrophoresis

SDS-polyacrylamide gel electrophoresis of LDL, HDL_3, and $apoHDL_3$ following isolation and sonication was performed using the methodology of Laemmli (1970). The concentration of polyacrylamide in the stacking and separating gels was 4 and 10%, respectively. The gels were stained with Coomassie brilliant blue R 250.

Electron Microscopy

The size distribution of the rHDL particles was determined by negative-staining electron microscopy with a Philips 300 electron microscope operating at 80 kV, using 2% ammonium molybdate pH 8.6 on 200 mesh Formvar carbon-coated grids. The rHDL was dialyzed against phosphate buffered saline pH 7.4 at 4°C prior to the negative staining procedure. Typically 0.5 mg protein/mL of the rHDL particles were deposited on the

Table II: Composition of rHDL Sonication Mixtures (mg) for DPPC/CO Incorporation Studies.

Study	Pr	[^{14}C]DPPC	DPPC	[^{14}C]CO	CO	Ch	SA[a]
1	12.2	6.0	-	-	3.2	0.8	38,000
2	50.0	21.3	-	-	20.4	-	16,510
3	20.1	-	9.7	5.3	-	1.4	93,880

[a] SA = specific activity (dpm/mg) of the labelled lipid

grid and allowed to stand for ≃2 minutes. The excess fluid was desorbed using Whatman filter paper. The stain solution was immediately applied and also removed after 2 minutes. The particle diameters were measured directly from the negative or by projecting the negative image onto a screen. The author is indebted to Dr. Yashpal Parmar and Ravinder Chana for obtaining the electron micrographs of the rHDL particles.

Lateral Diffusion Studies

Prior to NMR experiments, LDL and HDL_3 were dialysed into 0.15 *M* NaCl 0.02% Na_2EDTA pH 7.5 (hereafter referred to as saline). LDL was concentrated either by treatment with Aquacide or by using Millipore Immersible-CX Ultrafilters (CX-30). The viscosities of saline-glycerol mixtures were determined at 25 and 45 °C using an Ostwald viscometer.

Deuteroacetylation of GAGs

Chondroitin 4-sulfate and heparin were partially N-deacetylated essentially as described by Hook *et al.* (1982). [^{2}H]HEP was prepared as follows. A homebuilt bomb containing 110 mg of HEP, 5.5 mL of hydrazine, and 55 mg of hydrazine sulfate was heated at 100°C for 1.5 hours, after which it was cooled in an ice bath for 2 hours. The flask containing the HEP was removed and placed in a water bath at ≃40°C. Five mL of toluene was added, and the mixture was evaporated to dryness with stirring under a stream of N_2. The toluene additions were repeated twice more. Approximately 2 mL of absolute ethanol was then added to the deacetylated HEP, which was evaporated as above. The HEP was then dissolved in 5.5 mL of 0.2 *M* NH_4HCO_3 containing 0.02% NaN_3 and reisolated on a column (2.5 x 92 cm) of Sephadex G-50 eluted with the same buffer. Fractions containing HEP (assayed using Alcian Blue 8-GX (Gold, 1979)) were pooled and lyophilized. The HEP was dissolved in 20 mL of water and was lyophilized again.

N-deacetylated HEP (≃100 mg) was N-deuteroacetylated essentially as described (Hook *et al.*, 1982), with the exception that the addition of [$^2H_6$]acetic anhydride (1.1 mL) was performed at room temperature. The HEP was dissolved in 4 mL of 10% methanol containing 0.05 *M* Na_2CO_3, and the [$^2H_6$]acetic anhydride was added in eleven 0.1 mL aliquots over a period of 3.5 hours. The pH was maintained between 7-8 by the addition of 10% methanol saturated with Na_2CO_3. The reaction was stopped by the addition of 20 mL of water, and the [^{2}H]HEP was applied to a column (2.5 x 92 cm) of Sephadex G-50 and isolated as described above.

[^{2}H]C4S was prepared as follows. A homebuilt bomb containing 140 mg of C4S, 7 mL of hydrazine, and 70 mg of hydrazine sulfate was heated at 100°C

for 2.5 hours, after which it was cooled in an ice bath for 2 hours. The hydrazine was removed on a rotovap at ≃40°C after the addition of 7 mL toluene. The C4S was dissolved in 10 mL of 50% ethanol, and again evaporated to dryness with a rotovap. The C4S was then dissolved in 14 mL of water, and was precipitated by the addition of 5 volumes of 95% ethanol: saturated sodium acetate (4:1). The precipitate was collected by centrifugation (IEC clinical desktop), dissolved in 10 mL of 0.2 *M* NH_4HCO_3 containing 0.02% NaN_3 and reisolated on a column (2.5 x 92 cm) of Sephadex G-50 eluted with the same buffer. Fractions containing C4S (assayed using Alcian Blue 8-GX (Gold, 1979)) were pooled and lyophilized. The polysaccharides were checked for degradation on a column (2.5 x 81.5 cm) of Sephadex G-200 eluted with 1 *M* NaCl in 0.05 *M* Tris-HCl pH 8.0 containing 0.02% NaN_3. Percent deacetylation was estimated using the ninhydrin reaction (Spies, 1957) after residual NH_4^+ had been removed by desalting on a column (2.5 x 9 cm) of Sephadex G-25 eluted with 10% ethanol.

N-deacetylated HEP (60 mg) was N-deuteroacetylated as above using 0.6 mL of [$^2H_6$]acetic anhydride. Following deuteroacetylation, the [^{2}H]C4S was precipitated as above and reisolated on a column (2.5 x 10 cm) of Sephadex G-25 eluted with 1 *M* NaCl. After recovery by precipitation, the [^{2}H]C4S was dissolved in 10% ethanol and desalted on a column (2.5 x 9 cm) of Sephadex G-25 eluted with the same solvent. The [^{2}H]C4S was then lyophilized.

LDL-GAG Binding Studies

For the ^{2}H NMR experiments, LDL was first exhaustively dialysed against 0.05 *M* Tris-HCl pH 7.5 containing 0.3 m*M* Na_2EDTA, following which it was concentrated to ≃23 mg protein/mL for NMR experiments using Millipore

Immersible-CX Ultrafilters (CX-30). This and all subsequent dialyses and solvent exchanges were performed at 4°C. The sample volume was 1.5 mL. The residual ^{2}HOH signal was reduced by several exchanges (usually 6) with 0.05 *M* Tris-HCl pH 7.5 in deuterium-depleted water (resulting in a dilution of the original solvent of 800-fold). The [^{2}H]HEP and [^{2}H]C4S were lyophilized at least once in deuterium-depleted water prior to addition as solids to LDL.

For the ^{31}P NMR experiments in which the effect of increasing GAG was studied, LDL was concentrated to 14-20 mg protein/mL as above. The sample volume was 1.5 mL. Several exchanges (usually 5) were performed with the desired buffer, either 0.05 *M* Tris-HCl 0.02% Na_2EDTA pH 7.5 prepared in 50% ^2H_2O or 0.05 *M* HEPES 0.02% Na_2EDTA pH 7.5 prepared in 50% ^2H_2O. The GAGs were added as solids to the LDL and gently mixed just before NMR experiments. For the LDL-HEP concentration studies, the LDL was exhaustively dialysed against 0.05 *M* Tris-HCl 0.02% Na_2EDTA pH 7.5 prepared in 50% ^2H_2O, and the HEP was added as a solution (2 mg/mL) in the same buffer.

For the QELS experiments, LDL (4.9 mg protein/mL) was dialysed exhaustively against 0.05 *M* Tris-HCl 0.02% Na_2EDTA pH 7.5 or 0.05 *M* HEPES 0.02% Na_2EDTA pH 7.5. Stock solutions of HEP and CS were prepared in the appropriate buffer. Aliquots of GAG were added to the LDL, and the solution was then diluted to 0.2-0.8 mg protein/mL. The complexes were filtered directly into the sample cell (Gelman Acrodisc polysulfone filters; 0.2μm). In studies dealing with the effect of physiological concentrations of calcium, the buffer was 0.05 *M* Tris-HCl 2 m*M* $CaCl_2$ pH 7.5, and the protein concentration of the complex was 1 mg/mL.

Preparation of LDL-HEP Insoluble Complexes

LDL (5 mg protein/mL) was dialyzed against 0.15 *M* NaCl in 0.05 *M* HEPES pH 7.5. HEP (20 mg) and $CaCl_2$ (112 mg), both in the same buffer, were added to 4 mL LDL (20 mg protein) to give a final volume of 6 mL. The clear solution (no insoluble complexes formed due to presence of NaCl) was dialysed overnight against 0.05 *M* Tris-HCl pH 7.6 at 4°C. LDL-HEP insoluble complexes, formed in the dialysis tubing, were centrifuged at 5,000 rpm for 1 hour at 4°C in a Ti75 rotor. The solvent was decanted off the insoluble complexes, which were then transfered to an NMR tube for ^{31}P NMR.

Nuclear Magnetic Resonance

The ^{2}H NMR experiments were performed at 38.8 MHz with a home-built spectrometer and a 5.9 Tesla Nalorac superconducting magnet interfaced to a Nicolet BNC-12 computer or a Vax Workstation 1. Temperatures were controlled by a solid-state temperature controller with an accuracy of ±0.25°C built by the Simon Fraser University electronics shop. High-resolution spectra were obtained using a one-pulse sequence with phase alternation in order to minimize baseline distortion. The $[^{2}H_3]CO$ rHDL and $[^{2}H]$GAG spectra were obtained using a spinning probe while all other spectra were obtained on a broadband probe with a horizontally mounted coil. The samples were allowed to equilibrate for 30 min at a given temperature before acquiring data. The spectral parameters are given in the figure legends.

^{2}H spin-lattice relaxation times, T_1, were measured at 38.8 MHz by the inversion-recovery method

$(180°-\tau-90°-T)_n$, where signal intensities A were used to obtain T_1 from the expression $A_\tau = A_\infty(1 - 2e^{-\tau/T_1})$. The delay time T was 0.1 s for the [$^2H_2$]PC rHDLs at 25°C, and 0.26 and 0.20 s for the [$^2H_6$]TO rHDLs at 25 and -5°C, respectively.

^{2}H NMR powder spectra of neat [$^2H_3$]CO were obtained using the quadrupolar echo pulse sequence $(90°|_{0°}-\tau-90°|_{90°}-T)_n$. Data collection was accomplished with an Explorer IIIA digital oscilloscope while Fourier transformation was performed using a Nicolet BNC-12 computer. The spectra were symmetrized by zeroing the out-of-phase quadrature channel and reflecting the spectrum about the central (carrier) frequency. This results in an improvement in S/N by $\sqrt{2}$.

For the lipoprotein diffusion, rHDL, and LDL-HEP insoluble complex studies, the ^{31}P NMR experiments were performed at 102.2 MHz, without proton decoupling, on the home-built spectrometer, using the broad-band probe. For the LDL-GAG soluble complex studies, the ^{31}P NMR experiments were run at 40.5 MHz on a Bruker SY-100 spectrometer using inverse-gated proton noise decoupling (decoupler gated on during FID acquisition). Field frequency stabilization was obtained from the ^{2}HOH resonance of the solvent. Temperatures were controlled at 25°C using a Bruker temperature controller. The spectral parameters are given in the Figure legends.

The ^{2}H spectra shown in Figures 13, 16, 17, and 21 were analyzed using a seven-parameter iterative least-squares fit of the ^{2}HOH and [$^2H_3$]CO (Figure 13), [$^2H_6$]TO (Figures 16 and 17) or [$^2H_2$]PC (Figure 21) resonances to Lorentzian functions. Spectra of [$^2H_{31}$]PC/TO/apoHDL$_3$ in the presence of 2 *M* KBr and in deuterium-depleted water were analysed using both a 8- and 6- parameter fit to three Lorentzian functions (Figures 11 and 12). These

functions were chosen to approximate high- and low-order methylene segments and the terminal methyl group. For the 6- parameter fit, the areas under the three Lorentzians were constrained in the ratio 14:14:3, and the C^2H_3 chemical shift was offset 15 Hz upfield from that of the C^2H_2. For the 8-parameter fit, the only constraint was that the chemical shifts were offset as above. The ^2H NMR spectra in Figures 47 and 48 were analysed using a seven-parameter iterative least-squares fit of the ^2HOH and [^2H]GAG resonances to Lorentzian functions. The parameters which were fit included baseline, linewidth, intensity, and chemical shift. The program, provided by Dr. K.E. Newman and modified by Dr. W.D. Treleaven, both of the Chemistry Department, Simon Fraser University, was run using an IBM 3081 GX computer in the Computing Services Department of Simon Fraser University.

The ^{31}P NMR spectra of the rHDL samples (Figures 18 and 24) were analysed as above using a four-parameter fit to a single Lorentzian function. The ^{31}P NMR spectra of LDL and HDL_3 in the presence of increasing concentrations of glycerol (Figures 25, 29, and 32) were analysed as above using a five-parameter fit of the PC and SPM resonances to single Lorentzian functions. The chemical shift between the PC and SPM resonances was constrained at 0.6 ppm, and the linewidths of PC and SPM were assumed to be equal. The ^{31}P NMR spectra of LDL-GAG soluble complexes in Figures 42 and 43 were simulated by computer using a two Lorentzian lineshape function chemically shifted by 0.6 ppm (25.4 Hz), corresponding to the sphingomyelin and PC resonances of LDL. The linewidths of the two phospholipids were assumed to be equal. All spectra were plotted with low field to the left.

The ^{31}P NMR spectra of pelleted LDL (Figure 37) and LDL-HEP insoluble complexes were simulated using a program based upon the motional narrowing theories of Freed *et. al.* (1971), which assumes an axially-symmetric shielding tensor motionally narrowed by simple Brownian isotropic diffusion, as described by Burnell *et. al.* (1980). The program was kindly supplied by Dr. E. Burnell, Department of Chemistry, University of British Columbia.

Quasi-Elastic Light Scattering

Quasielastic light scattering (QELS) measurements were performed using a Nicomp Model 270 Submicron Particle Sizer. The scattering angle was 90°. The autocorrelation function was evaluated over 64 channels. The channel width varied from 2.8 to 5.0 μsec. The autocorrelation function can be evaluated by either a Gaussian analysis or a Bimodal Distribution analysis. The Gaussian analysis performs a least-squares fit of the autocorrelation function to a Gaussian distribution, using a chi-square test to assess the goodness of fit. The Distribution analysis makes no assumptions regarding the nature of the particle size distribution, but rather attempts to determine the set of exponentially decaying functions which will yield the measured autocorrelation function when added and squared. The sizes cited in the text, unless otherwise stated, were obtained from the Distribution analysis and are expressed as mean diameter ± standard deviation, obtained from repeated runs (usually 7-20) on the same sample. For LDL-GAG complexes, a Gaussian analysis of the data yielded chi-square values in the 0.5-20 range, with the majority of values in the range 5-10. The assumption of a Gaussian distribution of complex sizes does not, therefore, seem to be valid. In general, the sizes obtained from the Distribution analysis are

2-7 nm larger than the Gaussian sizes. However, it should be stressed that the same trends are observed with both methods of analysis, and the conclusions of our study are the same regardless of which analysis is used.

Preparation of [^{2}H,]DPPC Liposomes and Vesicles

Crude [^{2}H,]DPPC was purified on a column (2.5 x 51 cm) of silica gel eluted with chloroform:methanol:water (70:26:4). The solvent was removed by rotovap at 50-60°C until the [^{2}H,]DPPC was very viscous. The remainder of solvent was removed under vacuum (24 hours). The purity of [^{2}H,]DPPC was checked by TLC (silica gel) using chloroform:methanol:water (65:25:4) as the solvent and DPPC as the standard.

[^{2}H,]DPPC liposomes were prepared by co-dissolving 20 mg of [^{2}H,]DPPC and 180 mg of egg PC in chloroform, which was then removed under a stream of N_2. The lipids were placed under vacuum overnight to remove traces of solvent. The PC mixture was then mixed in 0.2 mL of deuterium-depleted water, and the sample was repeatedly mixed with a spatula, vortexed, and centrifuged (desktop) until smooth (≃45 minutes).

In order to prepare small unilamellar vesicles of 20 mol-% [^{2}H,]DPPC, the liposome sample was mixed and vortexed in 4 mL of 0.017 *M* Tris-HCl pH 7.5 prepared in deuterium-depleted water, followed by sonication on a Biosonics sonicator at 45°C until clear (15-20 minutes). The vesicles were centrifuged for 10 minutes on a clinical centrifuge to remove titanium.

DPPC and CO Incorporation Studies

Incorporation of [^2H_x]DPPC into LDL from Alcohol-Water Mixtures

In general, 2-10 mg of [^2H_x]DPPC and/or [^{14}C]DPPC was dissolved in ethanol or isopropanol, and added to stirring water to give a clear solution with an alcohol content of 2-10%. An equal volume of LDL was added to the solution to give a final concentration of 1% ethanol or 5% isopropanol. NaN_3 was added (0.02%), the mixture was flushed with N_2, and incubated at 25 or 45 °C for 24 hours. The amount of added PC was 20-30 mol-% of LDL phospholipid. Following incubation, the LDL was reisolated by ultracentrifugation at density 1.02 g/mL. The top fraction was removed and the LDL pellet was resuspended.

In order to verify association of the labelled PC with LDL and to assess incorporation, LDL was eluted on a column (2.6 x 100 cm) of Sepharose 4-B. The elution buffer was 0.15 *M* NaCl 0.02% Na_2EDTA 0.02% NaN_3 pH 7.6 and the flow rate was ≃20 mL/hour. In general, 6 or 8 mL fractions were collected. The void volume V_o and total volume V_t were 141 and 478 mLs, respectively.

Liquid scintillation counting was performed on a Wallac LKB 1217 Rackbeta liquid scintillation counter. The scintillation cocktail was composed of napthalene (60 g), methanol (100 mL), ethylene glycol (20 mL), liquifluor (42 mL), and dioxane (to 1 liter).

Incorporation of [^{14}C]DPPC and [^{14}C]CO into LDL from rHDL donor particles using plasma exchange proteins

The exchange experiments were performed by incubating rHDL with LDL under N_2 at 38°C in the presence of plasma exchange proteins obtained from lipoprotein-free plasma (LFP). LFP (ρ > 1.21) was dialysed against 0.15 M NaCl pH 7.7 containing 0.01% Na_2EDTA and 0.02% NaN_3 before use. The LDL used in study 2 came from a different pooled batch than the LDL used in studies 1 and 3.

In each of the incubations performed in studies 1 and 3, 2.5 mg of LDL protein was used, varying the amount of rHDL, in a total volume of 3 mL. The volume of LFP was 10 and 15 ml in studies 1 and 3, respectively. In study 2, approximately 25 mg of LDL protein was used, and the volume of LFP was 80 mL. The incubation times for studies 1, 2, and 3 were 13, 24, and 14 hours, respectively. The weight ratios of rHDL/LDL (mg/mg as defined) used in each study are given in Table XVII (Results and Discussion).

Analytical Techniques

Protein was determined by the method of Lowry *et al.* (1951) and phospholipid by the method of Ames (1966). Cholesteryl ester and triglyceride were determined enzymatically by the use of Boehringer Mannheim clinical test kits. The estimated error in these analyses, based on duplicate runs on the same sample, was ±2% for protein and phospholipid and ±10% for cholesteryl ester and triglyceride.

Acetylation of LDL lysine residues was accomplished by the addition of acetic anhydride to LDL in sodium acetate solution as described by Iverius (1972).

CHAPTER IV

RESULTS AND DISCUSSION

Lipid-Lipid Interactions in Reconstituted HDL

An important aspect of lipoprotein structure is that of interactions between the hydrophobic core and the phospholipid/protein monolayer. Interactions between these two domains of the lipoprotein particle may regulate the physical state of the particle surface and thereby affect such phenomena as receptor binding or lipid transfers between particles. The formation of LDL-GAG insoluble complexes has been shown to elevate the core ester phase transition temperature, an effect which may enhance the deposition of LDL in the arterial wall (Bihari-Varga *et al.*, 1981). Whether this is an important *in vivo* effect is not known, but it clearly demonstrates that interactions between LDL proteins and phospholipids with GAGs at the particle surface can influence the physical state of the core, and suggests the presence of a mechanism by which these two regions can communicate.

In order to search for such effects, reconstituted particles were chosen as a convenient means of varying the order of lipids in either region of the particle. Reconstituted HDLs (rHDLs) were chosen for two reasons: (i) they are the smallest of the lipoproteins, a factor which would facilitate the detection of core-monolayer interactions, which may be harder to observe in larger particles where a smaller percentage of core lipids would be in contact with the surface; (ii) they are easily formed by sonication of apoHDL$_3$ with lipids. In contrast, the preparation of rLDL (Walsh and Atkinson, 1983; Ginsburg *et al.*, 1984) involves the use of

sodium deoxycholate to stabilize the apo B-100, which may be difficult to completely remove. To date, the reconstitution of VLDL has not been reported.

Characterization of rHDLs

The question of interest in the present study was whether varying the order of either core or monolayer would affect the order of the neighboring domain. In order to assess this, three comparative studies have been performed using six different rHDLs. These may be summarized as follows: (1) [$^2H_3$]CO/DPPC/apoHDL$_3$ and [$^2H_3$]CO/egg PC/apoHDL$_3$ (2) two sizes of both [$^2H_6$]TO/DPPC/apoHDL$_3$ and [$^2H_6$]TO/egg PC/apoHDL$_3$ (3) [$^2H_2$]PC/CO/apoHDL$_3$ and [$^2H_2$]PC/TO/apoHDL$_3$.

In order for the comparisons within each study to be valid, it is necessary to show that the sizes and chemical compositions of the particles are approximately the same, and that the protein is not affected by the sonication procedure. It has been shown by circular dichroism measurements that the conformation of apoHDL$_3$ is identical in native and reconstituted particles (Hirz and Scanu, 1970), and that sonication of apo A-I does not result in structural changes of the apoprotein (Ritter and Scanu, 1977). The integrity of apo A-I after sonication has also been demonstrated by immunodiffusion, electrophoresis, and amino acid analysis (Ritter and Scanu, 1977). In order to ensure that the sonication conditions used in the present study did not damage the apoproteins, we have used SDS-polyacrylamide gel electrophoresis to compare the proteins of native HDL$_3$ and isolated apoHDL$_3$ with those of a sample of apoHDL$_3$/egg PC/cholesterol (24:72:4 by weight) sonicated for 30 minutes (Figure 7). The banding patterns of the native, isolated, and sonicated proteins were

essentially identical, and no degradation due to sonication could be observed. This represents the maximum sonication time employed in our study. In Figure 7, a human serum albumin (HSA) contaminant is present in the isolated apoHDL$_3$. This was effectively removed during ultracentrifugation following sonication, as shown in Figure 8 for [$^2H_6$]TO/DPPC/apoHDL$_3$ and [$^2H_6$]TO/egg PC/apoHDL$_3$ (diameter = 11 nm). The streaking observed with these rHDLs may be caused by the presence of lipid. In the gels shown in Figures 7 and 8, the apo A-II was present but was difficult to reproduce photographically. SDS gel electrophoresis of delipidated [$^2H_{31}$]PC/TO/apoHDL$_3$ is shown in Figure 9, where the apo A-II is clearly visible. The latter gel was run on a BIO-RAD Mini-PROTEAN II, which gives better resolution than the larger homemade slab gel apparatus used to run the other gels.

The size distributions were determined using electron microscopy and the particle compositions by chemical analysis. Figure 10 shows representative electron micrographs of [$^2H_6$]TO/egg PC/apoHDL$_3$ (diameter = 13.1 nm), [$^2H_6$]TO/DPPC/apoHDL$_3$ (diameter = 11.0 nm), and [$^2H_2$]PC/CO/apoHDL$_3$ (diameter = 8.7 nm). The particles look uniform in size and are spherical, as in the case of native HDL. The size distributions are shown beneath the micrographs, and were obtained from several different field measurements in each case. The mean diameters of the [$^2H_6$]TO/DPPC/apoHDL$_3$ and [$^2H_6$]TO/egg PC/apoHDL$_3$ were 13.2±4.3 and 13.1±4.0 nm, respectively. Following a second sonication, these sizes were reduced to 11.0±3.1 nm and 11.2±3.2 nm, respectively. The larger size of the [$^2H_6$]TO rHDLs is reflected in the increased percentage of core components (25% as compared with $\simeq$ 15% in the other rHDLs). The mean diameters of the [$^2H_2$]PC/CO/apoHDL$_3$ and [$^2H_2$]PC/TO/apoHDL$_3$ were 8.7±2.0 nm and 9.1±1.9 nm (Table III), with 56% and

Figure 7: Electrophoresis of apoHDL$_3$ on 10% SDS polyacrylamide gels. Well 1: 10 μL of a 3 mg/mL mixture of (1) myosin (MW 205,000), (2) β-galactosidase (MW 116,000), (3) phosphorylase B (MW 97,400), (4) bovine plasma albumin (MW 66,000), (5) egg albumin (MW 45,000), and (6) carbonic anhydrase (MW 29,000). The standards were obtained from Sigma (MW-SDS-200 Kit). Well 2: $\simeq$ 30 μg of native HDL$_3$ (as protein). Well 3: $\simeq$30 μg of isolated apoHDL$_3$. Wells 4 and 5: $\simeq$15 and 30 μg, respectively, of apoHDL$_3$ sonicated for 30 minutes in the presence of egg PC and cholesterol (apoHDL$_3$:egg PC:cholesterol 24:72:4 by weight). This sample was *not* subsequently centrifuged. Although difficult to reproduce photographically, three very faint bands running below the apo A-I are present in Wells 2-5. The apparent MW of the apo A-I (26,000-27,000) is the same in all three samples. The dark band of $M_r \simeq$ 66,000 observed in Wells 2-5 is a Human Serum Albumin (HSA) contaminant.

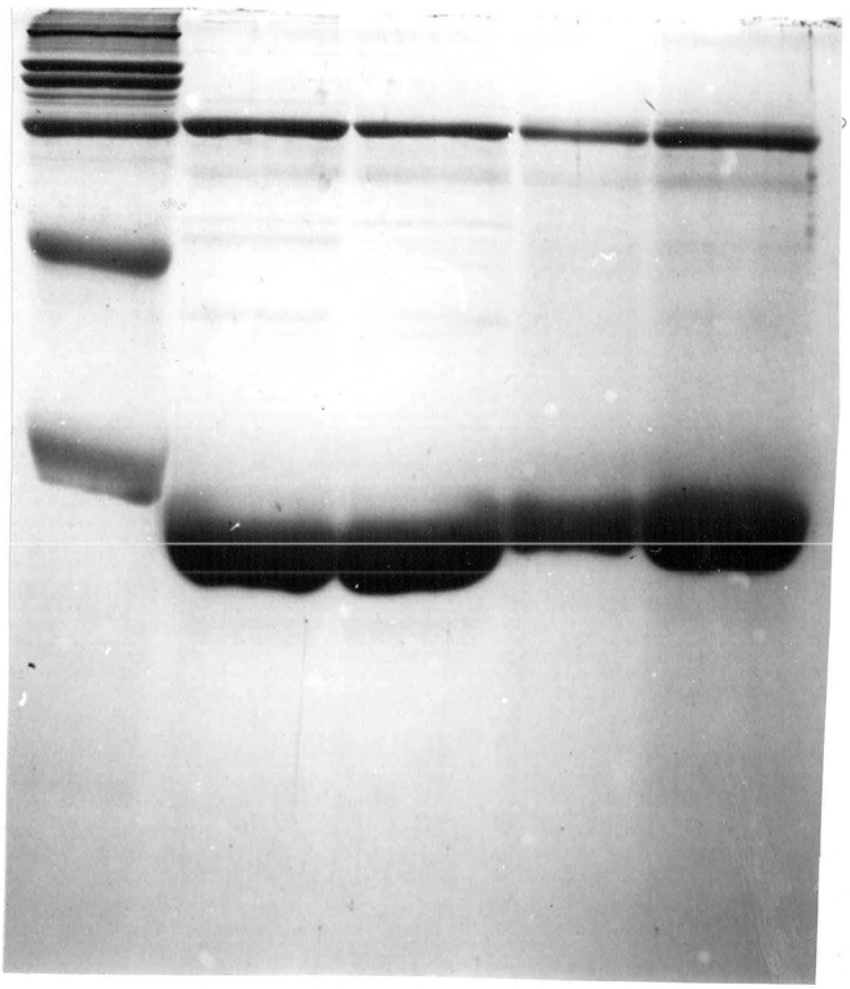

Figure 8: Electrophoresis of [$^2H_6$]TO/egg PC/apoHDL$_3$ and [$^2H_6$]TO/DPPC/apoHDL$_3$ on 10% SDS polyacrylamide gels. Wells 1-3: see caption for Well 1, Figure 7. Well 4: ≤20 μg [$^2H_6$]TO/egg PC/apoHDL$_3$ (as protein). Well 5: ≤20 μg [$^2H_6$]TO/DPPC/apoHDL$_3$ (as protein). The sonication time was ≃15 minutes.

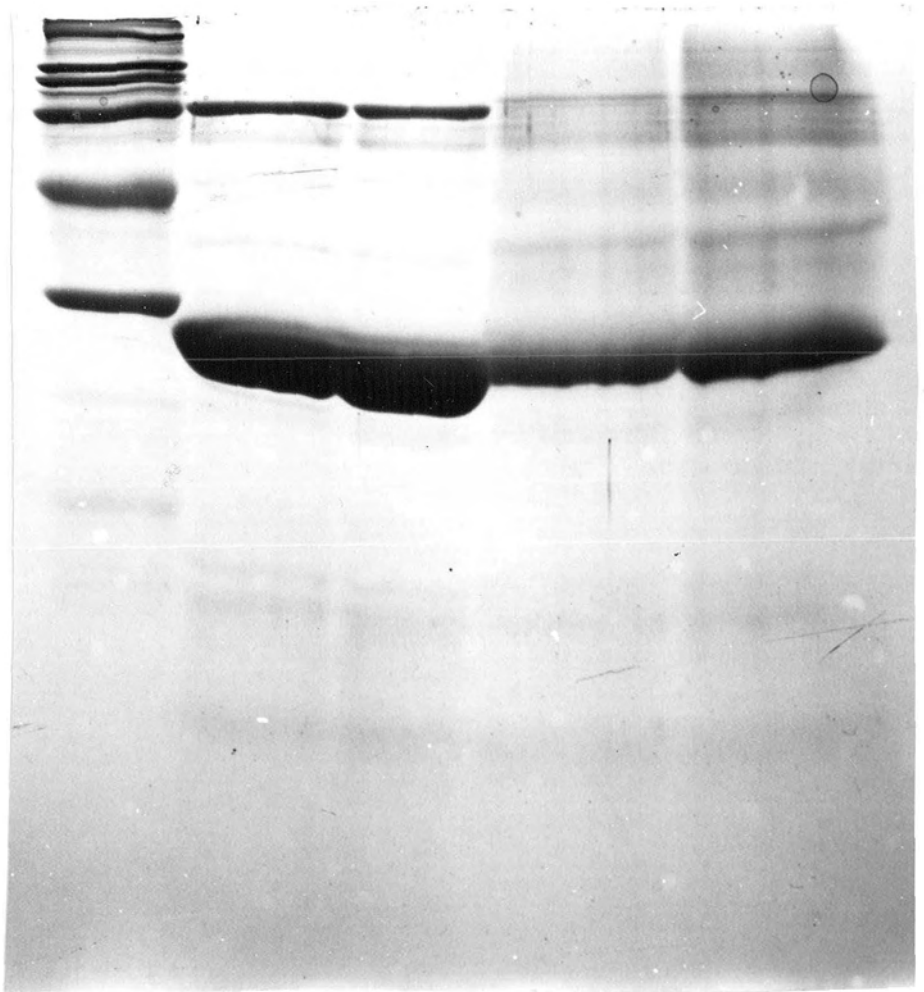

Figure 9: Electrophoresis of [$^2H_{31}$]PC/TO/apoHDL$_3$ on 10% SDS polyacrylamide gels. Well 1: see caption for Well 1, Figure 7. Wells 2 and 3: ≃30 and 100 μg, respectively, of native HDL$_3$ (delipidated). Wells 5 and 6: ≃20 and 60 μg, respectively, of delipidated [$^2H_{31}$]PC/TO/apoHDL$_3$, sonicated for 6 minutes. The apoHDL$_3$ run in wells 5 and 6 originates from a different batch of HDL$_3$ than that run in wells 2 and 3, which accounts for some of the minor differences in the banding patterns of the other proteins. The dark band of M_r ≃66,000 observed in Wells 2 and 3 is a Human Serum Albumin (HSA) contaminant.

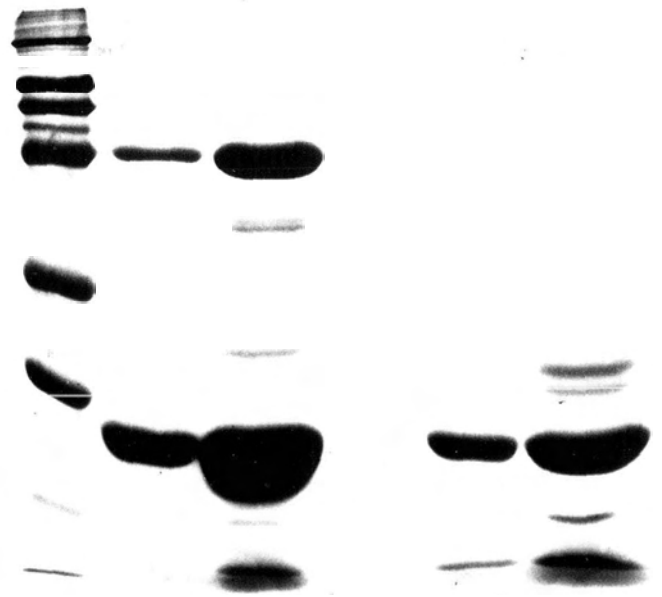

Figure 10: Representative electron micrographs and histograms of the size distributions of (a) [$^2H_6$]TO/egg PC/apoHDL$_3$ (diameter = 13 nm) (magnification = 175,000 times), (b) [$^2H_6$]TO/DPPC/apoHDL$_3$ (diameter = 11 nm) (magnification = 173,000 times), and (c) [$^2H_2$]PC/CO/apoHDL$_3$ (magnification = 130,000 times).

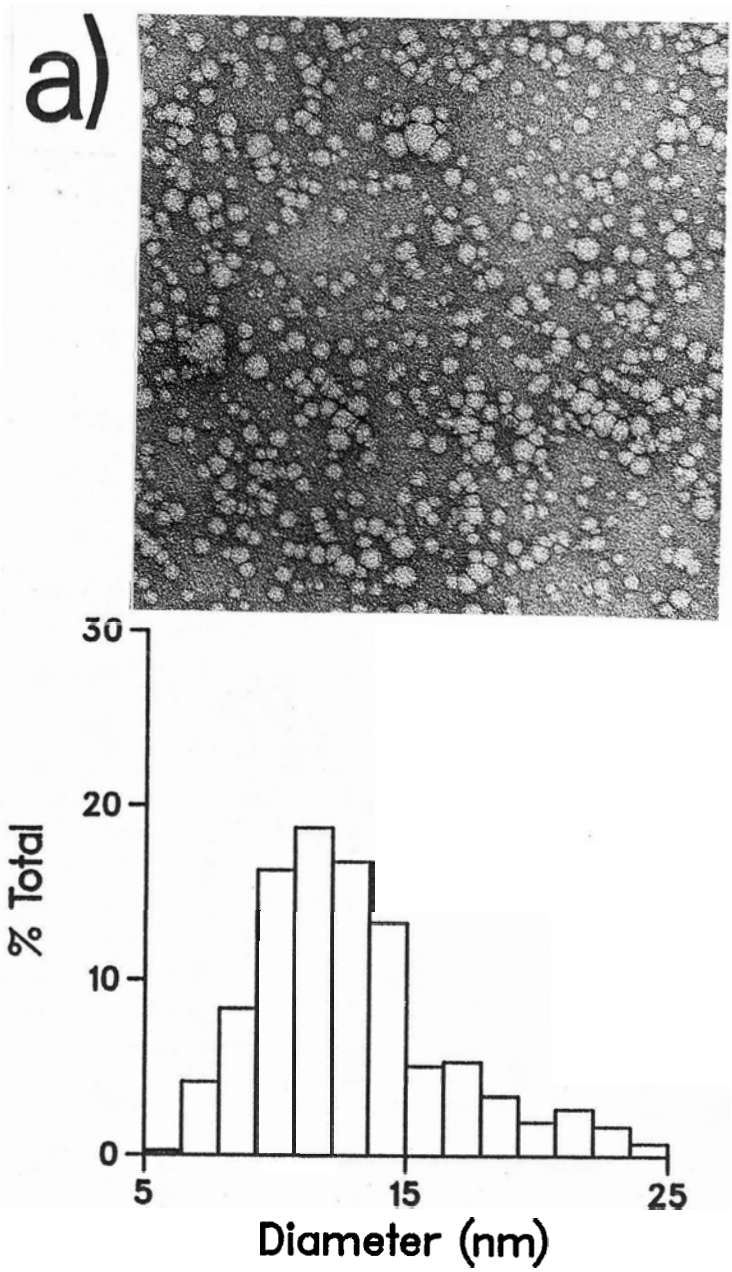
a)
30
20
10
0
% Total
5
15
25
Diameter (nm)

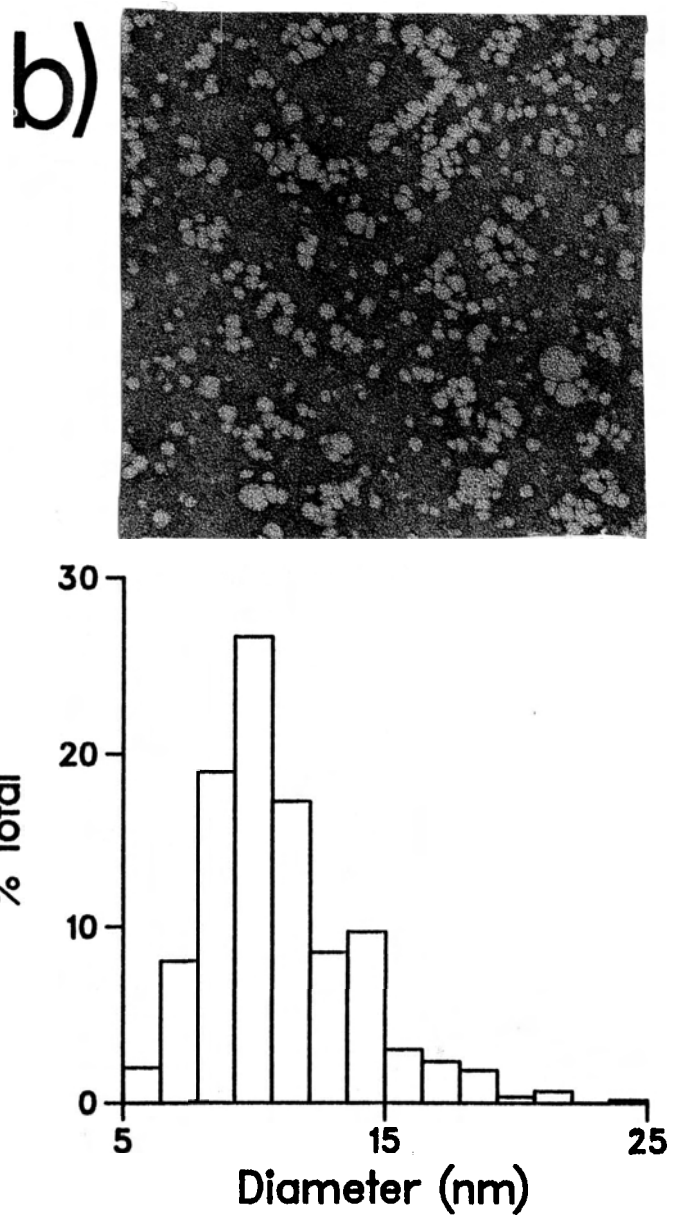
b)
30
20
10
0
% Total
5
15
25
Diameter (nm)

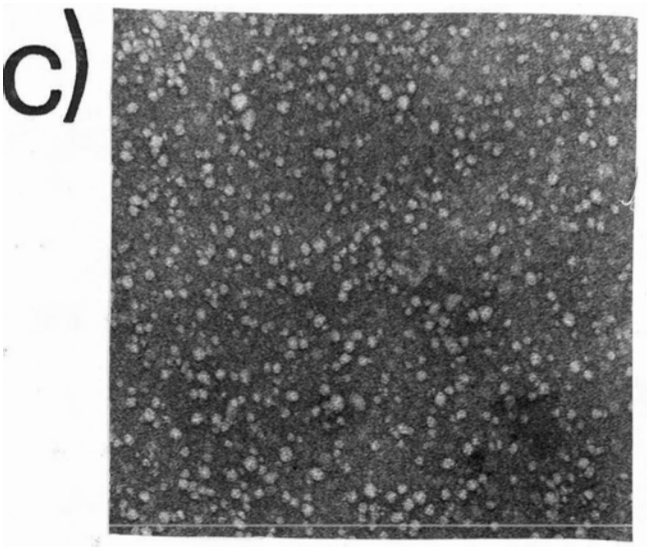
c)

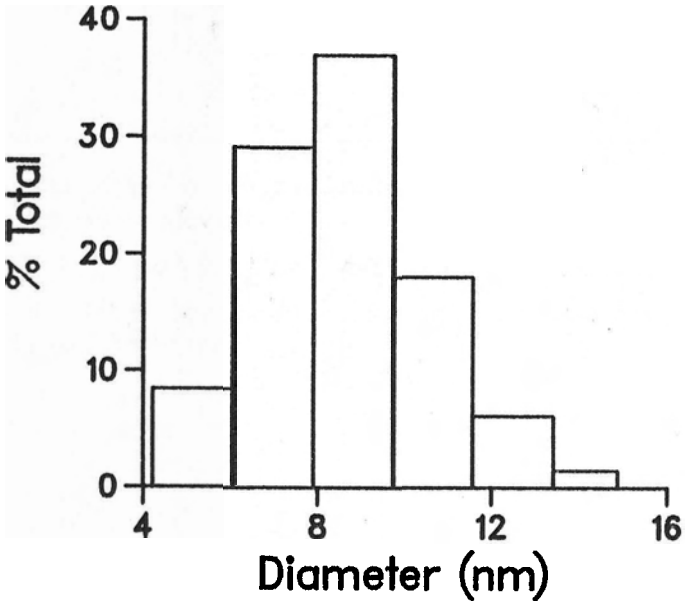
40
30
20
10
0
% Total
4
8
12
16
Diameter (nm)

Table III: Physical parameters of rHDLs reconstituted from apoHDL$_3$ and the indicated lipid mixtures, isolated in the density range 1.125-1.21 g/mL.

	[$^2H_3$]CO/DPPC	[$^2H_3$]CO/egg PC	[$^2H_2$]PC/CO	[$^2H_2$]PC/TO
Diameter[a] (nm)	9.0(±1.6[b])	8.7(±1.6)	8.7(±2.0)	9.1(±1.9)
Composition (wt %)				
Protein	46	46	53	53
PC	38	39	32	31
CO	16	15	15	-
TO	-	-	-	16
T_1 (ms)[c]	-	-	16	14

	[$^2H_6$]TO/DPPC	[$^2H_6$]TO/egg PC	[$^2H_6$]TO/DPPC	[$^2H_6$]TO/egg PC
Diameter[a] (nm)	13.2(±4.3)	13.1(±4.0)	11.0(±3.1)	11.2(±3.2)
Composition (wt %)				
Protein	53	54	55	56
PC	22	21	19	19
TO	25	25	26	25
T_1 (ms)[c]	17(-5°C)	19(-5°C)	-	
	33(25°C)	34(25°C)	-	

[a] Mean Diameter from EM measurements; between 200 and 600 particles were measured for each sample.

[b] The number in parentheses represents the standard deviation.

[c] Deuterium spin-lattice relaxation time of the deuterated lipid measured at 25°C or as indicated.

57% of the particles falling in the 7.3-9.5 nm size range, respectively. The mean diameters of [$^2H_3$]CO/DPPC/apoHDL$_3$ and [$^2H_3$]CO/egg PC/apoHDL$_3$ were 9.0±1.6 and 8.7±1.6 nm, respectively (Table III), and in both cases 64% of the particles fell in the 7.3-9.4 nm size range. The values for the [$^2H_3$]CO and [$^2H_2$]PC rHDLs are only slightly larger than those determined for the native HDL$_3$ from which the protein was isolated (mean diameter of 8.1±1.6 nm with 62% of the particles in the range 7.2-9.3 nm). Additionally, each pair of rHDLs within a given study have essentially identical chemical composition (Table III). Thus, the only major difference between the two [$^2H_3$]CO rHDLs and the [$^2H_6$]TO rHDLs lies in the fatty acyl chain composition of the phospholipid monolayer. Likewise, the two [$^2H_2$]PC rHDLs differ only in their core lipids. The average size of the [$^2H_3$]CO and [$^2H_2$]PC rHDLs, and the chemical composition of the [$^2H_3$]CO rHDLs, lie between the literature values for HDL$_2$ and HDL$_3$. The chemical composition of the [$^2H_2$]PC rHDLs is closer to that of HDL$_3$. The [$^2H_6$]TO rHDLs are in the size range of HDL$_2$. Although simpler in composition than the native particles, the rHDLs are good models of the native systems as far as size, relative proportion of core/monolayer components, and ^2H NMR parameters (see below) are concerned.

The rHDLs were isolated after ultracentrifugation in KBr of density 1.18 g/mL, which corresponds to a salt concentration of ≃2 *M*. The rHDLs were run as isolated to allow temperatures as low as -8°C to be studied. Observations made in this laboratory suggest that KBr has no effect on lipoprotein lipid organization and may act as a stabilizing agent. The order parameters of selectively deuterated phospholipids and fatty acids incorporated into the monolayer of VLDL are the same in the presence and absence of 2 *M* KBr, and the diffusion coefficients of phospholipids in the

monolayer at 25°C are similar (R. S. Chana, unpublished results). Also, KBr prevents VLDL aggregation at high VLDL concentrations (R. S. Chana, unpublished results). Nevertheless, to assess the effects of high salt concentrations on phospholipid order in the rHDL monolayer, studies were performed on [$^2H_{31}$]PC/TO/apoHDL$_3$. ^{2}H NMR spectra of [$^2H_{31}$]PC/TO/apoHDL$_3$ in 2 *M* KBr and in deuterium-depleted water are shown in Figures 11 and 12. The resulting spectra are super-Lorentzians resulting from the superposition of the narrow methyl resonance riding on the broader methylene resonances. It has previously been shown that the order parameter profile of the monolayer of native HDL$_2$ and HDL$_3$ containing ≤5 mol % (relative to phospholipid) selectively deuterated fatty acids is similar to that of liposomes (Parmar *et al.*, 1985, Parmar, 1985). Order in the monolayer is constant up to at least the 5,6- position (the plateau region), and then rapidly decreases until the end of the chain. However, the values of S_{CD} obtained (≃0.35 in plateau) were significantly greater than in liposomes (≃0.2 in plateau). The higher order in HDLs may be due to interactions with protein or with the core. The spectra in Figures 11 and 12 represent a superposition of resonances from the entire *sn*-2 chain, and therefore one cannot obtain meaningful order parameters from the measured linewidth. For this reason, two attempts were made to computer-simulate the spectra. In Figure 11, three Lorentzian functions were chosen to approximate the high order methylenes (plateau), the low order methylenes, and the terminal methyl group. Initially, the spectra were analysed using an 8-parameter fit to the data points in which the intensity *I* and the linewidth *W* of each Lorentzian were allowed to iterate to the best fit, with the baseline and methyl chemical shift comprising the other two parameters (the chemical shift of the methylenes was fixed 15 Hz

Figure 11: ^2H NMR spectra of [$^2H_{31}$]PC in HDL reconstituted with TO and apoHDL$_3$ at 25°C in 2 *M* KBr (a) and in deuterium-depleted water (b). The solid line represents an iterative least-squares fit of three Lorentzian lineshape functions to the data points (crosses). The three Lorentzians were chosen to represent high order C^2H_2, low order C^2H_2, and the terminal C^2H_3. The areas under the three Lorentzians were not constrained, and the C^2H_3 chemical shift was offset 15 Hz upfield from that of the C^2H_2. For illustrative purposes, every 5th data point is plotted. Spectral parameters: pulse width = 6.7 μs (flip angle = 90°). Sweep width = ±2.5 kHz. Number of acquisitions = 72000. Data sets = 4K. Delay between pulses = 0.85 s. Line broadening = 5 Hz. Delay before acquisition = 10 μs.

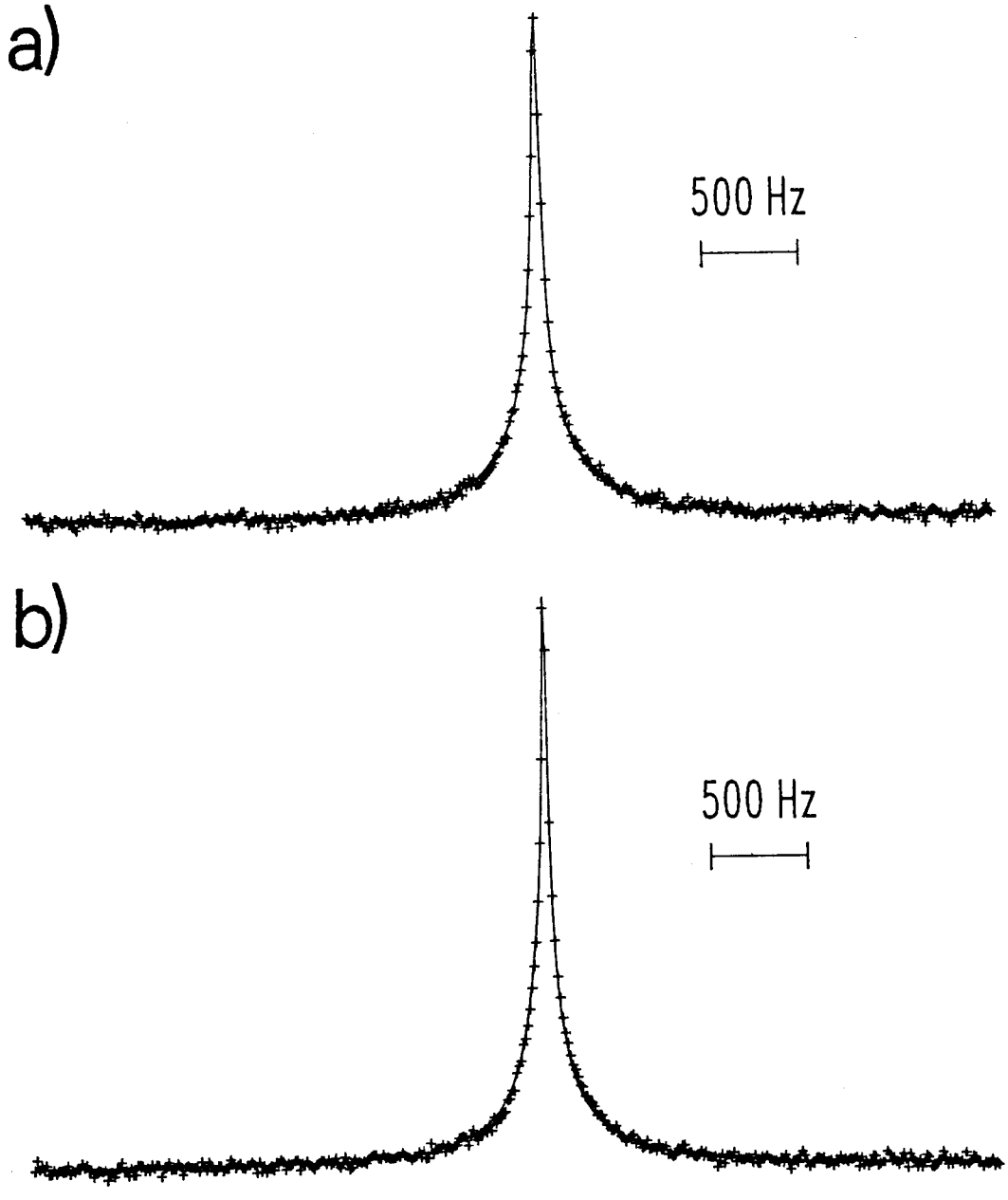
a)
500 Hz
b)
500 Hz

Figure 12: ^2H NMR spectra of [$^2H_{31}$]PC in HDL reconstituted with TO and apoHDL$_3$ at 25°C in 2 *M* KBr (a) and in deuterium-depleted water (b). The solid line represents an iterative least-squares fit of three Lorentzian lineshape functions to the data points (crosses). The three Lorentzians were chosen to represent high order C^2H_2 (positions 2-8), low order C^2H_2 (positions 9-15), and the terminal C^2H_3. The areas under the three Lorentzians were constrained in the ratio 14:14:3, respectively, and the C^2H_3 chemical shift was offset 15 Hz upfield from that of the C^2H_2. For illustrative purposes, every 5th data point is plotted. Spectral parameters same as in Figure 11.

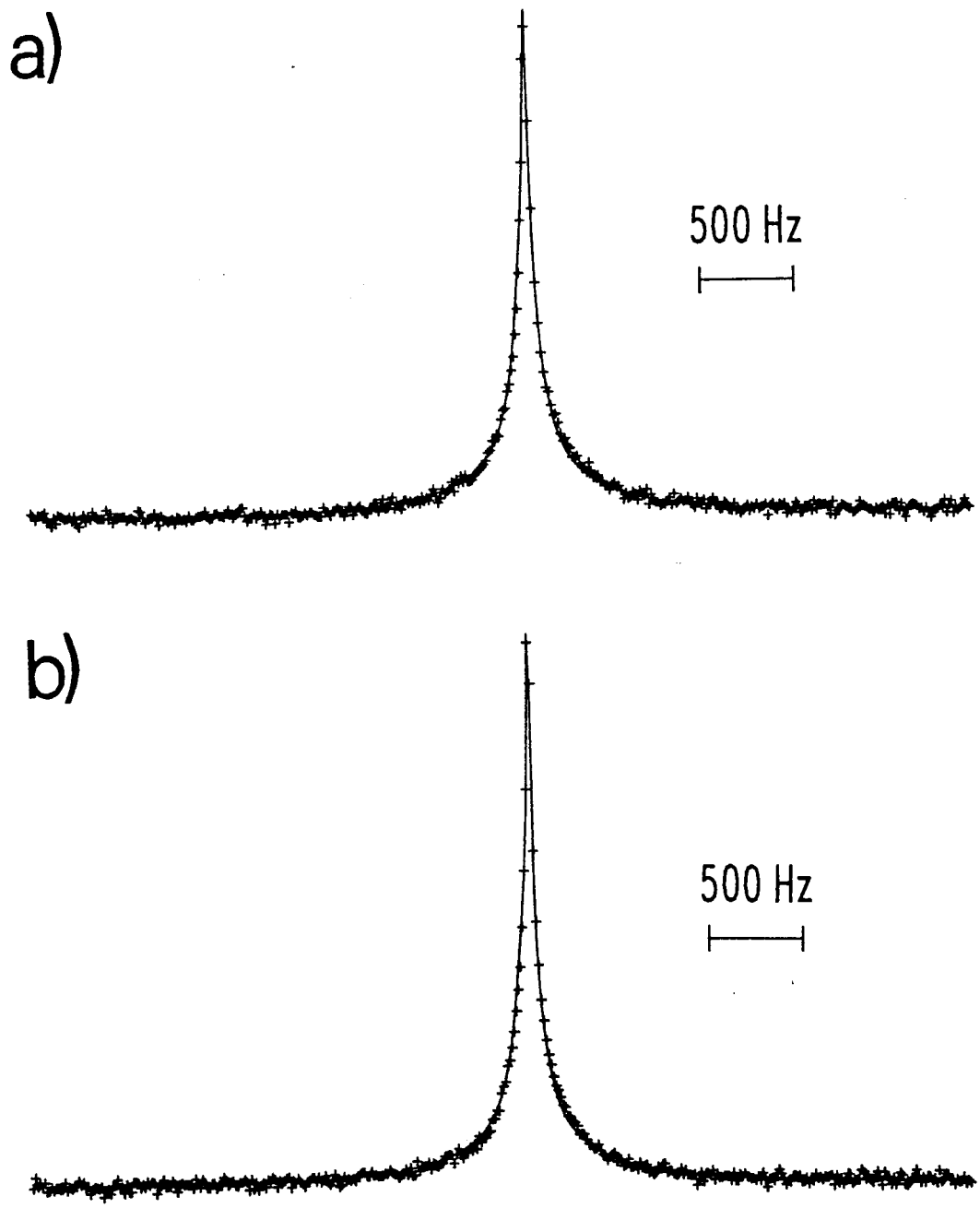
a)
500 Hz
b)
500 Hz

downfield from that of the methyl group). The computer-fit linewidths and order parameters are given in Table IV. Values of S_{CD} were calculated from eq 19, neglecting T_1 effects and assuming a radius of 5 nm. The values of S_{CD} are essentially identical in both 2 *M* KBr and water; however, the relative areas under each Lorentzian, as approximated by *WI* (Stone, 1973), were found to vary. Thus, the spectra were fit using 3 Lorentzian functions in which the areas were constrained in the ratio 14:14:3, to correspond to positions 2-8, 9-15, and 16. This is a reasonable although approximate choice, as only the 2,2-, 4,4-, 5,5,6,6-, 11,11,12,12-, and 16,16,16- positions have been examined using selectively deuterated fatty acids in native HDLs, and therefore it is not known precisely how far the plateau region extends down the chain. By comparing the sum of the areas of the three Lorentzians from the 8-parameter fit with the product of measured linewidth *W(SL)* times intensity *I(SL)*, it was found that the area of the super-Lorentzian was closely approximated by $2W(SL)I(SL)$. Thus, the area of Lorentzian 1 (L1) would be 14/31 of the total area, or

$$W(L1)I(L1) = (14/31)(2W(SL)I(SL)).$$

The intensity of L1 is thus $(28/31)(W(SL)/W(L1))I(SL)$, and by following the same procedure, L2 has intensity $(28/31)(W(SL)/W(L2))I(SL)$, and L3 has intensity $(6/31)(W(SL)/W(L3))I(SL)$. This gave a 6-parameter fit to the data points (*W(L1-L3)*, *I(SL)*, methyl chemical shift, and baseline), and the results are given in Figure 12 and Table IV. Again, no effect of salt on monolayer organization is observed. Finally, the values of S_{CD} and T_1 obtained for $[^2H_2]$PC rHDLs in 2 *M* KBr are nearly identical to the values obtained in water with $[5,5,6,6\text{-}^2H_4]$palmitic acid incorporated into native HDL_3 (Parmar *et al.*, 1985). The sum total of our observations thus argues strongly against any effect of high salt concentrations on the organization

of lipoprotein monolayers. However, if a small effect was present, it would most likely be constant throughout all the studies, and could be neglected.

Effect of Monolayer on Core. Results with [$^2H_3$]CO

Representative ^2H NMR spectra of rHDL containing [$^2H_3$]CO and either egg PC or DPPC as the surrounding monolayer are shown in Figure 13 as a function of temperature. In addition to the signal observed from the [$^2H_3$]CO, the spectra also contain a narrow resonance, ≃145 Hz downfield, due to the residual deuterium in water. The signals are simulated by single Lorentzian lineshape functions. The temperature dependence of the ^2H NMR linewidths $\Delta\nu_{1/2}$ for the two samples is given in Table V. The linewidths obtained are independent of whether the sample was heated or cooled over the temperature range studied. The observed linewidths are shown in Figure 14 as a function of η/T. The temperature dependence is more pronounced for the [$^2H_3$]CO/DPPC/apoHDL$_3$ (slope = 1.93 x 10^6 K·P^{-1}·s^{-1}) than for the [$^2H_3$]CO/egg PC/apoHDL$_3$ (slope = 3.37 x 10^5 K·P^{-1}·s^{-1}). The two curves are linear with correlation coefficients of 0.987 and 0.995, respectively. An examination of the ^2H NMR spectra in Figure 13 and the data in Table V reveals that the linewidth variation of [$^2H_3$]CO with temperature is highly dependent on the species of phospholipid present in each rHDL. At each temperature, the linewidths of the [$^2H_3$]CO/DPPC/apoHDL$_3$ are considerably broader than those of the [$^2H_3$]CO/egg PC/apoHDL$_3$. Since the rHDLs have similar size and composition (Table III), the broader linewidths observed for the [$^2H_3$]CO/DPPC/apoHDL$_3$, compared with the [$^2H_3$]CO/egg PC/apoHDL$_3$, must originate from more restricted motions of the C$^2H_3$ groups of the core cholesteryl esters. Several sources for this decrease in motion can be envisaged. One explanation of our results is that interdigitation of the

Table IV: Effect of 2 *M* KBr on monolayer order in [$^2H_{31}$]PC/TO/apoHDL$_3$.

	KBr		water	
	$\Delta\nu_{1/2}$ (Hz)	S_{CD}	$\Delta\nu_{1/2}$ (Hz)	S_{CD}
	8-parameter fit			
L1	538	0.37	672	0.40
L2	143	0.19	173	0.20
L3	46	0.11	31	0.09
	6-parameter fit			
L1	787	0.44	822	0.44
L2	151	0.19	153	0.19
L3	31	0.09	24	0.07

core esters with surface phospholipid of different order influences the motions of the core esters. Over the range 0-26°C, pure DPPC bilayers exist in the gel phase while pure egg PC bilayers are liquid crystalline. Although phospholipids may pack differently in HDLs than in bilayers due to the small radius of curvature of the lipoproteins, it is reasonable to assume that the DPPC monolayer would still be more ordered than the egg PC monolayer at any given temperature. Thus, the [$^2H_3$]CO linewidths would be broader in [$^2H_3$]CO/DPPC/apoHDL$_3$ than in [$^2H_3$]CO/egg PC/apoHDL$_3$ due to interactions with a more ordered monolayer. The difference in linewidths for the ester C$^2H_3$ is most pronounced at lower temperatures, while at 26°C the linewidths for the two samples are nearly identical.

An alternate explanation of our results is that as the temperature decreases and the DPPC chains become more ordered, DPPC excludes the core esters from the monolayer resulting in more restricted motions of the core esters due to packing in a smaller volume. Whatever the mechanism, it is

Figure 13: ^2H NMR spectra of [$^2H_3$]CO in HDL reconstituted with either DPPC (a-d) or egg PC (e-h) as a function of temperature. The plot width is 600 Hz in all cases. The solid line represents an iterative least squares fit to the data points (crosses). For illustrative purposes every third data point is plotted. Spectral parameters: pulse width = 20 μs (flip angle = 90°). Sweep width = 1 kHz. Number of acquisitions = 4021 (a), 2936 (b), 2048 (c,d), 2942 (e), 2208 (f), 2182 (g), 1457 (h). Data sets = 2K (a-g), 4K (h). Delay between pulses = 1.1 s (a-g), 2.1 s (h). Line broadening = 5 Hz (a,b), 2 Hz (c-h). Delay before acquisition = 10 μs.

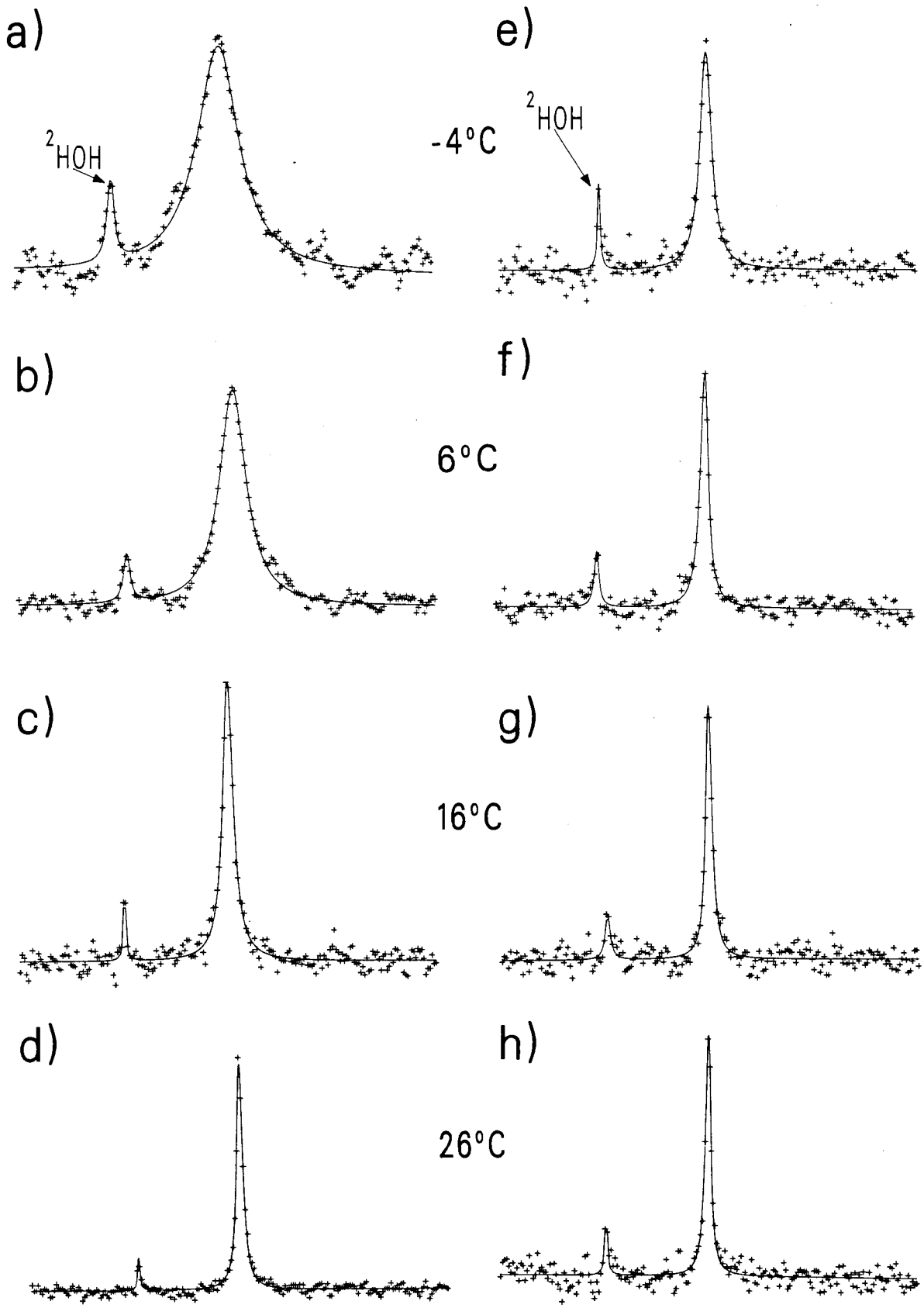
a)
^{2}HOH
e)
-4°C
^{2}HOH
b)
f)
6°C
c)
g)
16°C
d)
h)
26°C

Table V: Temperature dependent ^2H NMR linewidths[a] of $[^2H_3]CO$ and $[^2H_6]TO$ in rHDL containing either DPPC or egg PC.

T (°C)	$\Delta\nu_{1/2}$ - C (Hz)			
	$[^2H_3]CO$/DPPC	$[^2H_3]CO$/egg PC	$[^2H_6]TO$/DPPC[b]	$[^2H_6]TO$/egg PC[b]
-8.0	71			
-5.0			154	70
-4.0	64(65[c])	15(16[c])		
-2.3	57			
-2.0		13		
0.0	60			
1.0	50	12		
3.5	40			
5.0			78	45
6.0	38(38)	9.2(9.5)		
11.0	24	8.3		
15.0			45	34
16.0	13(13)	6.5(6.3)		
18.0	13			
20.0			33	
21.0	9.2			
25.0			26	24
26.0	5.9(5.9)	4.3(4.8)		
35.0			20	18
45.0			14	13

[a] The linewidths for the $[^2H_6]TO$ rHDLs were obtained from an iterative least squares fit of the $[^2H_6]TO$ resonance. Measured linewidths are accurate to ±10%.

[b] The mean diameters were 13.2±4.3 and 13.1±4.0 nm for the $[^2H_6]TO$/DPPC/apoHDL$_3$ and $[^2H_6]TO$/egg PC/apoHDL$_3$ rHDLs, respectively.

[c] The numbers in parentheses represent the linewidth obtained from an iterative least squares fit of the $[^2H_3]CO$ resonance.

Figure 14: ^2H NMR linewidths $\Delta\nu_{1/2}$ of $[^2H_3]CO$ in rHDL containing either DPPC (●) or egg PC (■) as a function of η/T. The error bars represent an estimated uncertainty in the linewidths of ±10%. The dashed lines are theoretical plots calculated from eq 12 using the measured temperature-dependence of $\Delta\nu_Q$ of neat $[^2H_3]CO$.

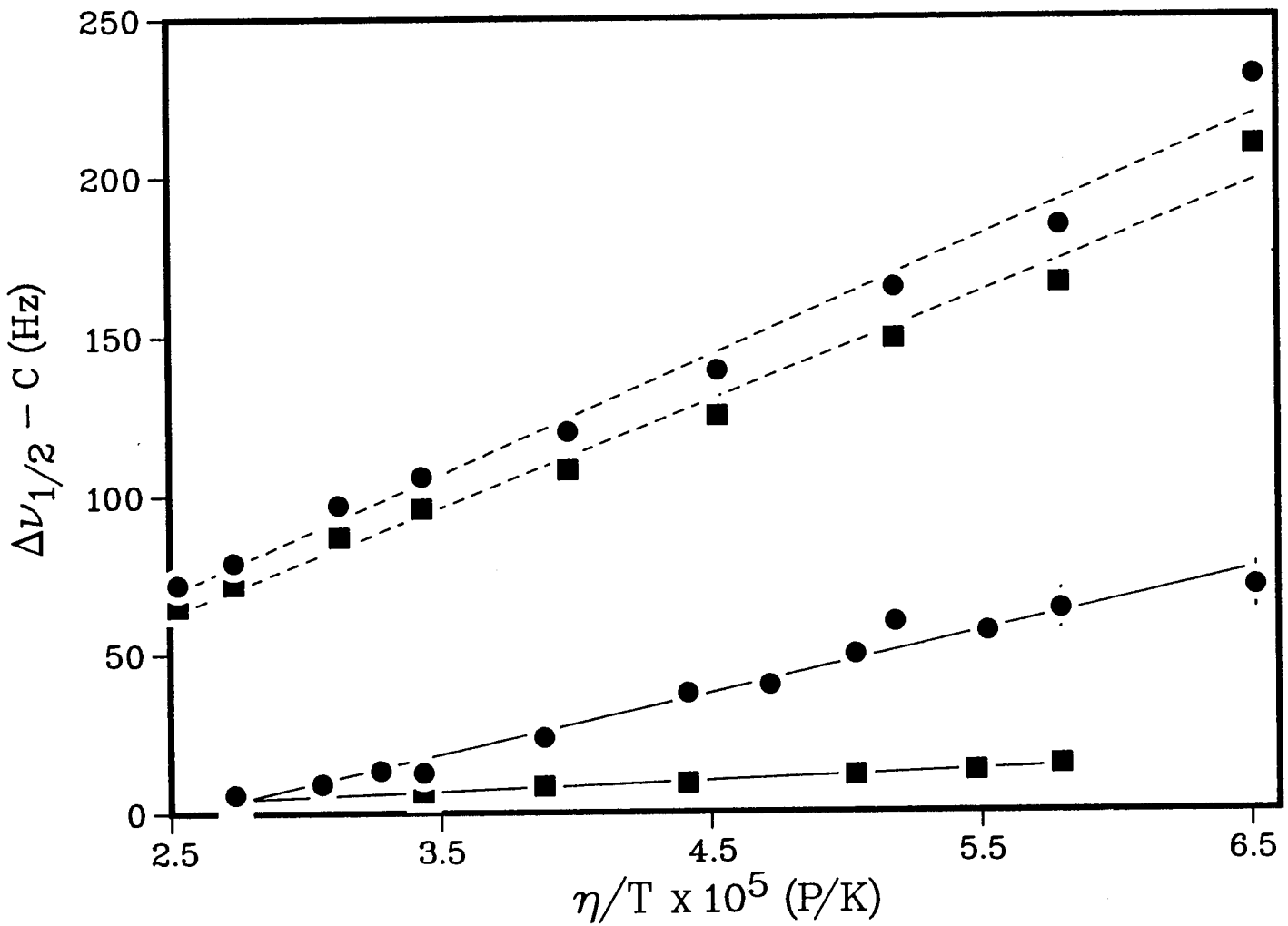
250
200
150
100
50
0
$\Delta\nu_{1/2} - C$ (Hz)
2.5
3.5
4.5
5.5
6.5
$\eta/T \times 10^5$ (P/K)

clear that the state of the monolayer profoundly affects the neighboring core.

To demonstrate that the packing is different in rHDL than it would be for neat esters, we have used eq 12 to calculate the theoretical $\Delta\nu_{1/2}$ for [$^2H_3$]CO in rHDL (dashed lines in Figure 14) using the measured values of $\Delta\nu_Q$ for neat [$^2H_3$]CO at various temperatures (representative spectra are given in Figure 15). Between -8 and 30°C, the values of $\Delta\nu_Q$ for neat [$^2H_3$]CO remain essentially constant at ≃20.7 kHz. It is only as the temperature is reduced to -39°C that the splittings approach the theoretical maximum value of 38 kHz, thus indicating significant motion for the neat ester C$^2H_3$ group to low temperature. The values of the linewidths for both rHDLs are much smaller than the theoretical linewidths, as shown in Figure 14, where both measured and theoretical linewidths are plotted for comparison. This demonstrates that the packing of [$^2H_3$]CO in the rHDLs is considerably different than in neat [$^2H_3$]CO. This is expected since it has been shown (Tall, 1980) that there are not enough ester molecules in HDL to form a separate ester phase. Also, the packing of esters in particles of small radius of curvature might be expected to differ from the neat phase. These two factors would be expected to result in a similar reduction of linewidth in both rHDLs however, since the particle size and number of ester molecules of the two [$^2H_3$]CO rHDLs are about the same. Therefore, the large differences in slope between the [$^2H_3$]CO/DPPC/apoHDL$_3$ and [$^2H_3$]CO/egg PC/apoHDL$_3$ plots (ratio of slopes = 5.7) suggests interactions between the core and the monolayer.

Figure 15: Temperature dependence of the ^2H NMR spectra of neat $[^2H_3]CO$. The plot width in all cases is ±50 kHz. Spectral parameters: pulse width = 8.0 μs (90° flip angle) (a-f); sweep width = ±100 kHz (a,b,d-f), ±50 kHz (c); line broadening = 200 Hz (a-d), 100 Hz (e,f); data set = 2K (a-f); τ = 75 μs (a-f); T = 1.0 s (a-d), 1.5 s (e,f). From the spectra, values of $\Delta\nu_Q$ of 35.5 (a), 33.5 (b), 29.4 (c), 21.7 (d), 20.4 (e), and 20.0 (f) kHz were obtained. The spectra have not been scaled to give equal areas under each curve. The origin of the narrow isotropic resonance which appears at temperatures above -28°C is unknown.

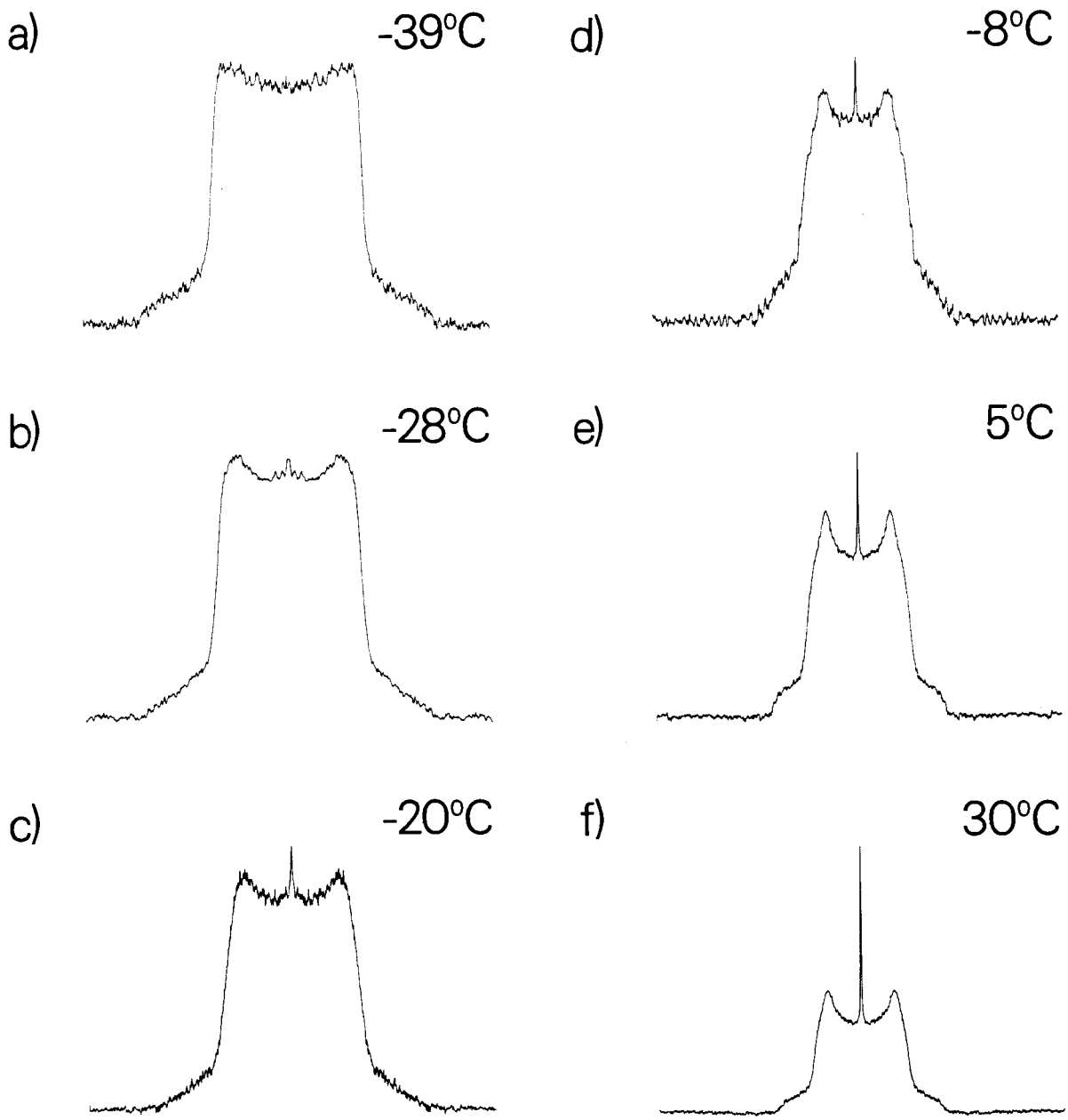
a)
-39°C
d)
-8°C
b)
-28°C
e)
5°C
c)
-20°C
f)
30°C

Effect of Monolayer on Core. Results with [$^2H_6$]TO.

In an effort to see if our observations extend to particles as large as HDL_2, we have made rHDLs containing [$^2H_6$]TO with mean diameters of 13 and 11 nm. Representative ^2H NMR spectra of rHDLs (diameter 13 nm) containing [$^2H_6$]TO as the core component and either DPPC or egg PC as the surrounding monolayer are shown in Figure 16 as a function of temperature. Representative spectra of 11 nm [$^2H_6$]TO rHDLs are shown in Figure 17. The spectra can be simulated by single Lorentzian lineshape functions. Temperature-dependent linewidths for the 13 nm samples are given in Table V.

^{31}P NMR spectra were obtained for the larger [$^2H_6$]TO rHDLs (13±4 nm) at 25°C, yielding linewidths of 53 and 55 Hz for the [$^2H_6$]TO/DPPC/apoHDL_3 and [$^2H_6$]TO/egg PC/apoHDL_3, respectively. These are the same within experimental error. The spectra are shown in Figure 18. As with the ^2H NMR spectra, the ^{31}P NMR spectra could be simulated with a single Lorentzian lineshape function. Although both the size and size distributions of the [$^2H_6$]TO rHDLs are larger than the other rHDLs, they are not sufficient to produce super-Lorentzian lineshapes, as is observed for unilamellar vesicles (Parmar *et al.*, 1984).

A plot of ^2H NMR $\Delta\nu_{1/2}$ as a function of η/T is shown in Figure 19 for both the 13 and 11 nm [$^2H_6$]TO rHDLs. As with the [$^2H_3$]CO rHDLs, the linewidths were broader in both sizes of DPPC-containing rHDL than in egg PC-containing rHDL at temperatures below 25°C. Above this temperature the linewidths were the same within experimental error. While the linewidth variation of the 13 and 11 nm [$^2H_6$]TO rHDLs differ slightly, the general trends are the same. Both the size distribution and chemical composition of

Figure 16: ^2H NMR spectra of [$^2H_6$]TO in HDL (diameter = 13 nm) reconstituted with either DPPC (a-d) or egg PC (e-h) as a function of temperature. The plot width is 1013 Hz in (a-c,e-g) and 500 Hz in (d) and (h). The solid line represents an iterative least squares fit to the data points (crosses). Spectral parameters: pulse width = 8 μs (flip angle = 90°). Sweep width = 5 kHz (a,b,e,f), 2 kHz (c,d,g,h). Number of acquisitions = 16,069 (a), 18,617 (b), 12,000 (c), 7,700 (d), 15,300 (e), 9,043 (f), 13,014 (g), 10,877 (h). Data sets = 2K (a,b,e,f), 1K zero-filled to 2K (d,h), 1K (c,g). Delay between pulses = 0.20 s (a,b,e,f), 0.26 s (c,d,g,h). Line broadening = 5 Hz (a,b,e,f), 4 Hz (c,g), 1 Hz (d,h). Delay before acquisition = 10 μs.

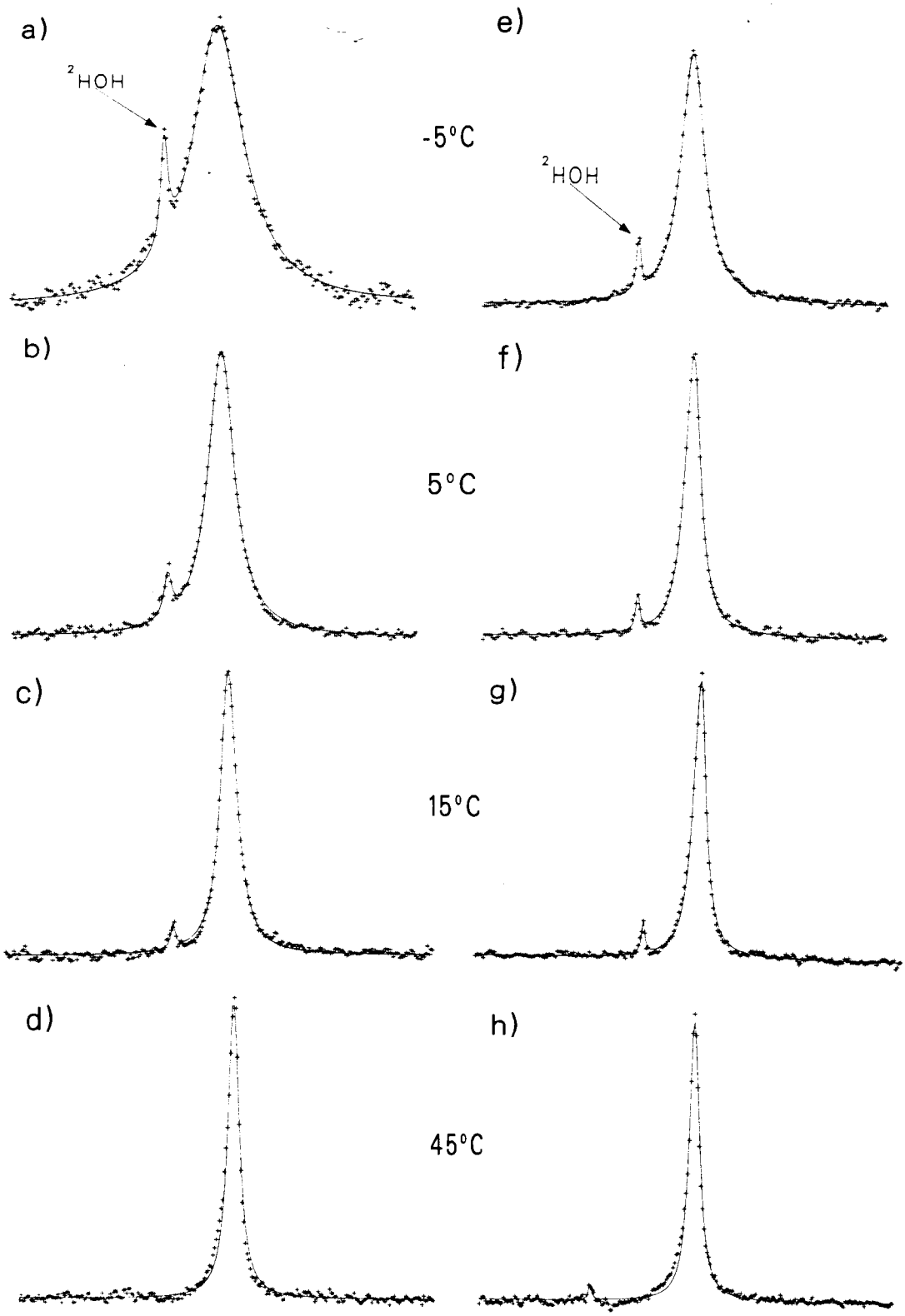
a)
^{2}HOH
e)
-5°C
^{2}HOH
b)
f)
5°C
c)
g)
15°C
d)
h)
45°C

Figure 17: ^2H NMR spectra of [$^2H_6$]TO in HDL (diameter = 11 nm) reconstituted with either DPPC (a-d) or egg PC (e-h) as a function of temperature. The solid line represents an iterative least squares fit to the data points (crosses). Spectral parameters: pulse width = 8 μs (flip angle = 90°). Sweep width = 10 kHz (a,b,e,f), 5 kHz (c,d,g,h). Number of acquisitions = 100,993 (a), 64,072 (b), 41,000 (c), 100,000 (d), 55,139 (e), 40,062 (f), 45,500 (g), 31,000 (h). Data sets = 2K zero-filled to 4K (a,b,e,h), 2K (c,d,g), 4K (f). Delay between pulses = 0.10 s (a,b,e), 0.20 s (c,d,f,g,h). Line broadening = 10 Hz (a), 5 Hz (b,e,f), 3 Hz (c,g), 2 Hz (d,h). Delay before acquisition = 10 μs.

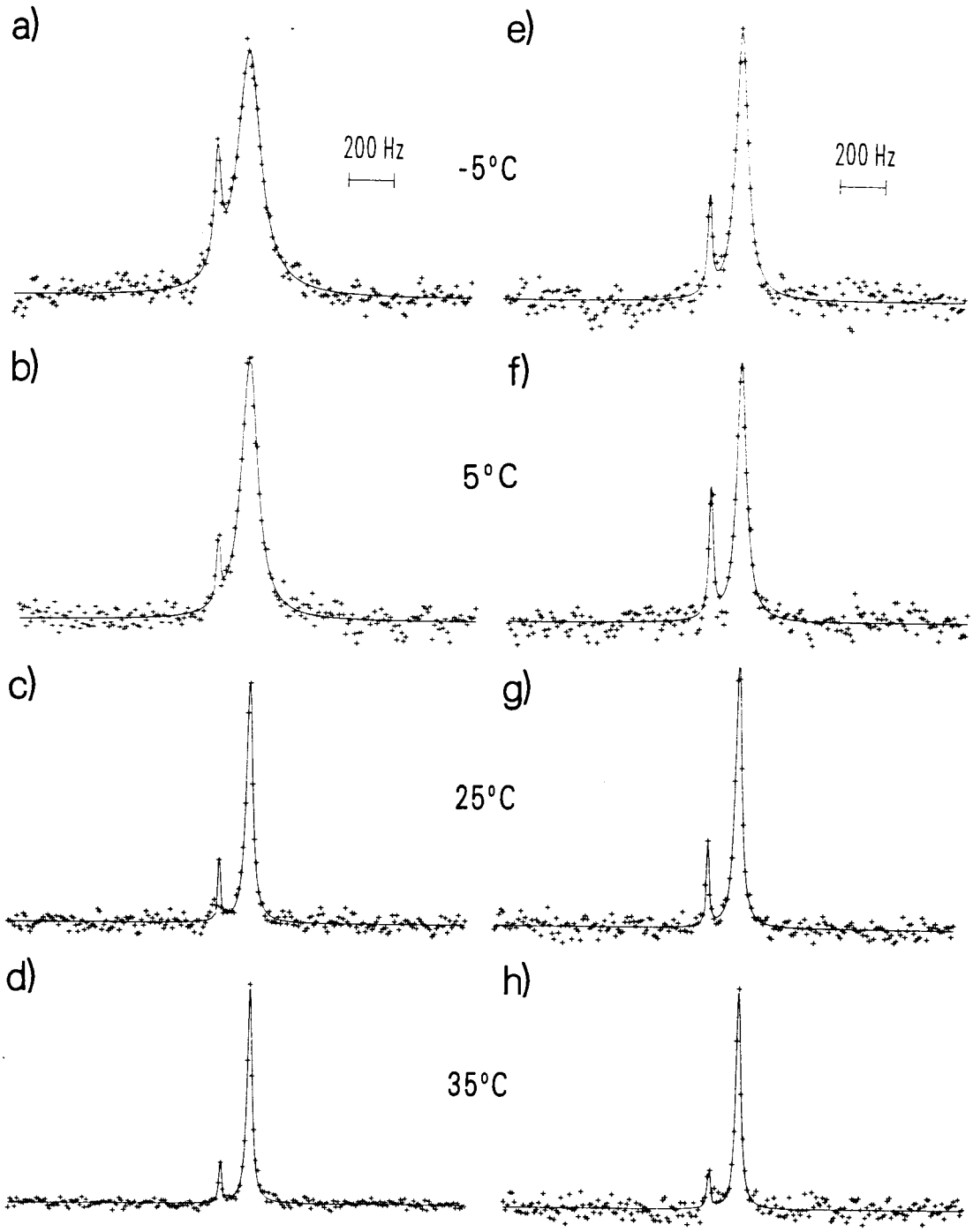
a)
200 Hz
-5°C
e)
200 Hz
b)
5°C
f)
c)
25°C
g)
d)
35°C
h)

Figure 18: Undecoupled ^{31}P NMR spectra of HDL reconstituted with [$^{2}H_{6}$]TO and either DPPC (a) or egg PC (b) at 25°C. The solid line represents an iterative least-squares fit of a single Lorentzian function to the data points (crosses), from which values for the linewidths $\Delta\nu_{1/2}$ of 55 (a) and 53 (b) Hz were obtained. For illustrative purposes, only every 4th point is plotted. Spectral parameters: pulse width = 5 μs (flip angle = 60°). Sweep width = 2 kHz. Number of acquisitions = 4500 (a), 3000 (b). Data sets = 2K. Delay between pulses = 1.5 s. Delay before acquisition = 10 μs. Line broadening = 5 Hz.

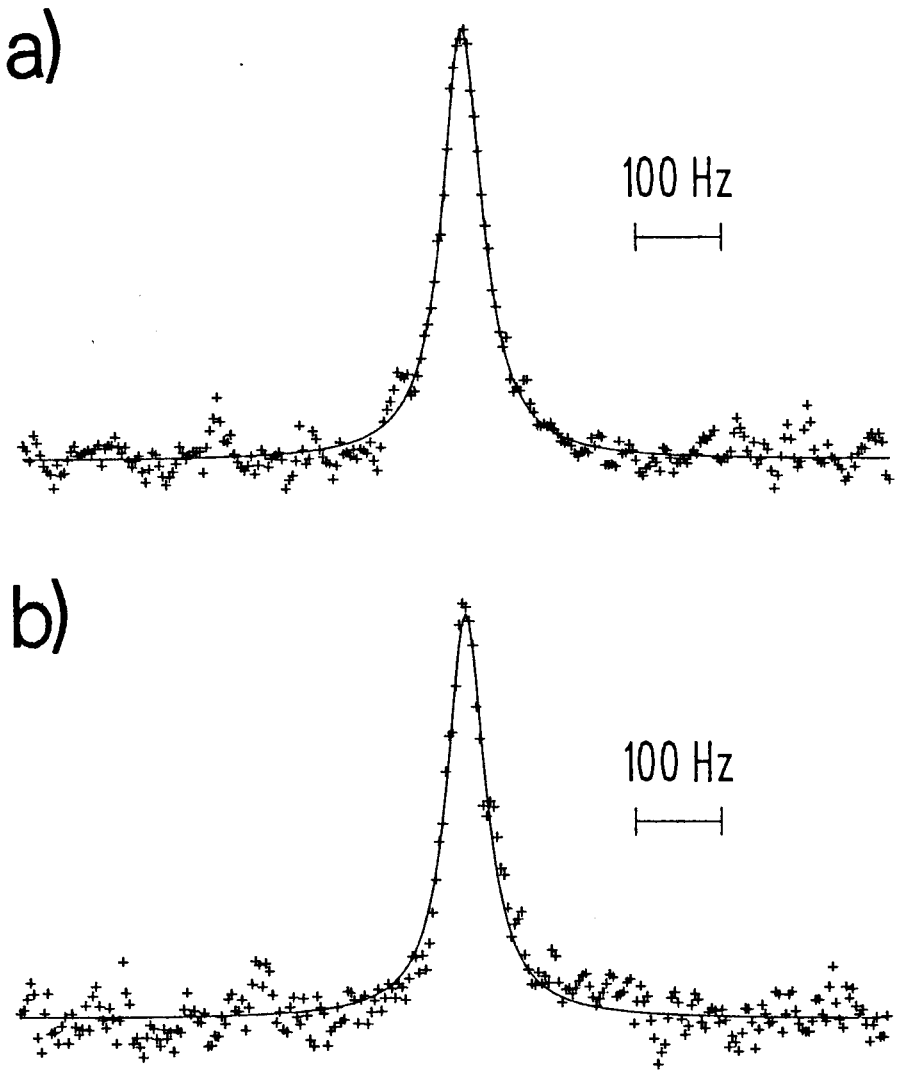
a)
100 Hz
b)
100 Hz

Figure 19: ^2H NMR linewidths $\Delta\nu_{1/2}$ of [$^2H_6$]TO rHDL containing either DPPC (circles) or egg PC (squares) as a function of η/T. The solid lines represent the 13 nm [$^2H_6$]TO/DPPC/apoHDL$_3$ (filled circles) and [$^2H_6$]TO/egg PC/apoHDL$_3$ (filled squares). The dashed lines represent the 11 nm [$^2H_6$]TO/DPPC/apoHDL$_3$ (open circles) and [$^2H_6$]TO/egg PC/apoHDL$_3$ (open squares). The curves are visual fits to the data points. The error bars represent an estimated uncertainty in the linewidths of ±10%.

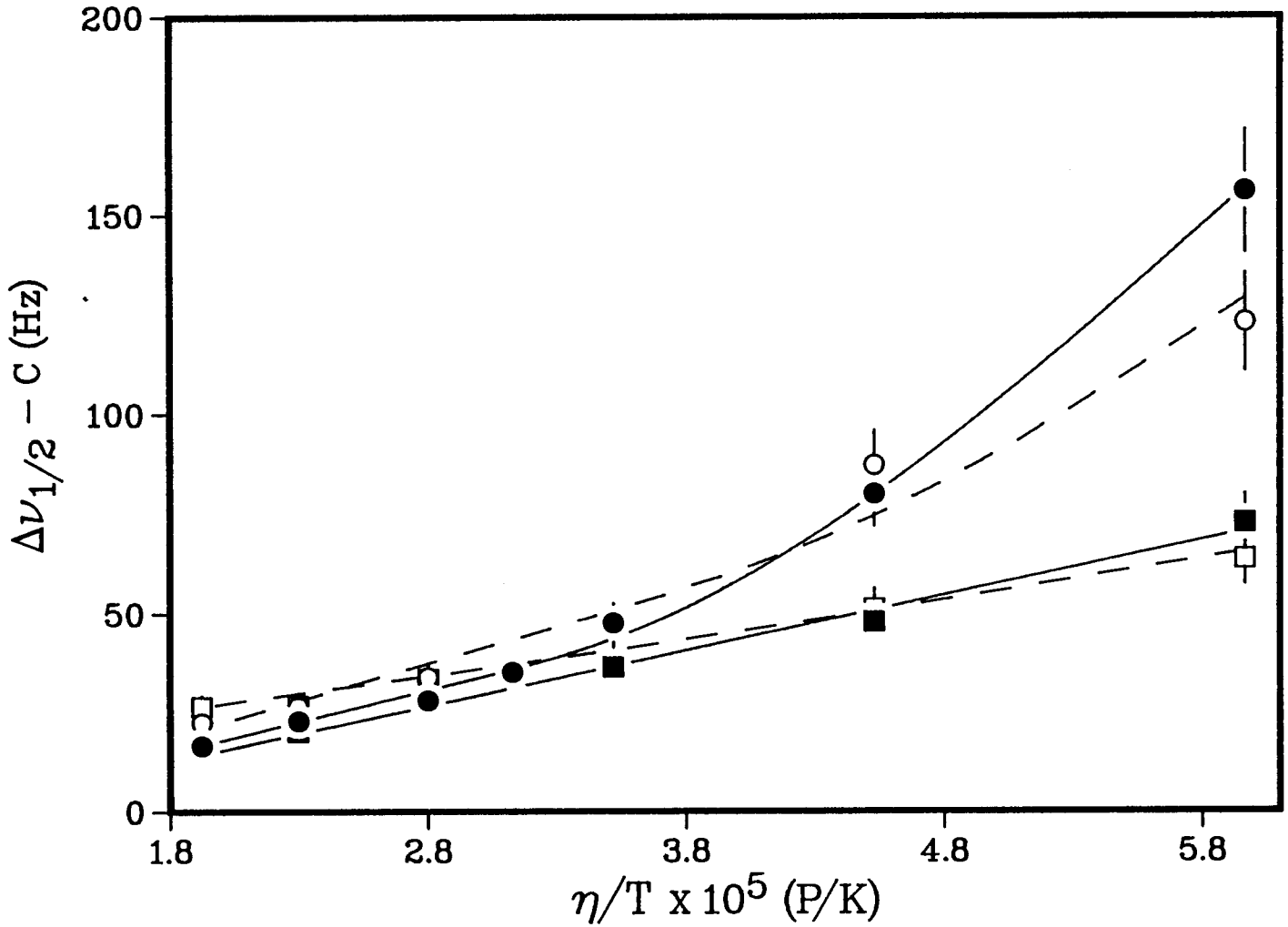
200
150
100
50
0
$\Delta\nu_{1/2} - C$ (Hz)
1.8
2.8
3.8
4.8
5.8
$\eta/T \times 10^5$ (P/K)

the 13 nm [$^2H_6$]TO/DPPC/apoHDL$_3$ and [$^2H_6$]TO/egg PC/apoHDL$_3$ are the same, and therefore the broader linewidths observed for [$^2H_6$]TO/DPPC/apoHDL$_3$ at low temperatures must originate from more restricted motions of the C$^2H_2$ groups, compared with the [$^2H_6$]TO/egg PC/apoHDL$_3$. Either of the mechanisms discussed above for [$^2H_3$]CO could account for this. The observation that the [$^2H_6$]TO linewidths are broader than those of [$^2H_3$]CO at any given temperature, implying higher order in the former, is explained by noting that the CO is labelled at the methyl group of the fatty acyl chain, which gives rise to narrower linewidths than do methylene positions. As well, the [$^2H_6$]TO rHDLs are significantly larger than the [$^2H_3$]CO rHDLs, which would lead to broader lines.

We assume that the effect of protein on the state of the core, if present at all, is approximately equal within each pair of [$^2H_3$]CO and [$^2H_6$]TO rHDLs, so that the differential effects we observe are attributed to phospholipid. Previous ^2H NMR studies of numerous protein-lipid systems have demonstrated a minimal effect of protein on lipid order (Bloom and Smith, 1985).

In order to determine whether the differential interactions between core component and the two monolayers had any effect on segmental reorientation rates, spin-lattice relaxation times T_1 were determined for the large [$^2H_6$]TO rHDLs at two temperatures. Plots of $\log(A_\infty - A_\tau)$ vs. τ are given in Figure 20 and the T_1 values are given in Table III. At -5°C, where the linewidth differences are largest, values of 17 and 19 ms were obtained for [$^2H_6$]TO/DPPC/apoHDL$_3$ and [$^2H_6$]TO/egg PC/apoHDL$_3$, which are the same within experimental error. Thus, the monolayer-core interactions appear to have no effect upon the rate of segmental motions. However, the

Figure 20: Plots of $\log(A_\infty - A_\tau)$ vs. τ for [$^2H_6$]TO/DPPC/apoHDL$_3$ at -5°C (a) and 25°C (b) and for [$^2H_6$]TO/egg PC/apoHDL$_3$ at -5°C (c) and 25°C (d). T_1's were measured by the inversion recovery method as described in the text.

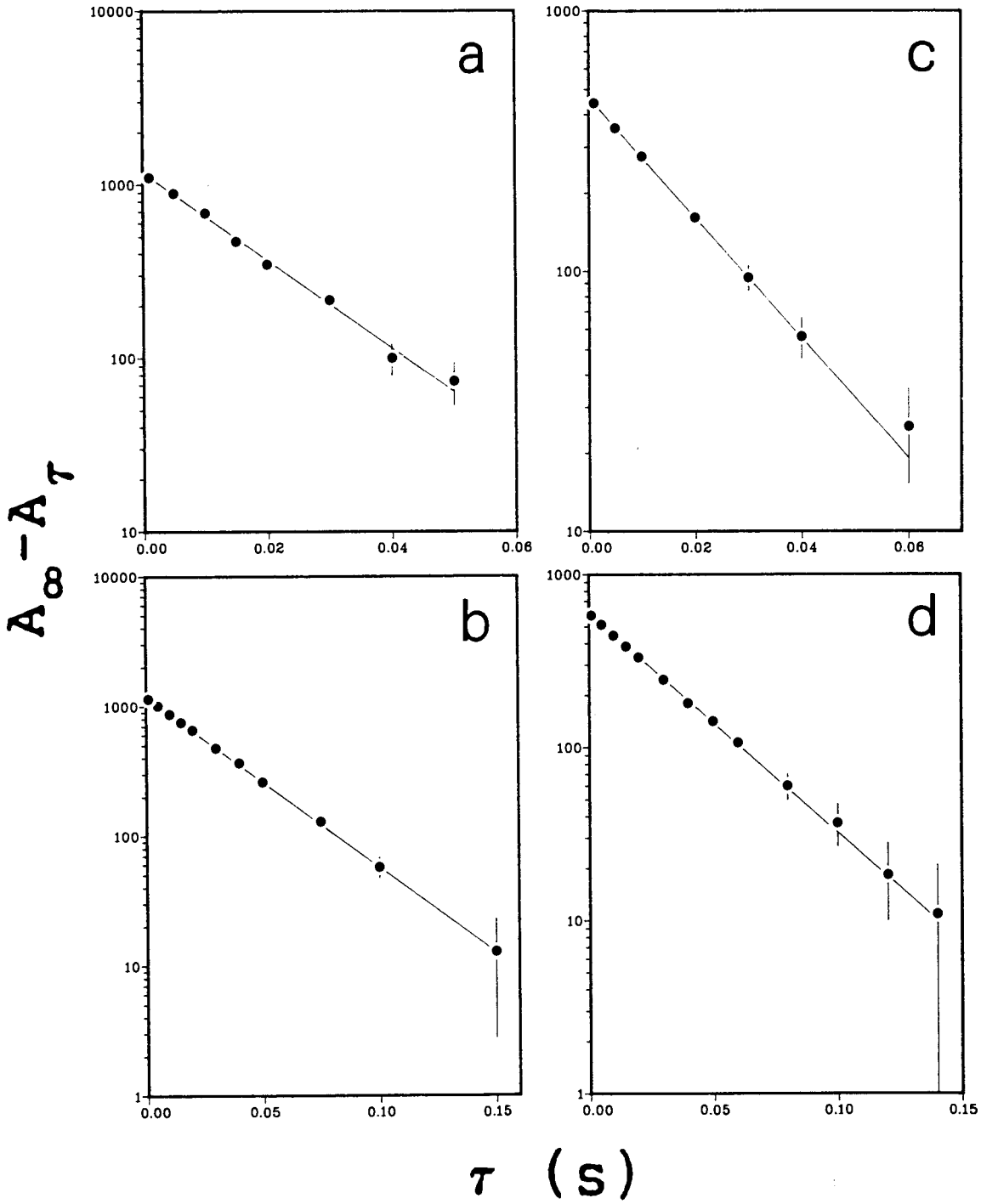
a
b
c
d
$A_\infty - A_\tau$
τ (s)
10000
1000
100
10
1
0.00
0.02
0.04
0.06
0.05
0.10
0.15

values obtained at 25°C (≃34 ms) are significantly different from the value of ≃60 ms observed at the same temperature for ≃2.5 mol% [$^2H_6$]TO incorporated into egg PC liposomes (Gorrissen *et al.*, 1982). This may indicate that the environment of triglycerides in the HDL core is significantly different from the environment in bilayers. It is also possible that the rapid tumbling of small particles such as HDL may influence T_1 (Parmar *et al.*, 1983).

In the case of native HDL, which contains triglycerides, the dynamic behaviour of the cholesteryl esters has been found to be comparable to cholesteryl ester/triglyceride mixtures by ^{13}C NMR measurements (Hamilton and Cordes, 1978). However, both the present study and that of Parmar *et al.*, (1983) demonstrate that cholesteryl esters in HDL can possess considerable motions in the absence of triglyceride, which we attribute largely to interactions with surface phospholipid.

Although the results from the [$^2H_3$]CO/egg PC/apoHDL$_3$ and [$^2H_6$]TO/egg PC/apoHDL$_3$ cannot be directly extrapolated to native HDL because of the simplicity of the model systems, the fatty acid composition of the phospholipid monolayers is similar (Scanu, 1979; Forrest, 1977). Therefore, it is possible that the existence of a state of disordered ester in native HDL above 0°C (Tall *et al.*, 1977; Jonas and Jung, 1975) can be partly explained on the basis of monolayer-core interactions. The greater compositional heterogeneity of the native system will also contribute to the disordering. Further studies using more complicated model systems are necessary to clarify this point.

Effect of Core on Monolayer.

The effect of different core components on the phospholipid monolayer was studied by comparing the temperature dependence of the ^2H NMR linewidths of [$^2H_2$]PC in [$^2H_2$]PC/CO/apoHDL$_3$ and [$^2H_2$]PC/TO/apoHDL$_3$. Representative ^2H NMR spectra of rHDL containing [$^2H_2$]PC and either CO or TO in the core are shown in Figure 21 as a function of temperature. The spectra can be simulated by single Lorentzian lineshape functions. Temperature-dependent linewidths for the two samples are given in Table VI, along with calculated values of the C-^2H order parameter, S_{CD} (see Theory).

The linewidths of [$^2H_2$]PC are seen to be broader at all temperatures in the particles containing CO than in those containing TO. Values of S_{CD} as a function of temperature are given in Table VI for [$^2H_2$]PC/CO/apoHDL$_3$ and [$^2H_2$]PC/TO/apoHDL$_3$, and a plot of S_{CD} versus T is given in Figure 22. The order parameter S_{CD} was determined from eq 19, using a value of D = 2 x 10^{-8} cm^2/s in the calculation. Values of D = (1.9±0.3)x 10^{-8} cm^2/s and D = (1.8±0.3) x 10^{-8} cm^2/s have been determined for phospholipids in HDL$_2$ using ^2H and ^{31}P NMR, respectively, and a value of D = (2.3±0.8)x 10^{-8} cm^2/s has been determined for HDL$_3$ using ^{31}P NMR (Cushley *et al.*, 1987; also see next section on phospholipid lateral diffusion).

In order to obtain order parameters from eq 19, it must be assumed that the mean diameter is a fair representation of all the particle sizes. In the case of HDLs, in which the particle sizes vary over ≤10 nm, this would appear to be a valid assumption, as the spectra of selectively deuterated positions can be fit by a single Lorentzian lineshape. Such is not the case for unilamellar vesicles, however, where sizes vary from 16 to 50 nm, and the ^2H NMR spectra resulting from selectively deuterated

Figure 21: ^2H NMR spectra of [$^2H_2$]PC in HDL reconstituted with either CO (a-d) or TO (e-h) as a function of temperature. The plot width is 10 kHz in all cases. The solid line represents an iterative least squares fit of Lorentzian functions to the data points (crosses). For illustrative purposes every third (a-c,g), fourth (d-f), or eighth (h) point is plotted. Spectral parameters: pulse width = 6.5 μs (flip angle = 90°). Sweep width = 10 kHz (d,h), 20 kHz (a-c,e-g). Number of acquisitions = 105,672 (a), 80,122 (b), 80,000 (c), 30,423 (d), 60,372 (e), 69,282 (f), 50,867 (g), 35,364 (h). Data sets = 2K (a-h). Delay between pulses = 0.1 s (d,h), 0.08 s (a-c,e-g). Line broadening = 70 Hz (a), 60 Hz (e), 50 Hz (b), 25 Hz (f), 15 Hz (c,g), 10 Hz (d,h). Delay before acquisition = 10 μs.

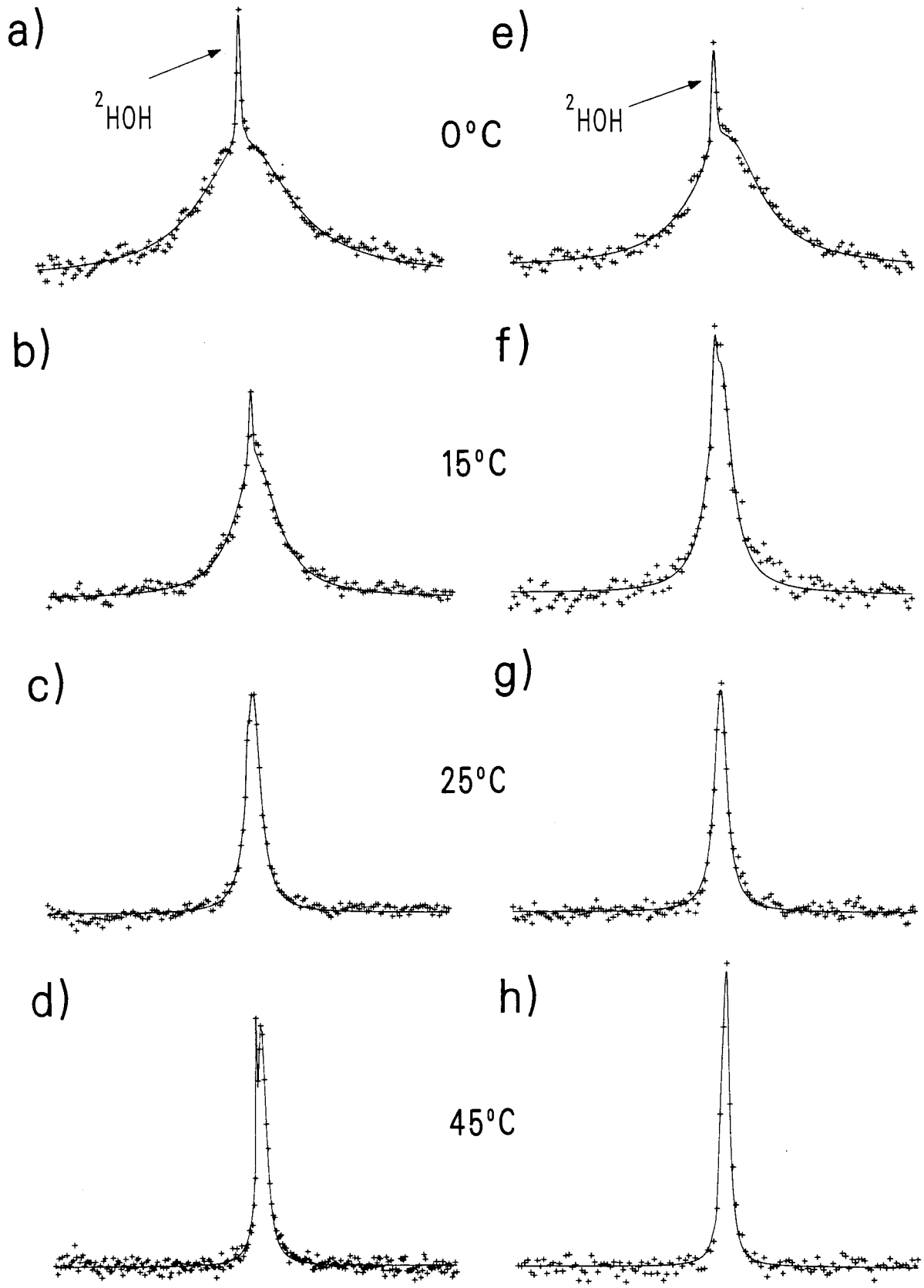
a)
^{2}HOH
e)
0°C
^{2}HOH
b)
f)
15°C
c)
g)
25°C
d)
h)
45°C

Table VI: Temperature dependent ^2H and ^{31}P NMR linewidths[a] of $[^2H_2]$PC in rHDL containing either cholesteryl oleate (CO) or triolein (TO).

T (°C)	CO			TO		
	$\Delta\nu_{1/2}$ (Hz)	S_{CD}[b]		$\Delta\nu_{1/2}$ (Hz)	S_{CD}[b]	
-5.0	3400	0.79		2684	0.66	
0.0	2718	0.75		2036	0.61	
2.5	2676	0.77		-		
5.0	2015	0.69		-	-	
6.0	-	-	[72[c]]	-	-	[74[c]]
7.5	2093	0.72		1096	0.49	
8.5	1917	0.70		-	-	
12.5	1420	0.63		-	-	
15.0	1303	0.62		684	0.42	
17.5	1013	0.56		-		
20.0	792	0.51		469	0.36	
22.5	707	0.49		-		
25.0	418	0.39	[59]	363	0.33	[60]
27.5	365	0.37		-	-	
32.5	375	0.39		271	0.31	
40.0	302	0.37		235	0.30	
45.0	258	0.36		216	0.31	

[a] Linewidths are accurate to ±10% and were obtained from an iterative least squares fit of the $[^2H_2]$PC resonance.

[b] Calculated using eq 19, assuming $D = 2 \times 10^{-8}$ cm²/s.

[c] The values in square brackets are ^{31}P NMR linewidths (Hz) obtained from an iterative least squares fit of the ^{31}P resonance of $[^2H_2]$PC.

Figure 22: Temperature dependence of the carbon-deuterium bond order parameter S_{CD} for [$^2H_2$]PC in rHDL containing either CO (circles) or TO (squares). The curves are visual fits to the data points.

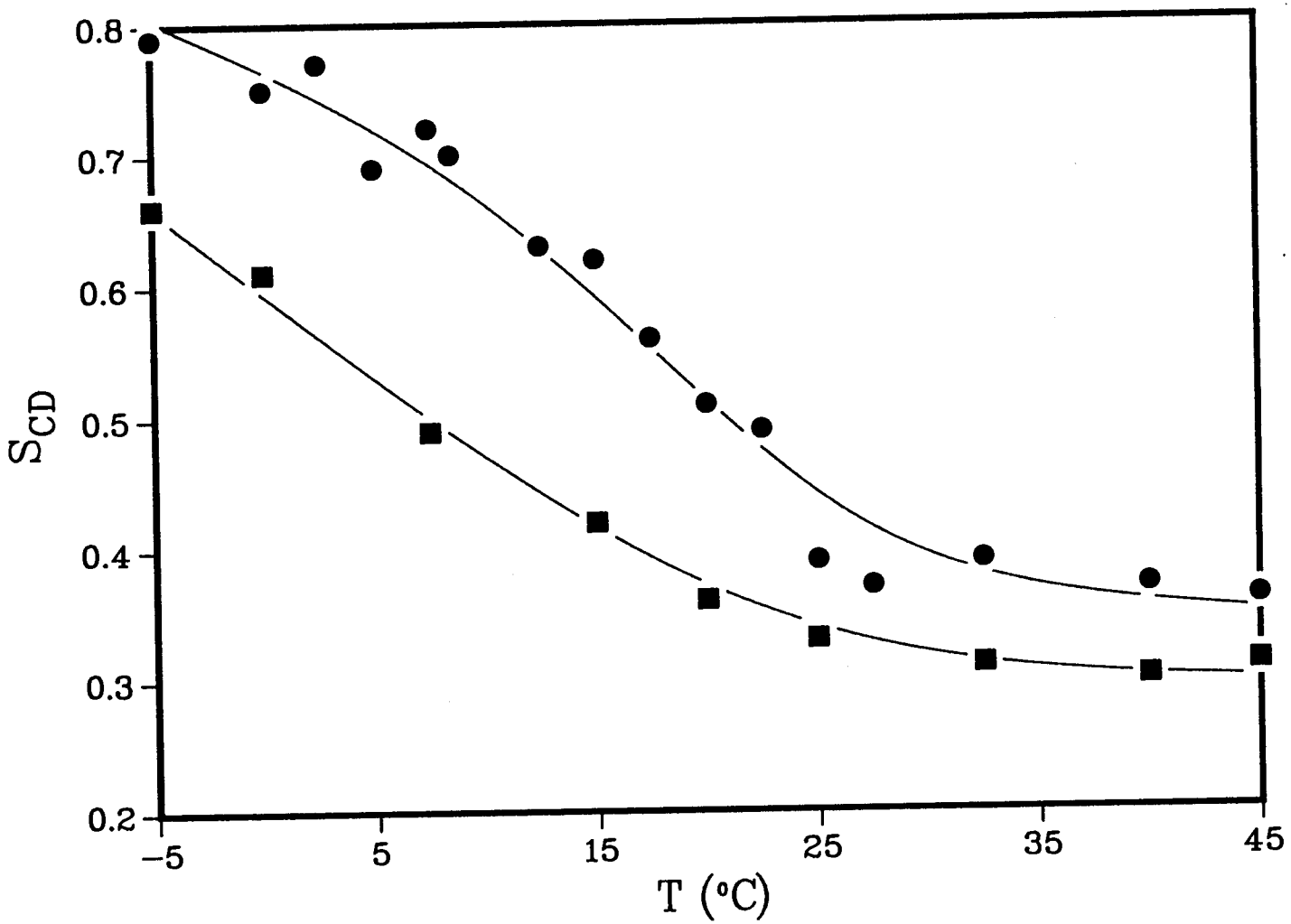
0.8
0.7
0.6
0.5
0.4
0.3
0.2
S_{CD}
−5
5
15
25
35
45
T (°C)

phospholipids or fatty acids are super-Lorentzian. In this case, S_{CD} was determined from simulations of super-Lorentzian lineshapes based on the distribution of particle sizes as determined by electron microscopy (Parmar, 1985). The order parameters of [$^2H_2$]PC/CO/apoHDL$_3$ have also been estimated at several temperatures using this approach. ^{2}H NMR spectra with computer simulations (neglecting the ^{2}HOH peak) are shown in Figure 23. Single Lorentzian fits to the spectra at 0 and 15°C are shown in Figure 21a and 21b. The values of S_{CD} obtained from the simulations are compared with values calculated from eq 19, neglecting T_1 effects, in Table VII. These values were found to be ≤5% higher than the single Lorentzian estimates, which is within the limit of ±10% error in linewidth. Hence, for the purposes of discussion, the S_{CD} values obtained from eq 19 will be used.

The values of S_{CD} = 0.39 and 0.33 obtained for [$^2H_2$]PC/CO/apoHDL$_3$ and [$^2H_2$]PC/TO/apoHDL$_3$ rHDLs, respectively, at 25°C, agree quite well with the values determined for native HDLs at approximately the same temperature. Values of S_{CD} = 0.37 (Parmar *et al.*, 1985) and 0.30 (Parmar, 1985) were obtained for ≤5 mol% of [5,5,6,6-$^2H_4$]palmitic acid incorporated into the monolayer of native HDL$_3$ and HDL$_2$, respectively. The deuterium T_1 values we obtained for [$^2H_2$]PC/CO/apoHDL$_3$ (16 ms) and [$^2H_2$]PC/TO/apoHDL$_3$ (14 ms) rHDLs (Table III) are also in close agreement with the values obtained for HDL$_3$ (16 ms) and HDL$_2$ (15 ms) (Parmar, 1985). Thus, the orientational order and relaxation rates of the phospholipid monolayer in the [$^2H_2$]PC/CO/apoHDL$_3$ and [$^2H_2$]PC/TO/apoHDL$_3$ systems at 25°C are essentially identical to the native systems. This further supports the use of simple model systems to elucidate properties of native lipoproteins.

Figure 23: Computer simulations of [$^2H_2$]PC/CO/apoHDL$_3$ based on electron micrograph size distribution from Figure 10c at 0 (a), 15 (b), 22.5 (c), 32.5 (d), and 40°C (e). The solid line is the computer simulated spectra for the value of S_{CD} which best fits the data points (crosses). The ^{2}HOH peak has been ignored.

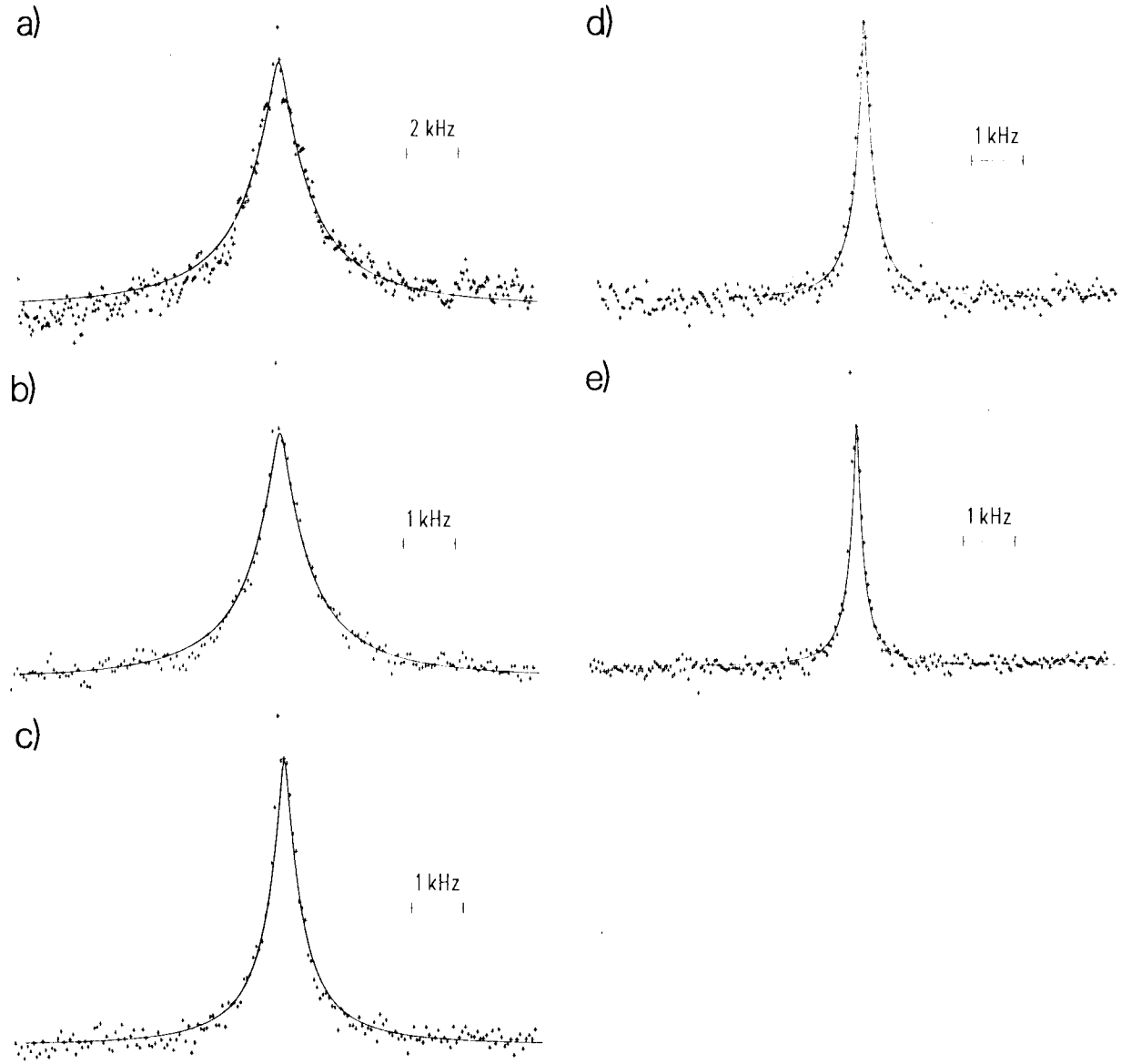
a)
2 kHz
b)
1 kHz
c)
1 kHz
d)
1 kHz
e)
1 kHz

Table VII: Order Parameters of [$^2H_2$]PC/CO/apoHDL$_3$ from super-Lorentzian simulations.

Temperature (°C)	S_{CD}	S_{CD} (single Lorentzian)
0	0.78	0.75
15	0.64	0.63
22.5	0.54	0.50
32.5	0.42	0.40
40	0.40	0.39

The order parameters of [$^2H_2$]PC in both the [$^2H_2$]PC/CO/apoHDL$_3$ and [$^2H_2$]PC/TO/apoHDL$_3$ decrease with increasing temperature, with the values of the [$^2H_2$]PC/CO/apoHDL$_3$ being larger over the entire temperature range (Figure 22). Over the range of -5 to 45°C, neat CO is a solid while neat TO is a liquid. Thus, we assume that CO in rHDL would be more ordered than TO at any given temperature. Although there may be too few molecules of each core component to form solid or liquid crystalline phases as found with neat components, some ordering of the core components (greater for CO than for TO) is expected on the basis of previous work with rHDL, in which considerable ordering of cholesteryl palmitate was observed (Parmar *et al.*, 1983). The larger values of S_{CD} observed with the [$^2H_2$]PC/CO/apoHDL$_3$ are then due to interactions of the PC acyl chains with the more ordered CO core.

The interactions observed between core and monolayer in the present study are maximal at low temperatures (Figures 14, 19, and 22). Above 25°C, the linewidths of the core lipids are the same within experimental error

whether egg PC or DPPC is present in the monolayer. However, S_{CD} of [$^2H_2$]PC is seen to be higher in rHDLs containing CO than in those containing TO at temperatures as high as 45°C (Figure 22) indicating that core-monolayer interactions are detected at physiological temperatures.

Over the temperature range studied, the order parameter versus temperature curve for the [$^2H_2$]PC/CO/apoHDL$_3$ is sigmoidal, whereas the [$^2H_2$]PC/TO/apoHDL$_3$ curve shows a smooth decrease with temperature. While the midpoint of the [$^2H_2$]PC/CO/apoHDL$_3$ curve of ≃18°C is very much less than the melting temperature of either DPPC multilamellar dispersions (42°C) or neat CO (51°C), large melting point depressions have been observed in other systems. For example, incorporation of ≃5 wt.% cholesteryl *cis*-parinarate into the core of LDL results in a 10-15°C depression in T_m of the core esters (Sklar *et al.*, 1982). Since ^2H NMR is more sensitive to changes in motional rates than bulk techniques such as DSC (Meier *et al.*, 1983; Thewalt *et al.*, 1986), it is possible that we are seeing small changes in cooperative motions of the phospholipids in the [$^2H_2$]PC/CO/apoHDL$_3$. Clearly, the order of the PC decreases with increasing temperature, with the shapes of the curves and the magnitude of the S_{CD} values influenced by the order of the core components.

The possibility of protein-lipid interactions contributing to the differential temperature behaviour of [$^2H_2$]PC in the [$^2H_2$]PC/CO/apoHDL$_3$ and [$^2H_2$]PC/TO/apoHDL$_3$ rHDLs seems unlikely since apoHDL$_3$ are surface proteins (Morrisett *et al.*, 1977) and in both cases the phospholipid is identical. Hence, the effects observed must originate from interactions with the core.

It is of considerable interest that the monolayer-core interaction is observable as far up the PC chain as the 5,5- position. In order to

determine whether the influence of the different cores of $[^2H_2]$PC/CO/apoHDL$_3$ and $[^2H_2]$PC/TO/apoHDL$_3$ extended to the headgroup region of the particles, ^{31}P NMR spectra of the rHDLs were recorded at 25 and 6°C. The spectra are shown in Figure 24, and the linewidths are given in Table VI. The linewidths of the two samples were essentially identical at each temperature, i.e., no differential effects originating from the core components were observed. The linewidths were slightly broader at 6°C, however ($\simeq$73 Hz compared to $\simeq$60 Hz at 25°C).

Our results with both the monolayer and core are most simply interpreted by a model wherein the core acyl chains interdigitate into the phospholipid monolayer. The fact that both core and monolayer are less ordered when in contact with lipids of lower order argues strongly for a direct interaction. Such a conclusion would be consistent with ^{2}H NMR studies of selectively deuterated cholesteryl palmitate in the core of rHDL (Parmar *et al.*, 1983), on the basis of which the ester was predicted to adopt an extended conformation. However, Hamilton and Cordes (1978) and Shen *et al.* (1977), on the basis of ^{13}C NMR and size/composition correlations, respectively, concluded that the core components exist in a separate liquid phase in HDL, with a sharply defined boundary between the hydrophobic core and the amphipathic layer surrounding it. In contrast, interdigitation of core components with phospholipid acyl chains is a feature of several models of HDL structure, based on size and compositional data (Verdery and Nichols, 1975), differential scanning calorimetry (Tall *et al.*, 1977), and X-ray diffraction (Laggner and Muller, 1978; Baumstark *et al.*, 1983). It is illustrative to apply the approach of Verdery and Nichols (1975) to our rHDL particles. For the purposes of discussion, we shall consider the $[^2H_3]$CO/$[^2H_2]$PC systems. From the size and compositional

Figure 24: ^{31}P NMR spectra of HDL reconstituted with [$^{2}H_{2}$]PC and either CO (a,b) or TO (c,d). The plot width is 1 kHz in all cases. The solid line represents an iterative least squares fit of a single Lorentzian function to the data points (crosses), from which values for the linewidths of 72 (a), 59 (b), 74 (c), and 60 (d) Hz were obtained. Spectral parameters: pulse width = 5.0 us (flip angle = 60°). Sweep width = 2 kHz. Number of acquisitions = 2173 (a), 1275 (b), 5677 (c), 1320 (d). Data sets = 2K. Delay between pulses = 1.8 s. Line broadening = 5 Hz. Delay before acquisition = 10 μs.

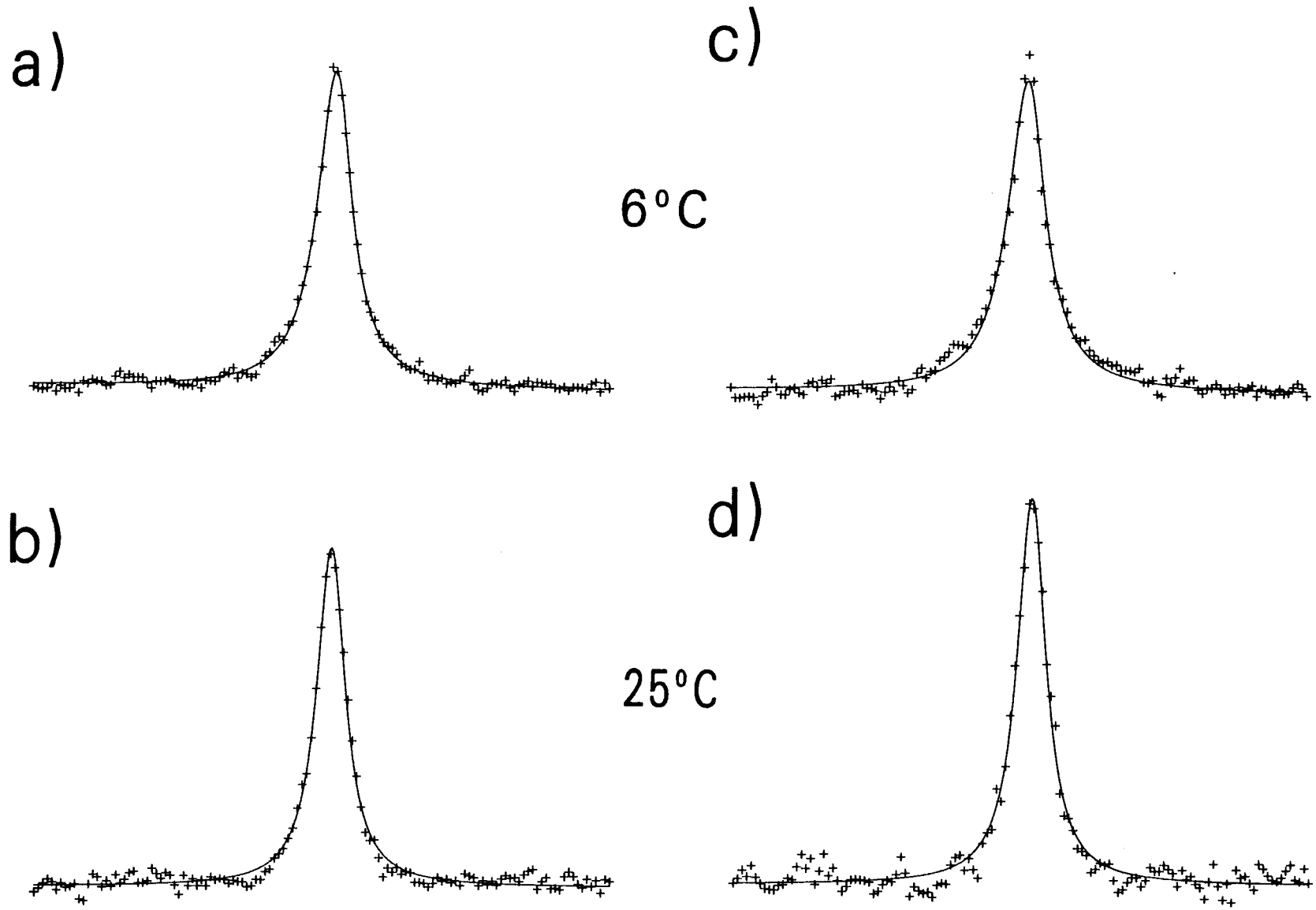
a)
c)
6°C
b)
d)
25°C

data in Table III, the number of molecules of protein, phospholipid, cholesteryl ester, and triglyceride in the four HDL samples can be calculated. Then, using the given molecular volumes of the constituent lipids and protein (Verdery and Nichols, 1975), the volume occupied by each domain can be estimated. In such an approach, it is common to divide HDL into (i) a polar surface containing protein and phospholipid headgroups, (ii) an outer hydrophobic core, $\simeq$ 2 nm thick, consisting of the fatty acyl chains of the phospholipid, and (iii) an inner hydrophobic core, extending to the center of the particle. For an rHDL of radius 4.5 nm, the total volume is 382 nm^3, with the polar surface occupying $\simeq$197 nm^3, the outer hydrophobic core $\simeq$170 nm^3, and the inner hydrophobic core $\simeq$15 nm^3 (average values from all four rHDL samples). The inner hydrophobic core ($\simeq$15 nm^3) is clearly far too small to contain all of the CO or TO molecules ($\simeq$68 nm^3), and the volume of the PC acyl chains ($\simeq$112 nm^3) is too small to fill the outer hydrophobic core ($\simeq$170 nm^3). This demonstrates that there is room in the outer hydrophobic core to accomodate some ester or triglyceride. In fact, the volume of the PC acyl chains plus esters or triglycerides ($\simeq$176 nm^3) is approximately equal to the volume of the two hydrophobic cores ($\simeq$185 nm^3). Further support for this view comes from the most recent x-ray diffraction data for HDL_3 (Baumstark *et al.*, 1983), in which a new evaluation theory was used to obtain the radial electron densities of three HDL subfractions. Based on their data, one can show that only $\simeq$6 nm^3 are available to form a separate core region in which no phospholipid acyl chains are located. Thus, an intrusion of the core components into the phospholipid monolayer seems highly probable. A notion which tempts speculation is whether the majority of esters orient with the acyl chains or cholesterol moieties protruding into the phospholipid chains. Verdery

and Nichols (1975) have suggested that in HDL_2 the esters are extended with the steroid moiety in the monolayer and the acyl chains in the core, whereas in HDL_3 the majority of esters are in the horseshoe conformation. In contrast, the data of Baumstark *et al.* (1983) suggests that the fatty acyl chains of both cholesteryl ester and phospholipid occupy together the outer hydrophobic core mentioned above. Our results suggest that a significant proportion of CO methyl groups and TO methylene groups are in contact with the monolayer, which would be consistent with the model of Baumstark *et al.* (1983).

While the data is consistent with an interdigitation model, the results do not provide proof of this view. However, other explanations of the data pose their own problems. For example, exclusion and compression of the core as a result of monolayer chain extension at low temperatures explains the effect of monolayer on core, but fails to explain the reverse effect, that of core on monolayer. While the present study demonstrates the existence of core-monolayer interactions, further studies are necessary to clarify the precise mechanism, and to see whether these observations extend to the other classes of lipoproteins.

Lateral Diffusion and Chemical Shift Anisotropy of Phospholipids in LDL and HDL_3

Measurement of D and Δσ in LDL at 25 and 45°C

The two major phospholipids found in LDL are phosphatidylcholine (PC) and sphingomyelin (SPM). PC is the more abundant, accounting for ≃65% of the total phospholipid (Scanu, 1973). The ^{31}P NMR linewidths of the PC and SPM resonances of LDL at 25°C are equal (≃70 Hz), suggesting that these lipids are homogeneously mixed in the monolayer. This is also the case for the native HDLs (Parmar, 1985). The lateral diffusion coefficients of these phospholipids have been measured using the method of Cullis (1976), whereby increasing concentrations of glycerol are used to broaden the ^{31}P linewidths. As the particle tumbling is slowed, diffusion becomes the dominant mechanism of line narrowing. By combining eq 12 to 15, the linewidth can be expressed as

$$(\Delta\nu_{1/2} - C)^{-1} = \eta^{-1}(3kT/4\pi R^3M_2) + (6D/R^2M_2). \qquad (27)$$

A plot of $(\Delta\nu_{1/2} - C)^{-1}$ versus η^{-1} gives a straight line from which the diffusion coefficient D can be obtained from the ratio of intercept to slope:

$$D = ((\text{intercept}/\text{slope})kT)/(8\pi R). \qquad (28)$$

The value of the second moment M_2, as defined in eq 26, can be obtained from the slope of eq 27 by $M_2 = 3kT/((\text{slope})4\pi R^3)$.

Representative ^{31}P NMR spectra of LDL in the presence of increasing concentrations of glycerol at 25°C are shown in Figure 25. The linewidths of the two resonances broaden and coalesce as the solvent viscosity is

Figure 25: Representative ^{31}P NMR spectra of LDL in the presence of increasing concentrations of glycerol at 25°C. The solid line represents an iterative least-squares fit of two (a-c) and one (d) Lorentzian function(s) to the data points (crosses). The concentrations of glycerol (weight-%) were approximately 0 (a), 21 (b), 47 (c), and 65 (d). Spectral parameters: pulse width = 5 μs (60°); sweep width = 10 kHz (a,b), 20 kHz (c), 50 kHz (d); number of acquisitions = 50,000 (a), 8,606 (b), 40,000 (c), 40,000 (d); data sets = 2K zero-filled to 4K; delay between pulses = 1.5 s; delay before acquisition = 10 μs; line broadening = 3 Hz (a), 5 Hz (b), 10 Hz (c), 40 Hz (d).

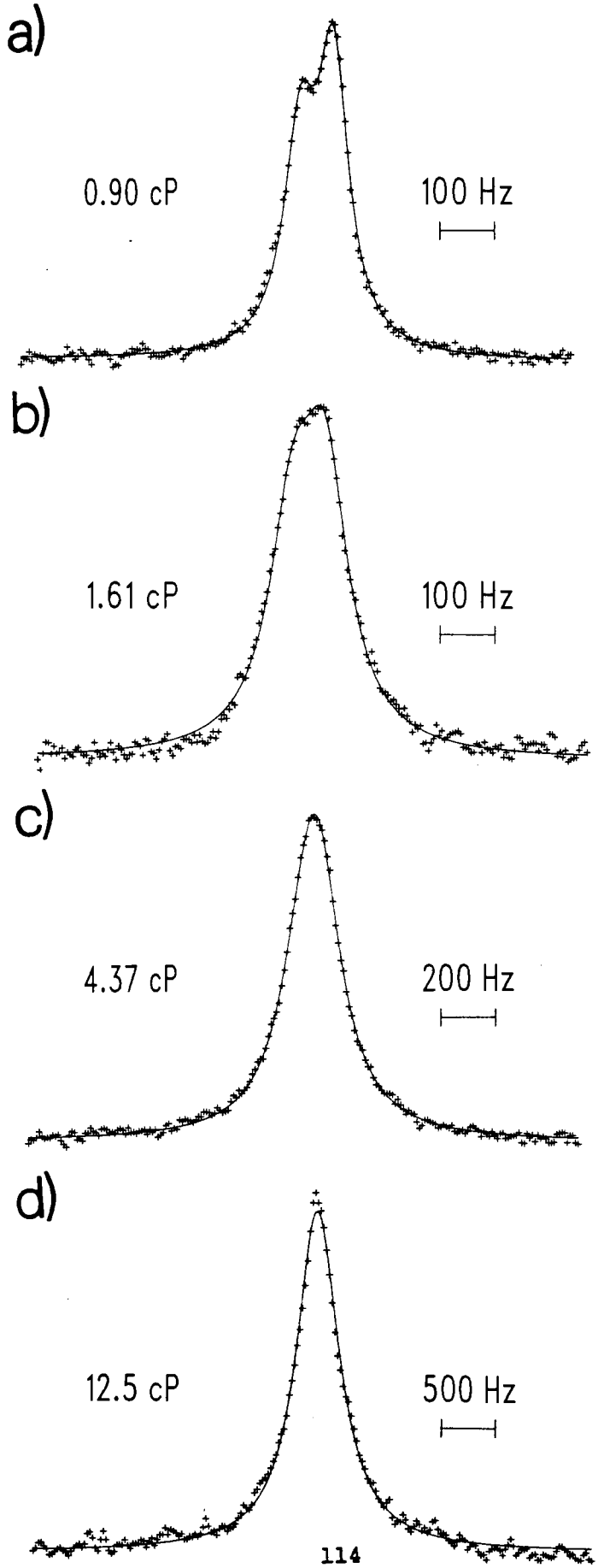
a)
0.90 cP
100 Hz
b)
1.61 cP
100 Hz
c)
4.37 cP
200 Hz
d)
12.5 cP
500 Hz

increased. The linewidths, given in Table VIII, were obtained from computer fits of the spectra to Lorentzian functions. The spectra in Figure 25(a) to (c) were fit with 2 Lorentzian functions, in which the peak separations were fixed at 60 Hz. However, at viscosities >4.4 cP, the two resonances could not be resolved and the spectra were fit with a single Lorentzian function. This may overestimate the linewidths slightly, but the errors should be small. No evidence of broad resonances due to immobilized lipid was observed over a 50 kHz sweep width (using a 60° pulse and a 10 second delay between pulses). No broad resonances can be observed in VLDL over a 50 kHz sweep width (R. S. Chana, unpublished results).

A plot of $(\Delta\nu_{1/2} - C)^{-1}$ versus η^{-1} is shown in Figure 26. The solid line is a weighted least-squares fit to the data points. In order to obtain D, the radius of the LDL particle and the value of the constant C must be known. The LDL radius was determined from QELS of LDL in 0.15 *M* NaCl 0.02% Na_2EDTA pH 7.5 to be 12 nm. The constant C, usually taken as the isotropic linewidth of the phospholipid, was determined to be ≃15 Hz from ^{31}P NMR of egg PC in chloroform/methanol (2:1) (Parmar, 1985). From eq 28, D was determined to be (1.4±0.5) x 10^{-9} cm^2/s. This is approximately an order of magnitude slower than observed in phospholipid bilayers (Mackay *et al.*, 1978 and references therein).

From eq 26 and 27, the value of $\Delta\sigma$ was found to be 49±1 ppm for LDL at 25°C. In order to see how the calculated values of D and $\Delta\sigma$ fit the experimental data points, a plot of $\Delta\nu_{1/2}$ versus η was constructed for several values of D ($\Delta\sigma$ = 49 ppm). This is shown in Figure 27. A good fit to the data points is obtained for D = 1.4 x 10^{-9} cm^2/s. Values of D a half-order of magnitude greater and smaller are outside the range of the

Table VIII: ^{31}P NMR linewidths of LDL as a function of solvent viscosity at 25°C.

η (cP)	$\Delta\nu_{1/2}$ (Hz)
0.90	69.6
1.16	72.9
1.61	102
2.03	114
2.72	139
4.37	206
7.27	299
12.5	470
22.0	859
28.1	1085
47.1	1648

error bars at viscosities >5 cP.

The value of $\Delta\sigma$ = 49±1 ppm obtained from the viscosity measurements is very close to $\Delta\sigma \simeq 45$ ppm observed in DPPC bilayers in the liquid crystalline phase at 48°C (Seelig, 1978). However, as it is possible that the glycerol may affect the orientation of the head group, especially at higher concentrations, we have also measured $\Delta\sigma$ from the field-dependence of the ^{31}P NMR linewidths. From eq 12 and 26, it can be seen that

$$(\Delta\nu_{1/2} - C) = (16/45)\pi\nu_0^2\Delta\sigma^2\tau_e \qquad (29)$$

where τ_e is defined in eq 13. $\Delta\sigma$ is obtained from a plot of $(\Delta\nu_{1/2} - C)$ versus ν_0^2. We have obtained the ^{31}P NMR spectra of LDL at three fields, and the linewidths are given in Table IX. From the plot in Figure 28, a

Figure 26: A plot of $(\Delta\nu_{1/2} - C)^{-1}$ versus η^{-1} for the ^{31}P NMR resonances of LDL at 25°C.

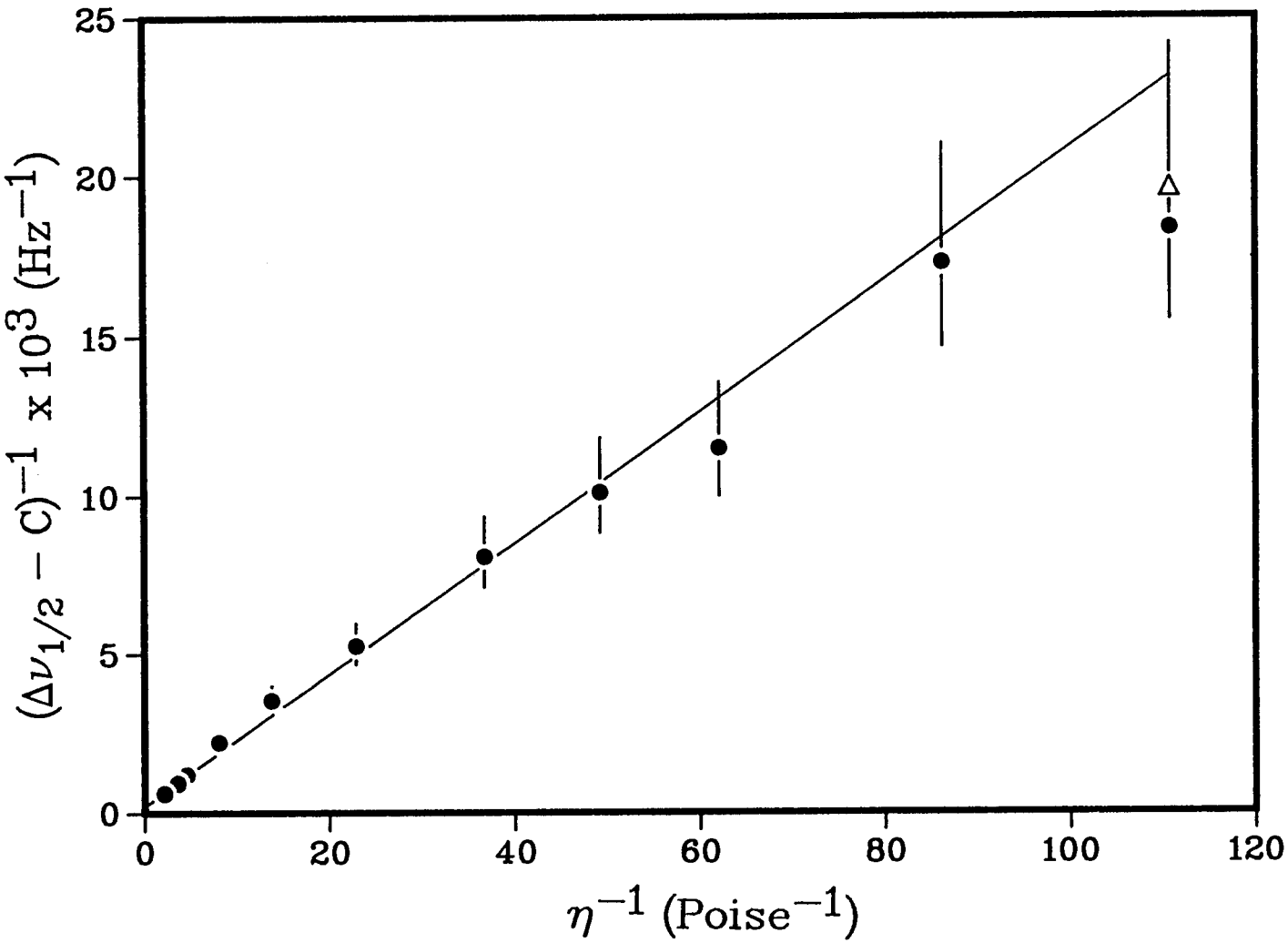
25
20
15
10
5
0
0
20
40
60
80
100
120
$(\Delta\nu_{1/2} - C)^{-1}$ x 10^3 (Hz^{-1})
η^{-1} (Poise^{-1})

Figure 27: ^{31}P NMR Linewidths of LDL as a Function of Solvent Viscosity at 25°C for D = 1 x 10^{-10} (a), 5 x 10^{-10} (b), 1.4 x 10^{-9} (c), 5 x 10^{-9} (d), 1 x 10^{-8} cm^2/s (e). The value of $\Delta\sigma$ was 49 ppm.

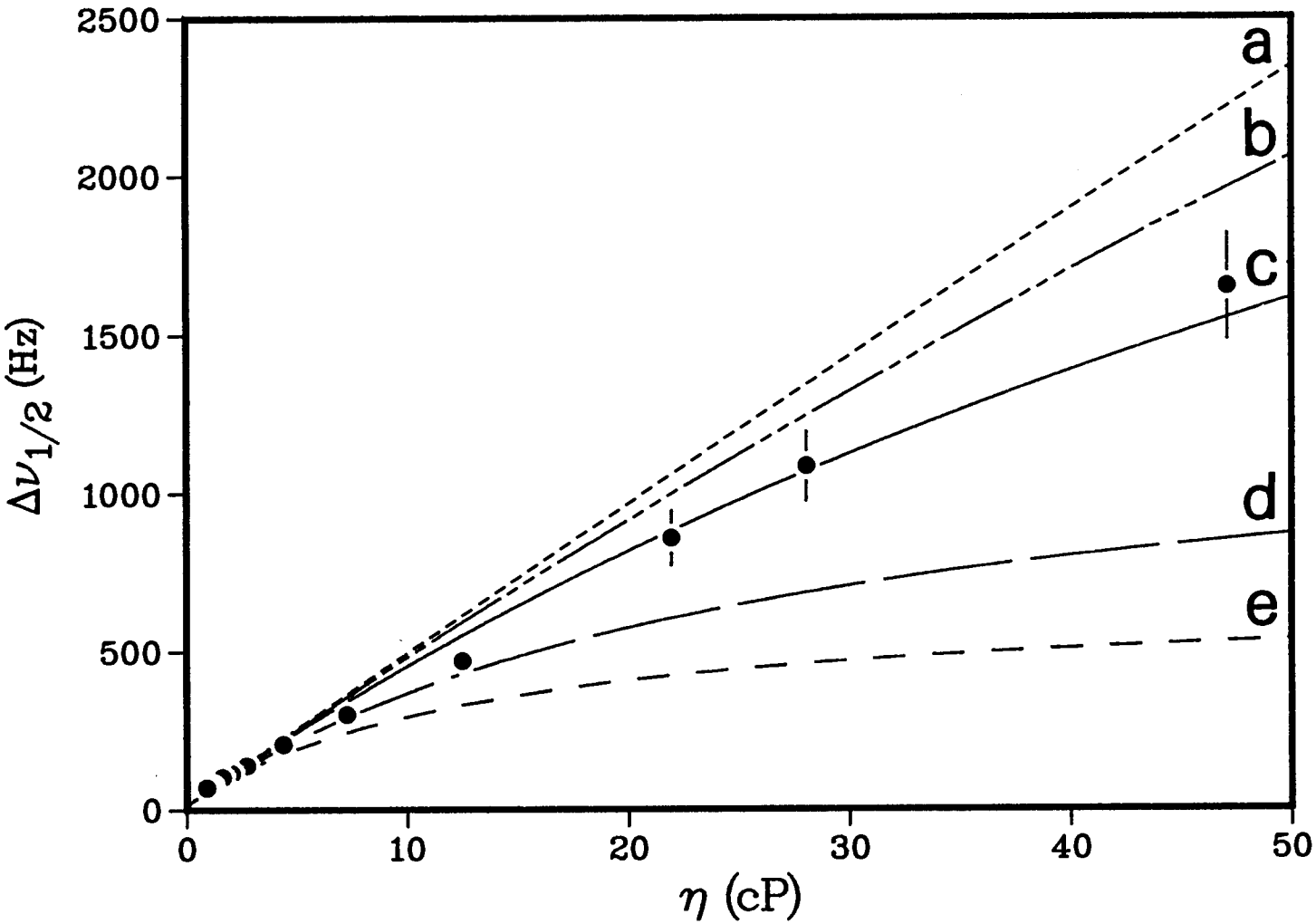
2500
2000
1500
1000
500
0
$\Delta\nu_{1/2}$ (Hz)
0
10
20
30
40
50
η (cP)
a
b
c
d
e

Table IX: ^{31}P NMR linewidths of LDL as a function of resonance frequency at 25°C.

ν_0 (MHz)	$\Delta\nu_{1/2}$ (Hz)
40.5	22
102.2	70
161.8	120

value of $\Delta\sigma$ = 50±4 ppm was obtained, in excellent agreement with the viscosity studies. This suggests that glycerol has a negligible effect on the order and orientation of the phospholipid head groups in LDL. This was verified by incubating LDL in 53 weight-% glycerol for 22 hours at 25°C, following which the glycerol was removed by exhaustive dialysis against 0.15 *M* NaCl 0.02% Na_2EDTA pH 7.5. Both the ^{31}P linewidths and mean diameters (determined by QELS) were found to be the same within experimental error before and after glycerol treatment, indicating that permanent changes in LDL structure are not induced by the glycerol. Parmar (1985) has previously shown that the linewidth changes caused by the addition of glycerol are reversible in HDL_2.

As phospholipid diffusion in LDL at 25°C is an order of magnitude slower than in phospholipid bilayers, we have also measured D at 45°C. Representative spectra are shown in Figure 29, and a table of linewidths versus solvent viscosity is given in Table X. In both Tables VIII and X, the highest viscosity measured was 80% glycerol by weight. From the double reciprocal plot shown in Figure 30, D = (1.1±0.2) x 10^{-8} cm^2/s and $\Delta\sigma$ = 52±2 ppm were obtained for LDL at 45°C. While the value of D was found to

Figure 28: $(\Delta\nu_{1/2} - C)$ as a function of ν_δ^2 for LDL at 25°C. The straight line is a weighted least-squares fit to the data points.

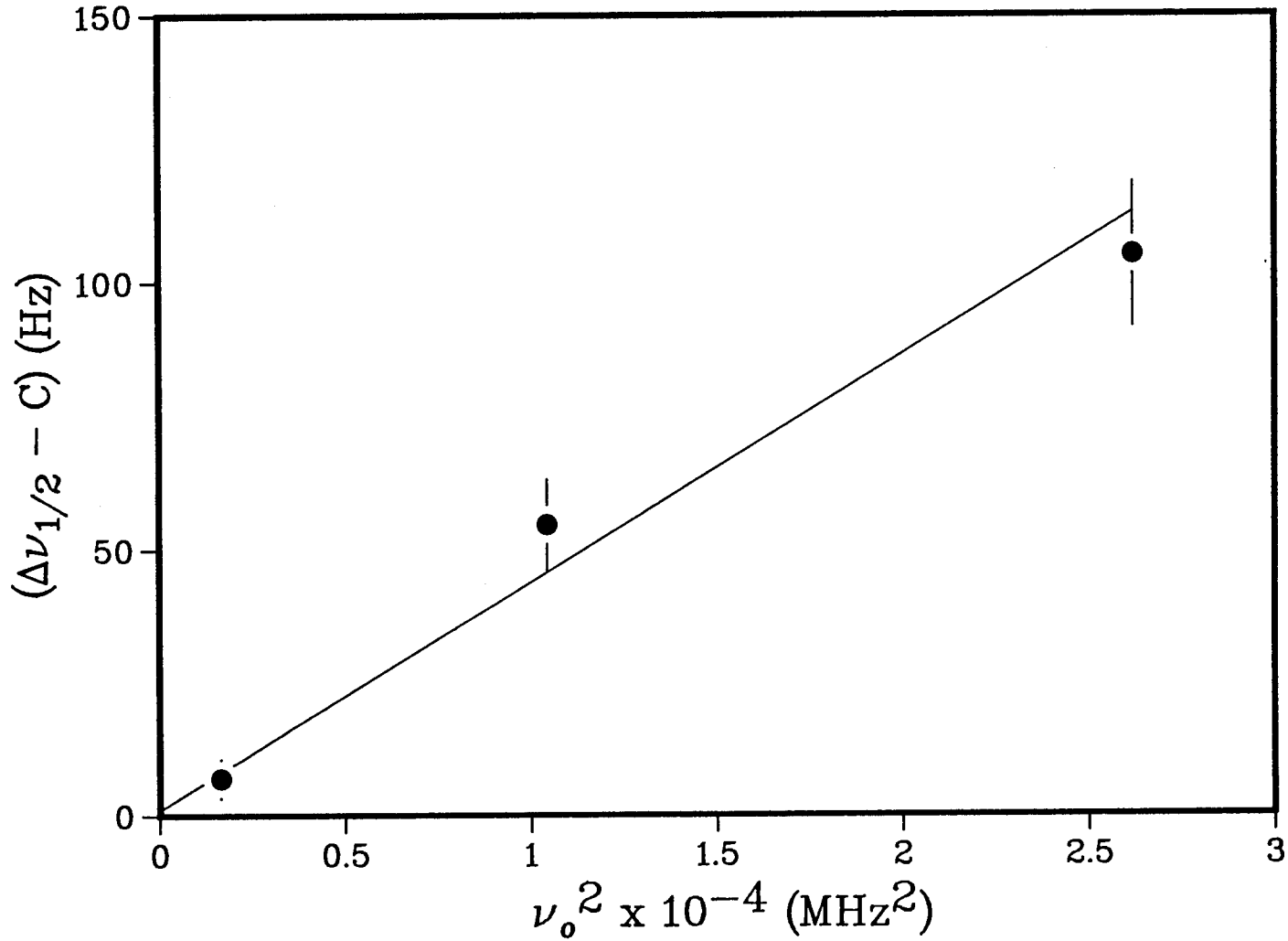
150
100
50
0
0
0.5
1
1.5
2
2.5
3
$(\Delta\nu_{1/2} - C)$ (Hz)
ν_o^2 x 10^{-4} (MHz^2)

Figure 29: Representative ^{31}P NMR spectra of LDL in the presence of increasing concentrations of glycerol at 45°C. The solid line represents an iterative least-squares fit of two (a,b) and one (c,d) Lorentzian function(s) to the data points (crosses). The concentrations of glycerol (weight-%) were approximately 0 (a), 40 (b), 72 (c), and 75 (d). Spectral parameters: pulse width = 5 μs (60°); sweep width = 5 kHz (a), 10 kHz (c-d); number of acquisitions = 35,393 (a), 12,000 (b), 30,000 (c), 30,000 (d); data sets = 4K; delay between pulses = 1.5 s; delay before acquisition = 10 μs; line broadening = 2 Hz (a), 10 Hz (b), 20 Hz (c), 30 Hz (d).

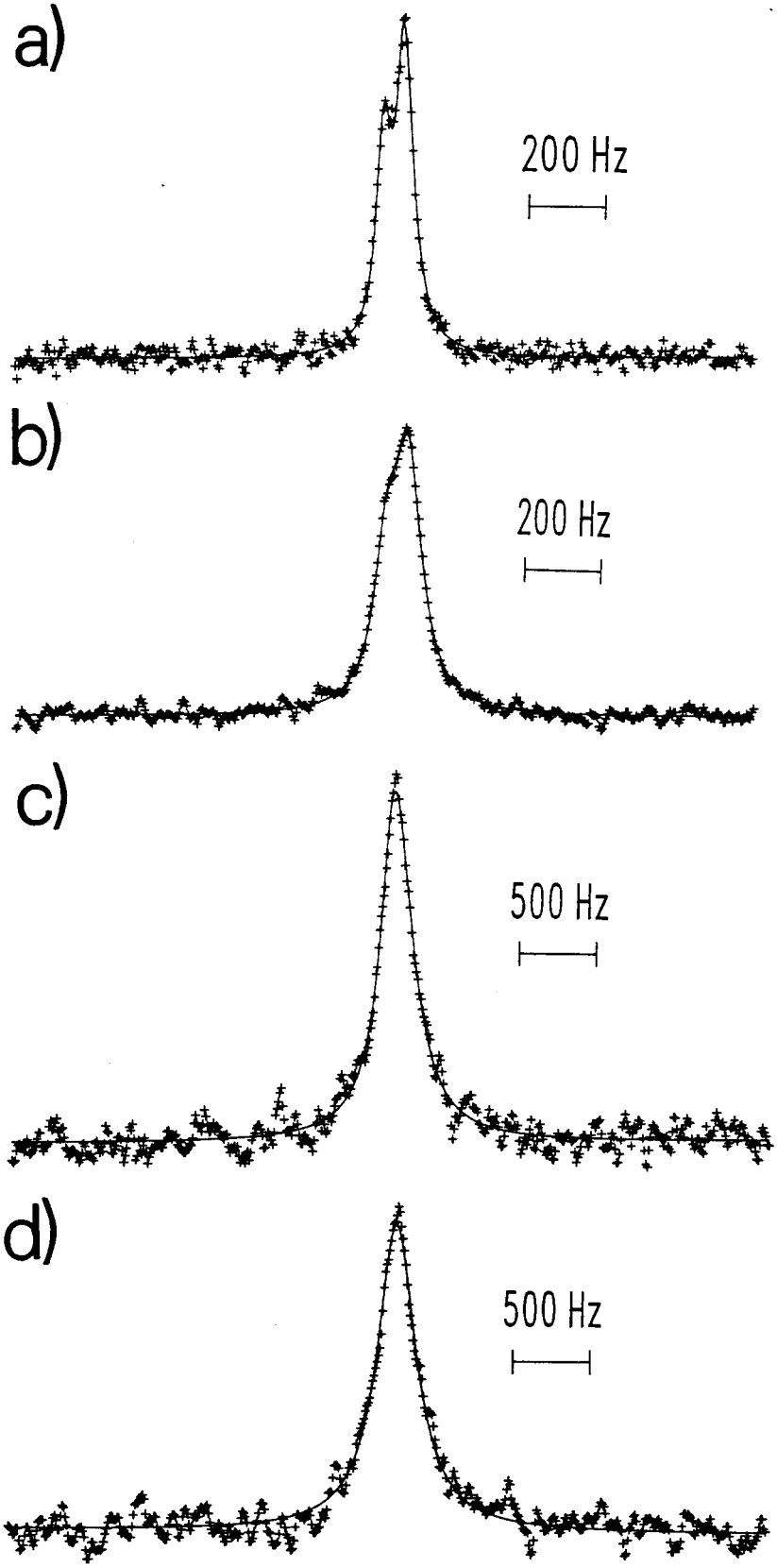
a)
200 Hz
b)
200 Hz
c)
500 Hz
d)
500 Hz

Table X: ^{31}P NMR Linewidths of LDL as a Function of Solvent Viscosity at 45°C.

η (cP)	$\Delta\nu_{1/2}$ (Hz)
0.61	50.8
0.80	60.1
1.00	60.2
1.24	64.0
1.94	89.2
2.66	121
9.32	263
11.9	317
18.0	431

increase by an order of magnitude going from 25 to 45°C, $\Delta\sigma$ remained essentially unchanged. This mirrors the insensitivity of $\Delta\sigma$ to temperature in DPPC bilayers above the gel-to-liquid crystalline phase transition (T > 41°C) (Seelig, 1978).

A plot of $\Delta\nu_{1/2}$ versus η is shown in Figure 31 for LDL at 45°C. The curve for D = 1.1 x 10^{-8} cm^2/s gives a good fit to the data points, and is clearly distinguished from diffusion a half-order of magnitude faster or slower.

Measurement of D and $\Delta\sigma$ in HDL_3 at 25°C.

Representative ^{31}P NMR spectra of HDL_3 in the presence of increasing concentrations of glycerol at 25°C are shown in Figure 32. The linewidths of the two phospholipids are equal. Again, increasing solvent viscosity

Figure 30: A plot of $(\Delta\nu_{1/2} - C)^{-1}$ versus η^{-1} for the ^{31}P NMR resonances of LDL at 45°C. For this sample of LDL, R = 11.8 nm.

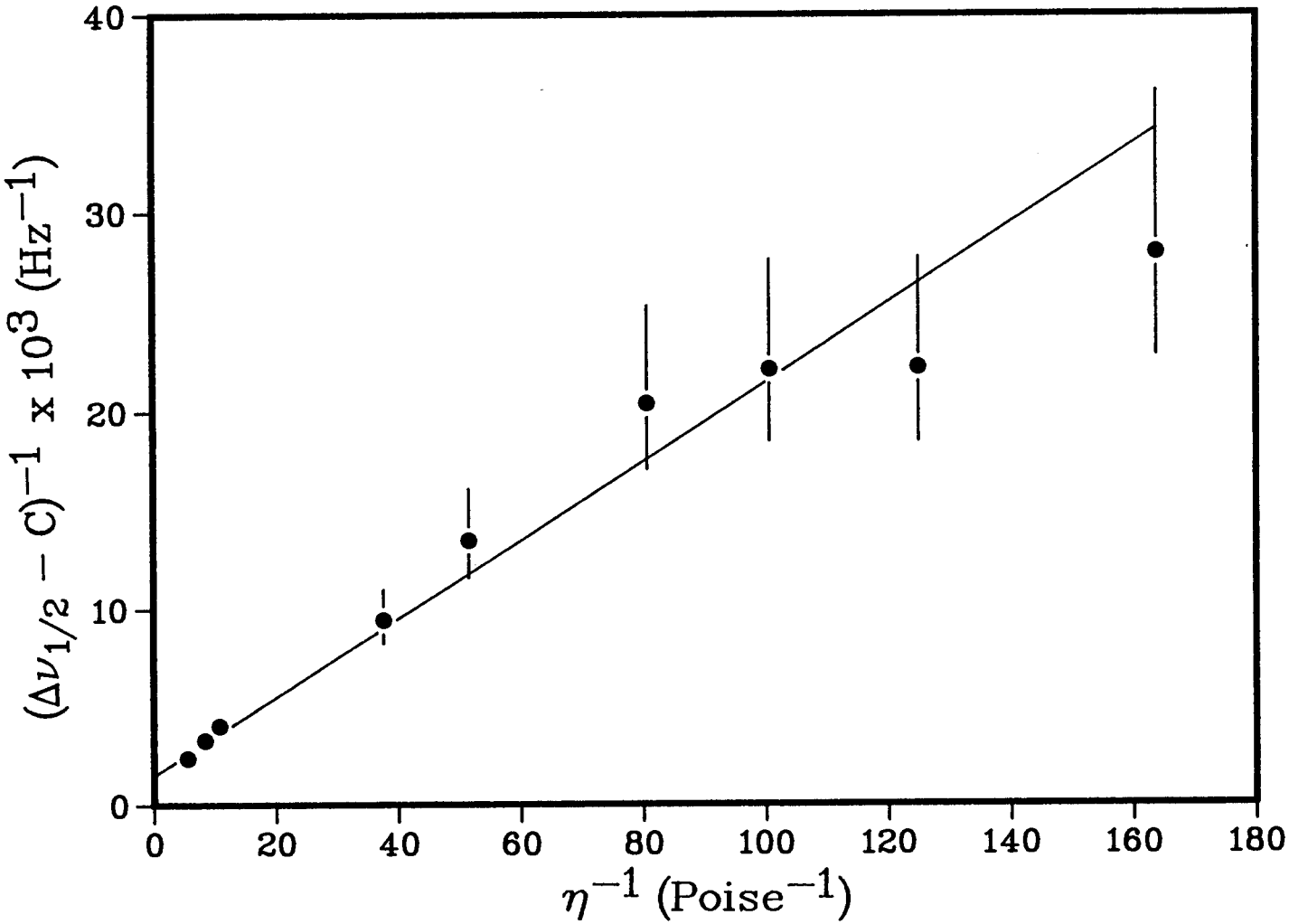
40
30
20
10
0
0
20
40
60
80
100
120
140
160
180
$(\Delta\nu_{1/2} - C)^{-1} \times 10^3$ (Hz^{-1})
η^{-1} (Poise^{-1})

Figure 31: ^{31}P NMR linewidths of LDL as a function of solvent viscosity at 45°C for D = 5 x 10^{-9} (a), 1.1 x 10^{-8} (b), 5 x 10^{-8} cm^2/s (c). The value of $\Delta\sigma$ was 52 ppm, and the value of R was 11.8 nm.

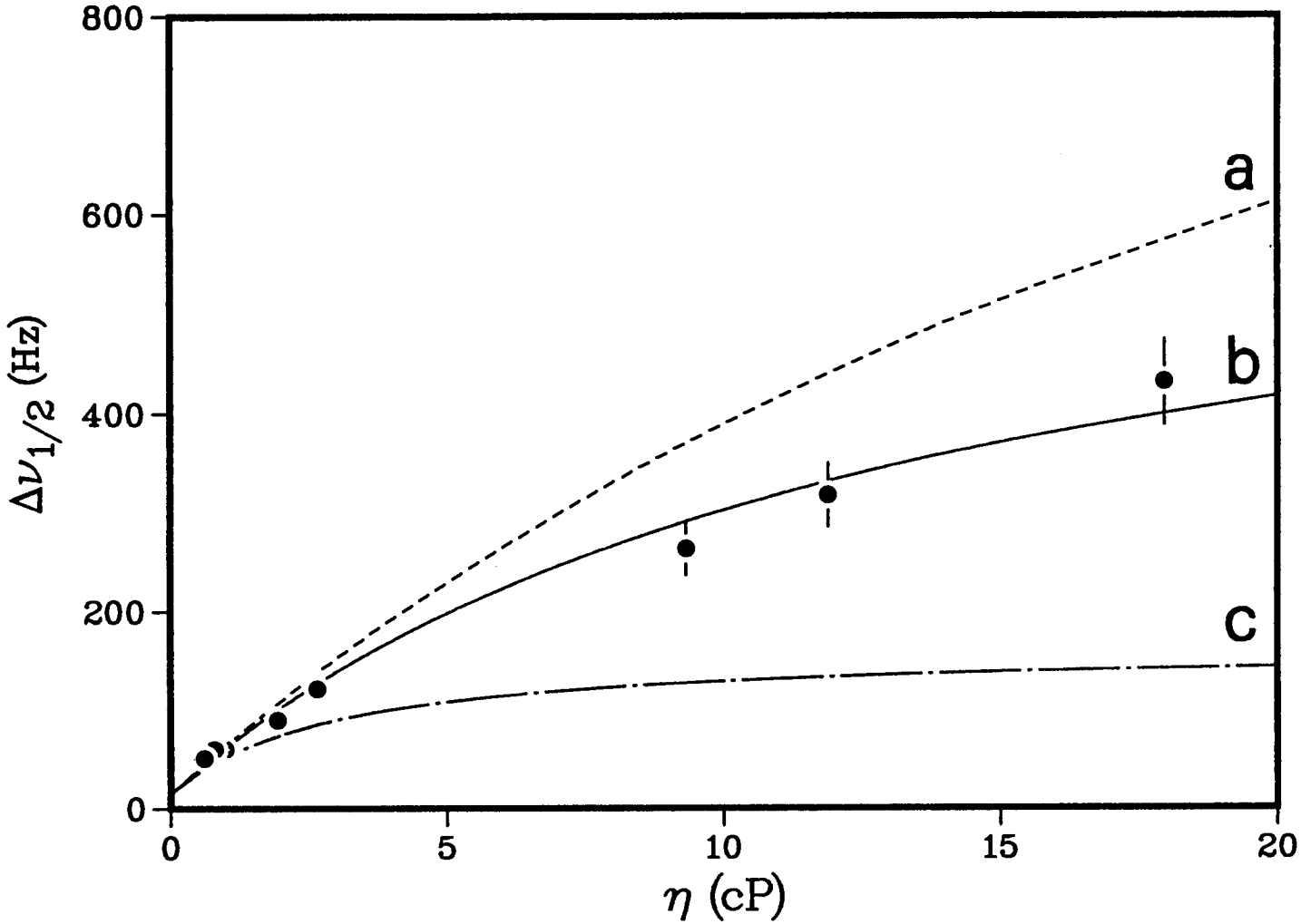
800
600
400
200
0
$\Delta\nu_{1/2}$ (Hz)
a
b
c
0
5
10
15
20
η (cP)

Figure 32: Representative ^{31}P NMR spectra of HDL_3 in the presence of increasing concentrations of glycerol at 25°C. The solid line represents an iterative least-squares fit of two (a-c) and one (d) Lorentzian function(s) to the data points (crosses). The concentrations of glycerol (weight-%) were approximately 0 (a), 46 (b), 64 (c), and 75 (d). Spectral parameters: pulse width = 5 μs (60°); sweep width = 5 kHz (a), 4 kHz (b-d); number of acquisitions = 6230 (a), 3800 (b), 20,000 (c), 20,000 (d); data sets = 4K (a), 2K (b-d); delay between pulses = 1.5 s; delay before acquisition = 10 μs; line broadening = 2 Hz (a), 5 Hz (b), 5 Hz (c), 10 Hz (d).

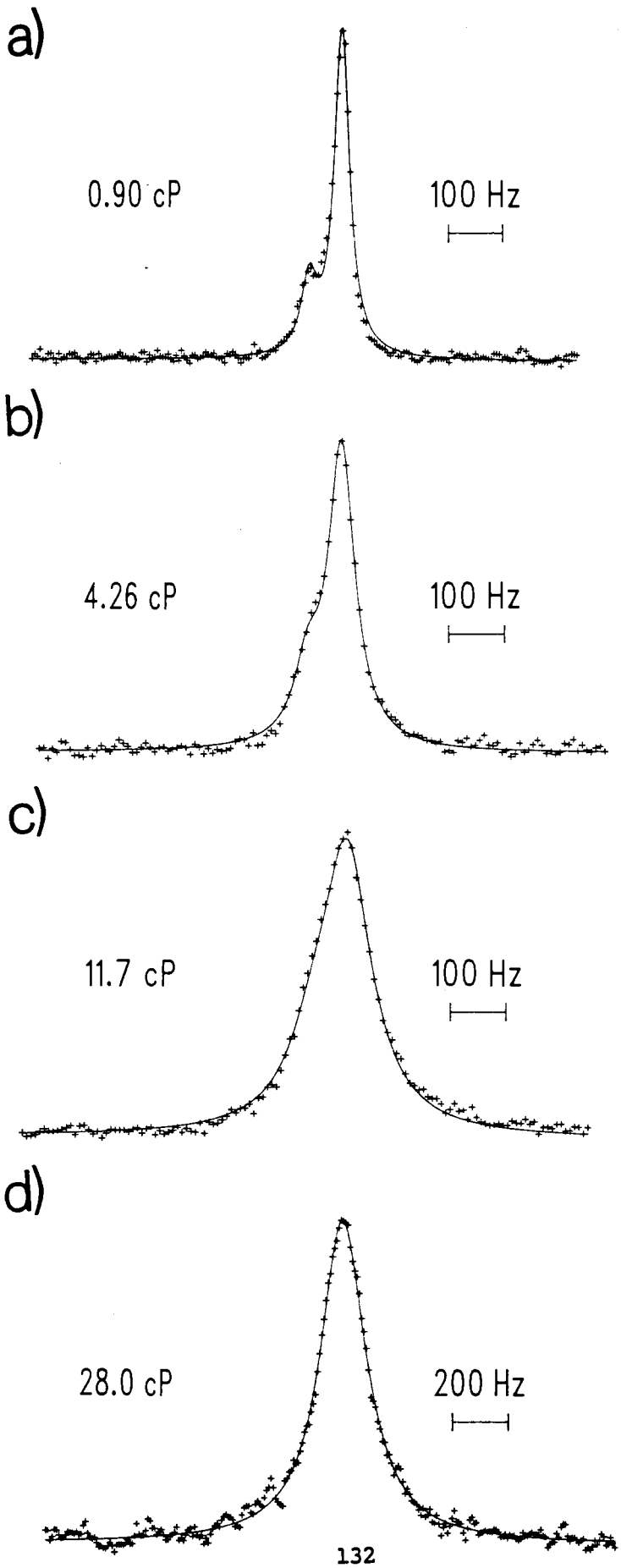
a)
0.90 cP
100 Hz
b)
4.26 cP
100 Hz
c)
11.7 cP
100 Hz
d)
28.0 cP
200 Hz

results in coalesence of the two resonances. The linewidths shown in Table XI were obtained from an iterative least-squares fit of the data to 2 (≤15.2 cP) or 1 (28 cP) Lorentzian function(s).

A plot of $(\Delta\nu_{1/2} - C)^{-1}$ versus η^{-1} is shown in Figure 33. The solid line is a weighted least-squares fit to the data points. Using R = 4.1 nm, a value determined in our lab for HDL_3 by electron microscopy, in agreement with literature values, we have obtained D = (2.3±0.8) x 10^{-8} cm^2/s and $\Delta\sigma$ = 136±11 ppm. The value of D is very close to that determined for HDL_2 (Parmar, 1985). However, an examination of Figure 33 reveals that there is a distinct curvature to the data points. It is difficult to ascertain whether this is significant due to the large uncertainties in each point at low viscosities. It should be stressed that the errors in determining D and $\Delta\sigma$ are intrinsically greater for HDL_3 than for the other lipoproteins. The narrower linewidths makes the accuracy of C more important, and magnifies experimental errors such as broadening due to magnetic field inhomogeneities. For example, if C = 20 Hz instead of 15, the appearance of the double reciprocal plot is considerably improved as shown in Figure 34. For C = 20 Hz, D = 1.2 x 10^{-8} cm^2/s and $\Delta\sigma$ = 116 ppm.

A plot of $\Delta\nu_{1/2}$ versus η is shown in Figure 35 for various values of D ($\Delta\sigma$ = 136 ppm), with the curve for D = 2.3 x 10^{-8} cm^2/s giving the best fit to the data points. The value of $\Delta\sigma$ = 136 ppm is almost double that observed for HDL_2 (69-75 ppm) (Parmar, 1985). To verify the large value of $\Delta\sigma$ using a glycerol-independent technique, we have obtained ^{31}P NMR spectra of HDL_3 at several frequencies (Table XII and Figure 36). From the field-dependence, $\Delta\sigma$ was found to be 156±30 ppm. The agreement between this value and that determined from the viscosity-dependence is not as good as

Table XI: ^{31}P NMR linewidths of HDL_3 as a function of solvent viscosity at 25°C.

η (cP)	$\Delta\nu_{1/2}$ (Hz)
0.90	34.6
1.58	38.2
2.04	44.3
2.79	45.9
4.26	57.4
7.25	71.9
11.7	104
15.2	122
28.0	195

for the other lipoproteins, but clearly with HDL_3, $\Delta\sigma$ is very large.

A few comments are in order regarding the experimental data points in Figure 35. The nearly linear dependence of the linewidth with viscosity could lead one to question whether lateral diffusion contributed significantly to line narrowing in HDL_3. Several lines of evidence suggest that diffusion is an important mechanism. One can calculate the predicted values of $\Delta\nu_{1/2}$ if particle tumbling was the only line-narrowing mechanism by putting D = 0 in eq 12 (i.e., letting $\tau_e = \tau_t$). This does not change the measured values of $\Delta\sigma$, which are still $\simeq$136 and 152 ppm from the viscosity- and field- dependence, respectively. It should also be noted that the value of $\Delta\sigma$ obtained from the field-dependent measurements is also independent of the value of C. Using $\Delta\sigma$ = 136 ppm and D = 0, one obtains theoretical plot *a* shown in Figure 35, in which it is seen that the

Figure 33: A plot of $(\Delta\nu_{1/2} - C)^{-1}$ versus η^{-1} for the ^{31}P NMR resonances of HDL_3 at 25°C.

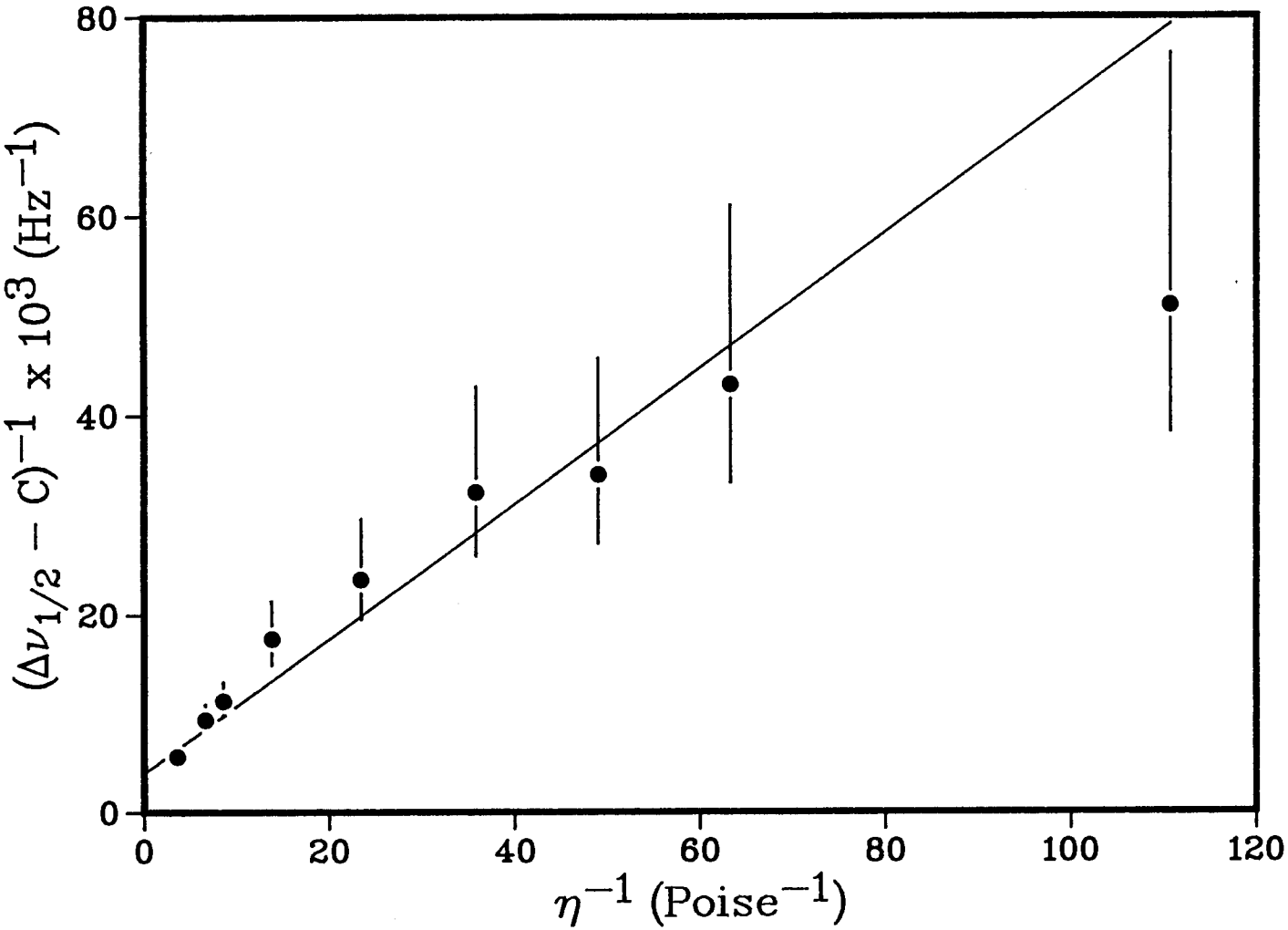
80
60
40
20
0
0
20
40
60
80
100
120
$(\Delta\nu_{1/2} - C)^{-1}$ x 10^3 (Hz^{-1})
η^{-1} (Poise^{-1})

Figure 34: A plot of $(\Delta\nu_{1/2} - C)^{-1}$ versus η^{-1} for the ^{31}P NMR resonances of HDL_3 at 25°C assuming C = 20 Hz.

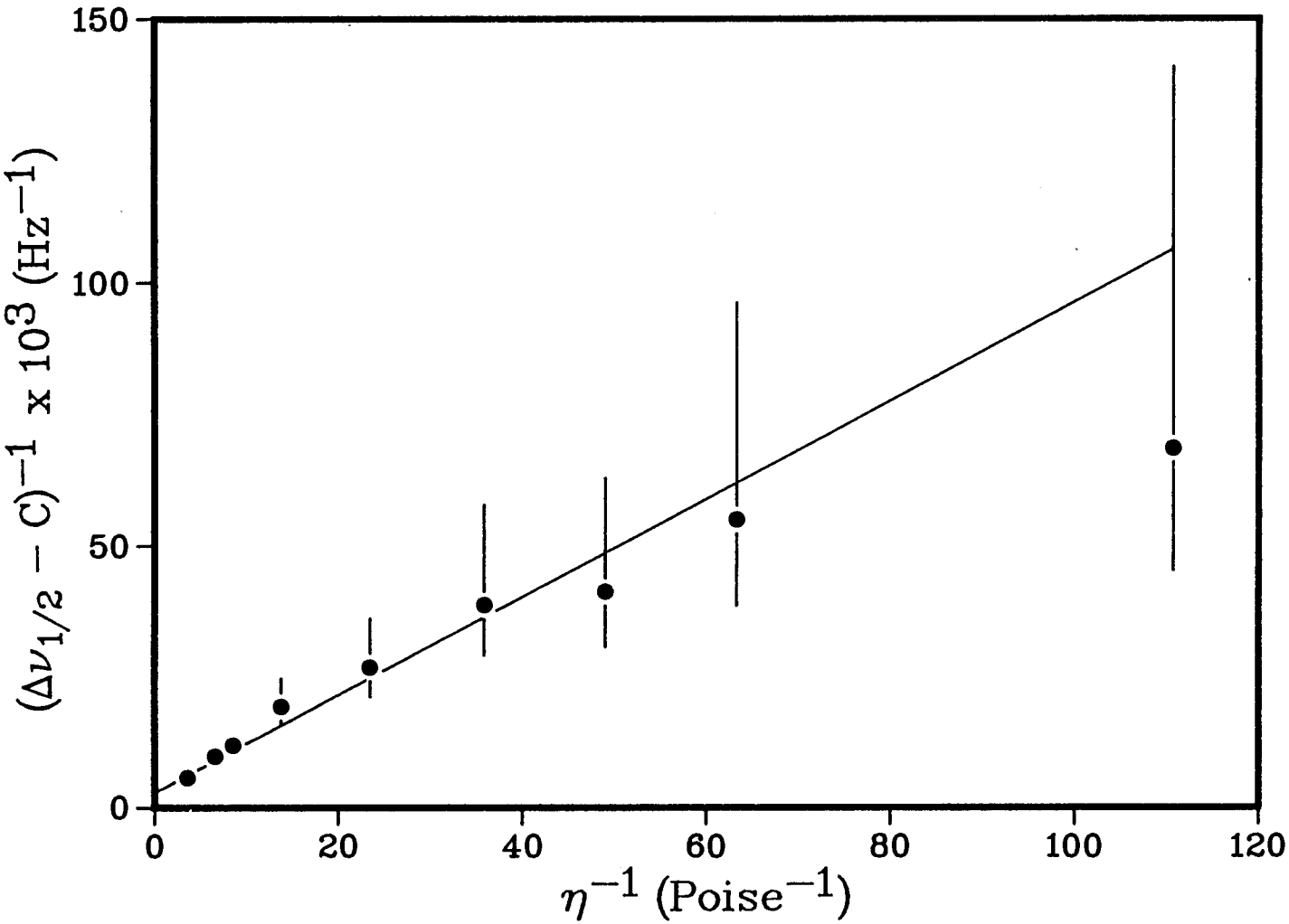
150
100
50
0
0
20
40
60
80
100
120
$(\Delta\nu_{1/2} - C)^{-1}$ x 10^3 (Hz^{-1})
η^{-1} (Poise^{-1})

Figure 35: ^{31}P NMR linewidths of HDL_3 as a function of solvent viscosity at 25°C for D = 0 (a), 1 x 10^{-8} (b), 2.3 x 10^{-8} (c), 5 x 10^{-8} (d). The value of $\Delta\sigma$ was 136 ppm.

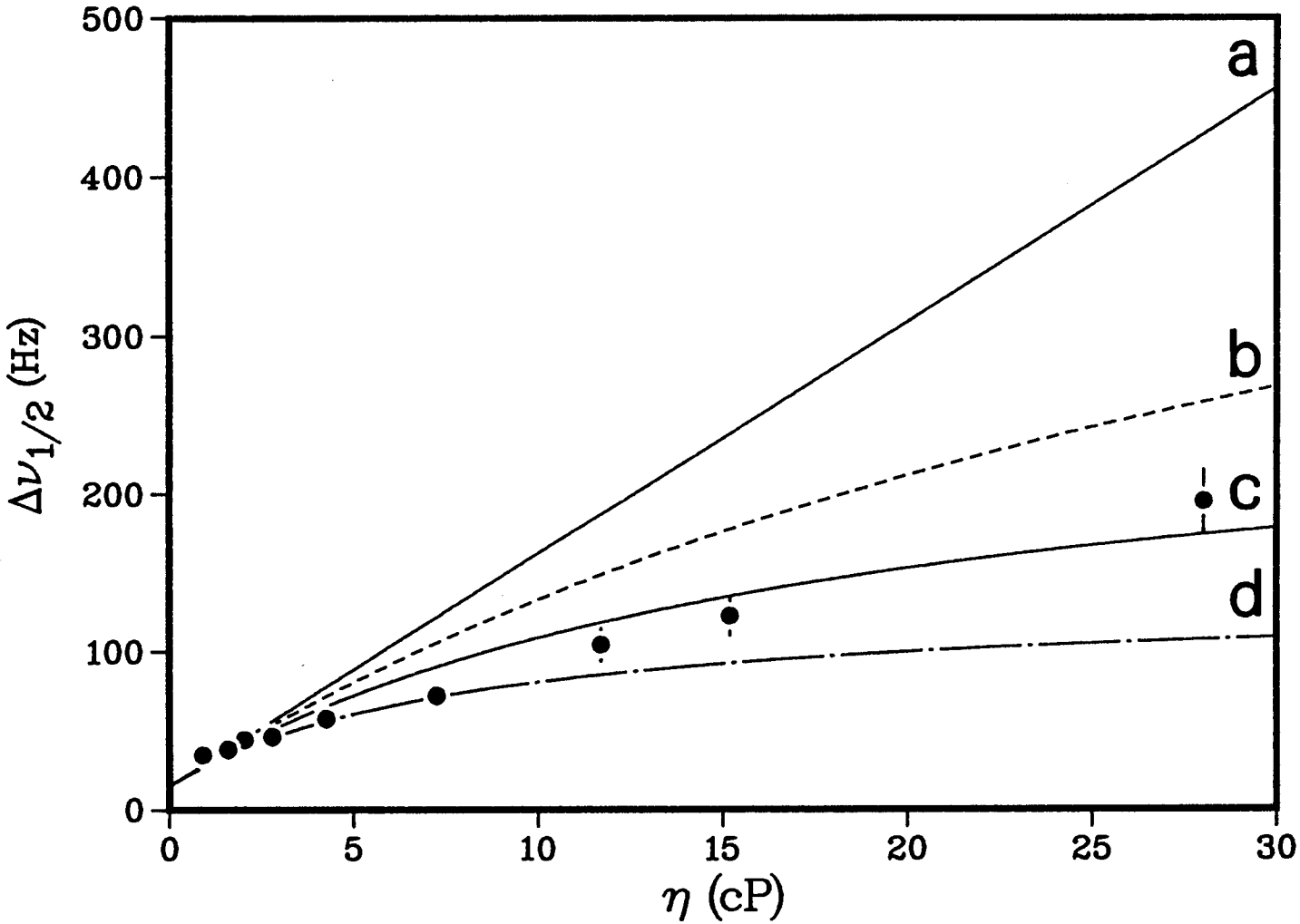
500
400
300
200
100
0
$\Delta\nu_{1/2}$ (Hz)
0
5
10
15
20
25
30
η (cP)
a
b
c
d

Table XII: ^{31}P NMR linewidths of HDL_3 as a function of resonance frequency at 25°C.

ν_o (MHz)	$\Delta\nu_{1/2}$ (Hz)
40.5	22
102.2	35
161.8	60

predicted linewidths are much broader than observed. Clearly, then, for a large $\Delta\sigma$, phospholipid diffusion is required to reduce the linewidths to their observed values. Furthermore, the leveling off of $\Delta\nu_{1/2}$ with increasing η is observed in HDL_2 (Parmar, 1985), which is only slightly larger than HDL_3.

The value of $\Delta\sigma$ obtained for HDL_3 is extremely large and approaches the limit that could be theoretically observed for an axially symmetric system (see below). Aside from C, the only other parameter which affects the calculated value of $\Delta\sigma$ is the particle radius. It is possible that the radius determined from electron microscopy may underestimate the hydrated particle radius. However, even if the radius was as large as 5.5 nm, which is the radius of HDL_2, $\Delta\sigma$ would still be 90-100 ppm.

Phospholipid Diffusion and Residual Chemical Shift Anisotropy in Human Serum Lipoproteins.

The values of D and $\Delta\sigma$ presented in the current study for LDL and HDL_3 have been compared with the values for HDL_2, VLDL, and egg PC/TO microemulsions (Cushley *et al.*, 1987; Parmar, 1985; R.S. Chana, unpublished

Figure 36: ($\Delta\nu_{1/2}$ - C) as a function of ν_0^2 for HDL_3 at 25°C. The straight line is a weighted least-squares fit to the data points.

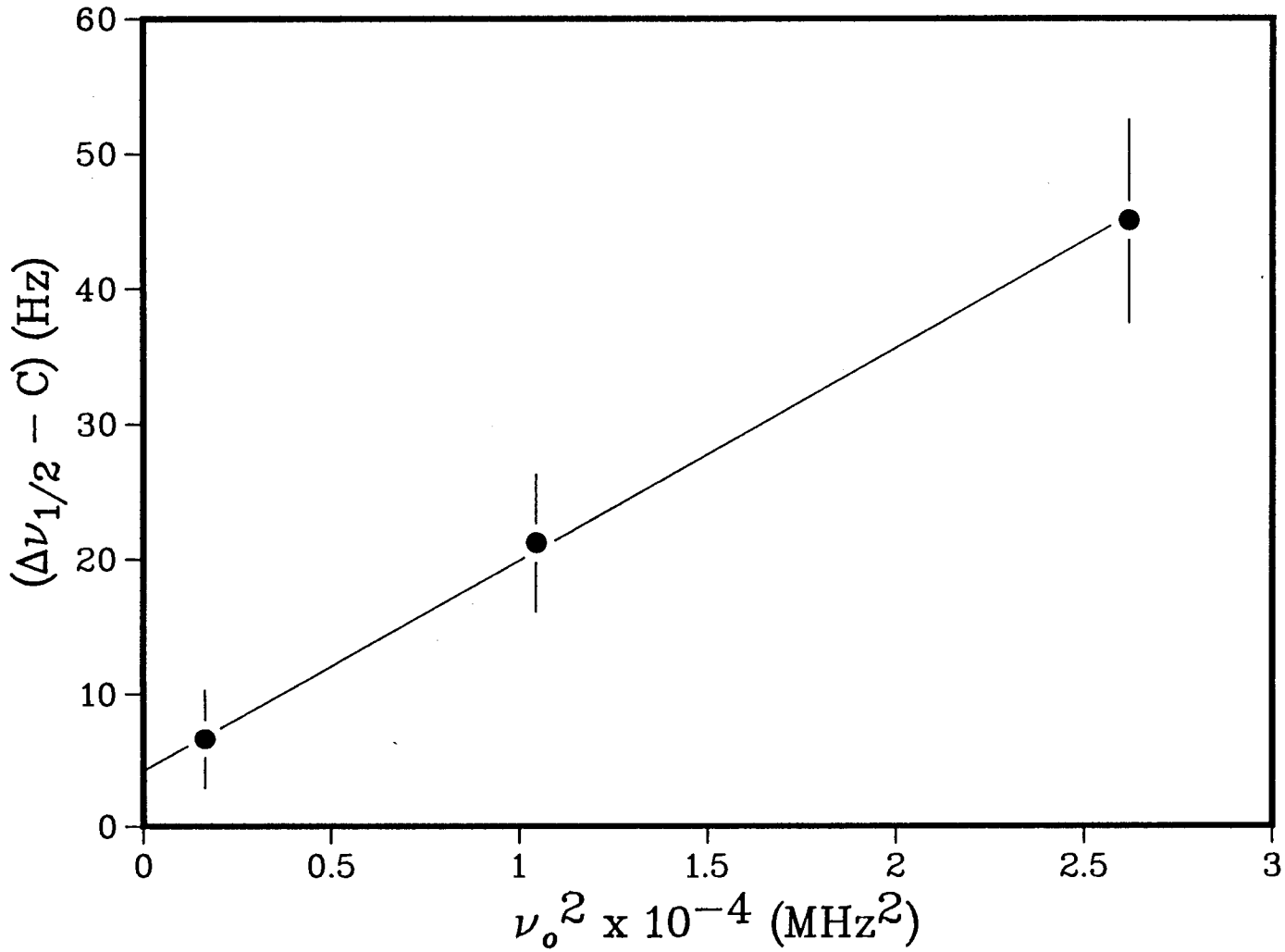
60
50
40
30
20
10
0
0
0.5
1
1.5
2
2.5
3
$(\Delta\nu_{1/2} - C)$ (Hz)
ν_o^2 x 10^{-4} (MHz^2)

results). These values, along with those observed in phospholipid bilayers, are presented in Table XIII.

For HDL_2 and HDL_3, D = 1.8 x 10^{-8} and 2.3 x 10^{-8} cm^2/s, respectively. These fall within the range of D observed in phospholipid bilayers by a variety of techniques ((1-7) x 10^{-8} cm^2/s (Mackay *et al.*, 1978 and references therein)). The value of 2.6 x 10^{-8} cm^2/s given in Table XIII for egg PC vesicles above the phase transition was measured from the viscosity dependence of the ^{31}P NMR linewidths (Cullis, 1976). A very similar rate of diffusion is observed in the monolayer of protein-free microemulsions (2.8 x 10^{-8}), which are better models of lipoproteins than pure bilayers.

In the larger lipoproteins VLDL and LDL, diffusion is significantly slower than in bilayers or microemulsions. The value of (9.1±1.0) x 10^{-9} cm^2/s observed for phospholipids in VLDL is ≃2 and 3 times slower than in the HDLs and microemulsions, respectively. This may be attributable to the higher cholesterol content of the VLDL monolayer. In vesicles, 20 mol % cholesterol slows the diffusion by a factor of 2 (Cullis, 1976). Other workers have reported a similar effect of cholesterol on lateral diffusion (Fahey *et al.*, 1977; Rubenstein *et al.*, 1979; Wu *et al.*, 1977). However, in at least one study, cholesterol was observed to cause a slight increase in D in bilayers made from several phospholipids (Lindblom *et al.*, 1981). In VLDL, the cholesterol to phospholipid ratio is 0.27, whereas in the HDLs it is <0.15.

In LDL, phospholipid diffusion is approximately one order of magnitude slower than in the HDLs. This significant decrease can only be partly explained by the cholesterol content of the LDL monolayer, which is roughly

Table XIII: Comparison of D and $\Delta\sigma$ for serum lipoproteins, microemulsions, and phospholipid bilayers.

	T (°C)	D (cm^2/s)
VLDL	25	$(9.1\pm1.0) \times 10^{-9}$ [a]
VLDL	40	$(1.2\pm0.2) \times 10^{-8}$ [b]
LDL	25	$(1.4\pm0.5) \times 10^{-9}$ [a]
LDL	45	$(1.1\pm0.2) \times 10^{-8}$
HDL_2	25	$(1.8\pm0.3) \times 10^{-8}$ [a]
HDL_3	25	$(2.3\pm0.8) \times 10^{-8}$ [a]
egg PC/TO	25	$(2.8\pm0.3) \times 10^{-8}$ [b]
egg PC vesicles	50	2.6×10^{-8} [c]

	T (°C)	$\Delta\sigma$ (ppm)	
		viscosity	field-dependence
VLDL	25	47±1 [b]	46±1 [b]
VLDL	40	42±1 [b]	
LDL	25	49±1	50±4
LDL	45	52±2	
HDL_2	25	75±10 [d]	≃69 [d]
HDL_3	25	136±11	156±30
egg PC/TO	25	28±1 [b]	
egg PC vesicles	30	45 [e]	
egg PC vesicles	50	32 [e]	
DPPC liposomes	30	56±10 [e]	
DPPC liposomes	50	45±10 [e]	

[a] Cushley *et. al.* (1987).

[b] R.S. Chana, unpublished results.

[c] Cullis (1976).

[d] Parmar (1985).

[e] McLaughlin *et. al.* (1975).

the same as in VLDL. While a definitive explanation of the slow diffusion in LDL cannot be given at this time, we will discuss three possibilities based on aspects of lipoprotein structure that are unique to LDL.

(1) LDL has the highest SPM content of the lipoproteins (≃40% of total phospholipid), followed by HDL_3 (20%), HDL_2 (15%), and VLDL (14%) (Cushley *et al.*, 1987). SPMs display complicated thermal behaviour as a result of fatty acyl chain heterogeneity, and the gel-to-liquid crystalline phase transition is often significantly higher than for PCs (Barenholz *et al.*, 1976). It is possible that the high content of SPM may decrease diffusion, although not by induction of a more gel-like monolayer as it has been shown that isolated phospholipids from LDL do not undergo a phase transition over the range 20-45°C. One possibility is that SPM interdigitates with the core components. Natural sphingolipids generally have long chain fatty acids, resulting in an asymmetric hydrocarbon region which has been proposed to cause interdigitation in sphingolipid membranes (Levin *et al.*, 1985; Boggs, 1987). However, this explanation appears to lose some strength when considering the SPM content of the other lipoproteins, which might be expected to mirror the diffusion rate. Such is not the case, as VLDL, which has slower diffusion than the HDLs, has less SPM.

(2) LDL contains a single molecule of apo B-100 (MW 514,000; Chen *et al.*, 1986) which is noted for its low water solubility and propensity to aggregate when isolated from lipid (Sparks and Sparks, 1985). The other apoproteins do not share these properties. Perhaps protein-lipid interactions that result in slower phospholipid diffusion are operative in LDL to a much greater extent than in the other lipoproteins. Yeagle *et*.

al. (1977) have suggested that protein-lipid interactions in LDL are responsible for the removal of ≃20% of the phospholipids from the high-resolution spectrum. These lipids would be immobilized and give rise to ^{31}P resonances too broad to detect. Trypsin treatment of LDL removed most of this immobilization, allowing detection of 96-99% of the phospholipid. No such immobilized phospholipid was detected in human HDL (Yeagle *et al.*, 1978). VLDL also contains apo B-100 as its major apoprotein.

(3) The LDL core is composed mainly of cholesteryl esters, which undergo a thermal liquid-crystalline to liquid phase transition over the range 20-40°C. The VLDL core, primarily triglycerides, is fluid over this range, and the amount of cholesteryl ester found in the HDL core is insufficient to form a separate ester phase. Hence, neither VLDL nor HDL display any detectable thermal events. At 25°C, the core esters of LDL are just into their phase transition. If core-monolayer interactions are operative in LDL, then the solid-like esters may be responsible for the slower diffusion of the phospholipids. This could occur through interdigitation of the acyl chains of PC and/or SPM with those of the core esters. As discussed above, the SPM may play an important role here. Consistent with this view is the observation that, at 45°C, above the phase transition, the diffusion of phospholipids in LDL increases by an order of magnitude, whereas in VLDL, going from 25 to 40°C, D remains essentially constant (R. S. Chana, unpublished results). In DPPC vesicles, increases of an order of magnitude in D occur only at the gel-to-liquid crystalline phase transition; above and below T_m, D is essentially constant with temperature (Cullis, 1976).

In summary, the lateral diffusion coefficients are significantly different in each class of lipoprotein at 25°C. Phospholipid diffusion is fastest in the smallest particles, the HDLs, and is decreased in the larger particles by other components in the monolayer and possibly, in LDL, through interactions with the core.

Perhaps more striking than the variation in diffusion rate is the profound differences in $\Delta\sigma$ observed in the lipoproteins (Table XIII). The values observed for VLDL and LDL are similar to values observed in unsonicated phospholipid bilayers, although they are larger than observed for sonicated vesicles at $T > T_m$ (30 ppm) and for microemulsions at 25°C (28 ppm); the latter two particles being closer in size and structure to lipoproteins. $\Delta\sigma$ increases from 47-50 ppm in VLDL and LDL to ≃70 ppm in HDL_2 and ≃136 ppm in HDL_3.

The larger $\Delta\sigma$'s observed in the HDLs could originate from differences in the orientation and/or order of the head group. ^{31}P NMR studies of phospholipid bilayers indicate a bent orientation of the head group, parallel to the membrane surface (Griffin *et al.*, 1978). Such an orientation is consistent with observed $\Delta\sigma$'s of 69 ppm and 47 ppm for DPPC in the gel and liquid crystalline states, respectively (Seelig and Gally, 1976; Griffin *et al.*, 1978). Depending on the amount of internal motions, then, a bent head group should give $\Delta\sigma$'s in the 47-69 ppm range.

If the phospholipid head group was extended parallel to the bilayer normal, with the O-P-O plane of the nonesterified oxygens parallel to the bilayer plane, the observed $\Delta\sigma$ values would be in the 80-125 ppm range, depending on the amount of internal motions (Griffin *et al.*, 1978; Herzfeld *et al.*, 1978). A theoretical study of the dependence of $\Delta\sigma$ on head group

orientation was reported by Thayer and Kohler (1981) for phosphatidylethanolamine. A simple model of rapid rotation about the long molecular axis (perpendicular to membrane surface), coupled with changes in the head group conformation achieved by varying the C3-O1 torsion angle (see Figure 5b), was found to account for a wide range of $\Delta\sigma$ values, including spectral lineshapes that were isotropic and hexagonal in nature. In particular, rotation of the head group up and away from the rest of the molecule was found to increase $\Delta\sigma$ from 47 ppm (torsion angle = -116.9°) to values as large as 123 ppm (-160° torsion angle). Even larger $\Delta\sigma$'s may be expected with PC, which has principal components σ_{11} = -87, σ_{22} = -25, and σ_{33} = 119 ppm (Kohler and Klein, 1977). Substitution of these values in eq 23 and 24, along with the Euler angles determined for PE (Thayer and Kohler, 1981), leads to a predicted value of $\Delta\sigma$ = -134 ppm for a torsion angle of -160°.

Based on the above, our results are consistent with a progressive change in head group orientation with increasing protein content, from roughly parallel to the lipoprotein surface in VLDL to roughly perpendicular to the surface in HDL_2 and HDL_3. Furthermore, the magnitude of $\Delta\sigma$'s observed in HDL_2 and HDL_3 suggests that the head group is significantly more ordered in the latter. This would not be unreasonable, as the ^2H NMR order parameters of the acyl chains in the plateau region of the HDLs are significantly higher ($\simeq$0.4; Parmar, 1985) than in liposomes ($\simeq$0.2) or other lipoproteins ($\simeq$0.3; Treleaven, 1985; R.S. Chana, unpublished results). Nevertheless, further studies are required to determine whether the large $\Delta\sigma$ observed in this lipoprotein results from the postulated change in head group orientation. As stressed by Thayer and Kohler (1981), other models which include more complicated motions could

predict similar $\Delta\sigma$ values for different head group conformations, and therefore one must be cautious in using ^{31}P NMR data alone to predict the head group orientation.

While the origin of the large $\Delta\sigma$'s observed in the HDLs cannot be determined from our data, some reasonable possibilities may be considered. The increase in $\Delta\sigma$ proceeding from VLDL to HDL_3 is coincident with (i) a decrease in particle size, and (ii) an increase in the weight-% or type of protein. Possibly, the packing constraints in particles as small as the HDLs, resulting from their high curvature, may force the phospholipid head group to adopt a conformation significantly different from that observed in bilayers or in the other lipoproteins.

A second possibility is that the change in $\Delta\sigma$ is caused by protein-lipid interactions. The weight-% protein increases from 8 and 21% in VLDL and LDL, respectively, to 46 and 61% in HDL_2 and HDL_3 (Scanu, 1979; Dolphin, 1985). As well, the major classes of apoproteins are different in VLDL (apo B and C's), LDL (apo B), and the HDLs (apo A's) (Lusis, 1988). In the HDLs, a larger percentage of phospholipid will be in direct contact with protein, as it has been calculated that the amount of phospholipid present is sufficient to cover only $\simeq$20% of the particle surface (Verdery and Nichols, 1975). This may allow an electrostatic interaction between phospholipid and protein to modulate $\Delta\sigma$ through alterations of the phospholipid head group conformation, which may explain why $\Delta\sigma$ is 20 ppm greater in VLDL than in protein-free egg PC/TO microemulsions. Unfortunately, the available experimental evidence involving biological membranes and reconstituted systems with both intrinsic and extrinsic proteins argues against such an effect (Watts, 1987; Seelig *et*

al., 1987; Ryba *et al.*, 1986; Dempsey *et al.*, 1986; Sixl *et al.*, 1984). Protein either disorders or has no effect at all on the head groups and acyl chains of phospholipids as assessed by ^{2}H quadrupolar splittings and ^{31}P CSA measurements. Deuterium relaxation time measurements suggest that protein causes a slight decrease in overall lipid reorientation, but does not invoke large-scale conformational changes (Watts, 1987). However, unlike integral and peripheral membrane proteins, the apoproteins possess a unique amphipathic helical structure which may permit interactions between amino acid side chains and phospholipids not available to most peripheral proteins (Segrest *et al.*, 1974). On the polar face of the helix, negatively charged amino acids are located at the center and positively charged amino acids at the periphery, which would allow direct electrostatic interactions with zwitterionic phospholipids (Segrest *et al.*, 1974). Furthermore, space-filling models of protein interacting with a PC predict an extended conformation of the head group (Segrest *et al.*, 1974). Our results may be the first evidence for electrostatic interactions between protein and lipid, a phenomenon which may be unique to proteins possessing amphipathic character.

It is of interest that the largest $\Delta\sigma$'s are observed in particles where phospholipid diffusion approximates that of bilayers and protein-free microemulsions. Based on our interpretation of the measured $\Delta\sigma$'s, protein-lipid interactions appear to be independent of the phospholipid lateral diffusion rate, indicating that both protein and lipid diffuse at the same rate (Clegg and Vaz, 1985).

It is clear that while the lipoproteins share a common structure, the dynamic properties of the monolayer phospholipids, as measured by ^{31}P NMR,

exhibit profound differences. The variation in both the orientation and/or order of the head group and in the phospholipid lateral diffusion rate suggest variation in the magnitude of lipid-lipid and lipid-protein interactions in each lipoprotein. While these differences may not be as great at physiological temperatures, they still may play an important role in such phenomena as receptor binding or interactions with important metabolic enzymes such as LCAT, lipoprotein lipase, and the plasma exchange proteins.

LDL-HEP Insoluble Complex Formation by ^{31}P NMR

In an initial attempt to probe for alterations in LDL structure resulting from insoluble complex formation with GAGs, we have chosen to examine the phospholipid headgroups by ^{31}P NMR. The increase in the phase transition temperature of the core esters observed upon insoluble complex formation (Bihari-Varga *et al.*, 1981) must be mediated via the particle surface, and could involve the protein and/or phospholipid. Srinivasan *et al.* (1975a) have proposed that the unique feature of insoluble complexes is the Ca^{2+} cross-linking between phospholipid head groups and GAG sulfate groups. More recently, Cardin *et al.* (1987), studying the interaction of a fluoresceinamine-derivatized high-reactive HEP with LDL, observed that acetylation of LDL prevented formation of insoluble complexes, suggesting a major role for the protein and a negligible or minor role for the phospholipid. The surface location of the phosphate groups makes ^{31}P NMR an ideal technique for studying the LDL surface, and allows the question of the involvement of the phosphate group in insoluble complex formation to be addressed. Changes in protein structure would be more accessible by other techniques such as FT-IR (Herzyck *et al.*, 1987).

In order to compare the native particle with the insoluble complexes, LDL was pelleted by ultracentrifugation. Representative spectra of pelleted LDL are shown in Figure 37 as a function of temperature. At temperatures <25°C, the spectral lineshapes are distinctly powder-like, with $\Delta\sigma$ increasing with decreasing temperature, verifying the assumption of effective axial symmetry for phospholipids in LDL. Observation of the residual $\Delta\sigma$ is possible only because particle tumbling has been greatly reduced, or stopped, in the viscous LDL pellet. As the temperature is

Figure 37: Representative ^{31}P NMR spectra (102.2 MHz) of pelleted LDL as a function of temperature. The spectral simulations assume an axially symmetric lineshape ($\Delta\sigma$ = 50 ppm) motionally narrowed by isotropic Brownian rotational diffusion with correlation times τ = 1.3 x 10^{-4} s (a), 1.15 x 10^{-4} s (b), 6.0 x 10^{-5} s (c), 3.0 x 10^{-5} s (d) (see Burnell *et. al.* (1980)). Spectral parameters: pulse width = 6.5 μs (90°); sweep width = 50 kHz; number of acquisitions = 2229 (a), 3933 (b), 2389 (c), 4433 (d); data sets = 2K; delay between pulses = 1.5 s; delay before acquisition = 20 μs (a-c), 10 μs (d); line broadening = 10 Hz. The chemical shift is given in ppm relative to external H_3PO_4.

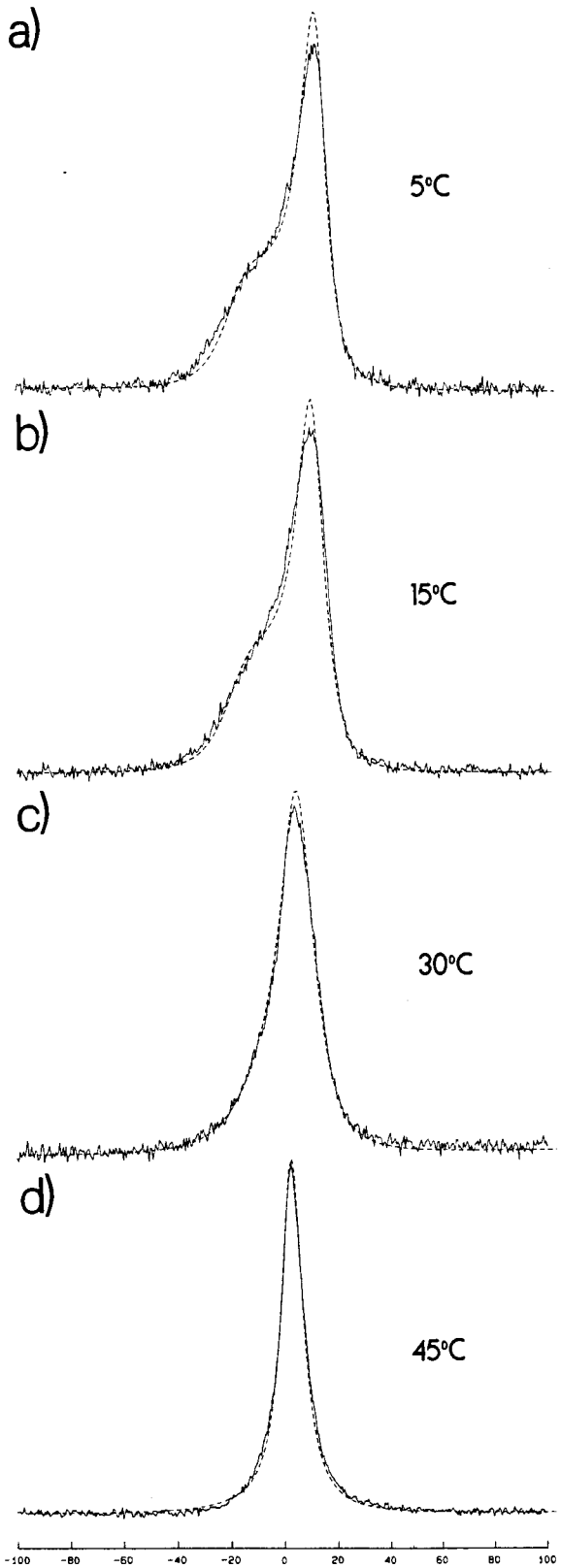
a)
5°C
b)
15°C
c)
30°C
d)
45°C
-100
-80
-60
-40
-20
0
20
40
60
80
100

increased, the anisotropy decreases until, at 45°C, the lineshape is nearly isotropic. Temperature-dependent ^{31}P NMR spectra of LDL-HEP insoluble complexes are shown in Figure 38. The general trends are the same as for pelleted LDL.

Two parameters that are useful in analysing powder spectra are $\Delta\sigma$ and $\Delta\nu_{1/2}$, the linewidth at half-height. Although the latter is an empirical parameter in the case of powder patterns, it has been used to give a quantitative measurement of phase transitions in membranes by ^{31}P NMR (Seelig, 1978). In the present case, it is possible to estimate $\Delta\sigma$ only at temperatures <25°C, and even then the uncertainty is large due to the poorly-resolved low-field shoulder. Hence, $\Delta\nu_{1/2}$ allows the spectra for both samples to be compared throughout the entire temperature range studied. The temperature-dependence of $\Delta\nu_{1/2}$ is given in Figure 39. For native LDL, the linewidths remain approximately constant until ≃25°C, at which point they begin to decrease as the temperature is raised to 45°C. This reduction in linewidth, probably due to increased lateral diffusion, occurs over the same temperature range as the phase transition of the core esters (20-40°C), suggesting interactions between the core and monolayer of LDL. The variation of $\Delta\nu_{1/2}$ with temperature is significantly different for LDL-HEP insoluble complexes. While the linewidths are comparable with those of pelleted LDL at temperatures <20°C, they decrease only slightly as the temperature is raised to 45°C. This suggests that the phospholipids have less motional freedom in the insoluble complexes than in native LDL, perhaps resulting from reduced lateral diffusion. However, the broader lines could also originate from a change in the headgroup orientation so as to increase $\Delta\sigma$. It thus appears that insoluble complex formation affects either the motions and/or orientation of the phospholipid headgroups in

Figure 38: Representative ^{31}P NMR spectra (102.2 MHz) of LDL-HEP insoluble complexes as a function of temperature. The spectra were simulated as described in the text and in the legend to Figure 37 with $\Delta\sigma$ = 60 ppm and τ = 9.0 x 10^{-5} s (a), 7.0 x 10^{-5} s (b), 5.0 x 10^{-5} s (c), and 4.0 x 10^{-5} s (d). Spectral parameters: pulse width = 6.0 μs (90°); sweep width = 50 kHz; number of acquisitions = 6549 (a), 6065 (b), 5089 (c), 3520 (d); data sets = 4K; delay between pulses = 1.5 s; delay before acquisition = 10 μs; line broadening = 50 Hz. The chemical shift is given in ppm relative to external H_3PO_4.

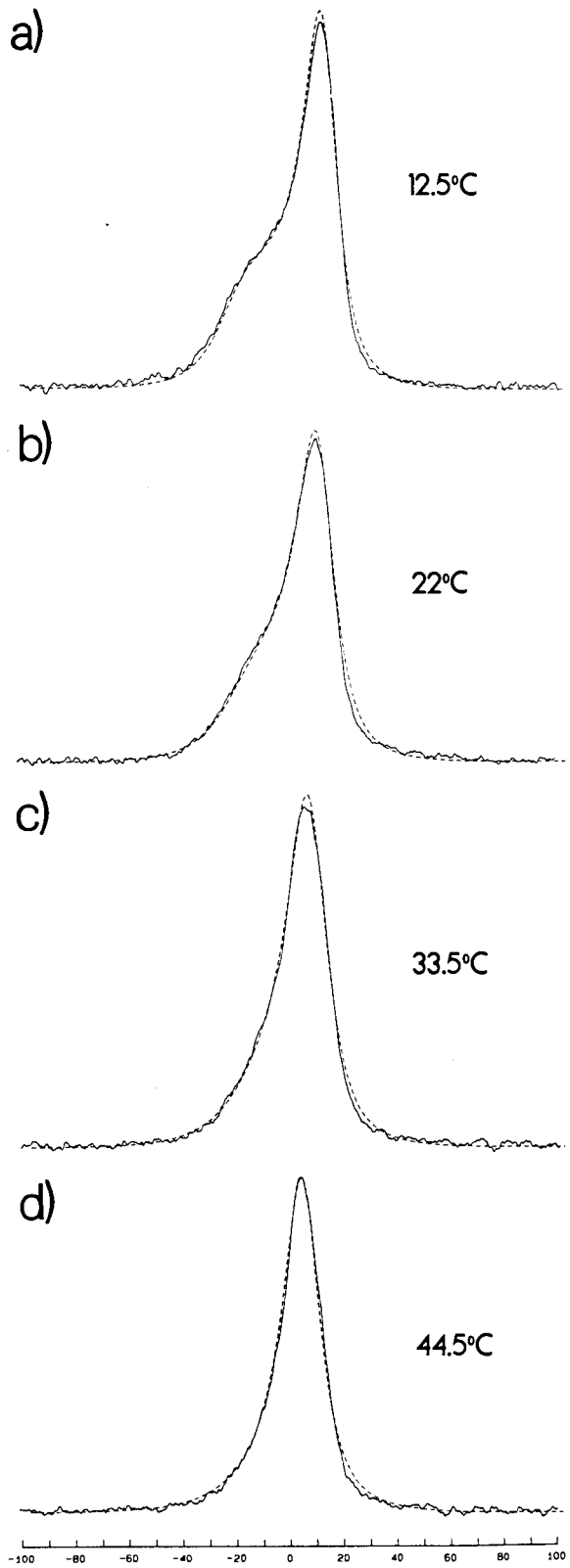
a)
12.5°C
b)
22°C
c)
33.5°C
d)
44.5°C
-100
-80
-60
-40
-20
0
20
40
60
80
100

Figure 39: Variation of $\Delta\nu_{1/2}$ of pelleted LDL (■) and LDL-HEP insoluble complexes (●) as a function of temperature. The error bars represent an estimated uncertainty of ±10%.

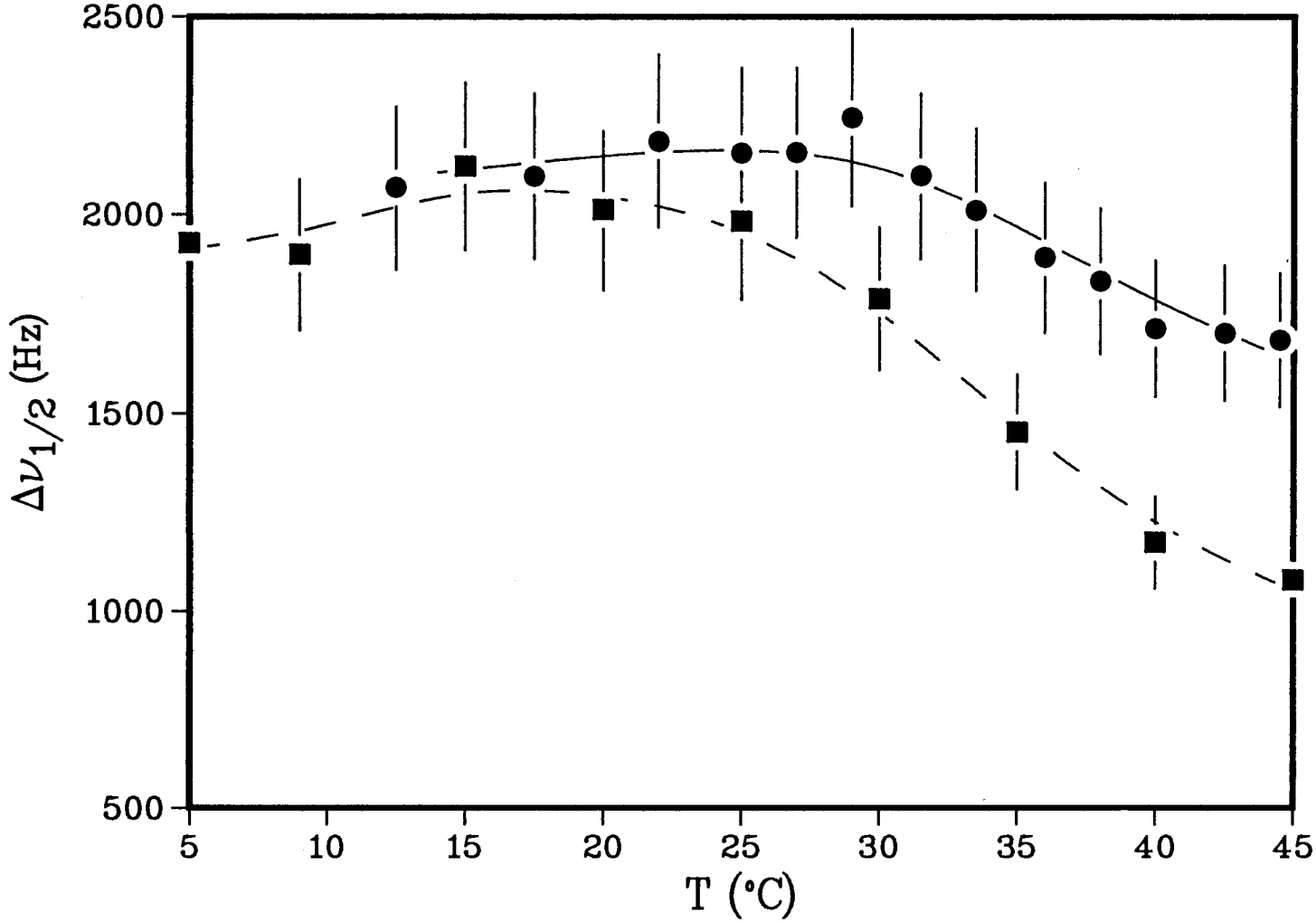
2500
2000
1500
1000
500
$\Delta\nu_{1/2}$ (Hz)
5
10
15
20
25
30
35
40
45
T (°C)

LDL.

The $\Delta\sigma$ values of $\simeq$32-36 ppm measured from Figures 37 and 38 for LDL and LDL-HEP complexes in the range 5-25°C are considerably smaller than the value of 50 ppm estimated from the viscosity- and field- dependence of the ^{31}P linewidths in solution (see *Lateral Diffusion and Chemical Shift Anisotropy of phospholipids in LDL and HDL*$_3$ in Results and Discussion). The observed $\Delta\sigma$ has most likely been reduced from 50 ppm by the lateral diffusion of the phospholipids, and is further reduced by increased lateral diffusion as the temperature is raised. In order to obtain a better understanding of the temperature dependent narrowing observed in Figures 37 and 38, the spectra were simulated assuming an axially-symmetric chemical-shift tensor motionally narrowed by isotropic diffusion, as described by Burnell *et. al.* (1980). The program, kindly supplied by Dr. E. Burnell, Physics Department, University of British Columbia, is based on the motional averaging theories of Freed *et. al.* (1971) and provides a convenient method for obtaining lateral diffusion coefficients D as a function of temperature, as recently described for phospholipids in erythrocyte microvesicles (Gawrisch *et al.*, 1986).

The LDL spectra in Figure 37 were simulated (dashed line) using $\Delta\sigma$ = 50 ppm (5110 Hz), an orientationally independent Lorentzian linewidth of 100 Hz, and isotropic correlation times τ ranging from 1.3 x 10^{-4} to 3 x 10^{-5}. If we assume that lateral diffusion is the dominant isotropic narrowing mechanism in the LDL pellet, then $\tau = \tau_d = R^2/6D$ (eq 15), where R = 12 nm, as measured from QELS. In this manner, values of D for LDL have been determined in the range 5-45°C, and the results are shown in Figure 40. D is observed to remain relatively constant at $\simeq$2 x 10^{-9} cm^2/s between

Figure 40: Variation of D for pelleted LDL and LDL-HEP insoluble complexes as a function of temperature. The diffusion coefficients were obtained from simulations of the spectra using $\Delta\sigma$ = 50 ppm for LDL (■) and $\Delta\sigma$ = 60 ppm for LDL-HEP insoluble complexes (●). Further details are given in the text.

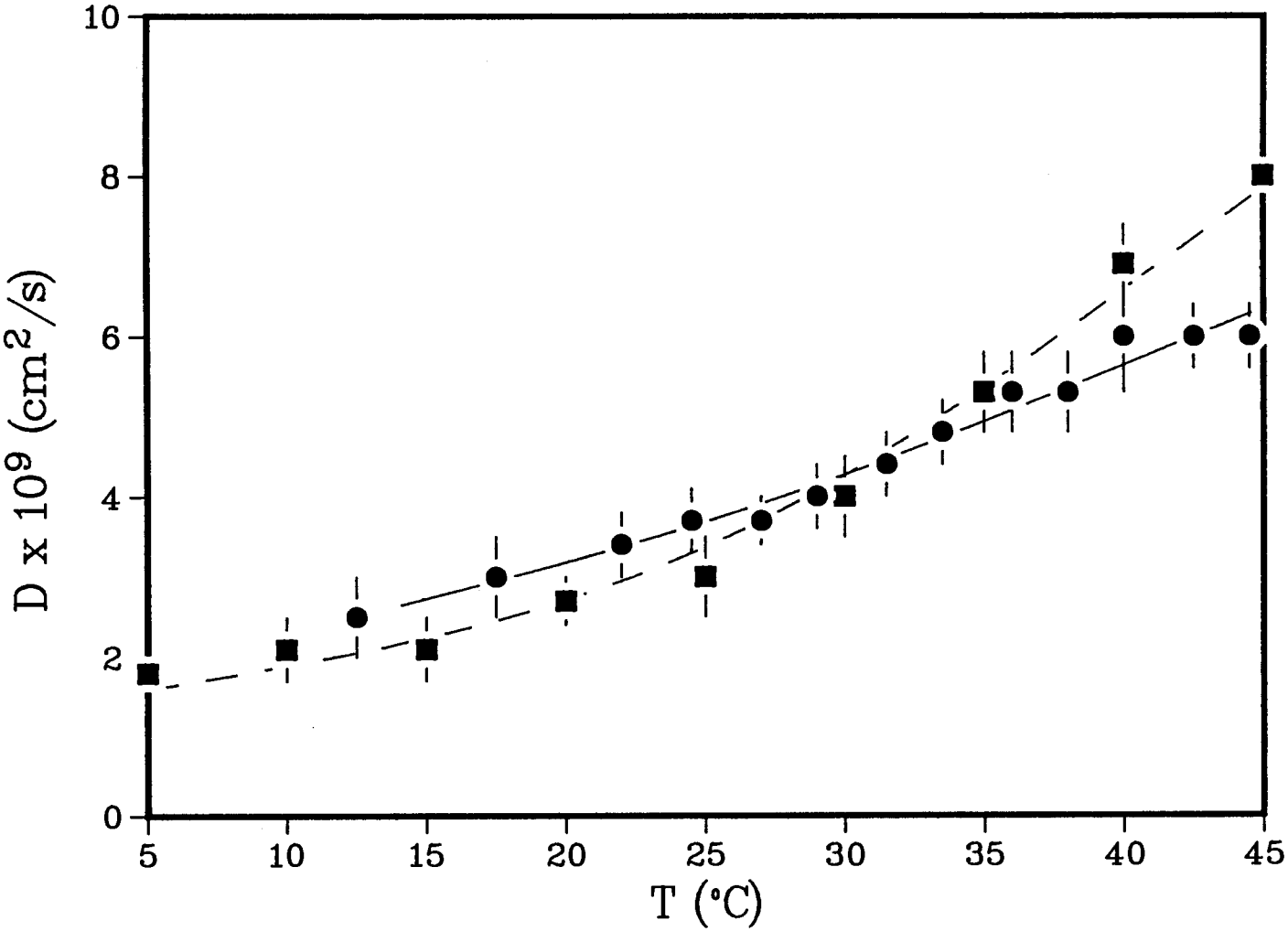
D x 10⁹ (cm²/s)
T (°C)
0
2
4
6
8
10
5
10
15
20
25
30
35
40
45

5 and 15°C, and increases gradually to 8 x 10^{-9} cm^2/s as the temperature is raised to 45°C. The increase in D occurs over the same temperature range as the phase transition of the core esters.

The value of D obtained for pelleted LDL (3.0±0.5 x 10^{-9} cm^2/s) at 25°C is twice that obtained at the same temperature from the viscosity-dependence of the ^{31}P NMR linewidths (1.4±0.5 x 10^{-9} cm^2/s). The value obtained at 45°C (8.0±0.5 x 10^{-9} cm^2/s) is smaller than obtained earlier (1.1±0.2 x 10^{-8} cm^2/s). Nevertheless, considering the errors involved, the agreement is reasonable. The rate of lateral diffusion in LDL is seen to be slow at low temperatures by both methods, and varies significantly with temperature, unlike VLDL.

In the LDL-HEP insoluble complexes, the spectra are broader at all temperatures by both the linewidths and $\Delta\sigma$. This might indicate that the presence of Ca^{2+} and HEP has increased $\Delta\sigma$, or that the cross-linking has decreased lateral diffusion in the complexes. Immobilization of phosphatidylserine by Ca^{2+} has been reported by Kohler and Klein (1977), with the values of the principal components of the shielding tensor remaining unchanged. Initial attempts to simulate the insoluble complex spectra using $\Delta\sigma$ = 50 ppm were unsuccessful, especially at low temperatures. In order to obtain good fits, a value of 60 ppm was required, as shown in Figure 38. To illustrate the point, attempts were made to simulate the 12.5°C spectrum using $\Delta\sigma$ values of 50 and 70 ppm. These are shown in Figure 41, and are clearly inferior to the simulations in Figure 38. The values of D obtained between 12.5 and 44.5°C for $\Delta\sigma$ = 60 ppm are the ones plotted in Figure 40. The temperature-dependence of D is reduced relative to LDL; the rate of lateral diffusion is significantly

Figure 41: Simulation of ^{31}P NMR spectra of LDL-HEP insoluble complexes at 12.5°C for $\Delta\sigma$ = 50 (a) and 70 (b) ppm, with τ = 1.3 x 10^{-4} (a) and 5.5 x 10^{-5} (b) cm^2/s.

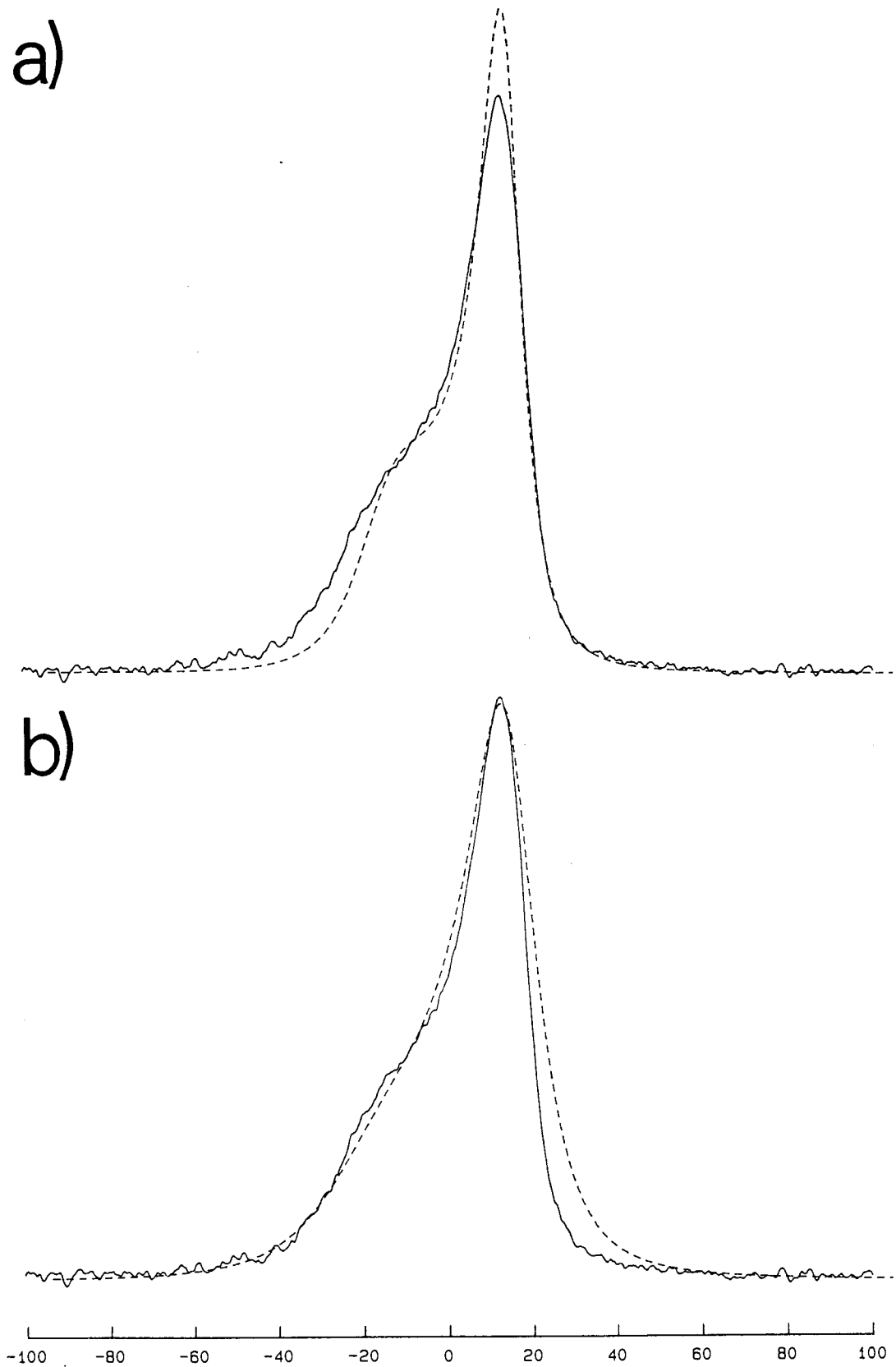
a)
b)
-100
-80
-60
-40
-20
0
20
40
60
80
100

reduced at 40 and 45°C. These results suggest that $\Delta\sigma$ is increased in LDL-HEP insoluble complexes, and that lateral diffusion is reduced at higher temperatures.

The increase in $\Delta\sigma$ may result from a change in orientation or increased order of the phosphate group. The most direct explanation is that the increase in $\Delta\sigma$ and the decreased values of D observed at higher temperatures results directly from an ionic interaction of the phosphate group with HEP-bound Ca^{2+}. This altered state of the monolayer may influence the organization of the core, contributing to the increased transition temperature of the esters. A similar model, suggested by Cardin *et al.* (1987), proposes that Ca^{2+} neutralizes positive charges on both LDL and HEP, resulting in a complex with reduced surface charge. The precipitation of the complex results from a 'salting out' effect in which hydrophobic patches on the surface promote aggregation. Such a process may also alter the orientation of the phospholipid headgroup and its rate of lateral diffusion. A third model could be envisaged wherein insoluble complex formation modifies the secondary structure of apo B-100, which in turn influences the core phase transition. In this model, the phospholipid monolayer may simply be monitoring a protein-induced core event. Cardin *et al.* (1987) have proposed that the protein plays a major role in insoluble complex formation. However, neither limited tryptic digestion of LDL or sialic acid removal was found to affect the phase transition temperature of cholesteryl esters in native LDL or in LDL-GAG insoluble complexes (Bihari-Varga *et al.*, 1982). The first two models therefore seem to be best supported by the data, and suggest that any effects on the core caused by insoluble complex formation are mediated through the phospholipid. However, further studies are needed to clarify this issue, with particular emphasis

on the role of the protein.

The results of the present study suggest that an investigation of both core and monolayer organization in LDL-GAG insoluble complexes by ^{2}H NMR may yield useful information. The quadrupolar splittings should be observable, allowing a direct measurement of orientational order. Furthermore, ^{2}H labels at various positions on the cholesteryl ester chain should provide information on the positional details of the melting process. To this end, techniques for incorporating labelled phospholipids and cholesteryl esters into LDL have been developed, and are described in a later section.

Soluble Complex Formation Between Low Density Lipoprotein and Glycosaminoglycans

^{2}H and ^{31}P NMR have been used to study the formation of soluble complexes of LDL with the glycosaminoglycans HEP, C4S, and C6S. This NMR approach allows each component of the complex to be monitored separately, and in detail, at protein concentrations in the range 15-24 mg/mL. As well, ^{31}P NMR and QELS have been used to provide information on the mean diameter and approximate size distribution of the overall complex at protein concentrations ranging from 0.2-20 mg/mL. The purpose was not only to obtain information on the properties of soluble complexes, but also to assess whether it would prove feasable to probe for perturbations in LDL structure as a result of complex formation.

^{31}P NMR and QELS Studies of the Interaction of HEP, C4S, and C6S with LDL.

In order to examine the behaviour of the lipoprotein component of LDL-GAG complexes, ^{31}P NMR was the method of choice. Figure 42 shows representative ^{31}P NMR spectra of LDL in 0.05 *M* Tris 0.02% Na_2EDTA pH 7.5 in 50% $^{2}H_2O$ in the presence of increasing concentrations of HEP. The SPM and PC resonances of native LDL (Figure 42(a)) are clearly resolved. The PC/sphingomyelin ratio of 1.63 obtained from the ^{31}P signal intensities compares well with literature values (Assman *et al.*, 1974). As the HEP concentration is increased, the linewidths broaden until resolution of the two resonances is lost (Figure 42(b)). With increasing HEP, the linewidths narrow and once more are resolved (Figure 42(c) and (d)). Similar results were obtained in HEPES buffer (not shown). The maximum linewidth of the LDL-HEP complexes occurs at a GAG/LDL ratio of 0.02-0.03.

Figure 42: ^{31}P NMR spectra of LDL (15.6 mg protein/mL) in 0.05 *M* Tris-HCl 0.02% Na_2EDTA pH 7.5 in the presence of increasing concentrations of HEP at 25°C. c_{HEP} (mg/mL) = 0 (a), 0.35 (b), 3.0 (c), 5.6 (d). Spectral parameters: pulse width = 20 μs (flip angle = 60°); delay between pulses = 2 s; data set = 2K zero-filled to 4K; number of acquisitions = 2000 (a), 2007 (b), 2000 (c), 2002 (d). Sweep width = 2000 Hz (a,c,d), 3000 Hz (b). Line broadening = 2 Hz (a,c,d), 5 Hz (b). The low-field sphingomyelin resonance appears on the left.

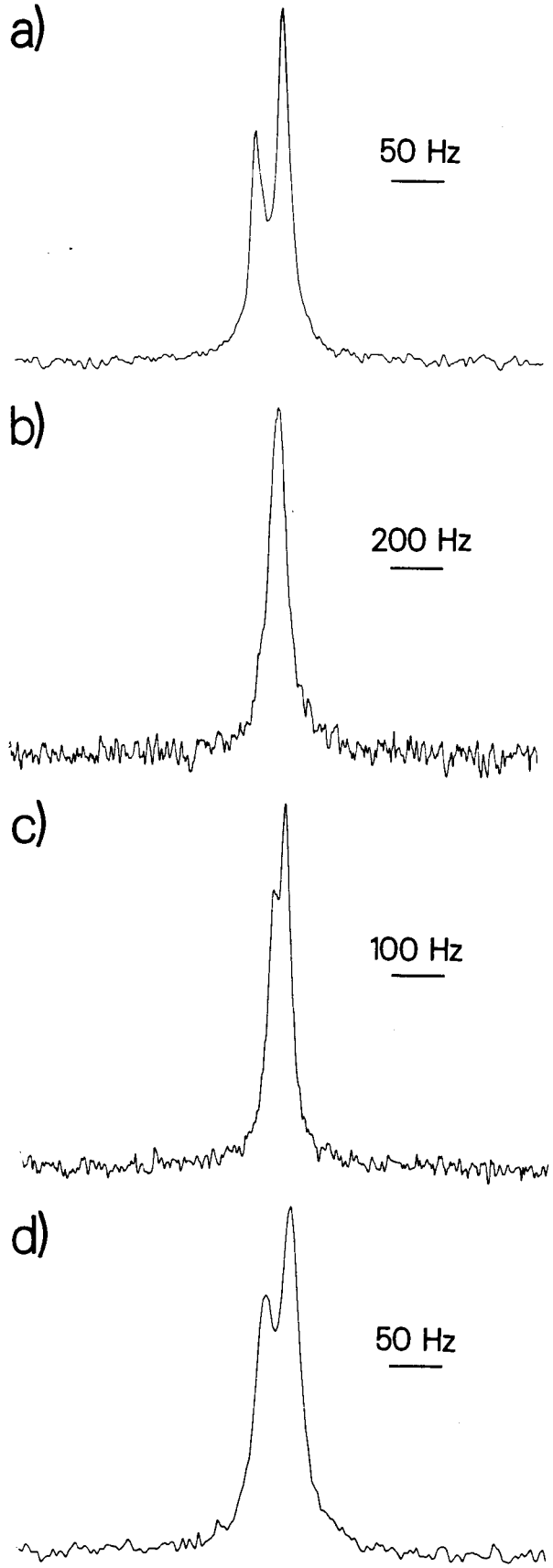
a)
50 Hz
b)
200 Hz
c)
100 Hz
d)
50 Hz

Figure 43 shows representative spectra of LDL in 0.05 *M* HEPES 0.02% Na_2EDTA pH 7.5 in 50% ^2H_2O in the presence of increasing concentrations of C6S. The linewidths are seen to broaden slightly but resolution of the PC and sphingomyelin resonances is never lost. Thus, the complexes formed with CS are strikingly different than those formed with HEP.

In order to obtain values for the ^{31}P linewidths of the PC and sphingomyelin resonances of LDL, the spectra were simulated by computer using two Lorentzian lineshape functions chemically shifted by 25.4 Hz (0.6 ppm). The chemical shifts were observed to remain constant in all cases. The results are shown in Figure 44, where the linewidth $\Delta\nu_{1/2}$ is plotted as a function of GAG/LDL ratio.

The addition of HEP to LDL (15-20 mg protein/mL) results in a rapid increase in ^{31}P NMR linewidths (Figures 37 and 39), with a maximum value of $\simeq$62 Hz observed at a HEP/LDL ratio of $\simeq$0.02 mg HEP/mg protein. Above this ratio, the linewidths decrease rapidly, levelling off at HEP/LDL $\simeq$0.2 (Figure 44). The broad ^{31}P linewidths observed at low HEP/LDL clearly result from complexes composed of several lipoproteins bound together by HEP, and it has been suggested that the stoichiometry (at much lower protein concentrations) is approximately 2-3 LDL particles per 1-2 HEP chains (Eigner *et al.*, 1982). As further HEP is added, the binding sites on LDL are saturated and the large complexes break down until, in the presence of excess HEP (HEP/LDL > 0.20), the ^{31}P NMR linewidths are slightly broader ($\simeq$20 Hz) than that of native LDL (13 Hz). From the ^{31}P NMR data, it is possible to arrive at an estimate of the complex diameters at higher protein concentrations. The relationship between the ^{31}P NMR linewidth $\Delta\nu_{1/2}$ and the correlation time for phospholipid reorientation τ_e

Figure 43: ^{31}P NMR spectra of LDL (13.7 mg protein/mL) in 0.05 *M* HEPES 0.02% Na_2EDTA pH 7.5 in the presence of increasing concentrations of C6S at 25°C. c_{CS} (mg/mL) = 0 (a), 0.32 (b), 7.6 (c). Spectral parameters: pulse width = 20 μs (flip angle = 60°); delay between pulses = 2 s; data set = 2K zero-filled to 4K; number of acquisitions = 1408 (a), 1663 (b), 2765 (c). Sweep width = 2000 Hz (a-c). Line broadening = 2 Hz (a-c).

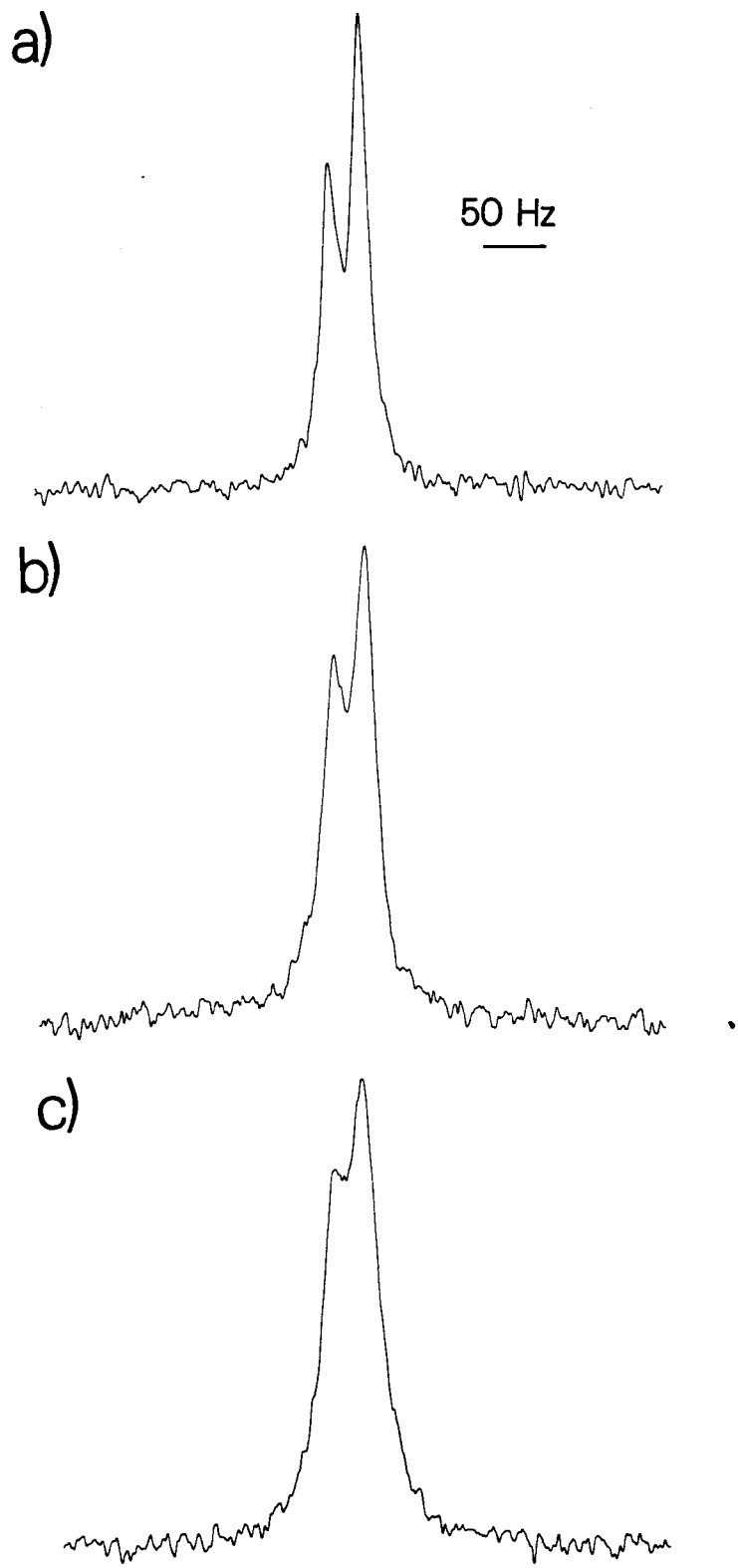
a)
50 Hz
b)
c)

Figure 44: ^{31}P NMR linewidth $\Delta\nu_{1/2}$ of the PC and sphingomyelin resonances of LDL as a Function of GAG/LDL Ratio at 25°C. Legend: HEP (Tris) (open circles), C4S (Tris) (open squares), C6S (HEPES) (filled circles), [^{2}H]C4S (HEPES) (filled squares). The linewidths were obtained from simulated spectra formed by the addition of two Lorentzian lineshape functions, representing the PC and sphingomyelin resonances of LDL. The chemical shift of the two resonances was kept constant at 25.4 Hz (0.6 ppm), and the linewidths were assumed to be equal. The error bars represent an estimated uncertainty in the linewidth of ±10%.

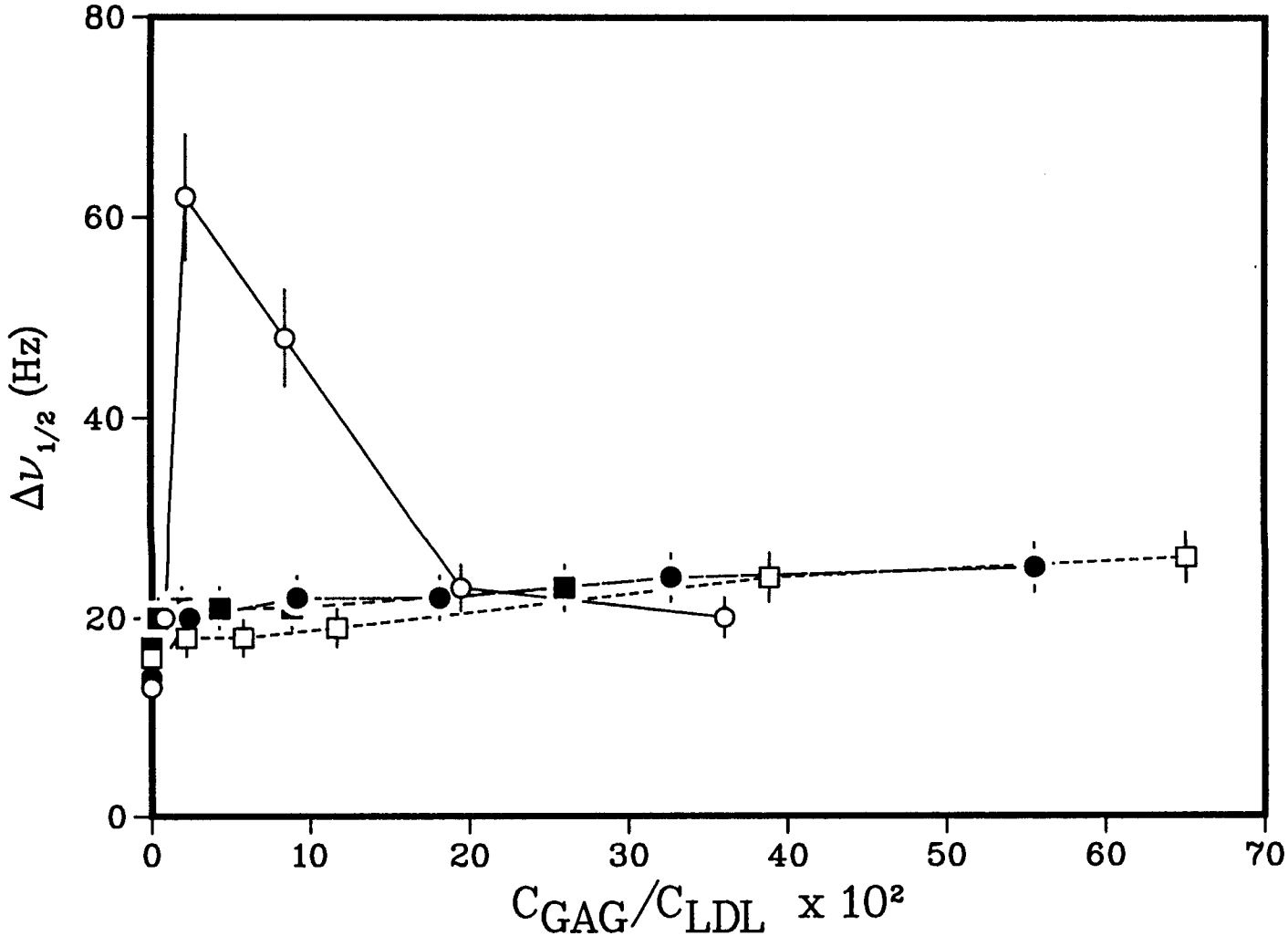
80
60
40
20
0
$\Delta\nu_{1/2}$ (Hz)
0
10
20
30
40
50
60
70
C_{GAG}/C_{LDL} x 10^2

is given by eq 12. τ_e contains contributions from particle tumbling (τ_t) and phospholipid lateral diffusion (τ_d) as defined in eq 13 to 15. In the native lipoprotein, the value of R (LDL radius) in eq 14 and 15 is identical. However, in the case of LDL-GAG soluble complexes involving more than a single lipoprotein particle, the values may differ. Assuming isotropic motion for the large LDL-HEP complexes ($R_1 \simeq 25$ nm; see below) complex reorientation occurs at a rate $1/\tau_t$. Since soluble complex formation involves the protein component of LDL, it is reasonable to assume that phospholipid diffusion remains unchanged. Thus, phospholipid lateral diffusion is still occuring at a rate $1/\tau_d$ with R_2 = 11.7 nm. Therefore, we assume that the soluble complexes are rigid enough that each LDL in the complex undergoes isotropic tumbling at a rate characterized by the overall complex radius R_1, and that phospholipid reorientation due to lateral diffusion occurs at a rate characterized by the radius R_2 of a single LDL particle. Then eq 12 to 15 can be combined to give

$$(R_1)^3 = (\Delta\nu_{1/2} - C)A/[(R_2)^2 - \{(\Delta\nu_{1/2} - C)B\}] \quad (30)$$

$$A = [3kTR_2^3/4\eta M_2] \quad (31)$$

$$B = [6D\pi/M_2] \quad (32)$$

where M_2 is defined in eq 26. As eq 30 is based on several approximations, its reliability was assessed by examining a single LDL-HEP sample (HEP/LDL = 0.022) by both ^{31}P NMR and QELS at a concentration of 2.2 mg protein/mL. Values of D = 1.4 x 10^{-9} cm^2/s and $\Delta\sigma$ = 50 ppm were used in the calculation. The value of the constant C in eq 30 ($\simeq$4 Hz) was estimated from ^{31}P NMR of egg PC (63 mg/mL) in C^2HCl_3:$CHCl_3$ (3:1) at 25°C. Substitution of these values into eq 30 yields a complex diameter of 39.4 nm, which agrees well with the QELS values of 39.3±4.3 and 39.6±0.2 nm obtained from the Distribution and Gaussian analyses, respectively. The

LDL-HEP complexes observed by ^{31}P NMR at 15-20 mg protein/mL are calculated to have mean diameters of 49±3 nm at HEP/LDL ratios of ≃0.02-0.03, and 31±2 nm in the presence of excess HEP.

In our hands, a QELS study of the LDL-HEP interaction (Figure 45*a*) yielded results which are in qualitative agreement with previous studies (Eigner *et al.*, 1982; Mitterer *et al.*, 1982). At the lower concentrations necessary for light scattering (<1 mg protein/mL), complexes with diameters of 37-40 nm are formed at 0.025-0.032 mg HEP/mg protein. In the presence of excess HEP (HEP/LDL = 0.57), the mean diameter (27.9±1.3 nm) is only slightly larger than that of native LDL (23.4±0.4 nm). At HEP/LDL ≃0.02, the complex diameters increase by 6-10 nm going from protein concentrations of <1 mg/mL (QELS) to 15-20 mg/mL (^{31}P NMR). These differences are real, as complex diameter exhibits a dependence on LDL concentration (see below; Table XIV). The sizes obtained by ^{31}P NMR and QELS for excess HEP are the same within experimental error.

In contrast to the behaviour observed with HEP, complexes formed with CS do not pass through a maximum diameter at low GAG/LDL ratios. This is shown by the ^{31}P NMR linewidth behaviour (Figures 38 and 39). While the ^{31}P linewidths of LDL-HEP complexes are much broader than those of LDL-CS complexes at GAG/LDL <0.2, the linewidths of both complexes are comparable at a ratio of ≃0.3, and even at ratios as high as 0.6, the LDL-CS linewidths are only slightly broader. At these high ratios, the diameters estimated from ^{31}P NMR are 35±2 nm for both C4S and C6S. Similarly, the addition of CS results in monotonic increases in QELS diameter until, at a ratio of 0.57 mg CS/mg protein, the diameter reaches a value of 32.6±0.4 nm for C6S and 29.3±0.3 nm for C4S, somewhat larger than observed with

Figure 45*a*: Mean diameter of LDL-GAG soluble complexes as a function of GAG/LDL ratio at 25°C as determined by QELS. Legend: HEP (filled circles), [^{2}H]HEP (open circles), C6S (open squares), C4S (filled squares). c_{LDL} (mg protein/mL) = 0.59 (HEP and [^{2}H]HEP), 0.59-0.66 (C6S and C4S). The error bars are standard deviations obtained from repeated runs on the same sample, and are smaller than the symbols where absent.

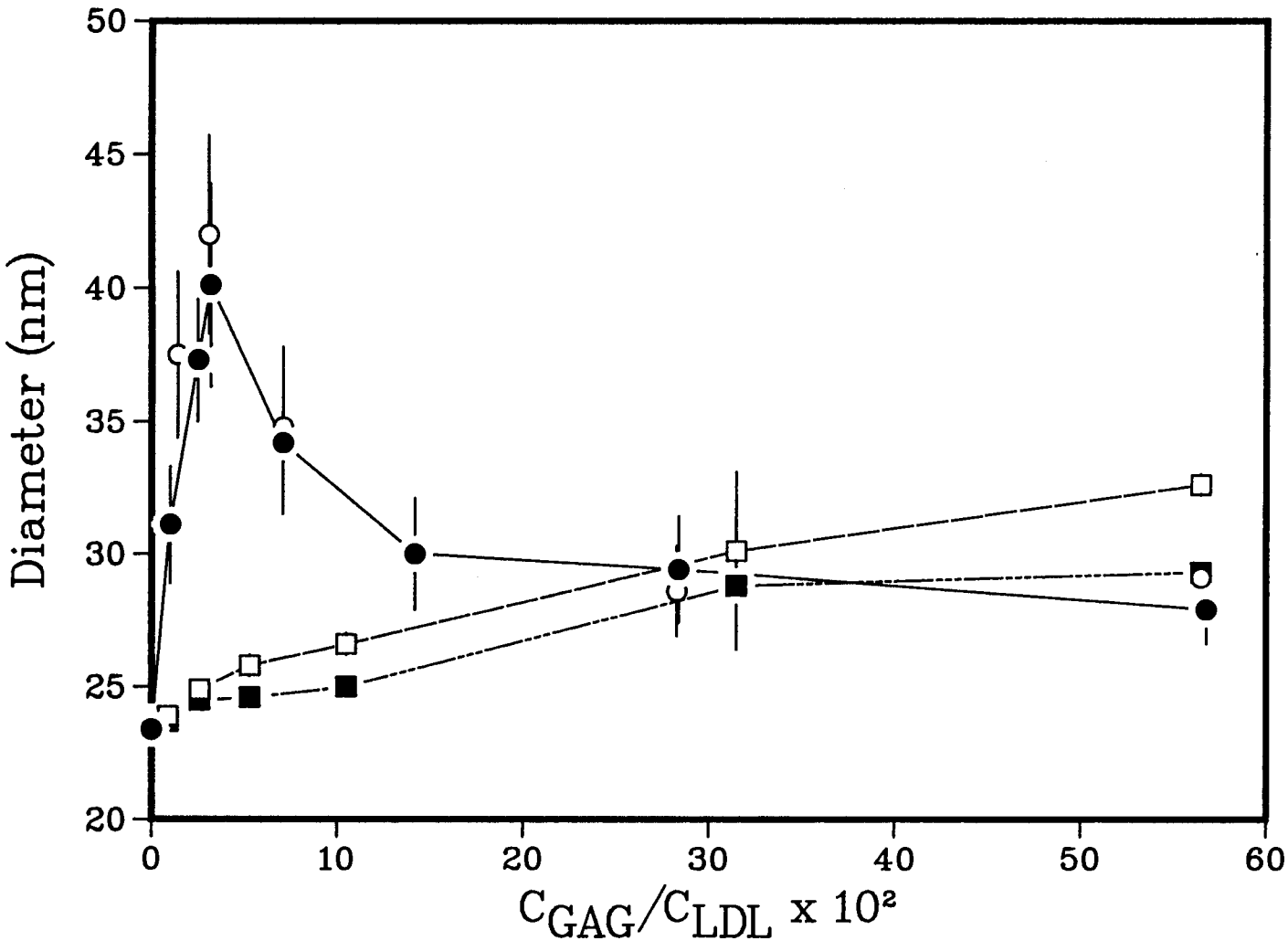
Diameter (nm)
50
45
40
35
30
25
20
0
10
20
30
40
50
60
C_{GAG}/C_{LDL} x 10^2

LDL-HEP complexes at the same ratio (Figure 45*a*).

The effect of physiological concentrations of Ca^{2+} on the LDL-GAG interaction was studied by QELS (Figure 45*b*). The presence of 2 m*M* Ca^{2+} had no effect on the binding of HEP, C6S, and C4S to LDL (compare Figures 45*a* and 45*b*), and soluble complexes were formed in all cases (calcium concentrations greater than 5 m*M* are required to effect precipitation (Cardin *et al.*,, 1986)). At all GAG/LDL ratios studied, the mean diameters in the presence of Ca^{2+} were within experimental error of the mean diameters in its absence. Similar results were obtained by Cardin *et al.* (1987), who examined the binding of fluoresceinamine-labeled HEP to LDL in the presence and absence of 3 m*M* Ca^{2+}, and found no differences in stoichiometry, affinity, or solubility.

By both ^{31}P NMR and QELS, the binding of C4S and C6S to LDL is similar. This is also observed in HEP-CS competition studies (see below; Table XV). Our binding results may be contrasted with a recent study in which C6S was found to be the only GAG retained on LDL-affinity columns in the presence of 50 m*M* Ca^{2+}, suggesting that the position of the CS sulfate groups may be of critical importance in the formation of insoluble complexes (Mourao *et al.*, 1981). We find little evidence to support such a claim for soluble complex formation, both in the absence and presence of physiological concentrations of Ca^{2+}.

Since our studies were performed over a wide range of protein concentrations due to the requirements of the techniques involved, we have investigated the effect of protein concentration on soluble complex formation. A comparison of the ^{31}P NMR and QELS data (Figures 39 and 40) shows that the shapes of the LDL-GAG binding curves are similar, and that

Figure 45*b*: Mean diameter of LDL-GAG soluble complexes in the presence of 2 m*M* Ca^{2+} as a function of GAG/LDL ratio at 25°C as determined by QELS. Legend: HEP (filled circles), C6S (open squares), C4S (filled squares). c_{LDL} = 1 mg protein/mL. The error bars are standard deviations obtained from repeated runs on the same sample, and are smaller than the symbols where absent. The solid lines are the mean diameters of C6S (a), C4S (b), and HEP (c) complexed to LDL in the absence of Ca^{2+} (see Figure 45*a*).

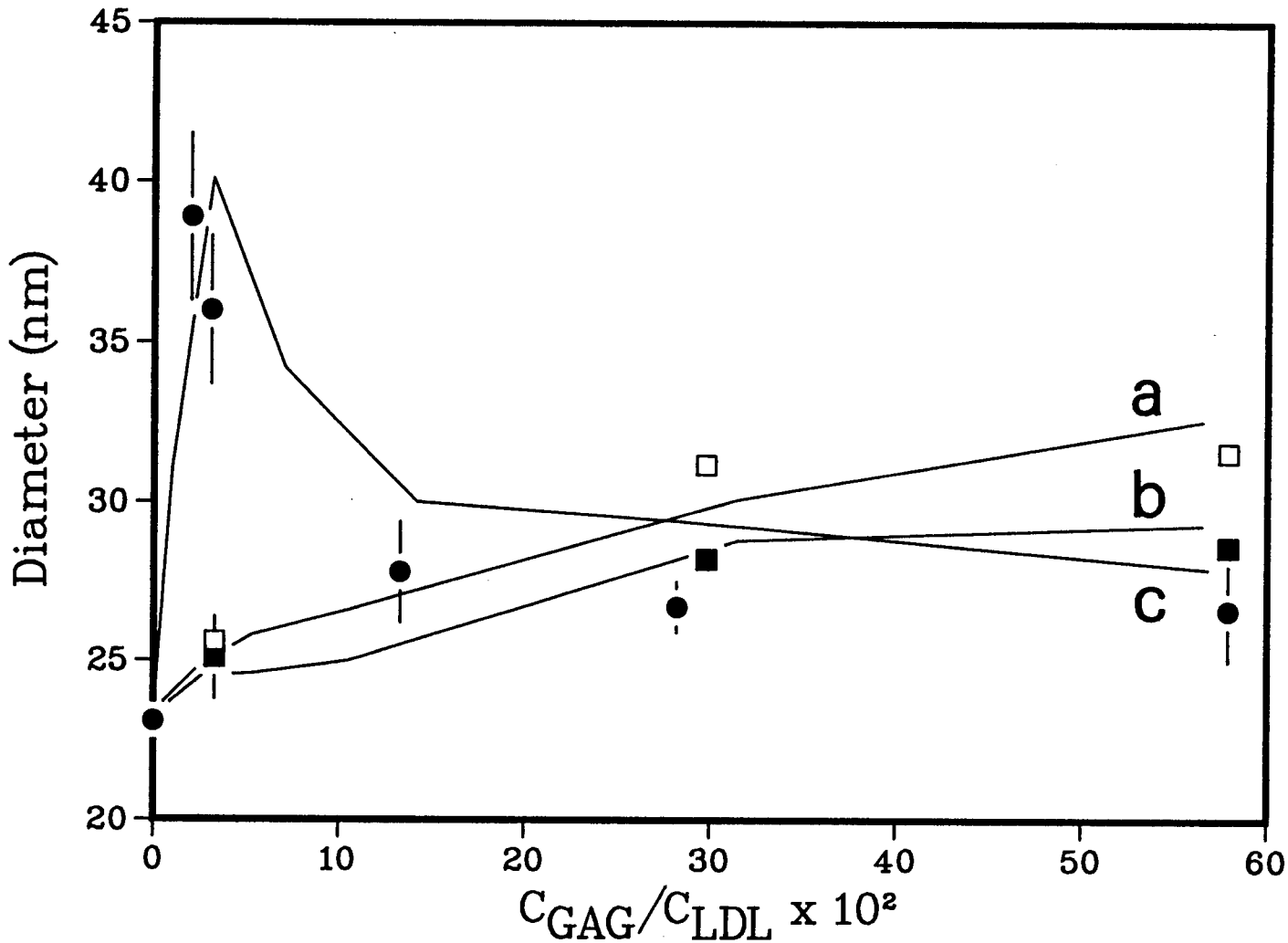
45
40
35
30
25
20
Diameter (nm)
0
10
20
30
40
50
60
C_{GAG}/C_{LDL} x 10^2
a
b
c

the HEP/LDL ratio at which the largest complexes are formed is approximately the same in both cases (0.02-0.03). To determine whether the complex size was dependent on protein concentration, several samples of HEP-LDL at a ratios of ≃0.02 and 0.032 were studied by NMR and QELS, and the results are given in Table XIV. As the complexes are diluted from ≃16 to 2 mg protein/mL, the ^{31}P linewidths narrow, indicating a decrease in the mean diameter of the complexes. Likewise, dilution of complexes from 0.8 to 0.2 mg protein/mL results in a slight decrease in diameter as determined by QELS. At the lower concentrations studied by QELS, the change in diameter is probably due to a shift in the equilibrium resulting in fewer multiple-LDL complexes and more single lipoproteins. At the higher concentrations studied by ^{31}P NMR, it is likely that some of the complexes are themselves complexing to form large aggregates (Mitterer *et al.*, 1982).

In order to assess which GAG had the greatest affinity for LDL, we have performed HEP-CS competition studies (Table XV). When an excess of C4S and C6S was added to LDL-HEP complexes (HEP/LDL = 0.025; diameter = 37.3±2.3 nm) to give a CS/LDL ratio of 0.57, the mean diameters were observed to increase slightly to 39.6±3.4 and 42.4±2.1 nm, respectively. In the absence of HEP, the same ratio of CS/LDL gave complex diameters of 29.3±0.3 and 32.6±0.4 nm for C4S and C6S, respectively. Thus, neither C4S or C6S was able to break down the LDL-HEP complexes. When HEP was added to LDL-C6S complexes (C6S/LDL = 0.57) to give a HEP/LDL ratio = 0.025, the complex diameter was 40.1±3.4 nm. Thus, even at a CS/HEP weight ratio of 23, the affinity of HEP for LDL is clearly greater than that of C4S and C6S. This is in agreement with previous studies (Iverius, 1972). As mentioned above, similar binding is observed with both C4S and C6S.

Table XIV: ^{31}P NMR and QELS concentration studies of LDL-HEP and LDL-[^{2}H]HEP soluble complexes in 0.05 *M* Tris-HCl 0.02% Na_2EDTA pH 7.5.

HEP/LDL[a]	concentration of LDL (mg protein/mL)	Mean Diameter ±S.D. (nm)	$\Delta\nu_{1/2}$ (Hz)
0.020	0.68	33.4±0.8	
	0.20	30.4±0.8	
0.021	0.79	(34.2±0.5[b])	
	0.20	(31.9±1.0[b])	
0.022	15.6		62
	4.4		45
	2.2	39.3±4.3	35
0.032	0.59	40.1±3.8	
	0.16	36.8±2.4	

[a] mg HEP/mg protein

[b] The numbers in parentheses represent studies involving [^{2}H]HEP.

Several studies have verified the ionic nature of the LDL-GAG interaction by consideration of the effect of ionic strength and pH on the degree of complex formation (Iverius, 1972; Pan *et al.*, 1978; Mitterer *et al.*, 1982). We have observed that increasing concentrations of NaCl result in a decrease in the mean diameter of LDL-HEP complexes formed at a HEP/LDL ratio of 0.02 (Table XVI). At physiological conditions (0.15 *M* NaCl), the small amount of HEP bound (Pan *et al.*, 1978) is complexed to single lipoprotein particles (diameter = 23.3±0.1 nm). [^{3}H]C6S has also been observed to bind to LDL at physiological conditions, as demonstrated by affinity chromatography of LDL-[^{3}H]C6S on albumin-agarose (Kuznetsov,

Table XV: Competition of HEP and CS for LDL binding sites as determined by QELS[a] in 0.05 *M* Tris-HCl 0.02% Na_2EDTA pH 7.5 at 25°C.

HEP/LDL[b]	CS/LDL[b]	Mean Diameter±S.D. (nm)	
		C4S	C6S
0.025	0	37.3±2.3	37.3±2.3
0.025	0.57	39.6±3.4[c]	42.4±2.1[c]
0.025	0.57		40.1±3.4[d]
0	0.57	29.3±0.3	32.6±0.4

[a] LDL concentration (c_{LDL}) = 0.59 mg protein/mL.

[b] mg GAG/mg protein

[c] HEP added first.

[d] CS added first.

1982). That various sulfated polysaccharides have been shown effective in the treatment of atherosclerosis (Weber *et al.*, 1979; Caruzzo, 1974; Morrison, 1971) is thus of some interest, and demonstrates the importance of understanding the precise factors involved in the LDL-GAG interaction *in vivo* as well as *in vitro*.

Table XVI: Effect of ionic strength on mean diameter of LDL-HEP soluble complexes (HEP/LDL = 0.020) at 25°C in 0.05 *M* Tris-HCl 0.02% Na_2EDTA pH 7.5 as determined by QELS.

[NaCl]	Mean Diameter ±S.D. (nm)
0.00	33.4±0.8
0.05	27.1±0.5
0.10	24.2±0.1
0.15	23.3±0.1

^2H NMR Studies of the Interaction of [^2H]HEP and [^2H]C4S with LDL.

Deuteroacetylated GAGs were chosen as a convenient means of monitoring the LDL-GAG interaction from the point of view of the polysaccharide component. The method used to obtain [^{2}H]GAGs has been shown to result in minimal perturbation of the GAG structure (Hook *et al.*, 1982). Because our procedure was modified slightly from that of Hook *et. al.* (see Experimental), the effect of chemical modification on GAG structure and binding properties was also examined. Deacetylated CS was examined for degradation on a Sephadex G-200 column eluted with 1 *M* NaCl in 0.05 *M* Tris-HCl pH 8.0 containing 0.02% NaN_3 (Figure 46). As well, the binding properties of [^{2}H]HEP and [^{2}H]C4S were compared with the unmodified GAGs by QELS and ^{31}P NMR, respectively (see Figures 39 and 40). The results indicate that hydrazinolysis does not degrade the polysaccharides

Figure 46: Fractionation of CS (•) and N-deacetylated CS (■) on Sephadex G-200 (2.5 x 81.5 cm) eluted with 1 *M* NaCl in 0.05 *M* Tris-HCl pH 8.0 containing 0.02% NaN_3 at a flow rate of ≃0.3 mL/minute. The fraction volume was 6.25 mL.

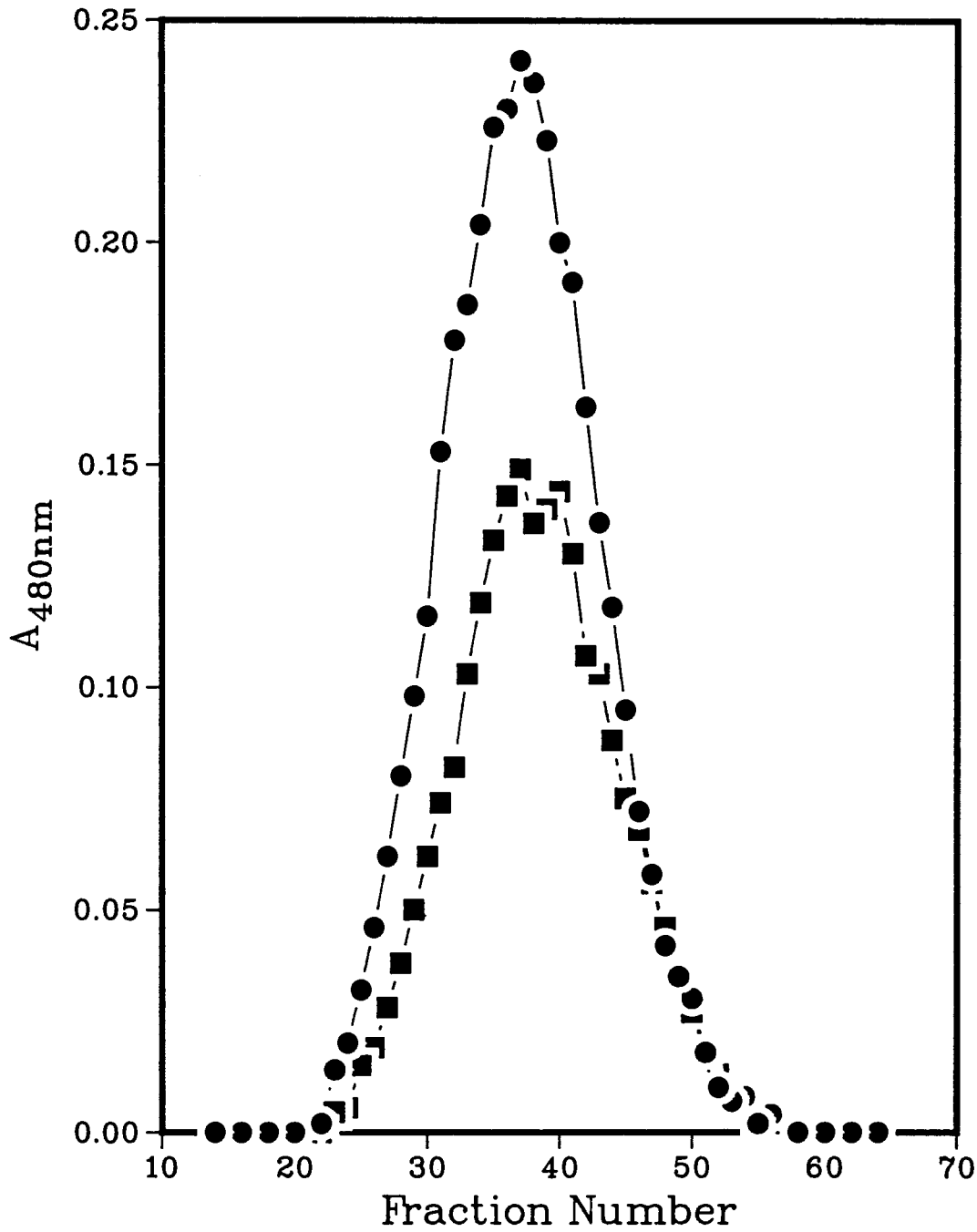
0.25
0.20
0.15
0.10
0.05
0.00
A_{480nm}
10
20
30
40
50
60
70
Fraction Number

significantly, and that deuteroacetylation does not significantly alter the binding behaviour of GAGs with LDL.

^{2}H NMR spectra of increasing concentrations of [^{2}H]HEP in the presence of LDL were obtained at 25°C and are shown in Figure 47. The solid line represents an iterative least-squares fit of the ^{2}HOH and [^{2}H]HEP resonances to single Lorentzian lineshape functions. The corresponding spectra of [^{2}H]C4S are shown in Figure 48. A plot of observed linewidth as a function of GAG/LDL ratio for [^{2}H]HEP and [^{2}H]C4S is shown in Figure 49.

^{2}H NMR provides the clearest demonstration of LDL-GAG soluble complex formation, especially for the chondroitin sulfates. The binding of both [^{2}H]HEP and [^{2}H]C4S to LDL is clearly evidenced by the broad resonances observed at low GAG/LDL ratios (Figures 42 and 43). A plot of linewidth versus [^{2}H]GAG/LDL is shown in Figure 49. In solution, [^{2}H]HEP and [^{2}H]C4S have linewidths of 13 and 32 Hz, respectively, at concentrations of ≃10 mg/mL. In the presence of LDL at ≃0.02 mg GAG/mg protein, these values increase 15-fold for [^{2}H]HEP to ≃220 Hz and 5-fold for [^{2}H]C4S to ≃160 Hz. By way of contrast, the addition of CS to LDL increases the ^{31}P NMR linewidths of LDL only by a factor of 1.6, even at high CS/LDL ratios. The ^{2}H NMR linewidths of [^{2}H]HEP are broader than those of [^{2}H]C4S at GAG/LDL <0.13. In order to verify that the ^{2}H NMR data is monitoring soluble complex formation, [^{2}H]HEP was added to acetylated LDL. It has been observed by others (Iverius, 1972; Mahley *et al.*, 1979) that acetylation of the lysine groups of apo B abolishes GAG binding. As shown in Figure 49, the linewidths of [^{2}H]HEP in the presence of acetylated LDL are considerably narrower than in the presence of native LDL, and remain constant over the range studied, suggesting that complex formation has been

Figure 47: ^{2}H NMR spectra of [^{2}H]HEP in the presence of LDL (22 mg protein/mL) in 0.05 *M* Tris-HCl pH 7.5 at 25°C. c_{HEP} (mg/mL) = 0.4 (a), 1.1 (b), 2.5 (c), 5.4 (d). Spectral parameters: pulse width = 14 μs (flip angle = 60°); delay between pulses = 0.1 s; sweep width = 5 kHz; number of data points = 1K zero-filled to 4K; number of acquisitions = 490,000 (a), 600,000 (b), 420,000 (c), 420,000 (d). Line broadening = 25 Hz (a), 20 Hz (b), 8 Hz (c), 5 Hz (d). The solid line is the best fit Lorentzian function to the ^{2}HOH (low field (left)) and [^{2}H]HEP resonances.

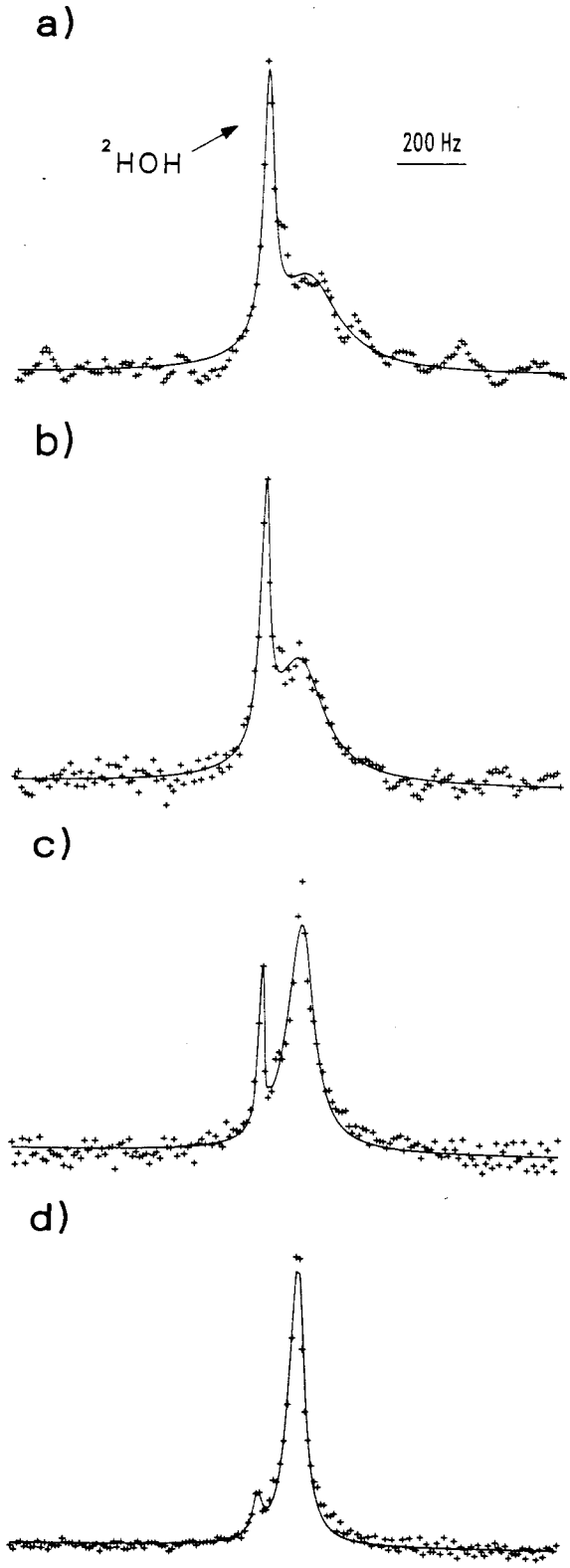
a)
^{2}HOH
200 Hz
b)
c)
d)

Figure 48: ^{2}H NMR spectra of [^{2}H]C4S in the presence of LDL (24 mg protein/mL) in 0.05 *M* Tris-HCl pH 7.5 at 25°C. c_{CS} (mg/mL) = 0.3 (a), 0.9 (b), 2.1 (c), 4.8 (d). Spectral parameters: pulse width = 14 μs (flip angle = 60°); delay between pulses = 0.1 s; sweep width = 5 kHz; number of data points = 1K zero-filled to 4K; number of acquisitions = 200,000 (a), 300,000 (b), 116,000 (c), 53,000 (d). Line broadening = 20 Hz (a,b), 10 Hz (c), 5 Hz (d). The solid line is the best fit Lorentzian function to the ^{2}HOH (low field (left)) and [^{2}H]C4S resonances.

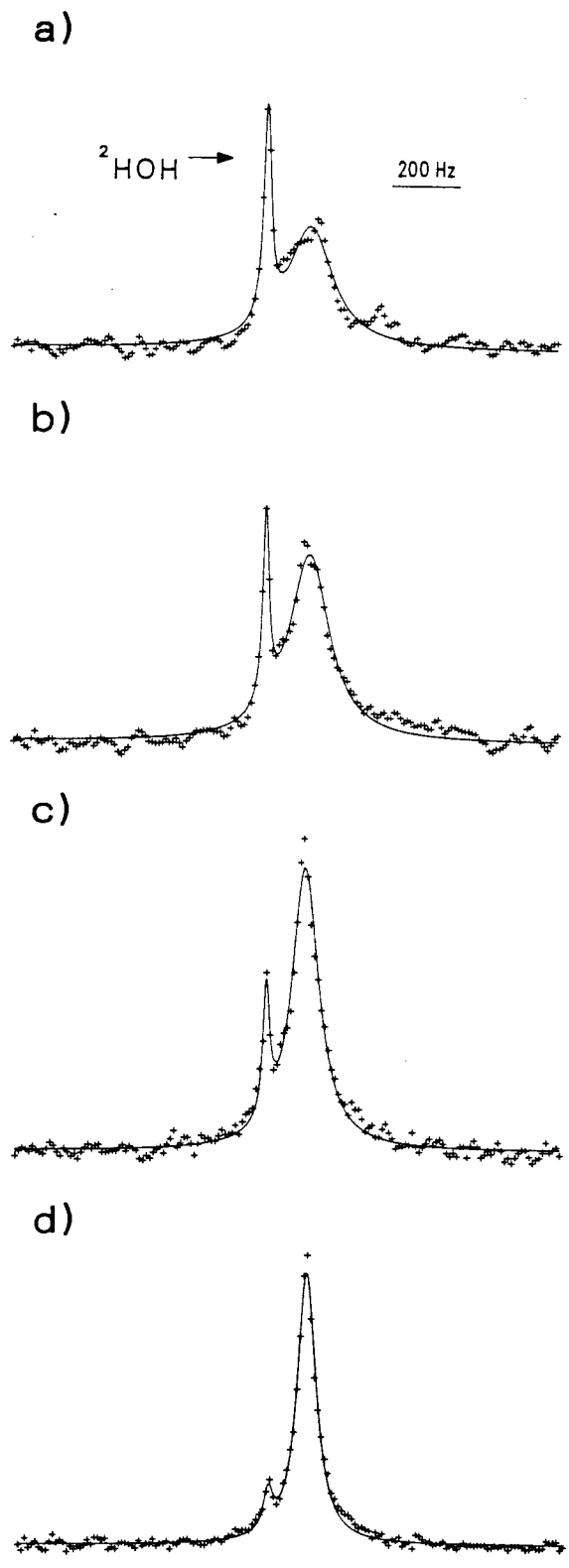
a)
^{2}HOH
200 Hz
b)
c)
d)

Figure 49: ^{2}H NMR linewidths $\Delta\nu_{1/2}$ of [^{2}H]HEP in the presence of LDL (filled circles) and acetylated-LDL (open circles), and of [^{2}H]C4S in the presence of LDL (filled squares) at 25°C. $c_{LDL} \simeq 23$ mg protein/mL for the native LDL studies and 13 mg protein/mL for the acetylated LDL study. The error bars represent an estimated uncertainty in the linewidth of ±10%.

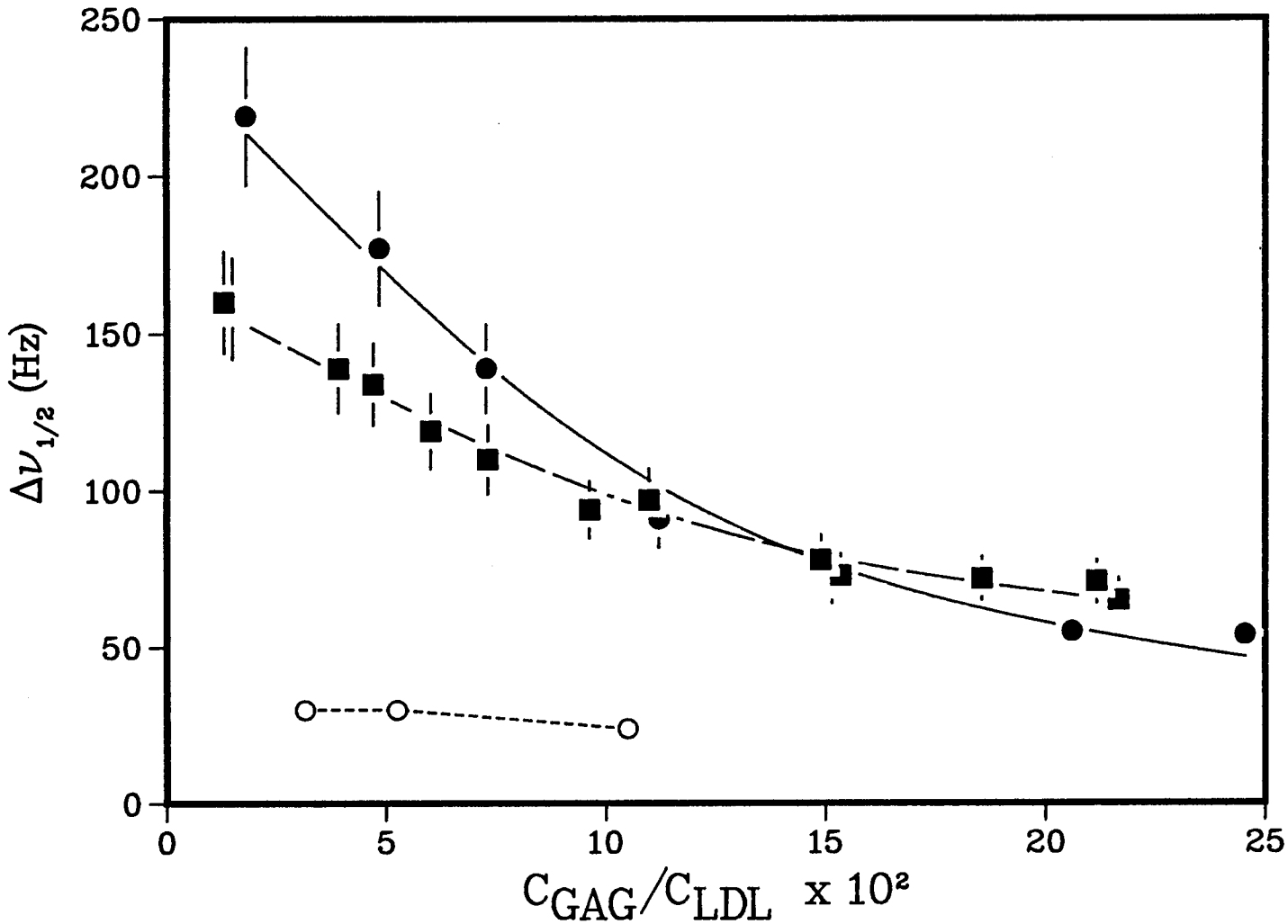
250
200
150
100
50
0
$\Delta\nu_{1/2}$ (Hz)
0
5
10
15
20
25
C_{GAG}/C_{LDL} x 10^2

greatly reduced.

There are several factors which may contribute to the observed linewidth of the [^{2}H]GAG. These include the statistical equilibrium constant for the dissociation of GAG and LDL (which determines the fraction of GAG bound to LDL), the overall size of the complex, and the presence of internal motions of the C^2H_3 group. It is difficult to separate these contributions on the basis of the ^{2}H NMR results alone. However, with the information on complex size provided by ^{31}P NMR and QELS, we may attempt a preliminary interpretation of the ^{2}H NMR data. For a quadrupolar nucleus (I = 1) undergoing isotropic rotation, and line width $\Delta\nu_{1/2}$, the transverse relaxation rate $T_2^{-1} = \pi\Delta\nu_{1/2}$ is given by (Abragam, 1961c)

$$T_2^{-1} = (4\pi^2/160)(e^2qQ/h)^2\{9J(0) + 15J(\omega_0) + 6J(2\omega_0)\} \qquad (33)$$

where (e^2qQ/h) is the quadrupolar coupling constant. The spectral densities $J(\omega)$ are

$$J(\omega) = 2\tau_c/(1 + \omega^2\tau_c^2) \qquad (34)$$

where τ_c is the effective correlation time for molecular motion. The spectral density $J(\omega)$ is the Fourier transform of the autocorrelation function describing the motion. From eq 33 and 34, we can calculate the correlation times for the C^2H_3 groups of [^{2}H]HEP and [^{2}H]C4S both free in solution and bound to LDL. The value of (e^2qQ/h) used in the calculation was that of deuterated acetone (174.5 kHz (Seelig, 1977)). Values of τ_c of 9.4 x 10^{-11} s and 2.2 x 10^{-10} s were obtained for [^{2}H]HEP and [^{2}H]C4S in solution, respectively, based on the free linewidths $\Delta\nu_f$. In order to obtain the values for [^{2}H]GAG complexed to LDL, values of the bound linewidth

$\Delta\nu_{bd}$ were estimated by extrapolation of a plot of $\log(\Delta\nu_{1/2})$ versus GAG/LDL to GAG/LDL = 0. This approach assumes that a single $\Delta\nu_{bd}$ is physically meaningful, which may not be the case if complexes with different stoichiometries (and therefore different sizes) are formed. However, the fact that all of the [^{2}H]GAG spectra, including the broad lineshapes observed at low GAG/LDL, could be computer-simulated with a single Lorentzian lineshape, suggests that the extrapolation was justified. For [^{2}H]HEP, a value of τ_c = (2.4±0.5) X 10^{-9} s was obtained from $\Delta\nu_{bd}$ = 260±30 Hz. For [^{2}H]C4S, τ_c = (1.3±0.2) X 10^{-9} s was obtained from $\Delta\nu_{bd}$ = 170±20 Hz. Thus, the correlation times of [^{2}H]HEP and [^{2}H]C4S increase 26-fold and 6-fold, respectively, when complexed to LDL.

The correlation time of bound [^{2}H]HEP is nearly twice that of bound [^{2}H]C4S, implying slower motions of the former. This could originate from the larger size of the LDL-HEP complexes, or from slower internal motions ("tighter" binding). If the [^{2}H]GAGs were tightly bound and rotating at the same rate as the overall complex, then the correlation time for motion would be given by eq 14 (τ_t). We can calculate a mean τ_c for the overall complex using the sizes obtained from ^{31}P and QELS, assuming that the complexes formed at low GAG/LDL ratios are approximately the same size as those observed at higher ratios, when all or most of the LDL is bound. For LDL-HEP complexes, this is the value observed at HEP/LDL $\simeq$ 0.03 (49±3 nm), and for LDL-CS the size observed at CS/LDL $\simeq$ 0.6 (35±2 nm). The size ratio R(LDL-HEP)/R(LDL-CS) = 1.4 is the same by both ^{31}P and QELS. Based on the ^{31}P values, eq 14 gives τ_c(LDL-HEP) = 1.5 x 10^{-5} s and τ_c(LDL-CS) = 5.5 x 10^{-6} s. A comparison of these values with those estimated for [^{2}H]GAG bound to LDL reveals that the C^{2}H$_3$ groups of both GAGs possess considerable spin rotation. Indications of further motions in either GAG could be found from

the ratio $\tau_c([^2H]GAG_{bd})/\tau_c(complex)$, which normalizes the correlation times with respect to complex size. Assuming a 10% uncertainty in τ_c(complex), the ratios are (1.6±0.5) x 10^{-4} for [^{2}H]HEP and (2.4±0.6) x 10^{-4} for [^{2}H]C4S. These are the same within experimental error. Therefore, the broader ^{2}H NMR linewidths observed for bound [^{2}H]HEP at GAG/LDL <0.13 can be explained on the basis of complex size. This implies that both GAGs have similar internal motions when bound to LDL.

Speculation on the Different Binding Behaviour of HEP and CS with LDL

LDL-GAG soluble complexes are thought to form via an attraction between the negatively charged sulfate and carboxyl groups of the GAG and the positively charged protein groups of LDL (Iverius, 1972). The results in the current study are consistent with this view. Acetylation of LDL, which neutralizes the positive charge on the lysine groups, abolishes the interaction of [^{2}H]HEP with LDL (Figure 49). Similarly, increasing the ionic strength of the solvent results in the dissociation of large LDL-HEP complexes (Table XVI). The different behaviour observed with HEP and CS in soluble complex formation with LDL probably originates from the different charge densities and molecular weights of HEP and CS. It is reasonable to speculate that a single HEP molecule (extended chain length ≃25 nm for 15,000 MW (Chakrabarti and Park, 1980; Mourao *et al.*, 1981; Mitterer *et al.*, 1982)) may not be long enough to interact with the 5-7 HEP binding sites of apo B (Weisgraber and Rall, 1987; Cardin *et al.*, 1987; Hirose *et al.*, 1987) or that to do so would bring the HEP chain into contact with regions of the LDL surface that possess a net negative charge. The formation of multiple-LDL complexes would allow maximal interaction between the limited number of HEP chains and the positively charged apo B binding

sites. At higher HEP concentrations, saturation of binding sites results in the dissociation of some of the complexes. In contrast to the behaviour observed with HEP, the lower affinity of CS for LDL results in the formation of fewer multiple-LDL complexes. It is also possible that the longer CS chain (Gelman and Blackwell, 1973; Chakrabarti and Park, 1980; Mourao *et al.*, 1981) may be able to interact with several binding sites on a single LDL, thereby decreasing the need to equalize surface charges by the 'sharing' of CS chains between lipoproteins.

Application of the techniques described in the present study, especially the estimate of sizes by ^{31}P NMR, could be used to probe for perturbations in lipoprotein structure resulting from soluble complex formation. The study of LDL labelled with various deuterated lipids may prove useful for this purpose. This would require a knowledge of the approximate sizes of LDL-GAG soluble complexes formed at various protein concentrations, since ^{2}H NMR linewidth changes are sensitive to both changes in lipid orientational order and changes in particle radius.

The Incorporation of DPPC and CO into LDL.

The formation of both soluble and insoluble complexes of LDL with arterial GAGs has been shown to alter the lipid structure of LDL (Nakashima *et al.*, 1975; Bihari-Varga *et al.*, 1981). Unfortunately, none of these studies have provided specific information on these changes in terms of orientational order or molecular motions of the lipid acyl chains. More detailed information on both insoluble and soluble complex formation might be obtained using LDL labelled with various deuterated lipids. This would allow specific locations of the monolayer and core to be investigated separately. Studies of this nature require methods for incorporating both phospholipids and cholesteryl esters into LDL. The most convenient methods developed to date utilize plasma exchange proteins, with large microemulsion particles as the source of the lipid (Sklar *et al.*,, 1982). Treleaven *et. al.* (1986) have recently used this approach to incorporate selectively deuterated CO into the core of LDL.

Since LDL-GAG insoluble complexes containing deuterated lipids are expected to display quadrupolar splittings, relatively high incorporations of lipid would be required in order to obtain acceptable S/N. Unfortunately, in the study mentioned above (Treleaven *et al.*, 1986), the incorporations of cholesteryl ester were too low. This section describes preliminary studies of CO and DPPC incorporation into LDL.

Incorporation of DPPC into LDL from alcohol-water mixtures.

Initial attempts to incorporate DPPC into LDL involved incubating LDL with vesicles formed by a modification of the alcohol injection technique (Batzri and Korn, 1973). The phospholipid, which was sometimes mixed with a

[^{14}C]DPPC tracer, was dissolved in either ethanol or isopropanol, and the mixture was injected into rapidly stirring buffer or water at ≃50°C, resulting in a clear solution. LDL was added to the PC/alcohol/water mixture to give a final alcohol concentration of 1 - 5%, and the mixture was incubated overnight (20-24 hours) at either 25 or 45°C (usually the latter). Following incorporation, the LDL was reisolated by ultracentrifugation prior to NMR or application to a column. Similar results were obtained regardless of the choice of alcohol or incubation temperature; the incorporation was always low and in some cases there was evidence of larger structures in the isolated LDL. Some representative results will be presented to compare with other methods described in the following section.

The phospholipid chosen for initial incorporation studies was PC which was deuterium-labelled in the choline methyl groups ([^{2}H$_{9}$]DPPC). Figure 50 shows ^{2}H NMR spectra of 20 mol % [^{2}H$_{9}$]DPPC in egg PC multilamellar liposomes and in unilamellar vesicles at 25°C. The quadrupolar splitting of ≃ 1 kHz observed in Figure 50(a) for the multilamellar dispersions agrees with previous studies (Stockton *et al.*, 1976). The unilamellar vesicles (Figure 50(b)) give a narrow Lorentzian line with $\Delta\nu_{1/2}$ = 23 Hz.

[^{2}H$_{9}$]DPPC (14 mg) was incubated with ≃ 50 mg LDL (as protein) for 20 hours at room temperature in the presence of 2% ethanol. The LDL was reisolated by ultracentrifugation in the density range 1.019 - 1.063 g/mL, and was prepared for ^{2}H NMR by several exchanges against 0.05 *M* Tris-HCl pH 7.5 prepared in deuterium-depleted water. The ^{2}H NMR spectra are shown in Figure 51 at 25 and 35°C. At the lower temperature (Figure 51(a)), there is a narrow signal, probably originating from [^{2}H$_{9}$]DPPC in LDL, with

Figure 50: ^2H NMR Spectra of [$^2H_9$]DPPC (20 mol %) in egg PC multilamellar dispersions (a) and unilamellar vesicles (b) at 25°C. Spectral parameters: pulse width = 7.0 μs (90°); sweep width = 50 kHz (a), 1 kHz (b); number of acquisitions = 1000 (a), 2177 (b); data sets = 4K (a), 2K (a); delay between pulses = 1.24 s (a), 3.2 s (b); delay before acquisition = 2 μs; line broadening = 20 Hz (a), 2 Hz (b). The chemical shift is given in Hz relative to external ^2H_2O.

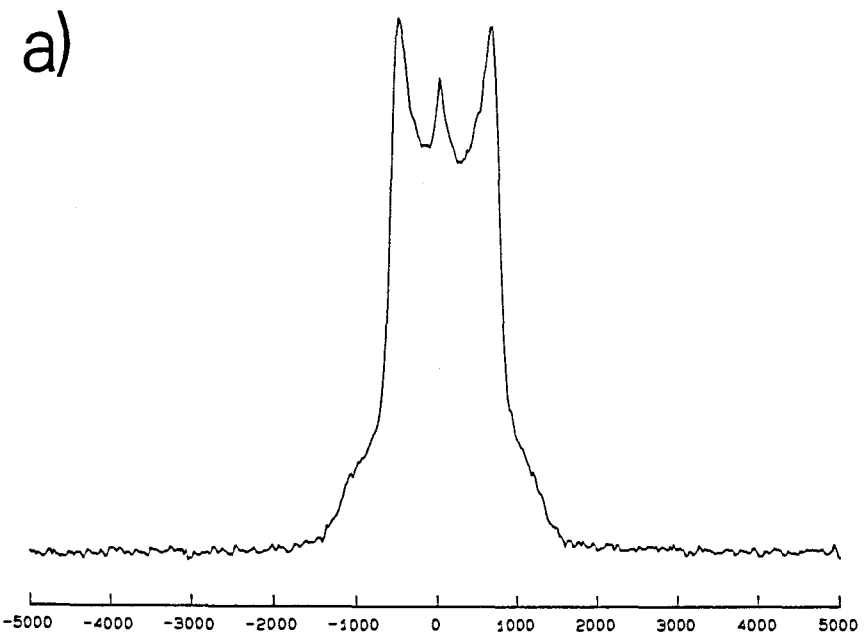
a)
-5000
-4000
-3000
-2000
-1000
0
1000
2000
3000
4000
5000

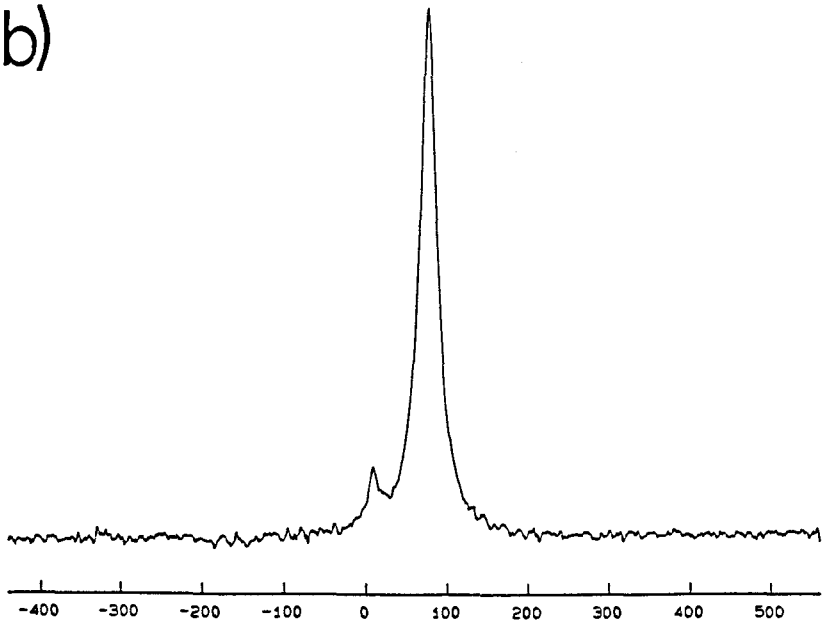
b)
-400
-300
-200
-100
0
100
200
300
400
500

Figure 51: ^2H NMR spectra of [$^2H_9$]DPPC incorporated into LDL by the ethanol method at 25°C (a) and 35°C (b). Spectral parameters: pulse width = 5 μs (60°); sweep width = 4 kHz; number of acquisitions = 102,000 (a), 27,183 (b); data sets = 4K; delay between pulses = 0.5 s; delay before acquisition = 2 μs; line broadening = 5 Hz. The chemical shift is given in Hz relative to external ^2H_2O.

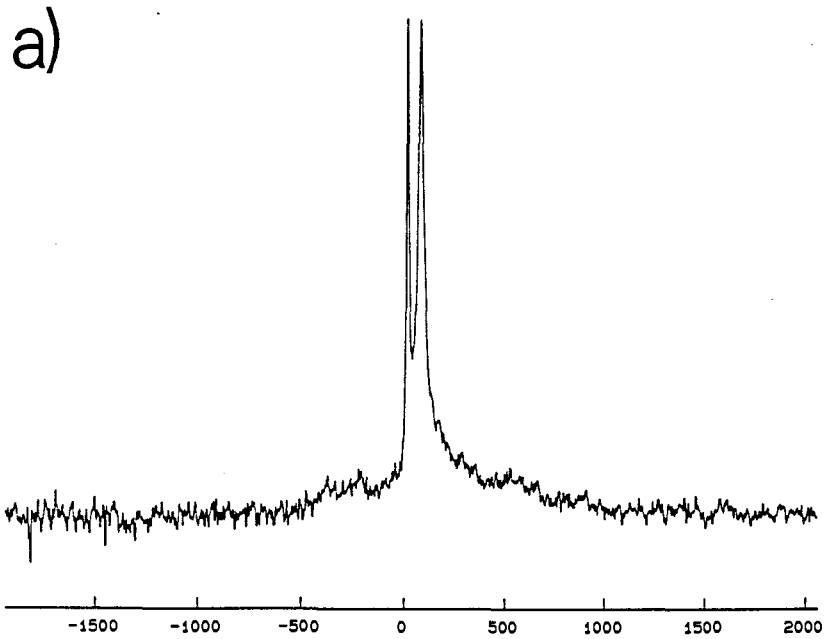
a)
-1500
-1000
-500
0
500
1000
1500
2000

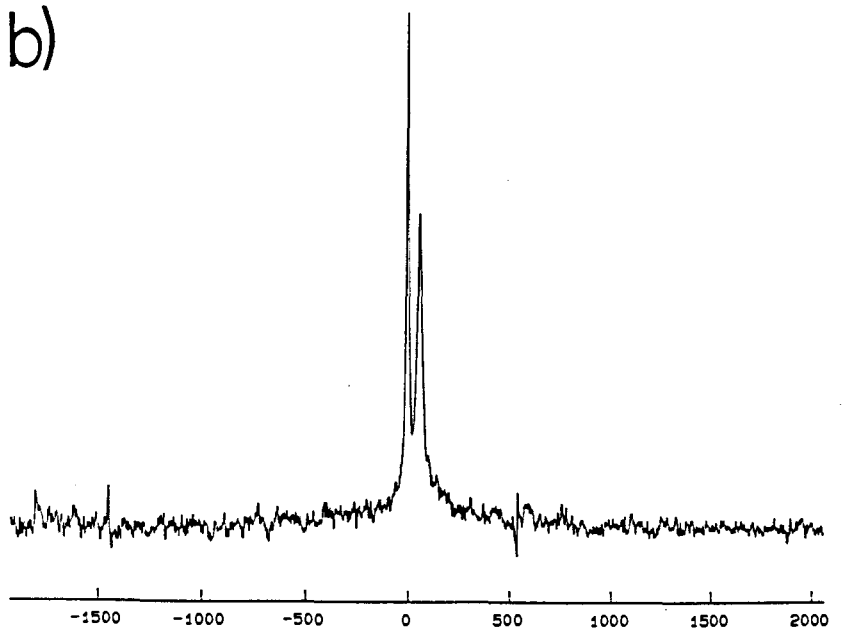
b)
-1500
-1000
-500
0
500
1000
1500
2000

a linewidth of 29-35 Hz, riding over what is suggestive of a broad resonance with an apparent quadrupolar splitting. This may indicate that some large structures are formed during the incubation process which are isolated with the LDL.

In order to verify the association of [^{2}H,]DPPC with LDL and to determine the incorporation, 2 mg of [^{14}C]DPPC (specific activity = 158,400 dpm/mg) was incubated with ≃ 7 mg LDL (as protein) at 45°C for 24 hours in a 1% ethanol solution. The ethanol concentration was lowered to safeguard against possible effects on LDL, and the temperature was increased to obtain a higher incorporation. The labelled LDL (containing 6.7 mg protein and 1.7 mg [^{14}C]DPPC) was isolated and applied to a column of Sepharose 4B. The elution profile is shown in Figure 52. Two peaks are observed; the first (fractions 20-30), containing ≃70% of the label, approximately at the void volume, and the second (LDL; fractions 54-100), containing ≃ 24% of the label. Lowry assays on fractions 26 and 59 revealed that the latter contained more than 11 times the amount of protein, even though its absorbance at 280 nm was only double that of the first peak. The identity of the first peak is thus unclear; possibly it represents large liposome structures not removed during centrifugation, or some contaminating VLDL.

From the total activity in the LDL fractions, the incorporation of [^{14}C]DPPC was calculated to be ≃ 4 mol % (relative to total LDL phospholipid).

In another study, 7.4 mg of [^{14}C]DPPC (specific activity = 73,700 dpm/mg) was incubated with ≃ 7 mg LDL protein at 46°C for 24 hours in a 5% isopropanol solution. Following incubation, the recovered LDL was found to contain 136,300 dpm. The elution profile on Sepharose 4B is shown in Figure

Figure 52: Elution of LDL containing [^{14}C]DPPC on Sepharose 4B. The [^{14}C]DPPC was incorporated by incubation in a 1% ethanol solution. The sample was eluted at 20 mL/hr, and the fraction volumes were $\simeq$ 6 mLs. Protein (●) was determined by the absorbance at 280 nm, and [^{14}C]DPPC activity (■) by liquid scintillation counting.

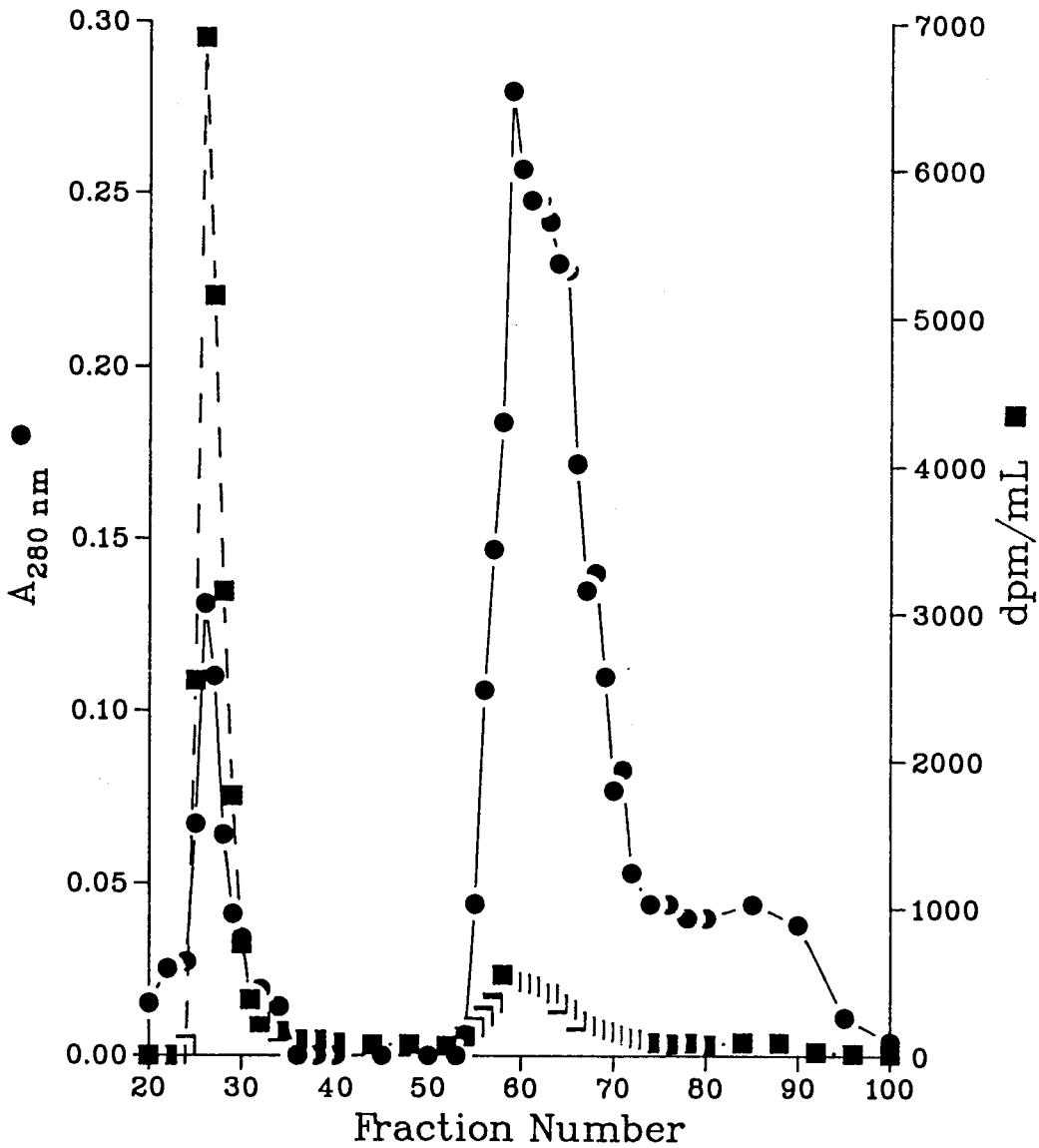
0.30
0.25
0.20
0.15
0.10
0.05
0.00
$A_{280\ nm}$
7000
6000
5000
4000
3000
2000
1000
0
dpm/mL
20
30
40
50
60
70
80
90
100
Fraction Number

53. Two peaks are observed as in Figure 52, and again the majority of label (≃ 120,000 dpm) is in the first peak. Only 25,600 dpm (0.35 mg [^{14}C]DPPC) were recovered in the LDL fractions. Assuming the same recovery of LDL as in the ethanol study, this would represent an incorporation of ≃ 5 mol %, the same as observed previously.

An attempt was made to incorporate [^{2}H,]DPPC into LDL using 5% isopropanol. In this study, 22.4 mg of [^{2}H,]DPPC containing a [^{14}C]DPPC tracer (specific activity = 16,600 dpm/mg) was incubated with ≃ 40 mg LDL (as protein) at 47°C for 19 hours. Following incubation, the LDL was applied directly to the Sepharose 4B column, and the LDL fractions were located from the absorbance at 280 nm. These fractions were pooled, and the LDL was concentrated by ultracentrifugation at density 1.063. The activity in the isolated LDL indicated the presence of 4.7 mg [^{2}H,]DPPC, an incorporation of ≃ 12 mol % if all the PC were associated with LDL. A ^{2}H NMR spectrum of this sample is shown in Figure 54. The narrow LDL resonance is riding on a broad lineshape with a quadrupolar splitting of ≃ 1 kHz. Hence, it appears that liposome contaminants are present, or that some LDL has aggregated. The former implies that the PC incorporation into LDL is much less than 11 mol %; the latter implies that the technique may damage LDL. On the basis of these experiments, it was concluded that other techniques were required for incorporating lipids into LDL.

Incorporation of DPPC and CO from rHDL particles into LDL using plasma exchange proteins.

Reconstituted HDLs containing either [^{14}C]DPPC or [^{14}C]CO were prepared as described in Materials and Methods. These were incubated with LDL under N_2 at 38°C in the presence of lipoprotein-free plasma (LFP; density > 1.21

Figure 53: Elution of LDL containing [^{14}C]DPPC on Sepharose 4B. The [^{14}C]DPPC was incorporated by incubation in a 5% isopropanol solution: The sample was eluted at 24 mL/hr, and the fraction volumes were 8 mLs. Protein (●) was determined by the absorbance at 280 nm, and [^{14}C]DPPC activity (■) by liquid scintillation counting.

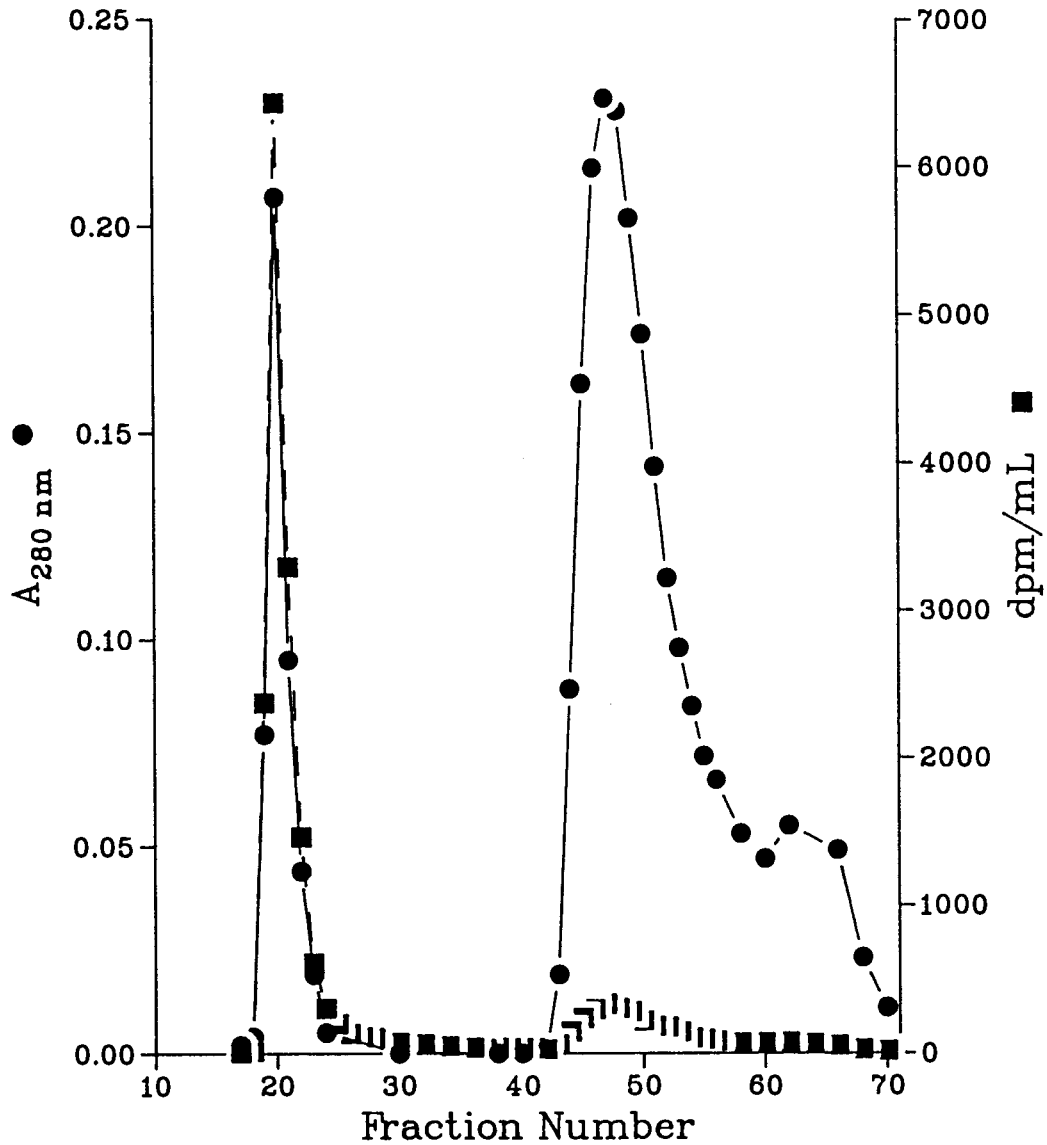
0.25
0.20
0.15
0.10
0.05
0.00
$A_{280\ nm}$
7000
6000
5000
4000
3000
2000
1000
0
dpm/mL
10
20
30
40
50
60
70
Fraction Number

Figure 54: ^2H NMR Spectrum at 25°C of LDL containing [$^2H_9$]DPPC incorporated using 5% isopropanol. The LDL was purified on a column of Sepharose 4B and concentrated by ultracentrifugation prior to NMR. Spectral parameters: pulse width = 6 μs (60°); sweep width = 5 kHz; number of acquisitions = 66000; data set = 2K; delay between pulses = 0.2 s; line broadening = 5 Hz. The chemical shift is given in Hz relative to external ^2H_2O.

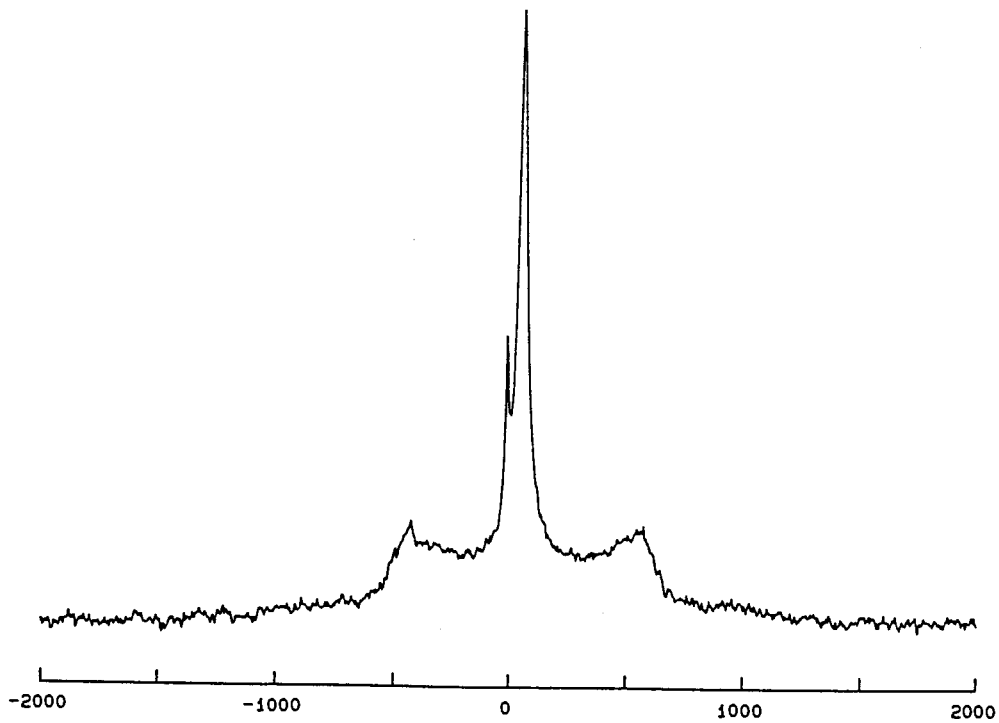
-2000
-1000
0
1000
2000

g/mL). Three studies were performed. Studies 1 and 2 involved [^{14}C]DPPC; in the former study, 3 ratios of rHDL/LDL were assayed. Study 3 involved [^{14}C]CO, and two rHDL/LDL ratios were assayed. Incubation times varied from 13-14 hours in studies 1 and 3 to 24 hours in study 2. Following lipid exchange, LDL was re-isolated and lipid incorporation was determined from liquid scintillation counting. Changes in LDL composition were assessed by protein, total cholesterol, free cholesterol, and triglyceride assays. The composition of each incubation mixture, the incorporation of labelled lipid obtained, and chemical assay results before and after exchange are given in Table XVII.

For [^{14}C]DPPC, incorporations of 15-22 mol % (relative to total LDL phospholipid) were obtained for rHDL/LDL ratios of 0.3-0.4 mg DPPC/mg protein. The amount of incorporated PC was almost as high after 13 hours (15 mol %; Study 1) as after 24 hours (22 mol %; Study 2). The effect of the exchange process on LDL composition was assessed from the ratios of free cholesterol (FC), cholesteryl ester (CE), and triglyceride (TG) to protein (Pr). The ratios of TG/Pr and CE/Pr before and after exchange are the same within experimental error. The ratio FC/Pr is slightly smaller after exchange, indicating a slight depletion of cholesterol, although the difference is small.

LDL phospholipid was not directly assayed, and therefore we cannot say whether there was any change in phospholipid/protein ratios. This was indirectly determined by obtaining ^{1}H-decoupled ^{31}P NMR spectra of LDL before and after the incorporation of 22 mol % of [^{2}H,]DPPC. These are shown in Figure 55, and the linewidths and PC/SPM ratios (obtained from the intensities of the two resonances) are given in Table XVIII.

Table XVII: Incorporation of [^{14}C]DPPC and [^{14}C]CO into LDL using plasma exchange proteins and rHDL donor particles.

	Study 1			Study 2	Study 3		native LDL
	1	2	3		1	2	
				Ratio of rHDL/LDL in Incubation Mixture			
DPPC/Pr[a]	0.38	0.21	0.15	0.32	3.0	1.3	
CO/Pr[a]					1.3	0.56	
CO/CE[a]					0.6	0.3	
				Incorporation of Labelled Lipid (mol %)			
[^{14}C]DPPC[b]	15	8	7	22			
[^{14}C]CO[b]					19	10	
				Effect of Exchange on LDL Composition			
FC/Pr	0.37	0.33	0.21	0.31	0.50	0.33	0.49±0.05
CE/Pr	2.06	2.04	2.31	1.95	2.54	2.37	1.99±0.23
TG/Pr	0.31	0.39	0.23	0.43	0.56	0.27	0.41±0.09

[a] Weight ratio of DPPC or CO of rHDL to protein (Pr) or cholesteryl ester (CE) of LDL. DPPC/Pr and CO/Pr ratios were determined from liquid scintillation counting and protein assays, except for Study 3, where DPPC/Pr was estimated assuming an rHDL composition of 46% Pr, 38% DPPC, and 16% CO. CO/CE was estimated assuming an LDL composition of 21% Pr, 21% phospholipid, and 42% CE. Other abbreviations: FC = free cholesterol, TG = triglyceride.

[b] DPPC incorporation is expressed as mol % of total LDL phospholipid (assuming 21% Pr and 21% phospholipid). CO incorporation is expressed as mol % of total LDL CE.

Figure 55: ^{1}H-decoupled ^{31}P NMR spectra (40.5 MHz) of native LDL (a) and LDL containing 22 mol % [$^{2}H_{9}$]PC (b) at 25°C. Spectral parameters: pulse width = 20 μs (60°); sweep width = 2000 Hz; number of acquisitions = 1576 (a), 1500 (b); data sets = 2K; delay between pulses = 2 s; line broadening = 2 Hz.

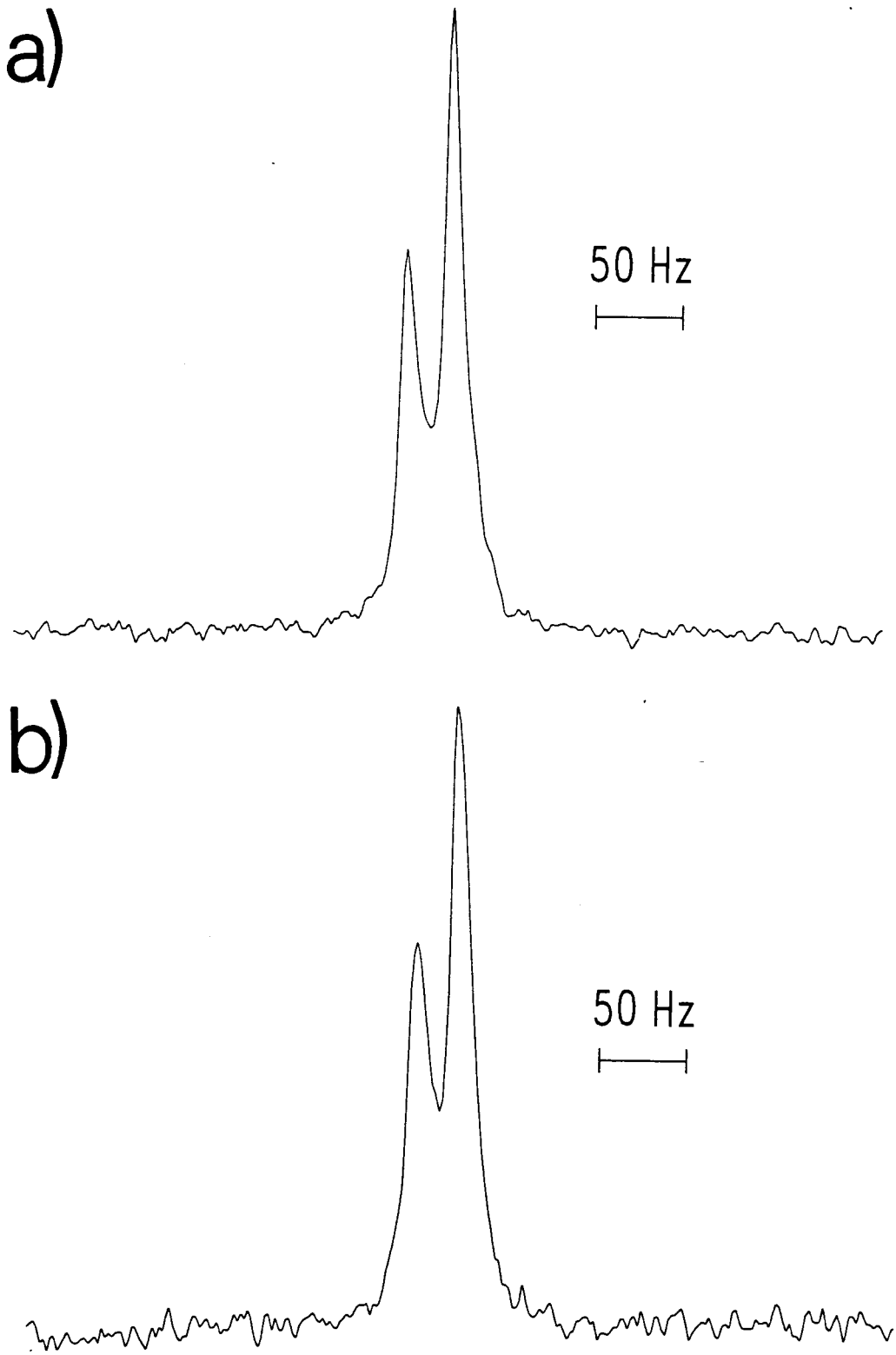
a)
50 Hz
b)
50 Hz

Table XVIII:

^{31}P NMR linewidths $\Delta\nu_{1/2}$ and PC/SPM ratios of LDL before and after incorporation of [^{2}H,]PC.

	$\Delta\nu_{1/2}$ (Hz)	PC/SPM
native LDL	13	1.63
labelled LDL	13	1.61

Both the linewidths and PC/SPM ratios are identical in the native and labelled LDL. Since no SPM is present in the rHDLs, the fact that the PC/SPM ratios are unchanged in LDL implies that PC exchange rather than net transfer is occuring.

For [^{14}C]CO, incorporations of 10 and 19 mol % (relative to total LDL cholesteryl ester) were obtained for rHDL/LDL ratios of 1.3 and 0.56 mg [^{14}C]CO/mg protein, corresponding to DPPC/protein ratios of $\simeq$3 and 1.3, respectively. Even at these much higher ratios of rHDL to LDL (compare with ratios for [^{14}C]PC exchange), the FC/Pr and TG/Pr ratios of the native and labelled LDL were the same within experimental error. However, the CE/Pr ratio indicates a slight increase in cholesteryl esters in LDL for the highest incubation ratio (rHDL(CO)/LDL(Pr) = 1.3).

In summary, for an incubation period of $\simeq$12 hours, minimal alterations in LDL composition occur in the rHDL/LDL (DPPC/Pr) range of 0.4-1.3. Within this range, high incorporations of both [^{14}C]DPPC and [^{14}C]CO can be obtained.

In order to demonstrate the potential of this method, ^2H NMR spectra of [$^2H_9$]DPPC in LDL were obtained at 35°C, as shown in Figure 56 (this was the LDL from Study 2). Figure 56(a) shows a 10 kHz plot, clearly demonstrating the lack of any broad component. The measured linewidth of the [$^2H_9$]DPPC at 35°C was 26 Hz. The LDL was then eluted on a column of Sepharose 4B as shown in Figure 57. As before, two peaks are resolved on the column. However, only $\simeq$ 5% of the label is in the first peak, with the remainder in LDL. This represents a significant improvement over the earlier attempts using alcohols. The identity of the first peak is still unclear, but most likely it represents a VLDL-contaminant. It should be noted that the small amount of label present in the first peak would not be detected by ^2H NMR, as evidenced by the absence of a second broader resonance over 10 kHz (Figure 56(a)). To verify this, fractions 35-60 were pooled, and the LDL was recentrifuged and concentrated for NMR. The ^2H NMR spectra of LDL isolated from the column is shown in Figure 58. The measured linewidth of 35 Hz at 25°C is broader than the linewidth at 35°C (26 Hz) due to differences in solvent viscosity. If we calculate τ_e for LDL at the two temperatures (assuming a value of D at 35°C intermediate to the values at 25 and 45°C), then from the ratio of correlation times we would predict the linewidth at 25°C to be 1.3 times greater than at 35°C, which in fact is what we observe. Therefore, the linewidths of [$^2H_9$]DPPC in LDL are the same before and after purification on the column. Further studies are needed to identify peak 1 and determine whether it is simply a lipoprotein-contaminant or whether the column may be causing degradation of some LDL. Clearly, however, the technique is promising, and future studies in this field should be rewarding.

Figure 56: ^2H NMR spectra of [^2H,]DPPC in LDL at 35°C. The [^2H,]DPPC was incorporated into LDL using plasma exchange proteins and rHDL donor particles. Spectrum (a) is a 10 kHz plot, and (b) is a 600 Hz plot. Spectral parameters: pulse width = 7 μs (76°); sweep width = 10 kHz; number of acquisitions = 12,144; data sets = 2K zero-filled to 8K; delay between pulses = 0.1 s; line broadening = 2 Hz. The chemical shift is given in Hz relative to external ^2H_2O.

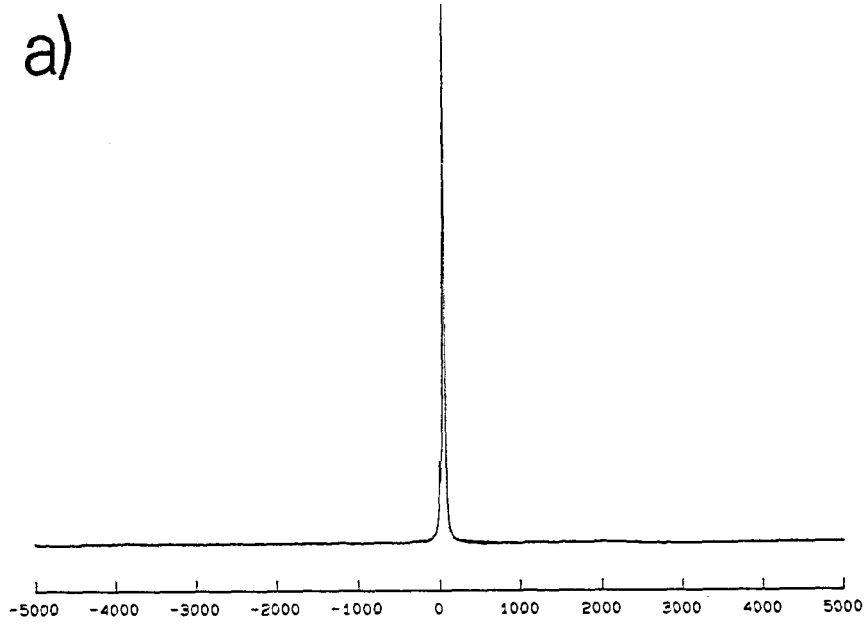
a)
-5000
-4000
-3000
-2000
-1000
0
1000
2000
3000
4000
5000

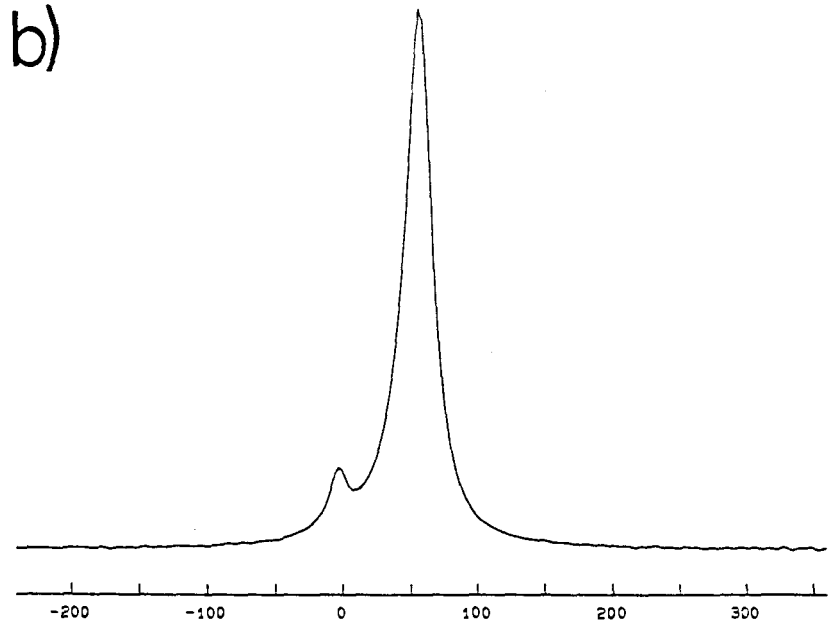
b)
-200
-100
0
100
200
300

Figure 57: Elution of LDL containing [^{14}C]DPPC on Sepharose 4B. The [^{14}C]DPPC was incorporated from rHDL particles using plasma exchange protein. The sample was eluted at 24 mL/hr, and the fraction volumes were 8 mLs. Protein (●) was determined by the absorbance at 280 nm, and [^{14}C]DPPC activity (■) by liquid scintillation counting.

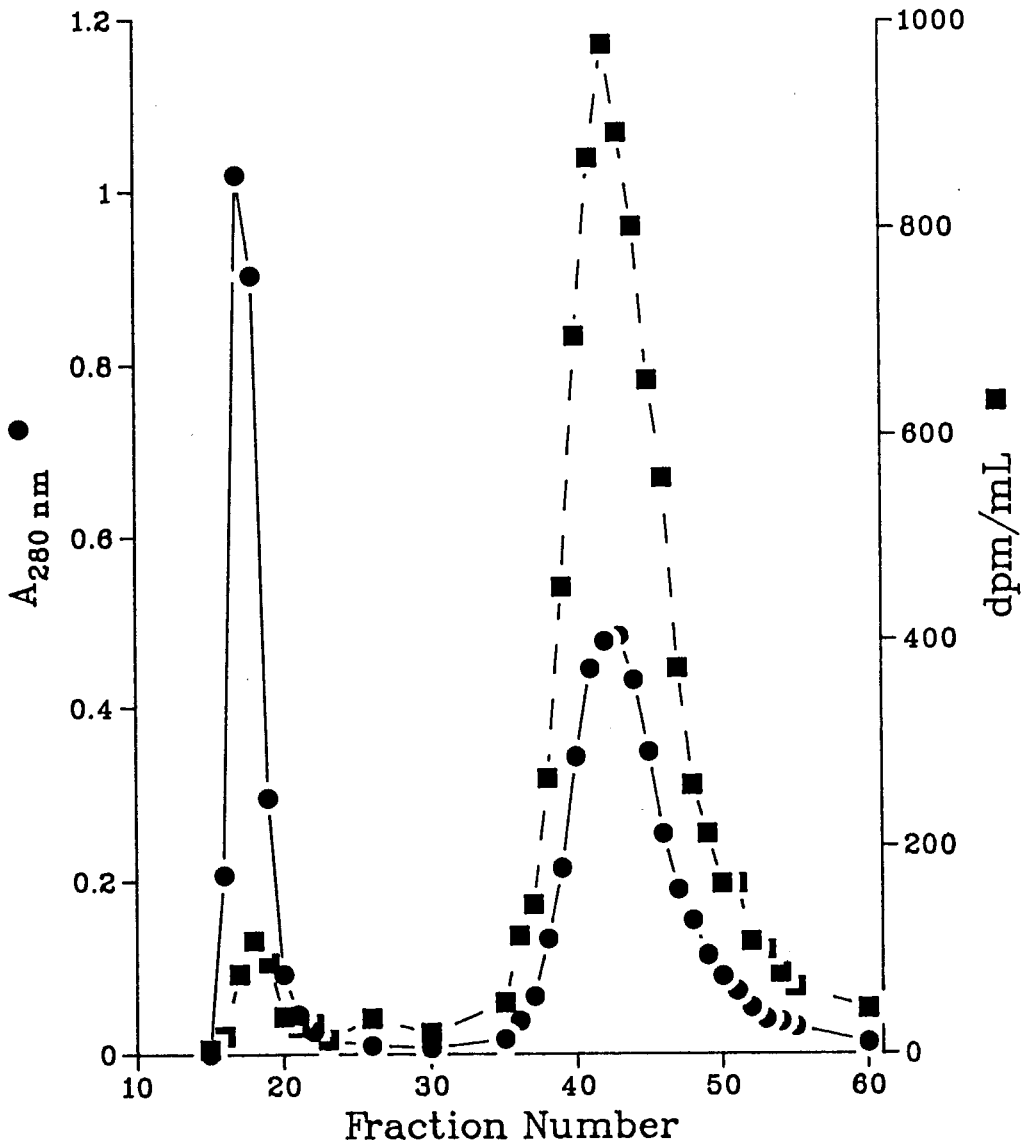
1.2
1
0.8
0.6
0.4
0.2
0
1000
800
600
400
200
0
10
20
30
40
50
60
Fraction Number
$A_{280\ nm}$
dpm/mL

Figure 58: ^2H NMR spectrum of [$^2H_9$]DPPC in LDL at 25°C after purification on Sepharose 4B. Spectral parameters: pulse width = 7 μs (76°); sweep width = 4 kHz; number of acquisitions = 8057; data sets = 2K; delay between pulses = 0.26 s; line broadening = 2 Hz. The chemical shift is given in Hz relative to external ^2H_2O.

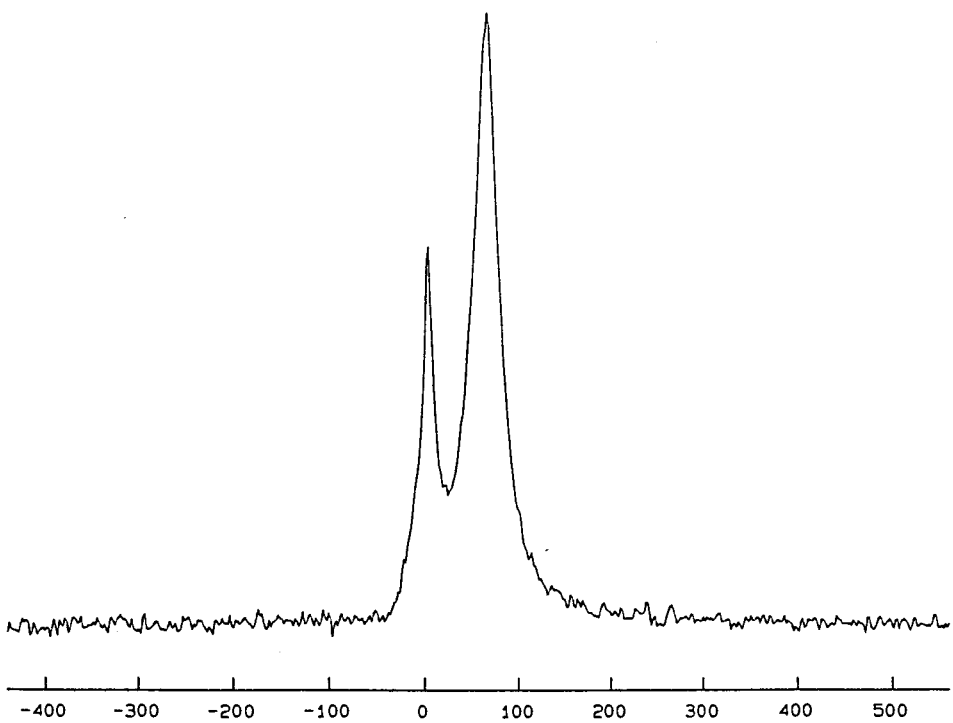
-400
-300
-200
-100
0
100
200
300
400
500

The values of the linewidths observed for [^{2}H,]DPPC in LDL are considerably broader than predicted from the quadrupolar splitting of [^{2}H,]DPPC in multilamellar dispersions. If the orientation and/or motions of the choline methyl groups are the same in LDL as in liposomes, then $\Delta\nu_{1/2}$ in LDL would be predicted to be 9 and 6 Hz at 25 and 35°C, respectively, using measured values of $\Delta\nu_Q$ = 1.3 (25°C) and 1.2 (35°C) kHz in eq 12 and 16. Conversely, the measured values in LDL would correspond to quadrupolar splittings of $\simeq$3 kHz in the absence of tumbling motions. Hence, the choline methyl groups may be slightly more ordered in LDL than in multilamellar dispersions. More information might come from studies using PC selectively deuterated in the methylene positions of the phosphorylcholine group.

CHAPTER V

CONCLUSIONS

The primary focus of the present investigations has been the study of lipid organization in HDL and LDL, with particular attention directed at the behaviour of the surface phospholipids and the extent of interaction between the monolayer and the core. A secondary focus has been the interaction of LDL with arterial GAGs, a topic of interest due to the possible role played by these macromolecules in the pathogenesis of atherosclerosis. The observation that insoluble complex formation may alter the phase transition of the core esters (Bihari-Varga *et al.*, 1981) suggests a role for monolayer-core interactions in this process.

Interactions between the Monolayer and Core of HDL

Lipid-lipid interactions between the core and monolayer have been studied using reconstituted high density lipoproteins (rHDL) composed of apoHDL$_3$ with either DPPC or egg PC as the monolayer and either CO or TO as the core. The effect of the monolayer on the core was observed by ^{2}H NMR studies of rHDLs containing the core component [$^2H_3$]CO or [$^2H_6$]TO surrounded by a monolayer of either DPPC or egg PC as a function of temperature. The reverse effect, that of the core on the monolayer, was examined by both ^{2}H and ^{31}P NMR studies of rHDLs containing [$^2H_2$]PC in the presence of CO or TO as a function of temperature. The ^{2}H NMR linewidths of [$^2H_3$]CO and [$^2H_6$]TO were considerably broader and showed a greater temperature dependence in rHDLs containing DPPC than in those containing egg PC. Similarly, the C-^{2}H order parameters of [$^2H_2$]PC were higher and showed a greater temperature dependence in rHDLs containing CO than in

those containing TO. In contrast, the ^{31}P NMR linewidths were identical for both [$^{2}H_2$]PC/CO/apoHDL$_3$ and [$^{2}H_2$]PC/TO/apoHDL$_3$ at 25°C and 6°C, showing only a slight temperature dependence. Thus, acyl chains of both the monolayer and core components show increased order when in contact with neighboring lipids of higher order. The data demonstrate a direct effect of core cholesteryl esters and triglycerides with the phospholipid monolayer of HDL. Effects of the core on the monolayer can be observed at least as high as the 5,5- position of the PC acyl chains. The results are consistent with a structure of HDL wherein interdigitation of core and monolayer components occurs, i.e., a model in which the core and monolayer are not separated by a distinct boundary. Nevertheless, further studies are necessary to clarify the mechanism of core-monolayer interactions, and to see whether these observations extend to the other classes of lipoproteins.

Phospholipid Lateral Diffusion in LDL and HDL$_3$

The lateral diffusion coefficient, D, of the phospholipids in LDL has been determined to be (1.4±0.5) x 10^{-9} cm^2/s at 25°C and (1.1±0.2) x 10^{-8} cm^2/s at 45°C, based on the viscosity-dependence of the ^{31}P NMR linewidths. The rate of diffusion at 25°C is 6-16 times slower than observed in multilamellar dispersions, unilamellar vesicles, or in the other lipoproteins. The temperature dependence of D in LDL was also determined by simulations of the ^{31}P NMR spectra of pelleted LDL over the range 5-45°C. At lower temperatures, the spectra are powder-like, narrowing as the temperature is raised. The simulations were performed assuming an axially-symmetric shielding tensor, motionally narrowed by isotropic diffusion (Burnell *et al.*, 1980). Assuming lateral diffusion to be the dominant narrowing mechanism in the viscous pellet, D was estimated to be

≃(2.0±0.5) x 10^{-9} cm^2/s at 5-15°C, increasing to (3.0±0.5) x 10^{-9} cm^2/s at 25°C and to (8.0±0.5) x 10^{-9} cm^2/s at 45°C. Although these values differ slightly from those above, they verify that diffusion is very slow in LDL at temperatures below 30°C, and that D varies significantly with temperature over the temperature range of the phase transition of the core cholesteryl esters. This contrasts with VLDL, where D remains essentially unchanged going from 25 to 40°C, and suggests that the rate of lateral diffusion of the phospholipids in the monolayer is sensitive to the physical state of the core.

The value of D in HDL_3 was found to be (2.3±0.8) x 10^{-8} cm^2/s at 25°C from the viscosity-dependence of the ^{31}P NMR linewidths. This value is similar to that obtained for HDL_2 (Parmar, 1985) and multilamellar dispersions and unilamellar vesicles.

Chemical Shift Anisotropy in LDL and HDL_3

The value of $\Delta\sigma$ in LDL was found to be 49±1 and 50±4 ppm at 25°C from the viscosity- and field- dependence of the ^{31}P NMR linewidths, respectively. From the viscosity-dependence, $\Delta\sigma$ = 52±2 ppm at 45°C. These values are similar to those determined for multilamellar dispersions and for VLDL (R.S. Chana, unpublished results). In contrast, $\Delta\sigma$ for HDL_3 = 136±11 and 156±30 ppm from the viscosity- and field- dependence of the ^{31}P NMR linewidths, respectively, at 25°C. These values approach the maximum possible value for an axially symmetric system, and suggest that the orientation and/or motions of the phosphate group is significantly different from that in VLDL or LDL. The value in HDL_2 is also quite large (≃70 ppm; Parmar (1985)). Based on the model of Thayer and Kohler (1981), the large $\Delta\sigma$ values may indicate an ordered orientation of the headgroup,

extended perpendicular to the plane of the lipoprotein surface, which may originate from interactions with the surface apoproteins.

Interactions of LDL with Arterial GAGs

LDL-HEP insoluble complexes were studied by ^{31}P NMR over the temperature range 12.5-44.5°C. As in the case of pelleted LDL, the spectra are powder-like at temperatures below 30°C. Simulations of the spectra as described above for pelleted LDL suggests that $\Delta\sigma$ is increased from 50 to 60 ppm in the insoluble complexes, and that lateral diffusion of the phospholipids is decreased from (8.0±0.5) x 10^{-9} cm^2/s in pelleted LDL to (6.0±0.4) x 10^{-8} cm^2/s in the insoluble complexes at 45°C. These alterations in the properties of the monolayer, presumably induced by the binding of HEP and Ca^{2+}, may contribute to the increased phase transition temperature of the core cholesteryl esters as observed by Bihari-Varga *et. al.* (1981), possibly via monolayer-core interactions.

Soluble complex formation between LDL and the glycosaminoglycans heparin (HEP) and chondroitin sulfate (CS) has been studied by ^{2}H and ^{31}P NMR and quasi-elastic light scattering (QELS). The use of ^{2}H and ^{31}P NMR allow us to elucidate details of binding of either the polysaccharide or the lipoprotein component, while QELS gives information on the overall complex size. [^{2}H]HEP and [^{2}H]chondroitin 4-sulfate ([^{2}H]C4S) were prepared by partial *N*-deacetylation (*via* hydrazinolysis) followed by treatment with [$^{2}H_6$]acetic anhydride. In the presence of LDL (≃23 mg protein/mL) at ratios <0.02 mg GAG/mg protein, the ^{2}H NMR linewidths of [^{2}H]HEP and [^{2}H]C4S increase 15- and 5- fold, respectively, over their unbound values. Analysis of the effective correlation time τ_c of the $C^{2}H_3$ group, obtained from estimates of the bound linewidths

$\Delta\nu_{bd}$ of the [^{2}H]GAGs, suggests that the observed linewidths are determined by the complex size, and that both [^{2}H]HEP and [^{2}H]C4S have similar motions when bound to LDL. The ^{31}P NMR data demonstrate that large LDL-HEP complexes are formed with diameters of ≃50 nm at HEP/LDL weight ratios of 0.02-0.03 mg HEP/mg protein (protein concentration = 15 mg/mL). As the HEP/LDL ratio is increased, the large complexes break down into complexes with diameters on the order of 30 nm. Complexes of LDL with C4S and chondroitin 6-sulfate (C6S) do not exhibit this behaviour. The mean diameter of these complexes increases continuously over the range of CS concentrations studied, reaching values of 32-35 nm, as estimated by ^{31}P NMR, at CS/LDL ratios of 0.6. At the lower protein concentrations studied by QELS (<1 mg/mL), the same trends are observed, although the mean diameters are less than those estimated by ^{31}P NMR. ^{31}P NMR and QELS dilution studies demonstrate that complex size varies with protein concentration. The binding of C6S and C4S to LDL was examined by CS binding studies and HEP-CS competition studies, and in both cases was found to be similar.

Incorporation of DPPC and CO into LDL

Techniques have been developed for the incorporation of labelled phospholipids and cholesteryl esters into the monolayer and core of LDL, respectively, using rHDL donor particles as the source of the lipid and plasma exchange proteins as the means of transfer. Preliminary results indicate that incorporations of up to 20 mol-% of the total phospholipid and cholesteryl ester can be achieved, with minimal alterations to LDL structure. This could allow a detailed study of the effects of LDL-GAG soluble- and insoluble- complex formation on the structure of the LDL core

and monolayer.

REFERENCES

Abragam, A. (1961a) *The Principles of Nuclear Magnetism,* Clarendon Press, Oxford, pp. 232-236.

Abragam, A. (1961b) *The Principles of Nuclear Magnetism,* Clarendon Press, Oxford, pp. 424-427.

Abragam, A. (1961c) *The Principles of Nuclear Magnetism,* Clarendon Press, Oxford, p. 315.

Alavi, M. Z. and Moore, S. (1987) *Atherosclerosis* **63**, 65-74.

Ames, B. N. (1966) *Methods Enzymol.* **8**, 115.

Assmann, G. and Brewer, H. B. (1974) *Proc. Nat. Acad. Sci. USA* **71**, 1534-1538.

Assmann, G., Sokolski, E. A. and Brewer, H. B. (1974) *Proc. Nat. Acad. Sci. USA* **71**, 549-553.

Atkinson, D., Deckelbaum, R. J., Small, D. M., and Shipley, G. G. (1977) *Proc. Natl. Acad. Sci. USA* **74**, 1042-1046.

Atkinson, D. and Small, D. M. (1986) *Ann. Rev. Biophys. Biophys. Chem.* **15**, 403-456.

Atkinson, D., Small, D. M., and Shipley, G. G. (1980) *Ann. N. Y. Acad. Sci.* **348**, 284-298.

Atkinson, D., Tall, A. R., Small, D. M., and Mahley, R. W. (1978) *Biochemistry* **17**, 3930-3933.

Barenholz, Y., Suurkuusk, J., Mountcastle, D., Thompson, T. E., and Biltonen, R. L. (1976) *Biochemistry* **15**, 2441-2447.

Batzri, S. and Korn, E. D. (1973) *Biochim. Biophys. Acta* **298**, 1015-1019.

Baumstark, M., Welte, W., and Kreutz, W. (1983) *Biochim. Biophys. Acta* **751**, 108-120.

Bernfeld, P., Nisselbaum, J. S., Berkeley, B. J. and Hanson, R. W. (1960) *J. Biol. Chem.* **235**, 2852-2859.

Bihari-Varga, M., Sztatisz, J. and Gal, S. (1981) *Atherosclerosis* **39**, 19-23.

Bihari-Varga, M., Goldstein, S., Lagrange, D. and Gruber, E. (1982) *Int. J. Biol. Macromol.* **4**, 438-441.

Bihari-Varga, M., Camejo, G., Horn, M. C., Szabo, D., Lopez, F. and Gruber,

E. (1983) *Int. J. Biol. Macromol.* **5**, 59-62.

Bloom, M. and Smith, I. C. P. (1985) in *Progress in Protein-Lipid Interactions (Volume 1)* (Watts, A. and De Pont, J.J.H.H.M., eds.) Elsevier Science Publishers, pp. 61-88.

Boggs, J. M. (1987) *Biochim. Biophys. Acta* **906**, 353-404.

Brown, M. S. and Goldstein, J. L. (1986) *Angew. Chem. Int. Ed. Engl.* **25**, 583-602.

Buldt, G. and Wohlgemuth, R. (1981) *J. Membrane Biol.* **58**, 81-100.

Burnell, E. E., Cullis, P. R., and De Kruijff, B. (1980) *Biochim. Biophys. Acta* **603**, 63-69.

Burnett, L. J. and Muller, B. H. (1971) *J. Chem. Phys.* **55**, 5829-5831.

Camejo, G., Lalaguna, F., Lopez, F. and Starosa, R. (1980) *Atherosclerosis* **35**, 307-320.

Camejo, G., Ponce, E., Lopez, F., Starosta, R., Hurt, E., and Romano, M. (1983) *Atherosclerosis* **49**, 241-254.

Cardin, A. D., Randall, C. J., Hirose, N., and Jackson, R. L. (1987) *Biochemistry* **26**, 5513-5518.

Cardin, A. D., Ranganathan, S., Hirose, N., Wallhausser, L., Harmony, J. A. K., and Jackson, R. L. (1986) *Biochemistry* **25**, 5258-5263.

Caruzzo, C. (1974) in *Atherosclerosis IV* (Schettler, G. and Weizel, A., eds.) Springer-Verlag, Berlin, pp. 751-757.

Chakrabarti, B. and Park, J. W. (1980) *CRC Critical Reviews in Biochemistry* **8**, 225-313.

Chen, S-.H., Yang, C.Y., Chen, P.-F., Setzer, D., Tanimura, M., Li, W.H., Gotto, A.M., Jr., and Chan, L. (1986) *J. Biol. Chem.* **261**, 12918-12921.

Clegg, R. M. and Vaz, W. L. C. (1985) in *Progress in Protein-Lipid Interactions (Volume 1)* (Watts, A. and De Pont, J.J.H.H.M., eds.) Elsevier Science Publishers, pp. 173-229.

Cullis, P. R. (1976) *FEBS Lett.* **70**, 223-228.

Cullis, P. R. and De Kruijff, B. (1979) *Biochim. Biophys. Acta* **559**, 399-420.

Cushley, R. J., Treleaven, W. D., Parmar, Y. I., Chana, R. S., and Fenske, D. B. (1987) *Biochem. Biophys. Res. Comm.* **146**, 1139-1145.

Dalferes, Jr., E. R., Ruiz, H., Kumar, V., Radhakrishnamurthy, B., and Berenson, G. S. (1971) *Atherosclerosis* **13**, 121-131.

Davis, J. H. (1983) *Biochim. Biophys. Acta* **737**, 117-171.

Dawson, G., Kruski, A. W., and Scanu, A. M. (1976) *J. Lipid Res.* **17**, 125-131.

Deckelbaum, R.J., Shipley, G.G., and Small, D.M. (1977) *J. Biol. Chem.* **252**, 744-754.

Dempsey, C. E., Ryba, N. J. P., and Watts, A. (1986) *Biochemistry* **25**, 2180-2187.

Dolphin, P. J. (1985) *Can. J. Biochem. Cell Biol.* **63**, 850-869.

Eigner, W. -D., Mitterer, A., Schurz, J. and Jurgens, G. (1982) *Bioscience Reports* **2**, 413-417.

Fahey, P. F., Koppel, D. E., Barak, L. S., Wolf, D. E., Elson, E. L. and Webb, W. W. (1977) *Science* **195**, 305-306.

Finer, E. G., Henry, R., Leslie, R. B., and Robertson, R. N. (1975) *Biochim. Biophys. Acta* **380**, 320-337.

Forrest, B. J. (1977) Ph.D. Thesis, Simon Fraser University, p. 53.

Forte, G. M., Nichols, A. V., and Glaeser, R. M. (1968) *Chem. Phys. Lipids* **2**, 396-398.

Fransson, L. -A. (1985) in *The Polysaccharides* (Aspinall, G.H., ed.), vol. 3, Academic Press, New York, pp. 337-415.

Freed, J. H., Bruno, G. V., and Polnaszek, C. F. (1971) *J. Phys. Chem.* **75**, 3385-3399.

Gawrisch, K., Stibenz, D., Mops, A., Arnold, K., Linss, W., and Halbhuber, K.-J. (1986) *Biochim. Biophys. Acta* **856**, 443-447.

Gelman, R. A. and Blackwell, J. (1973) *Biochim. Biophys. Acta* **297**, 452-455.

Ginsburg, G.S., Walsh, M.T., Small, D.M. and Atkinson, D. (1984) *J. Biol. Chem.* **259**, 6667-6673.

Gold, E. W. (1979) *Anal. Biochem.* **99**, 183-188.

Goldstein, J. L., Basu, S. K., Brunschede, G. Y. and Brown, M. S. (1976) *Cell* **7**, 85-95.

Goldstein, J. L. and Brown, M. S. (1977) *Ann. Rev. Biochem.* **46**, 897-930.

Gordon, V., Innerarity, T. L. and Mahley, R. W. (1983) *J. Biol. Chem.* **258**, 6202-6212.

Gorrissen, H., Tulloch, A. P., and Cushley, R. J. (1982) *Chem. Phys. Lipids*

31, 245-255.

Griffin, R. G. (1976) *J. Am. Chem. Soc.* **98**, 851-853.

Griffin, R. G. (1981) *Methods Enzymol.* **72**, 108-174.

Griffin, R. G., Powers, L., and Pershan, P. S. (1978) *Biochemistry* **17**, 2718-2722.

Hamilton, J. A. and Cordes, E. H. (1978) *J. Biol. Chem.* **253**, 5193-5198.

Hamilton, J. A., Cordes, E. H. and Glueck, C. J. (1979) *J. Biol. Chem.* **254**, 5435-5441.

Hamilton, J.A. and Morrisett, J.D. (1986) *Methods Enzymol.* **128**, 472-515.

Hauser, H., Radloff, C., Ernst, R. R., Sundell, S., and Pascher, I. (1988) *J. Am. Chem. Soc.* **110**, 1054-1058.

Havel, R. J., Elders, H. A. and Bragdon, J. H. (1955) *J. Clin. Invest.* **34**, 1345-1353.

Henderson, T. O., Kruski, A. W., Davis, L. G., Glonek, T., and Scanu, A. M. (1975) *Biochemistry* **14**, 1915-1920.

Herzfeld, J., Griffin, R. G., and Haberkorn, R. A. (1978) *Biochemistry* **17**, 2711-2718.

Herzyk, E., Lee, D. C., Dunn, R. C., Bruckdorfer, K. R., and Chapman, D. (1987) *Biochim. Biophys. Acta* **922**, 145-154.

Hirose, N., Blankenship, D. T., Krivanek, M. A., Jackson, R. L., and Cardin, A. D. (1987) *Biochemistry* **26**, 5505-5512.

Hirz, R. and Scanu, A. M. (1970) *Biochim. Biophys. Acta* **207**, 364-367.

Hoff, H. F. and Wagner, W. D. (1986) *Atherosclerosis* **61**, 231-236.

Hook, M., Riesenfeld, J. and Lindahl, U. (1982) *Anal. Biochem.* **119**, 236-245.

Iverius, P. -H. (1972) *J. Biol. Chem.* **247**, 2607-2613.

Jonas, A. (1977) *Biochim. Biophys. Acta* **486**, 10-22.

Jonas, A. and Jung, R. W. (1975) *Biochem. Biophys. Res. Comm.* **66**, 651-657.

Kane, J. P. (1983) *Annu. Rev. Physiol.* **45**, 637-650.

Kennedy, J. F. (1979) *Proteoglycans - Biological and Chemical Aspects in Human Life*, Elsevier, Amsterdam.

Kohler, S. J. and Klein, M. P. (1976) *Biochemistry* **15**, 967-973.

Kohler, S. J. and Klein, M. P. (1977) *Biochemistry* **16**, 519-526.

Kokkonen, J. O. and Kovanen, P. T. (1987) *Biochem. J.* **241**, 583-589.

Kroon, P.A. (1981) *J. Biol. Chem.* **256**, 5332-5339.

Kuznetsov, A. S. (1982) in *Vessel Wall in Athero- and Thrombogenesis* (Chazov, E.I. and Smirnov, V.N., eds.) Springer-Verlag, Berlin Heidelberg New York, pp. 91-98.

Laemmli, U. K. (1970) *Nature* **227**, 680-685.

Laggner, P., Kostner, G. M., Rakusch, U., and Worcester, D. (1981) *J. Biol. Chem.* **256**, 11832-11839.

Laggner, P. and Muller, K. W. (1978) *Quart. Rev. Biophys.* **11**, 371-425.

Levin, I. W., Thompson, T. E., Barenholz, Y., and Huang, C. (1985) *Biochemistry* **24**, 6282-6286.

Li, W.-H., Tanimura, M., Luo, C.-C., Datta, S., and Chan, L. (1988) *J. Lipid Res.* **29**, 245-271.

Lindblom, G., Johansson, L. B.-A., and Arvidson, G. (1981) *Biochemistry* **20**, 2204-2207.

Lowry, O. H., Rosebrough, N. J., Farr, A. L. and Randall, R. J. (1951) *J. Biol. Chem.* **193**, 265-275.

Lusis, A. J. (1988) *J. Lipid Res.* **29**, 397-429.

Mahley, R. W., Weisgraber, K. H. and Innerarity, T. L. (1979) *Biochim. Biophys. Acta* **575**, 81-91.

Mahley, R. W. and Innerarity, T. L. (1983) *Biochim. Biophys. Acta* **737**, 197-222.

Mackay, A. L., Burnell, E. E., Nichol, C. P., Weeks, G., Bloom, M., and Valic, M. I. (1978) *FEBS Lett.* **88**, 97-100.

Mateu, L., Avila, E. M., Camejo, G., Leon, V., and Liscano, N. (1984) *Biochim. Biophys. Acta* **795**, 525-534.

McLaughlin, A. C., Cullis, P. R., Berden, J. A. and Richards, R. E. (1975) *J. Mag. Reson.* **20**, 146-165.

Mehring, M., Griffin, R. G., and Waugh, J. S. (1971) *J. Chem. Phys.* **55**, 746-755.

Meier, P., Ohmes, E., Kothe, G., Blume, A., Weidner, J., and Eibl, H. -J. (1983) *J. Phys. Chem.* **87**, 4904-4912.

Miller, G. J. and Miller, N. E. (1975) *Lancet* **1**, 16-19.

Mitterer, A., Eigner, W. -D., Schurz, J., Jurgens, G. and Holasek, A. (1982) *Int. J. Biol. Macromol.* **4**, 227-232.

Morrisett, J. D., Jackson, R. L., and Gotto, A. M., Jr. (1977) *Biochim. Biophys. Acta* **472**, 93-133.

Morrison, L. M. (1971) *Angiology* **22**, 165-174.

Mourao, P. A. S., Pillai, S. and Ferrante, N. D. (1981) *Biochim. Biophys. Acta* **674**, 178-187.

Mourao, P. A. S. and Bracamonte, C. A. (1984) *Atherosclerosis* **50**, 133-146.

Nakashima, Y., Di Ferrante, N., Jackson, R. L. and Pownall, H. J. (1975) *J. Biol. Chem.* **250**, 5386-5392.

Pan, Y. T., Krushi, A. W. and Elbein, A. D. (1978) *Arch. Biochem. Biophys.* **189**, 231-240.

Parmar, Y. I. (1985) Ph.D. Thesis, Simon Fraser University, p. 162.

Parmar, Y. I., Gorrissen, H., Wassall, S. R. and Cushley, R. J. (1983) *J. Biol. Chem.* **258**, 2000-2004.

Parmar, Y. I., Gorrissen, H., Wassall, S. R. and Cushley, R. J. (1985) *Biochemistry* **24**, 171-176.

Parmar, Y.I., Wassall, S.R., and Cushley, R.J. (1984) *J. Amer. Chem. Soc.* **106**, 2434-2435.

Patterson, B.W., Miller, N.H., and Fisher, W.R. (1987) *Biochim. Biophys. Acta* **920**, 266-276.

Phillips, M. C. (1977) *NATO Adv. Studies Series* **15**, 91-114.

Radhakrishnamurthy, B., Ruitz, H. A., Srinivasan, S. R., Preau, W., Dalferes, Jr., E. R. and Berenson, G. S. (1978) *Atherosclerosis* **31**, 217-229.

Rance, M. and Byrd, R. A. (1983) *J. Magn. Reson.* **52**, 221-240.

Rifici, V. A. and Eder, H. A. (1984) *J. Biol. Chem.* **259**, 13814-13818.

Ritter, M.C. and Scanu, A.M. (1977) *J. Biol. Chem.* **252**, 1208-1216.

Roden, L. (1980) in *The Biochemistry of Glycoproteins and Proteoglycans* (Lennarz, W. J., ed.), Plenum, New York, pp. 267-371.

Ross, R. and Glomset, J. A. (1976) *N. Engl. J. Med.* **295**, 369-377.

Rubenstein, J. L. R., Smith, B. A., and McConnell, H. M. (1979) *Proc. Natl. Acad. Sci. USA* **76**, 15-18.

Ryba, N. J. P., Dempsey, C. E., and Watts, A. (1986) *Biochemistry* **25**, 4818-4825.

Segrest, J. P., Jackson, R. L., Morrisett, J. D., and Gotto, Jr., A. M. (1974) *FEBS Lett.* **38**, 247-253.

Scanu, A. M. (1973) in *Atherogenesis: Initiating Factors*, Elsevier Scientific Publishers, pp. 223-250.

Scanu, A. M. (1979) in *The Biochemistry of Atherosclerosis* (Scanu, A. M., Wissler, R. W. and Getz, G. S., eds.) Marcel Dekker, New York, pp. 3-8.

Scanu, A. M., Toth, J., Edelstein, C., Koga, S. and Stiller, E. (1969) *Biochemistry* **8**, 3309-3316.

Schneider, W. J., Beisiegel, U., Goldstein, J. L., and Brown, M. S. (1982) *J. Biol. Chem.* **257**, 2664-2673.

Sears, B., Deckelbaum, R. J., Janiak, M.J., Shipley, G. G., and Small, D. M. (1976) *Biochemistry* **15**, 4151-4157.

Seelig, J. (1977) *Q. Rev. Biophys* **10**, 353-418.

Seelig, J. (1978) *Biochim. Biophys. Acta* **515**, 105-140.

Seelig, J. and Gally, H.-U. (1976) *Biochemistry* **15**, 5199-5204.

Seelig, J., Gally, H.-U., and Wohlgemuth, R. (1977) *Biochim. Biophys. Acta* **467**, 109-119.

Seelig, J., Macdonald, P. M., and Scherer, P. G. (1987) *Biochemistry* **26**, 7535-7541.

Shen, B. W., Scanu, A. M., and Kezdy, F. J. (1977) *Proc. Natl. Acad. Sci. USA* **74**, 837-841.

Sirtori, C. R., Catapano, A., Ghiselli, G. and Malino, W. R. (1976) *Artery* **2**, 390-399.

Sixl, F., Brophy, P. J., and Watts, A. (1984) *Biochemistry* **23**, 2032-2039.

Sklar, L. A., Mantulin, W. W., and Pownall, H. J. (1982) *Biochem. Biophys. Res. Commun.* **105**, 674-680.

Smith, I.C.P., Stockton, G.W., Tulloch, A.P., Polnaszek, C.F., and Johnson, K.G. (1977) *J. Coll. Int. Sci.* **58**, 439-451.

Sparks, J.D. and Sparks, C.E. (1985) *Adv. Lipid Res.* **21**, 1-46.

Spies, J. R. (1957) *Methods Enzymol.* **3**, 467-471.

Srinivasan, S. R., Lopez-S., A., Radhakrishnamurthy, B. and Berenson, G. S. (1970) *Atherosclerosis* **12**, 321-334.

Srinivasan, S. R., Dolan, P., Radhakrishnamurthy, B. and Berenson, G. S. (1972) *Atherosclerosis* **16**, 95-104.

Srinivasan, S. R., Radhakrishnamurthy, B. and Berenson, G. S. (1975a) *Arch. Biochem. Biophys.* **170**, 334-340.

Srinivasan, S. R., Dolan, P., Radhakrishnamurthy, B., Pargaonkar, P. S. and Berenson, G. S. (1975b) *Biochim. Biophys. Acta* **388**, 58-70.

Srinivasan, S. R., Radhakrishnamurthy, B., Dalferes, Jr., E. R. and Berenson, G. S. (1979) *Atherosclerosis* **34**, 105-118.

Srinivasan, S. R., Yost, K., Radhakrishnamurthy, B., Dalferes, Jr., E. R. and Berenson, G.S. (1980) *Atherosclerosis* **36**, 25-37.

Staprans, I. and Felts, J. M. (1985) *J. Clin. Invest.* **76**, 1984-1991.

Steele, R. H., Wagner, W. D., Rowe, H. A., and Edwards, I. J. (1987) *Atherosclerosis* **65**, 51-62.

Stockton, G. W., Polnaszek, C. F., Tulloch, A. P., Hasan, F., and Smith, I. C. P. (1976) *Biochemistry* **15**, 954-966.

Stone, A. J. (1973) *Nucl. Instr. and Methods* **107**, 285-291.

Tall, A. R. (1986) *J. Lipid Res.* **27**, 361-367.

Tall, A. R. (1980) *Ann. N.Y. Acad. Sci.* **348**, 335-351.

Tall, A. R. (1986) *J. Lipid Res.* **27**, 361-367.

Tall, A. R., Deckelbaum, R. J., Small, D. M. and Shipley, G. G. (1977) *Biochim. Biophys. Acta* **487**, 145-153.

Thayer, A. M. and Kohler, S. J. (1981) *Biochemistry* **20**, 6831-6834.

Thewalt, J. L., Tulloch, A. P., and Cushley, R. J. (1986) *Chem. Phys. Lipids* **39**, 93-107.

Treleaven, W. D. (1985) Ph. D. Thesis, Simon Fraser University, pp. 134-158.

Treleaven, W. D., Parmar, Y. I., Gorrissen, H. and Cushley, R. J. (1986) *Biochim. Biophys. Acta* **877**, 198-210.

Verdery, R. B., III and Nichols, A. V. (1975) *Chem. Phys. Lipids* **14**, 123-134.

Vijayagopal, P., Srinivasan, S. R., Jones, K. M., Radhakrishnamurthy, B.,

and Berenson, G. S. (1985) *Biochim. Biophys. Acta* **837**, 251-261.

Vijayagopal, P., Srinivasan, S. R., Jones, K. M., Radhakrishnamurthy, B., and Berenson, G. S. (1988) *Biochim. Biophys. Acta* **960**, 210-219.

Walsh, M.T. and Atkinson, D. (1983) *Biochemistry* **22**, 3170-3178.

Walton, K. W. and Williamson, N. (1968) *J. Atheroscler. Res.* **8**, 599-624.

Watts, A. (1987) *J. Bioenergetics Biomembranes* **19**, 625-653.

Weber, G., Fabbrini, P., Resi, L., Sforza, V. and Tanganelli, P. (1979) *Pharmacol. Res. Comm.* **11**, 341-348.

Weisgraber, K. H. and Rall, Jr., S. C. (1987) *J. Biol. Chem.* **262**, 11097-11103.

Wu, J., Jacobson, K. and Papahadjopoulos, D. (1977) *Biochemistry* **16**, 3936-3941.

Yeagle, P. L., Langdon, R. G., and Martin, R. B. (1977) *Biochemistry* **16**, 3487-3491.

Yeagle, P. L., Martin, R. B., Pottenger, L., and Langdon, R. G. (1978) *Biochemistry* **17**, 2707-2710.

Yla-Herttuala, S., Jaakkola, O., Solakivi, T., Kuivaniemi, H., and Nikkari, T. (1986) *Atherosclerosis* **62**, 73-80.

Zilversmit, D. B. (1984) *J. Lipid Res.* **25**, 1563-1569.